# Electroporation of Tissue and Cells for Drug Delivery Applications

by

Mark R. Prausnitz

B.S. Chemical Engineering, Stanford University, 1988

Submitted to the Department of Chemical Engineering
in partial fulfillment of the requirements for the degree of

Doctor of Philosophy in Chemical Engineering

at the

Massachusetts Institute of Technology
September 1994



Signature of Author .....
Department of Chemical Engineering
July 14, 1994

Certified by .....
Robert Langer
Thesis Supervisor

Certified by .....
James C. Weaver
Thesis Supervisor

Accepted by .....
Robert E. Cohen
Chairman, Committee for Graduate Students

# Electroporation of Tissue and Cells for Drug Delivery Applications

by

Mark R. Prausnitz

Submitted to the Department of Chemical Engineering
on July 14, 1994 in partial fulfillment of the
requirements for the degree of
Doctor of Philosophy in Chemical Engineering

## Abstract

Basic quantitative studies of transport due to electroporation were performed in single and multiple bilayer systems. This thesis provides, for single bilayer systems: (a) a systematic study of the absolute number of molecules transported over a range of electroporation conditions and (b) measurements of electroporation transport with time resolution shorter than that of the pulse. Considering tissue electroporation, this thesis provides: (a) the first demonstration that electroporation of mammalian skin occurs, (b) a systematic study of transdermal transport due to electroporation, suggesting that electroporation of skin may be useful for drug delivery applications, and (c) theoretical analysis supporting the occurrence of skin electroporation.

Electroporation involves creation of transient aqueous pathways in lipid bilayers by the application of short (μs, ms) electric field pulses. We measured the net number of molecules transported into erythrocyte ghosts over a broad range of electroporation conditions. A plateau in uptake was found at large field strength, which did not represent an absolute maximum in transport, but represented the maximum effect of increasing field strength, for a particular pulse protocol. Moreover, sub-millisecond measurements of electroporative transport

demonstrated that under some conditions transport occurs predominantly by electrophoresis and/or electroosmosis during a pulse, while under other conditions transport occurs in part or almost completely by post-pulse diffusion.

Widespread clinical use of transdermal drug delivery has been limited, due largely to the remarkable barrier properties of stratum corneum's intercellular lipid bilayers. We found that electroporation occurs in the skin by a mechanism involving transient structural changes in these intercellular lipids, supported by experimental results and theoretical characterization. Flux increases up to four orders of magnitude have been observed with human skin *in vitro* for three molecules having charges between -1 and -4 and molecular masses up to 1000 Da. Similar flux increases have been observed *in vivo* with hairless rat skin. The area fraction of skin available to transport during electroporation was determined to be up to 0.1 %. Electroporation-mediated transport was rapidly responsive to changes in electrical conditions, where (a) skin transport properties changed over a time scale of microseconds or faster and (b) steady-state transdermal flux could be achieved on a time scale of minutes.

Thesis Supervisor: Dr. Robert Langer
Title: Kenneth J. Germeshausen Professor of Chemical and Biochemical Engineering
Department of Chemical Engineering, MIT

Thesis Supervisor: Dr. James C. Weaver
Title: Senior Research Scientist
Harvard/MIT Division of Health Sciences and Technology, MIT

## Acknowledgements

I am deeply indebted to my friends, co-workers, and mentors:

Bob Langer for his unique insight into what is important and how to accomplish it.

Jim Weaver for his scientific rigor and attentive involvement with my research.

Vanu Bose for trying to make me into an electrical engineer.

Uwe Pliquett for good experiments and discussions.

Jung Gimm, Becky Lau, Caroline Lee, Cindy Liu, Tina Milano, Judy Pang, and Tej Preet Singh, my undergraduate collaborators, for invaluable laboratory help.

The many members of Langer Labs, especially Mark Johnson and Samir Mitragotri for transdermal and political discussions; David Edwards for convective dispersion and other theoretical insights; and Smadar Cohen for being my scientific big sister.

The people of Bldg. 20, especially Elizabeth Gift for helpful discussions, Gail Harrison for teaching me how to electroporate, Tani Chen for electroporating with me, and Yuri Chizmadzhev and Steve Burns for their insight.

Alex Kon and Dee Dee Seddick for spending their summer in Boston with me electroporating rats; and Bob Marini for helping.

Chris Cullander, Richard Guy, and the UCSF skin team for their hospitality, guidance, and confocal microscopy expertise.

Shoshi Frankenburg, Sidney Klaus, and the Hadassah Dermatology research group for their "iruach" and my leishmaniasis gift.

Jim Corbett and David Golan for late night microscopy to reggae.

Stewart Conner and Glenn Paradis for flow cytometry expertise.

Russ Potts, Janet Tamada, and others at Cygnus for their valuable insight into skin.

Aruna Nathan, Mark Lovich, Elazer Edelman, and members of the Edelman lab for heparin and other topics.

William Deen and Frederick Schoen for their guidance as members of my thesis committee.

Ron Haak, Rick Gyory, and my former co-workers at Alza for introducing me to transdermal drug delivery.

The National Disease Research Interchange; Wilson Hayes, Aaron Hecker, and Amir Kahn of Harvard Medical School; and the Departments of Pathology at Beth Israel, Brigham and Women's, and Massachusetts General Hospitals for tissue acquisition.

Cygnus Therapeutic Systems for providing a fellowship to support this thesis and the MIT Undergraduate Research Opportunities Program for partially funding my undergraduate collaborators.

Pam Brown, Joann Sorrento, and Terry Parekh for maintaining administrative sanity.

Tushar Merchant and Grace Colon, my house-mates; my friends from Boston and California; Judy; and, of course, Mom and Dad.

# Table Of Contents

## ELECTROPORATION OF RED BLOOD CELL GHOST MEMBRANES

## List Of Figures

## List Of Tables

# INTRODUCTION

## 1 Introduction

Because the method of drug administration is now recognized to be of critical importance to a drug's therapeutic effect, the field of drug delivery has grown rapidly [Chien, 1991; Kydonieus, 1992; Langer, 1990; Robinson and Lee, 1988; Tyle, 1988]. Drug delivery across skin shows potential as a noninvasive, user-friendly, and controllable approach. However, transdermal drug delivery is presently limited by the remarkable barrier properties of skin, afforded primarily by skin's outermost later, the stratum corneum. The stratum corneum is a dead tissue composed of flattened cells filled with crosslinked keratin and intercellular lipids arranged largely in bilayers [Bouwstra et al., 1991; Elias, 1991]. Intercellular pathways are generally believed to be the most important routes for transdermal transport. Therefore, permeabilization of the lipid bilayers occupying these intercellular pathways would be expected to increase transdermal transport.

Electroporation involves the creation of transient aqueous pores in lipid bilayer membranes by the application of a brief electric-field pulse [Chang et al., 1992; Neumann et al., 1989; Orlowski and Mir, 1993; Tsong, 1991; Weaver, 1993b]. Dramatically increased electrical conductance and transport of molecules, including macromolecules, are generally associated with electroporation of lipid bilayers, including membranes of artificial planar and spherical systems, as well as those of living cells. Electric field exposures causing electroporation typically generate transmembrane potentials of approximately 1 V and last 10 μs to 10 ms. Electroporation of isolated single cells is well established, but electroporation of cells that are part of an intact

tissue has received little attention. Electroporation of stratum corneum has not been previously demonstrated.

This thesis presents a novel approach to enhancement of transdermal transport involving skin electroporation, believed to create aqueous pathways in the multilamellar, intercellular lipid bilayers of the stratum corneum. Here, basic studies of molecular transport associated with electroporation in a single bilayer system (red blood cell ghost membranes) are first performed to provide a deeper quantitative understanding of the phenomenon. Then, the possibility of electroporating the intercellular, multilamellar lipid bilayers of the stratum corneum is explored and its potential usefulness to enhance transdermal drug delivery is assessed.

# BACKGROUND

## 2 Transdermal Drug Delivery

### 2.1 Advantages And Limitations

Transdermal drug delivery offers many potential advantages over conventional methods of drug administration, such as injections or pills [Bronaugh and Maibach, 1989; Champion et al., 1992; Cullander and Guy, 1992; Hadgraft and Guy, 1989; Hsieh, 1994; Shah and Maibach, 1993]. First, by delivering drugs across the skin and into the systemic blood stream, potential degradation due to the stomach, intestine, or liver is reduced. Degradation can be a significant problem for many drugs, especially if taken orally. Second, patience compliance may be improved, since a transdermal delivery device might only need to be applied to the skin once per day or less frequently. In contrast, many patients find it difficult or inconvenient to take medication many times each day, which is often required when injections or pills are used. Finally, transdermal delivery has the potential for controlled release, where (a) drug can be continuously provided to the body to maintain a desired therapeutic and non-toxic drug level or (b) drug delivery rates can be varied, according to pulsed or other more complex delivery profiles, if needed.

Despite the potential advantages of transdermal delivery, few drugs are now administered clinically across the skin. This is primarily because transdermal transport occurs for most drugs at sub-therapeutic rates. Skin's low permeability is due largely to the remarkable barrier properties of the stratum corneum, the outermost layer of skin.

## 2.2 Skin Anatomy

Skin is the largest organ in the human body and has a surface area of ~ 2 $m^2$. Skin's two principle components are the outer epidermis, derived from surface ectoderm, and the underlying dermis, of mesodermal origin (Fig 2-1) [Champion et al., 1992; Monteiro-Riviere, 1991].

The epidermis is 50 - 100 μm thick and contains no blood vessels, lymphatics or nerves, exchanging metabolites by diffusion to and from the dermis. Keratinocytes, or corneocytes, are the predominant cell type, although melanocytes, Merkel cells, Langerhans' cells, and indeterminate cells are found in epidermis as well. Epidermal cells can be classified in layers above the dermal-epidermal junction: (1) The first layer is the stratum basale, a single layer of biochemically active columnar or cuboidal cells immediately above the basement membrane. (2) The second is the stratum spinosum, which contains several layers of irregular polyhedral shaped cells. (3) Third is the stratum granulosum, composed of irregularly-shaped, flattened cells which are oriented parallel to the dermal-epidermal junction. Granules inside these cells contain lamellar structures which are later released to form the intercellular lipid matrix of the stratum corneum. (4) The outermost layer, stratum corneum, contains flattened cornified cells of 14-sided polygonal structure. Each cell is approximately 30 μm across and 0.5 - 0.8 μm thick. The stratum corneum is 10 - 50 cells thick, usually measuring 10 - 20 μm. Although these cells are generally stacked in columns, they are sometimes interdigitated [Champion et al., 1992; Monteiro-Riviere, 1991].

The stratum corneum is unlike any other tissue in the body. First, its "cells" are filled with bundles of cross-linked keratin and keratohyalin surrounded by a thickened (15 nm) cell membrane [Champion et al., 1992; Monteiro-Riviere,

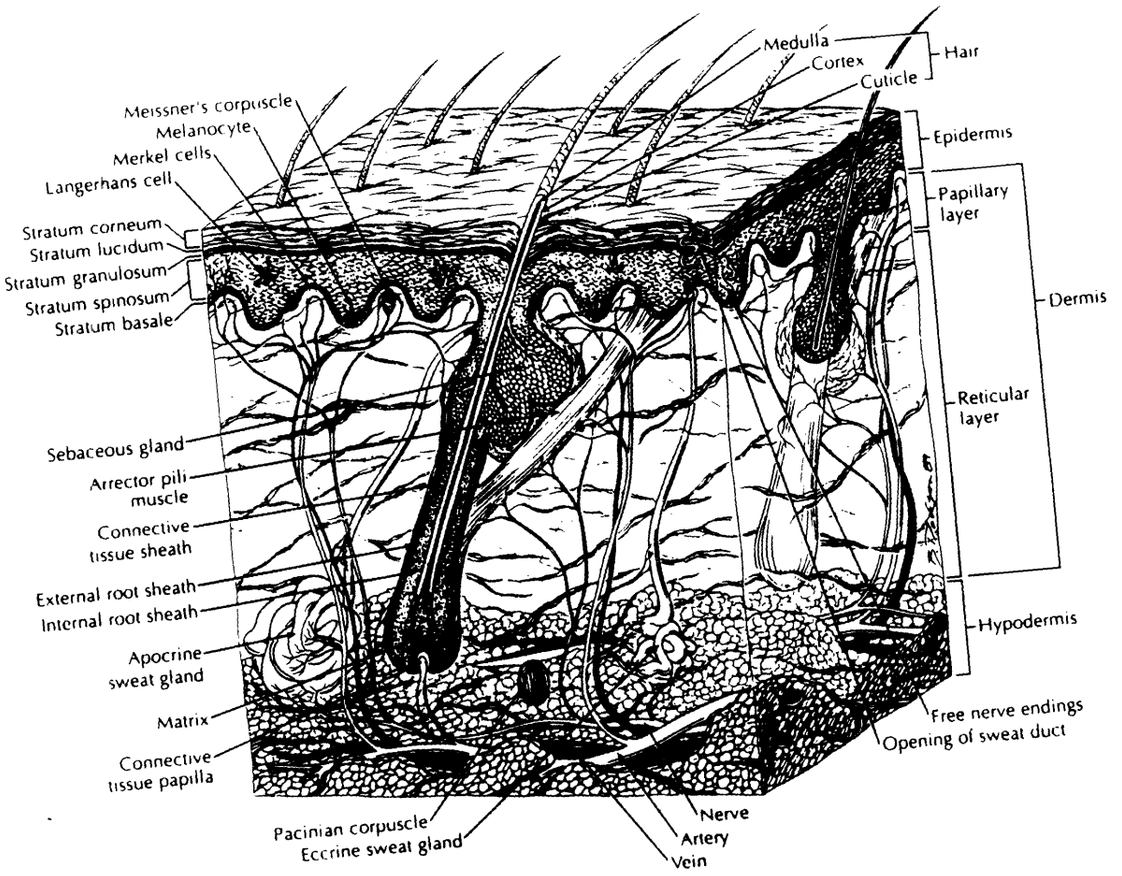


**Fig. 2-1A.** Schematic representation of human skin. The principle components of skin are shown in a composite representation of skin structure typically found in various regions of the body. Reproduced from [Monteiro-Riviere, 1991].

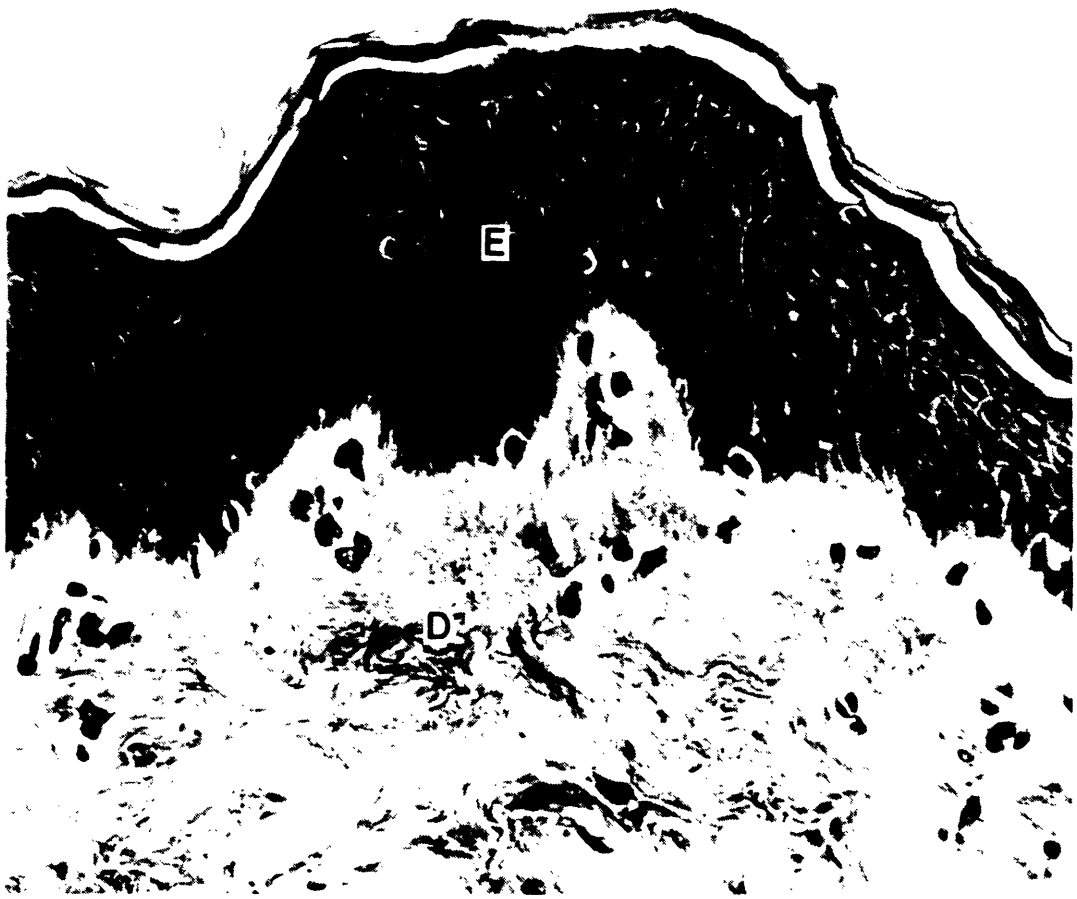


**Fig. 2-1B.** Light micrograph of human breast skin, stained with hematoxylin and eosin. Epidermis (E) and dermis (D) are indicated. Reproduced from [Monteiro-Riviere, 1991].

1991]. Second, the intercellular spaces of stratum corneum, which contain almost no water (estimated at one water molecule per lipid molecule [Mak et al., 1991]), are made of lipids arranged largely in bilayers (Fig 2-2) [Bouwstra et al., 1991; Elias, 1991]. Unlike the phospholipids of cell membranes found elsewhere in the body, stratum corneum lipids are primarily ceramides, cholesterol, and fatty acids [Elias, 1988; Lampe et al., 1983a; Lampe et al., 1983b]. It is this structure of keratin-filled blocks surrounded by multilamellar lipid bilayers, which is believed to give skin its barrier properties and prevents therapeutic transdermal administration of many drugs.

The dermis is 1 - 3 mm thick, mostly containing dense irregular connective tissue made up of 60 - 70 % water. This amorphous matrix, called ground substance, also contains fibrous proteins, such as collagen, elastin, and reticulin. The predominant cell types are fibroblasts, mast cells, and macrophages. Blood vessels, lymphatics, and nerves also reside within the dermis [Champion et al., 1992; Monteiro-Riviere, 1991].

Appendages, including hair follicles and sweat ducts, exist within skin. Hair follicles have three concentric layers: (1) the inner root sheath, composed of keratinized cells, (2) the outer root sheath, continuous with and structurally similar to viable epidermis, and (3) the connective tissue sheath, continuous with and structurally similar to dermis. At the base of the hair follicle is the bulb with the hair matrix. Arrector pili muscles and sebaceous glands are also connected to hair follicles. Sweat ducts are coiled, tubular structures primarily associated with eccrine sweat glands. Apocrine sweat glands also exist in a few parts of the body (e.g., axilla, pubis) [Champion et al., 1992; Monteiro-Riviere, 1991].

**Fig. 2-2.** Electron micrograph of hairless mouse stratum corneum. The two large dark regions are keratinocytes, while the central striped band is the intercellular domain. Within the intercellular region, series of electron-dense and electron-lucent bands are seen, corresponding to the lipid bilayers of the intercellular lamellae. Reproduced from [Elias, 1991].

## 2.3 Pathways Of Transport

There are three potentially important pathways by which molecules cross skin. First, a pathway directly across the stratum corneum is possible, where molecules cross multiple keratinocytes and lipid bilayers. However, because transport across bilayers and through keratinocytes is believed to be slow, this path is usually not expected to be important. Second, a tortuous pathway through the intercellular lipids is possible, where transport through keratinocytes does not occur. This pathway might involve little transport across bilayers, where molecules travel laterally within tail group regions, if hydrophobic, or within head group regions, if hydrophilic. Experimental data support an intercellular lipid pathway under conditions of passive diffusion [Boddé et al., 1989; Boddé et al., 1991; Cullander, 1992; Potts and Guy, 1991; Potts et al., 1992]. Finally, a route through sweat ducts and/or hair follicles (referred to as the shunt pathway) may provide a direct route which circumvents the stratum corneum barrier. Although shunts make up only ~ 0.1 % of human skin's surface area, experimental evidence suggests that this pathway may also be important, especially for ion transport in the presence of electric fields [Abramson and Gorin, 1940; Burnette and Marrero, 1986; Burnette and Ongpipattanakul, 1988; Cullander, 1992; Grimnes, 1984; Potts et al., 1992; Scott et al., 1993; Scott et al., 1992].

## 2.4 Transport Enhancement

Because rates of transdermal delivery are slow for many drugs, a number of approaches to enhancing transport across skin have been investigated, including the use of chemicals, electricity, ultrasound, and prodrugs [Banga and Chien, 1988; Bronaugh and Maibach, 1989; Chien and Banga, 1989; Cullander and Guy, 1992; Hadgraft and Guy, 1989; Hsieh, 1994; Shah and Maibach, 1993;

Sloan and Soltani, 1986]. Chemical enhancement has received the most attention. A chemical enhancer may increase transport by: (a) increasing drug solubility in the delivery vehicle (outside the body), (b) increasing drug solubility in the skin, (c) increasing the effective volume in the skin into which drug can partition, or (d) physically altering the skin. Although chemical enhancers have received extensive attention in both the scientific [Bronaugh and Maibach, 1989; Hadgraft and Guy, 1989; Hsieh, 1994; Shah and Maibach, 1993] and patent [Santus and Baker, 1993] literature, mechanistic insight and broadly-applicable approaches to enhancement are limited. Identification of chemicals which both affect transport significantly and are safe for human use has proved difficult. Nevertheless, chemical enhancers, such as ethanol, are presently used in transdermal patches approved by the U.S. Food and Drug Administration (FDA).

Electrical enhancement using small electric fields, termed iontophoresis, usually involves the application of a dc electric field across the skin to increase the migration of charged species. The delivery of charged drugs can be enhanced by electrophoresis. Because at physiological pH the skin carries a net negative charge, transport of uncharged drugs can also be enhanced by electroosmosis due to convection caused by electrophoresis of mobile cationic counter-ions. Iontophoresis has been used clinically [Abramson, 1941; Arvidsson et al., 1984; Banga and Chien, 1988; Chien and Banga, 1989; Duvanel et al., 1988; Ledger, 1992; Meyer et al., 1990; Schwarz et al., 1968; Singh and Roberts, 1989; Sloan and Soltani, 1986], but no drugs are presently approved by the FDA for iontophoretic delivery. Iontophoresis is limited by the maximum current which can be applied without pain or irritation. For larger patches (~ 100 $cm^2$), this limit may be up to 0.5 $mA/cm^2$ [Banga and Chien, 1988; Burnette and Ongpipattanakul, 1988; Ledger, 1992; Zlotogorski, 1987].

Ultrasound has been reported by a number of investigators to increase transdermal transport, even for macromolecules [Antich, 1982; Benson et al., 1991; Bommannan et al., 1991a; Bommannan et al., 1991b; Kost and Langer, 1993; Kost et al., 1989; Levy et al., 1989; Miyazaki et al., 1991; Novak, 1964; Tachibana and Tachibana, 1991; Tachibana and Tachibana, 1993; Tyle and Agrawala, 1989]. Although flux enhancement is sometimes small, ultrasound has been shown to dramatically reduce transport lag times, to as little as minutes. Typically ultrasound at 1 - 10 MHz and $\leq 2$ W/cm$^2$ has been employed, selected largely because of existing FDA-approved ultrasound protocols for other uses (e.g., heating for physical therapy). Mechanistic understanding of ultrasound enhancement is limited, but may involve mixing, acoustic streaming, heating, cavitation, and effects of mechanical stresses.

Prodrugs have been proposed to address a variety of drug delivery problems, including those of transdermal delivery. For skin, a prodrug would involve modification of the original drug in such a way that (a) in its modified form, the prodrug has improved transport characteristics (e.g., more hydrophobic), and (b) once the prodrug enters the body, the modification is undone or removed by enzymatic cleavage, hydrolysis, or some other mechanism, to yield the original drug. Prodrugs for transdermal delivery have received only limited attention and success [Sloan, 1992; Tojo and Lee, 1991].

## 2.5 Clinical Products

Only nine drugs are currently sold in the United States as transdermal drug delivery products: clonidine, estradiol, fentanyl, isosorbide dinitrate, nicotine, nitroglycerin, norethisterone, scopolomine, and testosterone [Santus and Baker, 1993]. A few other drugs, such as salicylate and non-steroidal anti-inflammatory

agents, have been approved in other countries. However, it is believed that many more transdermal drug delivery systems are currently being considered by the FDA, including iontophoretic devices, and may be on the market within a few years.

# 3 Electroporation

## 3.1 Overview

Electroporation involves the creation of transient aqueous pathways in lipid bilayer membranes by the application of an electric field pulse (Fig. 3-1) [Chang et al., 1992; Neumann et al., 1989; Orlowski and Mir, 1993; Tsong, 1991; Weaver, 1993b]. Permeability and electrical conductance of lipid bilayers, such as cell membranes, are increased by many orders of magnitude. Moreover, the associated local electric field can simultaneously contribute to transmembrane molecular transport by electrophoresis and/or electroosmosis. These membrane changes can persist for up to hours, but are reversible or irreversible, depending mainly on pulse magnitude and duration, as well as membrane composition. Electroporation has been demonstrated in many different mammalian, plant, yeast, bacterial, and other cells, as well as in artificial planar and spherical membranes. Thus, electroporation appears to be universal in lipid bilayers, with onset largely independent of their exact composition or structure. Although the creation of transient aqueous pathways, or electropores, is the proposed mechanism by which electroporation occurs, the exact physical nature of an electropore and the possibility of imaging them by any form of microscopy remain unresolved (Fig. 3-2) [Chang et al., 1992; Chang and Reese, 1990; Neumann et al., 1989; Orlowski and Mir, 1993; Weaver, 1993a].

Electrical exposures typically involve square-wave or exponential-decay electric field pulses which generate transmembrane potentials of approximately 1 V and last 10 μs to 10 ms [Chang et al., 1992; Neumann et al., 1989; Orlowski and Mir, 1993; Tsong, 1991; Weaver, 1993b]. For lipid bilayers on the order of 10 nm thickness, this corresponds to a local field strength within the membrane of order $10^6$ V/cm. Based largely on electrical and optical measurements,

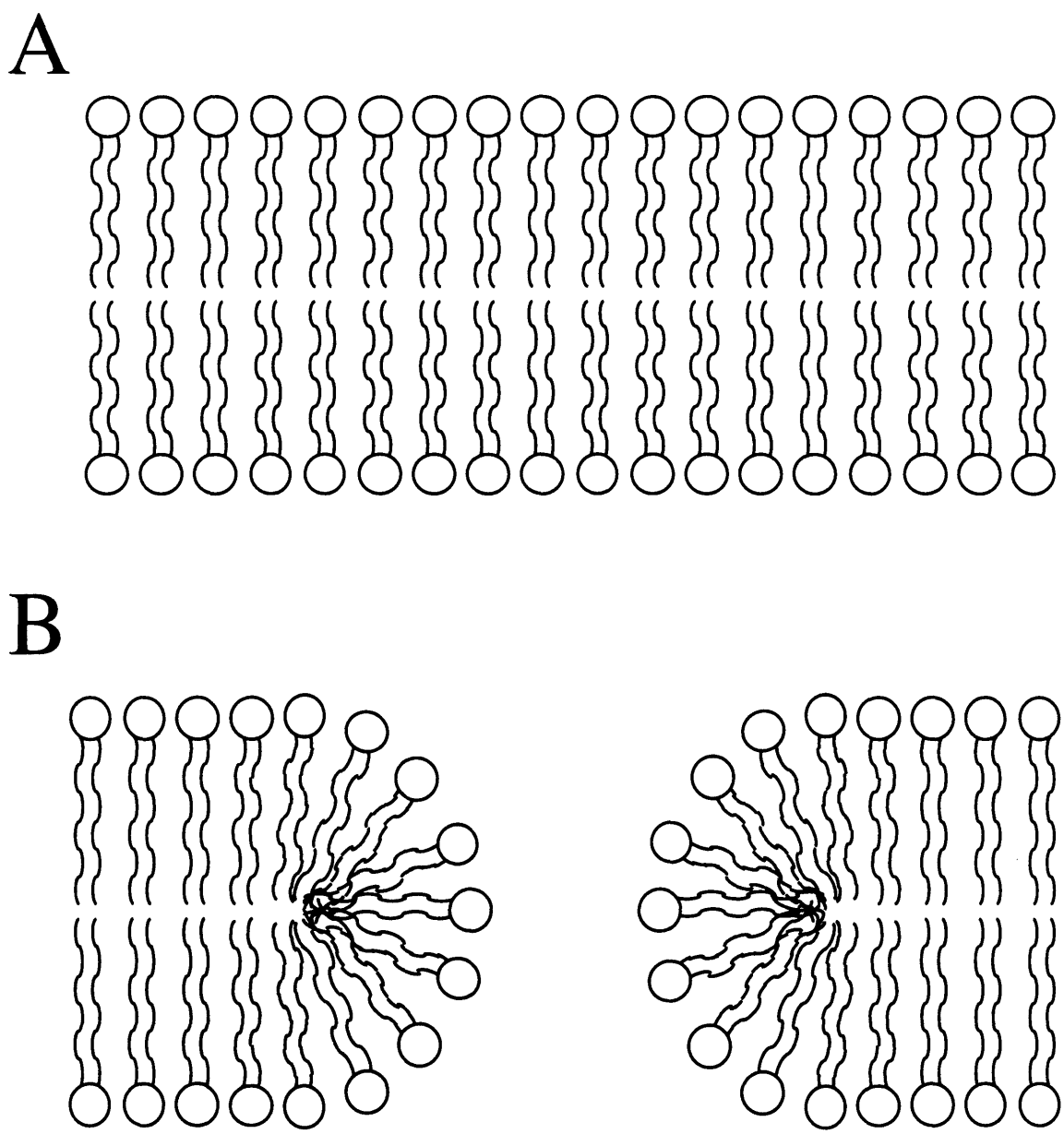


**Fig. 3-1.** Membrane reorganization by which metastable electropores might be created. A) Intact lipid bilayer. B) Lipid bilayer with a metastable aqueous pathway, or electropore. Such a reorganization might explain the existence of pores which exist well after the electric field pulse. Based on a drawing from [Glaser et al., 1988].

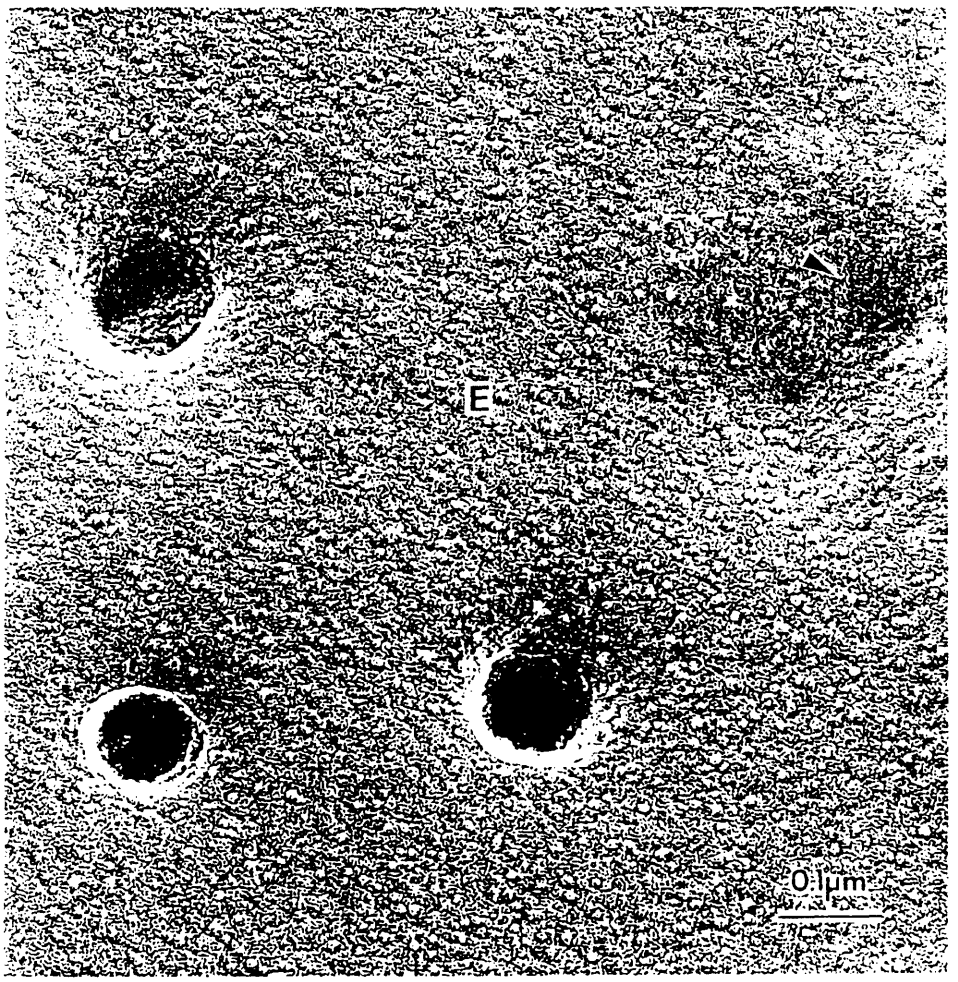


**Fig. 3-2.** Freeze-fracture electron micrograph of pore-like structures in a red blood cell membrane, showing three pores and one depression (arrow). Suspended red blood cells were pulsed (4 - 5 kV/cm, 0.3 ms) and then rapidly frozen in a liquid propane/ethane mixture (-80 °C). The large size (20 - 120 nm) and delayed appearance (3 ms post pulse) of these pore-like structures suggest that their formation may have involved secondary events following those which occurred during the pulse. Reproduced from [Chang and Reese, 1990].

electropores are thought to be created on the sub-microsecond time scale [Benz et al., 1979; Hibino et al., 1991; Neumann et al., 1992; Serpersu et al., 1985]. They are believed to continue growing in size for the duration of the electrical exposure, where maximum pore diameters are believed to up to order 10 nm, although a distribution in sizes is expected (Fig. 3-3) [Barnett and Weaver, 1991; Freeman et al., in press]. After the pulse, pores are believed to shrink to a metastable state, over a characteristic time of milliseconds [Chernomordik et al., 1983; Glaser et al., 1988]. These long-lived metastable pores are thought to be ~1 nm in radius [Abidor et al., 1979; Glaser et al., 1988]. Having lifetimes from sub-second to hours, these pores eventually disappear completely, under reversible conditions. The onset of electroporation has been shown to occur largely independent of exact membrane composition and experimental conditions. However, the time scale of recovery is a strong function of conditions, especially temperature, where low temperature (i.e., 4°C) increases pore lifetimes [Chang et al., 1992; Neumann et al., 1989].

Although electroporation has been demonstrated under a variety of conditions, there exists a range of electrical parameters for which electroporation is known to occur, and a smaller range for which electroporation is reversible (Fig 3-4). Both the magnitude and duration of the induced transmembrane voltage are important to the occurrence of electroporation. For example, electroporation generally occurs for short pulses (0.1 - 10 μs) which generate a transmembrane voltage slightly greater than 1 V, medium-length pulses (10 - 100 μs) of 0.5 - 1 V, and long pulses (≥ 1 ms) of 0.2 - 0.5 V [Benz and Zimmermann, 1980; Neumann, 1989]. Less work has been done on pulses shorter than 0.1 μs.

While electrical characterization of electroporation is important to mechanistic understanding, most applications have emphasized electroporation's ability to

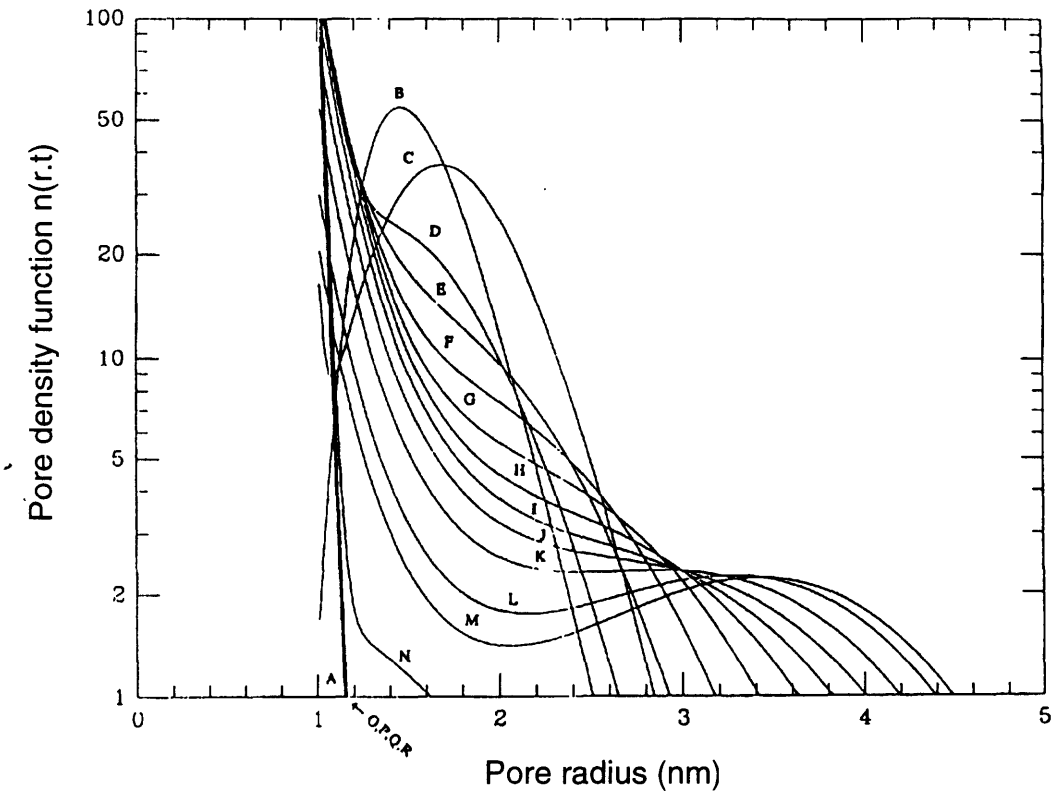


**Fig. 3-3.** Theoretical prediction of pore size distributions in an electroporated cell membrane as a function of time. Initially, there are no pores (curve A). However, during a 50 μs, 10 kV/cm square-wave pulse, a pore population with a changing distribution of sizes is created (curves B - L). After the pulse, the pores rapidly close (curves M - R). Reproduced from [Weaver and Barnett, 1992]

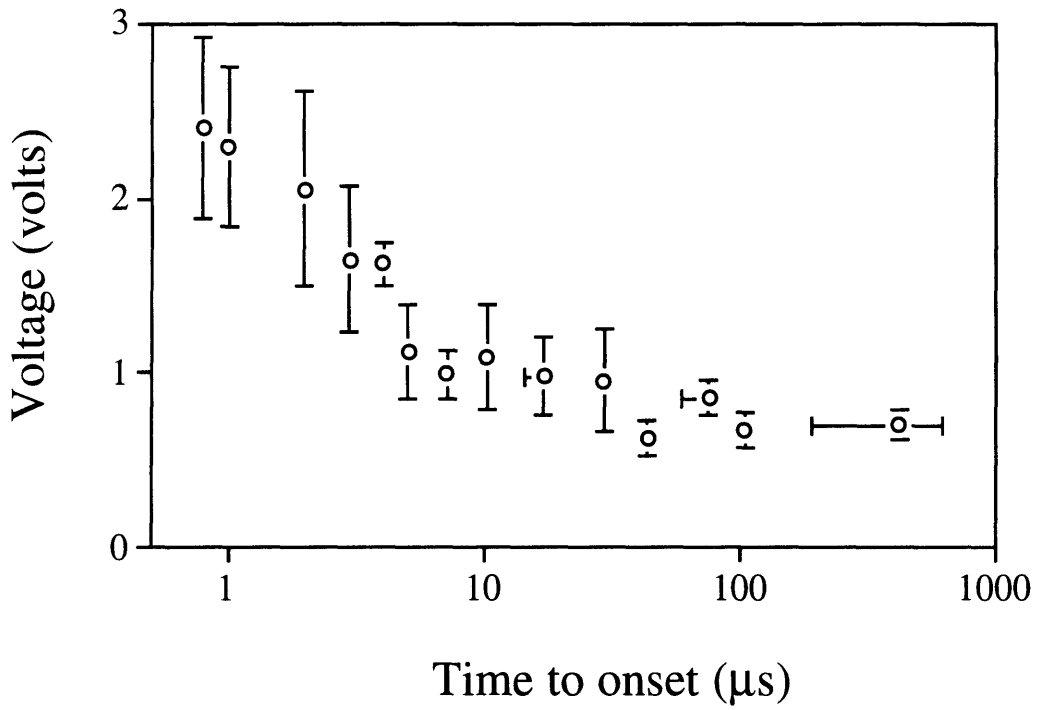


**Fig. 3-4A.** Transmembrane voltage plotted versus pulse length required for onset of electroporation in *Valonia utricularis* cell membranes. Standard deviation bars are shown. Data from [Benz and Zimmermann, 1980]

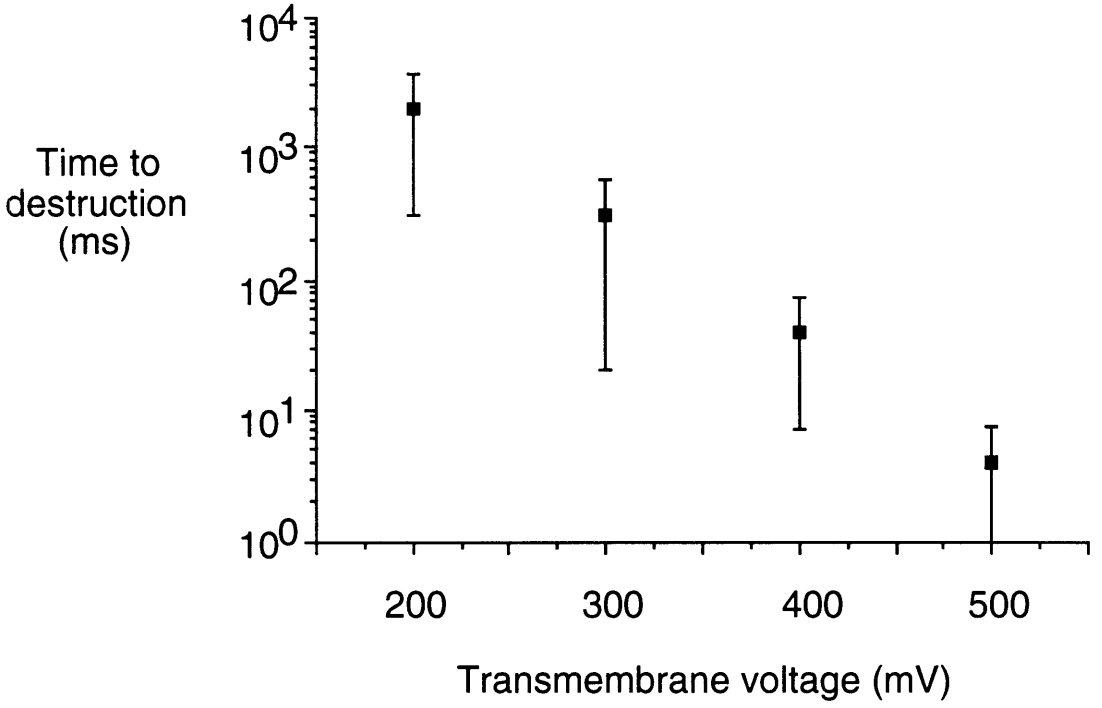


**Fig. 3-4B.** Time to cell membrane destruction (irreversibility) shown at different transmembrane voltages. Using a patch-clamp method, red blood cell membrane conductivity was measured. Cell membrane destruction was determined by irreversible membrane conductivity increases of orders of magnitude. Data from [Chernomordik et al., 1987].

increase molecular transport across lipid bilayers. Many different molecules have been transported across membranes by electroporation, ranging progressively in size from small ions to sugars to oligonucleotides to proteins to DNA to virus particles [Orlowski and Mir, 1993]. Electroporation has found widespread application in molecular biology as a method to introduce DNA into cells for gene transfection [Chang et al., 1992; Neumann et al., 1989]. Other possible applications exist, including introduction of foreign proteins into cells [Berglund and Starkey, 1991; Graziadei et al., 1991; Hashimoto et al., 1989; Lambert et al., 1990; Mir et al., 1988; Zimmermann et al., 1975], release of cellular contents for intracellular assays [Knight and Scrutton, 1986; Suprynowicz and Mazia, 1985; Swezey and Epel, 1988], and cell killing for sterilization [Hulsheger et al., 1981; Jayaram et al., 1992; Sale and Hamilton, 1967].

## 3.2 Tissue Electroporation

Recently, electroporation has been demonstrated in cells in monolayers [Kwee et al., 1990; Raptis and Firth, 1990] as well as in cell membranes and other lipid-containing structures within intact tissues [Dev and Hofmann, 1994; Orlowski and Mir, 1993; Weaver, 1993b].

The prospect of transiently enhancing transport across a tissue by electroporation suggests a variety of compelling research and biomedical applications [Chang et al., 1992; Neumann et al., 1989; Orlowski and Mir, 1993; Tsong, 1991; Weaver, 1993b]. For example, electroporation of cells within a selected tissue could cause increased local uptake of drug, allowing drug targeting. Moreover, some drugs are ineffective because they are unable to cross cell membranes under normal physiological conditions. However, electroporation could allow these drugs to enter their target cells and become

therapeutically useful. Another possible application is electroporation of skin to enhance transdermal drug delivery.

To date, electroporation of tissue has been reported by only a few research groups. Okino et al. first demonstrated in rats that electroporation at the site of a tumor could increase the effect of a chemotherapeutic agent on tumor destruction relative to pulse-only or drug-only controls [Kanesada, 1990; Okino and Esato, 1990; Okino et al., 1987; Okino and Mohri, 1987; Okino et al., 1992; Okino et al., 1991]. Following systemic administration of bleomycin, cylindrical electrodes were inserted through the skin on opposite sides of the tumor (2 - 2.5 cm spacing) and a single square-wave or exponential-decay pulse of $\leq$ 10 kV and $\leq$ 7.25 ms was applied. These electrodes produce a highly non-uniform electric field, with a very large field near the electrodes.

Related studies have been done in mice by Mir et al., employing surface, parallel-plane electrodes placed across the tumor (6.6 mm spacing) (Fig. 3-5) [Belehradek et al., 1991; Belehradek et al., 1994; Mir et al., 1991a; Mir et al., 1991b; Mir et al., 1992a; Mir et al., 1992b]. These electrodes provide a nominally uniform electric field, with departures from uniformity due mainly to tissue heterogeneity. A series of 8 square-wave pulses (100 μs width) at 1 pulse per second (pps) was applied using 900 - 1500 V/cm. Mir and coworkers have also shown tumor regression in human patients by administering bleomycin with a similar pulsing protocol [Belehradek et al., 1993; Mir et al., 1991a]. Both Okino's and Mir's groups report transient edema as the only significant side effect. Finally, using a different protocol, Mir and coworkers have recently demonstrated electroporation-enhanced cancer chemotherapy for treatment of brain tumors in rats [Salford et al., 1993].

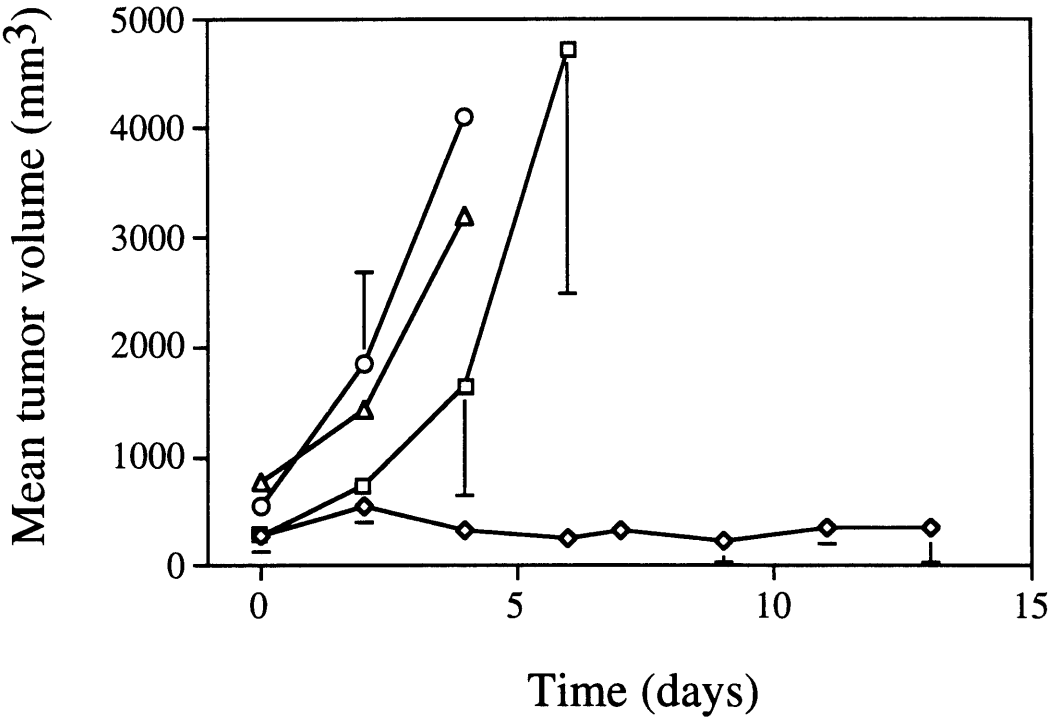


**Fig. 3-5.** The effects of bleomycin and electroporation on B16 melanomas in the flanks of C57B1/6 mice: [◇] drug (+), electroporation (+); [△] drug (+), electroporation (-); [○] drug (-), electroporation (-); [□] drug (-), electroporation (+). Only tumors which received both bleomycin (500 μg) and electroporation pulses (8 pulses of 100 μs and 1000 V/6.6 mm at 1 Hz) did not grow. Standard deviation bars are shown. Data from [Mir et al., 1991b]

Of relevance to gene therapy, Titomirov et al. have used surface electrodes to electroporate dermal cells in mice, thereby enhancing uptake and resulting in expression of plasmid DNA injected subcutaneously [Sukharev et al., 1994; Titomirov et al., 1991]. Two exponential-decay pulses of opposite polarity were applied at 400 - 600 V, 100 - 300 μs, resulting in tissue necrosis at higher voltages.

Grasso et al. have demonstrated electrofusion of cells to rabbit corneal epithelium, potentially important for novel approaches to drug delivery, wound healing, and development of new animal models [Grasso et al., 1989; Heller and Gilbert, 1992; Heller and Grasso, 1990]. Electrofusion is a phenomenon which is believed to be mechanistically related to electroporation [Chang et al., 1992; Neumann et al., 1989; Tsong, 1991]. Using an electrode which fit the curvature of the eye and a counter electrode attached to the buccal mucosa, three pulses of 20 V, 20 μs were applied at 1 pps. Ocular inflammation or more severe damage was not observed.

Finally, Powell et al. have demonstrated electroporation of viable frog skin [Powell et al., 1989]. Transient changes ($\leq$ 3 min) in skin electrical properties were measured after application of an electric pulse of 2 - 20 V in magnitude and 10 - 100 μs in duration. Skin viability appeared not to be affected.

# METHODS

## 4 Red Blood Cell Ghosts

### 4.1 Net Transport Measurement[1]

#### 4.1.1 Introduction

Most electroporation studies have used one of the following four methods of analysis: (A) expression of an introduced gene, (B) total population methods, (C) image analysis, or (D) flow cytometry.

(A) Studies focusing on the uptake and expression of exogenous DNA by a living cell are relevant to transfection applications, but are inherently coupled to other processes. For example, whether a cell grows into a colony which expresses the introduced gene depends on many more factors than just transport of DNA across the cell membrane.

(B) Total population methods, such as turbidity changes in cell suspensions and radioactivity measurements of cell populations pulsed in the presence of radiolabelled molecules, better isolate electroporative transport, but are responsive only to the average electroporative behavior of cells. There are, however, fundamental physical and biological reasons for expecting a heterogeneous electroporation response within a cell population [Weaver and Barnett, 1992], and indeed heterogeneity is observed experimentally [Lambert et al., 1990; Liang et al., 1988; Mir et al., 1988; Rosemberg and Korenstein, 1990; Tekle et al., 1991; Weaver et al., 1988]. Although the average transport per cell is of interest, it is important to determine whether the average reflects behavior of a single population with similar responses, or of two or more distinct subpopulations with significantly different responses.

---

[1] These methods have also been described in [Prausnitz et al., 1993d] and [Prausnitz et al., 1994].

(C) Image analysis of individual cells provides the power of spatial and temporal resolution. However, limitations include: (1) restricted ability to measure kinetics on the microsecond level, the time scale during which electroporation phenomena are believed to occur, based on experimental observations [Benz and Zimmermann, 1980; Benz et al., 1979; Hibino et al., 1991] and on theoretical grounds [Barnett and Weaver, 1991; Weaver and Barnett, 1992], (2) difficulty in observing molecules entering cells (as opposed to those exiting), even though it is uptake which is relevant to most applications [Weaver and Barnett, 1992], and (3) restriction to measuring only a few cells at a time, with the consequence that population distributions of behavior are difficult to obtain.

(D) Flow cytometry provides large numbers of quantitative optical measurements on individual cells at rates of $10^2$ to $10^4$ cells per second [Melamed et al., 1990; Shapiro, 1988]. Although flow cytometry is not attractive for measuring rapid kinetics, it provides quantitative and statistically significant end point measurements on large numbers of individual cells. Molecular uptake and cell damage can be independently assessed. Light scatter is responsive to morphology and calibrated fluorescence provides a quantitative measurement of the number of fluorescent molecules. At their present performance levels, image analysis and flow cytometry are complementary, with neither able to provide all of the important types of measurements.

Here, flow cytometry has been used because of its quantitative nature at the single cell level, to conduct a systematic study of the effects of electric and other parameters on molecular transport due to electroporation.

We have chosen erythrocyte ghosts as model cells because of the following advantages: (1) large, consistent supply from which ghosts are easily prepared,

(2) relatively simple spherical geometry for most ghosts, and (3) existence of many previous electroporation studies [Auer et al., 1976; Chang and Reese, 1990; Dimitrov and Sowers, 1990; Kinosita and Tsong, 1977a; Sale and Hamilton, 1968; Zimmermann et al., 1976]. Because electroporation has been shown to occur universally in lipid bilayers, irrespective of the details of their composition [Chang et al., 1992; Neumann et al., 1989], results from red blood cell ghosts are expected to be representative of cells in general. However, disadvantages include: (1) heterogeneity of red blood cell ghost size, shape, and age in usual preparations (including ours) and (2) likely existence of a single, persistent defect (pore) in each ghost as the result of ghost formation [Lange et al., 1982; Lieber and Steck, 1982a; Lieber and Steck, 1982b].

### 4.1.2 Red Blood Cell Ghost Preparation[2]

Human blood was obtained from healthy adult volunteers, heparinized, and stored for < 24 h at 4 °C (Vacutaner tube, Becton Dickinson, Franklin Lake, NJ). Red blood cells were separated and washed at least three times with Dulbecco's phosphate-buffered saline (PBS; pH 7.4; 150 mM total salts: 138 mM NaCl, 8.1 mM $Na_2HPO_4$, 2.7 mM KCl, 1.1 mM $KH_2PO_4$) (centrifugation at 450 g, 12 min. 4 °C). Red blood cells were then immediately converted into erythrocyte ghosts by hypotonic lysis (5 mM PBS, pH 8.5, 20 min; wash four times with 20 mM PBS, pH 8.5, centrifuge at 10,000 g, 20 min, 4°C; [Dodge et al., 1963]). Ghosts were stored as a pellet at 4 °C and used within four days.

To preload ghosts with calcein, after lysis and one wash, ghosts were placed in lysis buffer (5 mM PBS, pH 8.5) containing $10^{-3}$ M calcein at 4 °C for 1 h. Then, an equal volume of resealing buffer (40 mM PBS, pH 8.5) containing $10^{-3}$ M calcein

---

2 See detailed protocol in Appendix 1.

was added and the mixture was stored at room temperature (23 ± 1 °C) for two hours. Ghosts were then washed four times and stored as above.

4.1.3 Electroporation Protocol[3]

Approximately $10^7$ ghosts/ml were suspended in PBS (20 mM, pH 8.2 ± 3) containing $10^{-4}$ M calcein (lot 10A-3, Molecular Probes, Eugene, OR) or $10^{-5}$ M of one of the following fluorescent macromolecules: (1) fluorescein-labeled lactalbumin (lot 9A, Molecular Probes), (2) fluorescein-labeled bovine serum albumin (BSA; lots 10C and 65111, Molecular Probes and lot 29F9318, Sigma Chemical Co., St. Louis, MO), or (3) fluorescein isothiocyanate (FITC)-dextran (average MW = 71 kDa, lots 105F-5029 and 118F-0821, Sigma). Unlike proteins, with known molecular weight and structure, dextrans have distributions in size. One therefore does not know if uptake of dextran molecules represents transport of dextrans of all molecular weights or, for example, of only the dextrans of low molecular weight. In spite of this disadvantage, many investigators, including us, have used dextran [Bartoletti et al., 1989; Dimitrov and Sowers, 1990; Liang et al., 1988; Rosemberg and Korenstein, 1990; Sowers and Lieber, 1986; Weaver et al., 1988].

Pulsing was performed with a Gene Pulser (BioRad, Richmond, CA) or an ECM 600 (BTX, San Diego, CA), using 2 mm gap cuvettes with parallel-plate aluminum electrodes (BioRad). Cuvettes were reused up to ten times each. Unless otherwise noted, exponential-decay electric field pulses (exponential decay time constant, $\tau$, between 1 - 2 ms) of various magnitudes were used. Five minutes after the pulse, ghosts were washed twice with PBS (20 mM, pH 8.2 ± 3; centrifuge at 10,000 g, 3 min, room temperature), suspended in PBS (20 mM, pH

---

[3] See detailed protocol in Appendix 2.

8.2 ± 3) containing fluorescent latex microspheres (beads; ~$10^6$/ml; d = 5.8 μm; Polysciences, Warrington, PA) and stored at 0 - 4 °C until analysis the same day.

Samples were pulsed either at room temperature (23 ± 1 °C) or 0 - 4 °C, unless otherwise indicated. Samples pulsed at 0 - 4 °C were kept on ice, while samples pulsed at 37 °C were kept in a 37 °C water bath (VWR Scientific, Cleveland, OH) before and after pulsing. Samples pulsed at 23 °C were kept at room temperature throughout. In multiple pulse experiments with inter-pulse spacing, $t_{inter}$ = 60 s, samples were kept on ice between pulses, while for $t_{inter}$ = 5 s, samples were on ice only before and after all pulses were applied. Sample temperature was not controlled for the 5 - 10 s during which samples were placed in the pulsing unit.

In experiments where the time before pulsing during which BSA could adsorb to ghosts was controlled, two solutions were prepared: one contained twice the desired ghost concentration and no BSA, while the other contained twice the desired BSA concentration and no ghosts. At the appropriate time these solutions were mixed. For example, to expose ghosts to BSA 5 s post-pulse, a sample containing the concentrated ghost suspension was first pulsed. Five seconds later, the concentrated BSA solution was added and shaken by hand, yielding a preparation with the desired final ghost and BSA concentrations.

Reported electric field values are nominal electric fields (applied voltage divided by electrode spacing), as commonly used in the literature. The nominal electric field was determined by dividing the voltage (displayed by the pulsing device) by the electrode gap: $E_{nominal} = V_{output}/d_{electrode}$. However, if significant potential drops existed outside the ghost suspension (e.g., at the electrode/electrolyte interfaces), the field to which the ghosts were exposed would be lower. In this study, we determined the actual field within the ghost suspension

using a method described previously [Bliss et al., 1988]: we measured the ghost suspension electrical conductivity, measured the current though the cell suspension by placing a 5 Ω sampling resistor in series with the cuvette, and then computed the electric field pulse magnitude within the ghost suspension. We determined that, under the conditions of this study, the actual electric field within the cuvette was up to 10% less than the nominal electric field. Although only nominal electric fields are generally reported in the literature, differences between nominal and actual electric fields are probably present in many electroporation protocols.

After most experiments had been performed, it was brought to our attention that pulsing with standard cuvettes can cause pH shifts. Since our system was only weakly buffered, pH changes occurred (final range between pH 8 and 9), which increased with pulse voltage. To assess the effect of pH, we performed additional studies of BSA uptake at different voltages using $7.4 \leq pH \leq 10$. In each case the uptake vs. voltage graph (i.e., Fig. 7-6) was of the same form (plateau observed) and the absolute values of molecular transport between pH 8 and 9 were within 20% of each other. We therefore conclude that pH had only a weak effect on uptake under the conditions of our experiments.

In summary, upon electroporation resulting in sufficiently large pores in the ghost membrane, fluorescent molecules were able to enter the ghosts. After waiting five minutes and then washing the ghosts, fluorescent molecules inside the ghosts were measured by the flow cytometer. Fluorescent beads were co-suspended (at a fixed concentration) with the ghosts as an internal volumetric standard. This provided a basis for determining if ghosts were destroyed by electroporation or otherwise lost during sample handling and washing:

determination of the ghost/bead ratio provided a relative ghost concentration which could be compared to control samples.

### 4.1.4 Flow Cytometry Measurements[4]

Individual measurements on ghosts and beads were performed by a FACStar Plus flow cytometer (Becton Dickinson) using Consort 40 software (Becton Dickinson) on a microVAX computer (Digital Equipment Corp., Maynard, MA). Fluorescence data were collected using a custom-modified three or four-log decade amplifier. Collection of scatter data was with a standard four-log decade amplifier. Multiple optical measurements were made at a rate of up to 3000 ghosts/s, which allowed rapid collection of large amounts of statistically meaningful data at the individual ghost level. Ghosts were diluted into a carrier fluid (Isoton II balanced electrolyte solution, Coulter Diagnostics, Hialeah, FL) and passed though a 488 nm laser beam (Innova-90 argon ion laser; 5 W; Coherent, Palo Alto, CA). Measurements of light scatter of the ghosts gave an indication of object size and shape, allowing discrimination between ghosts, microspheres, and debris. With calibration, fluorescence measurements provided a quantitative determination of the number of fluorescent molecules associated with each ghost. Microscopy of electroporated ghosts generally showed uniformly fluorescent solid circles, as opposed to fluorescent rings, supporting the interpretation that ghost fluorescence was due to molecules inside the ghost rather than molecules bound to the membrane.

In a typical experiment in this study, measurement of ghost fluorescence proceeded as follows: as a ghost passed though the flow cytometer, it scattered light from the laser. This triggered collection of light scatter and fluorescence

---

[4] See detailed protocol in Appendix 3.

data (90° light scatter trigger used). Fluorescein was excited at 488 nm and the resulting fluorescence emission was collected though a 530 nm band pass filter.

### 4.1.5 Quantitative Fluorescence Calibration

Quantitative calibration beads (Flow Cytometry Standards, Research Triangle Park, NC) were used to convert fluorescein fluorescence measurements into quantitative numbers of molecules contained inside each ghost [Bartoletti et al., 1989]. These calibration beads provided the equivalent fluorescence of specified numbers of fluorescein molecules free in solution. For example, one bead may be as bright as $10^6$ free fluorescein molecules. However, our fluorescent tracer molecules may fluoresce differently from free fluorescein, e.g., $10^6$ BSA molecules with multiple bound-fluorescein labels may have a different fluorescence intensity than $10^6$ free fluoresceins. Therefore, the fluorescence of each type of fluorescent molecule must be determined relative to that of free fluorescein before proper calibration can be done.

This was accomplished by comparing the fluorescence intensities of known concentrations of each fluorescent molecule to that of known concentrations of free fluorescein (lot 20H-3413; Sigma) in a spectrofluorimeter (Fluorolog-2, model F112AI; Spex Industries, Edison, NJ), using the same filter for collection of fluorescent light as is used in the flow cytometer. Sample excitation was performed at 488 nm with a 4.6 nm bandwidth. Under the conditions of this study, the ratios, R, of fluorescent molecule fluorescence to free fluorescein fluorescence were: $R_{calcein} = 0.65 \pm 0.28$; $R_{lactalbumin} = 0.51 \pm 0.26$; $R_{BSA} = 1.11 \pm 0.39$ (lot 10C), $0.74 \pm 0.21$ (lot 65111), and $0.37 \pm 0.12$ (lot 29F9318); $R_{dextran} = 3.05 \pm 0.61$ (lot 105F-5029) and $1.63 \pm 0.62$ (lot 118F-0821). The error ranges are attributed to different degrees of fluorescent sample bleaching.

## 4.2 Transport Kinetics Measurement[5]

### 4.2.1 Erythrocyte Ghost Preparation

The preparation of erythrocyte ghosts, and their loading with fluorescent molecules, has been described previously in this chapter. Briefly, human erythrocytes were washed and lysed by hypotonic shock. Calcein (molecular mass, M = 623 Da; net charge, z = -4; Molecular Probes, Eugene, OR) was loaded into the ghosts before resealing by exposure to a solution of 1 mM calcein. Loaded ghosts were stored as a pellet at 4 °C for up to one day and washed again before use. Erythrocyte membranes are commonly used in electroporation studies [Chang and Reese, 1990; Dimitrov and Sowers, 1990; Kinosita and Tsong, 1977a; Prausnitz et al., 1993d; Sale and Hamilton, 1968; Zimmermann et al., 1976].

### 4.2.2 Pulsing Chamber Design

The pulsing chamber is shown in Figure 4-1. A mounting stand made of microscope slides adhered to each other with silicone rubber (RTV silicone rubber, General Electric Co., Waterford, NY) provided mechanical stability and electrical insulation from the metal microscope stage. Two stainless steel electrodes (4 x 1 x 0.2 mm, with polished surfaces and 90° corners) were affixed (RTV silicone rubber) in parallel to the mounting stand, with an interelectrode spacing of 1.6 mm. The electrodes were further polished with emery cloth until the top surfaces were flat and co-planar. An enclosed trough was made by filling the interelectrode spaces on the outer edges with silicone rubber.

---

5 These methods have also been described in [Prausnitz et al., submitted, a]

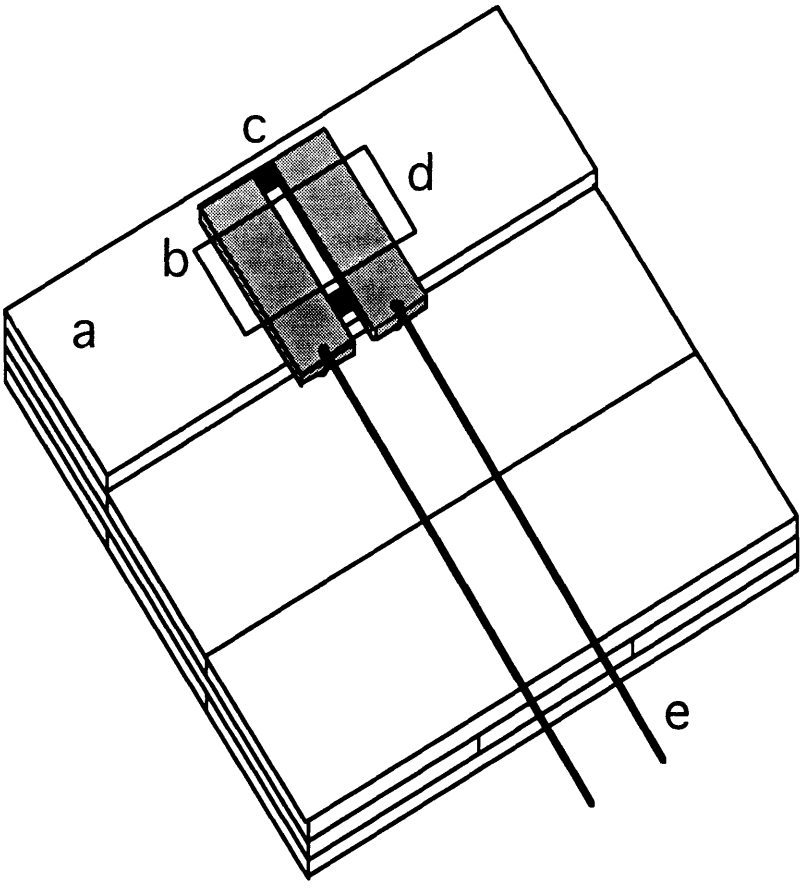


**Fig. 4-1.** Pulsing chamber design. A mounting stand (a) provided a platform for two parallel, co-planar stainless steel electrodes (b). To form an enclosed trough, the interelectrode spaces on the outer edges were filled with silicone rubber (c). A cover slip (d) coated on its underside with erythrocyte ghosts was placed on top. This design allowed imaging of ghosts by fluorescence microscopy during and after electroporation.

### 4.2.3 Electroporation Protocol

To perform an experiment, ghosts were adhered to one side of a glass cover slip (16 x 16 mm) coated with Cell-Tak cell adhesive (20 - 180 min adhesion time; Becton Dickinson Labware, Bedford, MA). The experimental chamber, between the electrodes, was filled with phosphate-buffered saline (20 mM total salts). A cover slip was then placed on top of the chamber, with the ghost-coated surface facing down, bathed in saline. A small drop of silicone grease (high vacuum grease, Dow Corning Corp., Midland, MI) was placed over one or two corners of the cover slip to prevent it from moving. The chamber was positioned under a fluorescence microscope (see below) so that a single adherent and isolated ghost was illuminated by the excitation beam. A 5 μm radius beam, slightly larger than a ghost, was used to assure that the ghost remained within the excitation beam even if the ghost moved or deformed slightly during the pulse. After waiting one to two minutes to verify that the ghost was well anchored, an exponential-decay electric field pulse was applied across the chamber using a capacitor-discharge power supply (Gene Pulser, Bio Rad, Richmond, CA). The internal trigger signal which started the pulse output from the power supply was used to initiate data collection.

### 4.2.4 Fluorescence Measurements

Fluorescence measurements were made using an instrument modified from a fluorescence imaging apparatus described previously [Corbett and Golan, 1993]. The light source for fluorescence excitation was a 5 watt argon ion laser (Spectra-Physics 164-08, Mountain View, CA) tuned to 488 nm. Intensity modulation by an acousto-optic modulator (Newport Electro-Optics N35083-3, Melbourne, FL) provided the two light intensities required for (a) locating cells

(low intensity) and (b) following changes in fluorescence after the application of an electrical pulse (high intensity). Before entering a fluorescence microscope (Leitz Orthoplan/MPV-3, Rockleigh, NJ), the intensity-modulated light was passed through a 500 mm biconvex lens (Ealing Corp., Natick, MA). This beam was directed onto the microscope stage by a 515 nm dichroic (Leitz), and focused at the sample plane by an adjustable short focal length lens within the body of the microscope followed by a strain-free 40X 0.65 N.A. air objective. Experiments were performed at room temperature (~23 °C).

Fluorescence emission from the sample was collected by the microscope objective and filtered by the dichroic and a 520 nm long pass filter. Emitted light was detected by a single-photon counting system composed of a thermionically cooled (Products for Research TE-104RF, Danvers, MA) photomultiplier tube (PMT; Thorn EMI 9658RA, city) driven by a high voltage power supply (EG&G 1109, Princeton, NJ). An adjustable field diaphragm was used to discriminate against fluorescence from regions other than the ghost of interest. PMT pulses were amplified and discriminated to 100 mV (EG&G 1121A). The resulting transistor-transistor logic pulses were fed into a multi-channel scaler (Nicolet 370, Madison, WI), triggered by the pulsing unit to begin data collection at the beginning of the electric field pulse. After each experiment, data were sent to a computer workstation (Sun 386i/250, Mountain View, CA) for processing.

### 4.2.5 Electric Field Validation

Because ghosts adhered to cover slips were located slightly above the electrodes, the local electric field was less than the nominal electric field between the electrodes. Using the microscope, we determined that ghosts were at most 100 μm above the plane of the upper surfaces of the electrodes. Numerically

solving by finite element analysis (Maxwell 2D Field Simulator, Ansoft Corp., Pittsburgh, PA) for the field in the chamber using the geometry of our apparatus, the electric field experienced by the ghosts was estimated to be within 1% of the nominal electric field.

# 5 In Vitro Skin[6]

## 5.1 Materials

Phosphate-buffered saline (PBS) was prepared, containing 138 mM NaCl, 8.1 mM $Na_2HPO_4$, 2.7 mM KCl, and 1.1 mM $KH_2PO_4$ (Mallinckrodt, Paris, KY), and adjusted to pH 7.4 by adding NaOH or HCl (Mallinckrodt). Calcein was obtained from Sigma (St. Louis, MO) or Molecular Probes (Eugene, OR). Lucifer Yellow and erythrosin - 5 - iodoacetamide were obtained from Molecular Probes. To make the sulfur alkylated erythrosin derivative, erythrosin - 5 - iodoacetamide was reacted with excess 6 - mercapto - 1 - hexanol in PBS at 25 °C for over 12 h.

## 5.2 Skin Preparation[7]

Using established skin sample preparation methods, full thickness excised cadaver skin was obtained within 48 h *post mortem* and stored at 4 °C / 95 % humidity for up to 1 week [Bronaugh and Maibach, 1989; Hadgraft and Guy, 1989]. Full thickness samples were prepared by gently scraping off subcutaneous fat. Epidermis samples were heat separated by submerging full thickness skin in 60 °C water for 2 min and then gently removing the epidermis [Gummer, 1989]. All samples were stored at 4 °C / 95 % humidity for less than 3 weeks. Tissue was obtained from four sources (three local hospitals and the National Disease Research Interchange) to minimize any artifacts of tissue acquisition. Tissue was generally from the abdomen, removed just lateral to the midline, although tissue from the breast, back, and thigh was used as well.

Because the primary barrier to transport is the stratum corneum (the upper 10 - 20 μm of the epidermis), the use of epidermis rather than full-thickness skin is a

---

6 These methods have also been described in [Prausnitz et al., 1993a] and [Prausnitz et al., submitted, b].

7 See detailed protocol in Appendix 4

well-established model for transdermal drug delivery [Bronaugh and Maibach, 1989; Champion et al., 1992; Cullander and Guy, 1992; Hadgraft and Guy, 1989]. In the literature, transdermal drug delivery is commonly understood to mean transport of drugs across the skin (not just the dermis) [Bronaugh and Maibach, 1989; Hadgraft and Guy, 1989]. When systemic delivery is desired, a drug must traverse the stratum corneum, the viable epidermis, and some fraction of the dermis before entering blood vessels of the systemic circulation. Since capillaries exist near the dermal-epidermal junction, drugs can enter the systemic circulation without crossing the whole dermis [Bronaugh and Maibach, 1989; Champion et al., 1992; Hadgraft and Guy, 1989]. Thus, transport across full-thickness skin misrepresents the actual transport pathway. For these reasons, following established practice [Bronaugh and Maibach, 1989; Hadgraft and Guy, 1989], we have performed the majority of our studies with human epidermis, and have established agreement with select results from full-thickness human skin.

## 5.3 Electroporation Protocol

### 5.3.1 Aliquot Method[8]

Prepared skin samples were mounted in side-by-side permeation chambers [Friend, 1992] containing well-stirred phosphate-buffered saline (PBS; pH 7.4, 150 mM total salts; Sigma, St. Louis) (Fig. 5-1). To assure initially intact skin barrier function, we used only skin samples which had $\geq$ 100 k$\Omega$ cm$^2$ resistance and which exhibited a passive calcein flux below our detection limit (of order $10^{-4}$ $\mu$g/cm$^2$h). After allowing skin to hydrate (12 - 18 h, 4 °C), the temperature was raised to 37 °C and a donor solution of 1 mM fluorescent compound (calcein, Lucifer Yellow, or erythrosin derivative) in PBS was placed in the donor

---

[8] See detailed protocol in Appendix 5

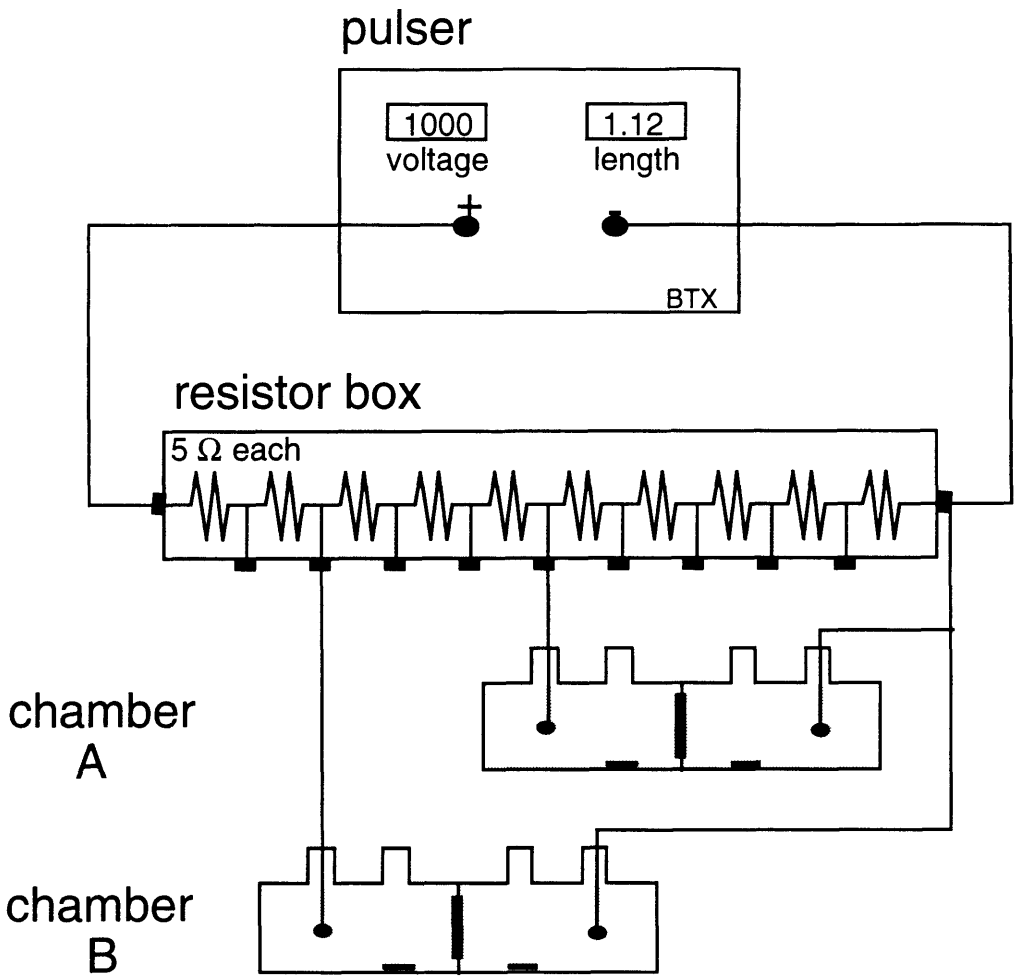


**Fig. 5-1.** Schematic of the apparatus for in vitro transdermal drug delivery by skin electroporation. The pulser applies a voltage pulse across a resistor box containing ten 5 Ω resistors. By providing a constant load of 50 Ω, the pulse length of a capacitive-discharge pulse ($\tau = R\,C$) is held constant even if chamber resistances change (chamber resistance is >> 50 Ω). Moreover, the resistor box is used as a voltage divider so that different chambers can be pulsed simultaneously at different voltages. For example, chamber A is pulsed at 50 %, while chamber B is pulsed at 80 %, of the voltage applied by the pulser.

compartment, facing the stratum corneum (0.7 $cm^2$ exposed skin). Contents of the receptor compartment (facing the viable epidermis) were periodically removed, replaced with fresh PBS, and analyzed for fluorescence by calibrated spectrofluorimetry (Fluorolog-2, model F112AI, SPEX Industries, Edison, NJ) to determine rates of transdermal transport.

Exponential-decay (decay time constant, $\tau$ = 1.0 - 1.3 ms, unless otherwise noted; ECM 600, BTX, San Diego, CA or GenePulser, BioRad, Richmond, CA) or square-wave (model 350 pulser with model 350-12 plug-in unit, Velonex, Santa Clara, CA; 200 $\Omega$ minimum load) electric field pulses were applied for 1 h, unless otherwise noted. Constant-current iontophoresis was performed by providing a constant current through the permeation chamber for 1 h using a constant-current power supply. Constant-voltage iontophoresis was performed by maintaining a constant voltage across the skin using a constant-voltage power supply (model 721A, Hewlett-Packard, Palo Alto, CA). Alternating-voltage iontophoresis was performed by providing a sinusoidally-varying voltage across the skin for 1 h using a test oscillator power source (model 651A, Hewlett-Packard). Ag/AgCl electrodes (In Vivo Metrics, Healdsburg CA) were used, each located ~ 3 cm from the skin. The negative electrode was in the donor compartment, while the positive electrode was in the receptor compartment, unless otherwise noted. Electrical properties were measured with an oscilloscope (model 54602A, Hewlett-Packard), where (a) permeation chamber voltage was measured directly and (b) the corresponding current was calculated using Ohm's law by measuring the voltage across a sampling resistor in series with the chamber.

Reported voltages are average transdermal values determined during the first of each hour-long sequence of pulses. Because significant voltage drops

occurred within donor and receptor solutions and electrodes, applied voltages during these pulses were approximately three-fold higher [Bose, 1994; Pliquett and Weaver, submitted, a]. Moreover, because skin resistance decreased further as pulsing progressed, transdermal voltages during subsequent pulses were lower than the first-pulse values [Pliquett and Weaver, submitted, a]. Reported iontophoresis voltages are also transdermal values, where transdermal voltage was directly measured by Ag/AgCl electrodes located on either side of the skin.

Pulse voltages were determined ~100 μs after the onset of the pulse. During a pulse, the apparent resistance of the chamber, without skin (but including electrodes, saline, and interfacial resistances), was 480 Ω, independent of the pulse voltage. The apparent resistance of the chamber with skin varied from 900 Ω during lower-voltage pulses (~ 50 V across skin) to 600 Ω during higher-voltage pulses (~ 500 V across skin). Transdermal voltages were determined by calculating the ratio of the apparent skin resistance to the apparent total chamber (with skin) resistance. This ratio is equal to the ratio of the transdermal voltage to the voltage across the whole chamber (with skin). By applying a voltage pulse and measuring the resulting current, apparent resistances were calculated by dividing the applied voltage by the measured current.

Post-pulse skin electrical characterization was performed using a four-electrode impedance measurement system [Bose, 1994]. A current step (0.1 - 2 $\mu A/cm^2$) was applied and the resulting transdermal voltage was measured. Using a Fourier transform, skin impedance was calculated over a range of frequencies (1 - 1000 Hz) by dividing the measured transdermal voltage by the applied current.

5.3.2 Flow-Though Method

The experimental methods have been described previously [Pliquett et al., submitted; Pliquett and Weaver, submitted, b; Prausnitz et al., 1993a]. Briefly, heat stripped human epidermis was loaded into a side-by-side, flow-through permeation chamber containing well-stirred phosphate-buffered saline (PBS; pH 7.4, 150 mM total salts; Sigma, St. Louis, MO) at 21 ± 3 °C. A donor solution of 1 mM calcein (Sigma) in PBS was placed in the donor compartment, facing the stratum corneum (0.7 $cm^2$ exposed skin). Contents of the receptor compartment (facing the viable epidermis) were continuously flowed through a spectrofluorimeter ($\lambda_{excitation}$ = 488 nm, $\lambda_{emission}$ = 515 nm; Fluorolog-2, model F112AI, SPEX Industries, Edison, NJ) allowing continuous determination of receptor solution fluorescence. Deconvolution and calibration of the fluorescence measurements allowed calculation of transdermal fluxes with 10 s resolution [Pliquett et al., submitted].

After allowing skin to hydrate for 1 - 2 h, electric field pulses (exponential-decay time constant, $\tau$ = 1.1 m) were applied with an ECM 600 (BTX, San Diego, CA) using Ag/AgCl electrodes (In Vivo Metrics, Healdsburg, CA), each located 3 cm from the skin. Iontophoresis was performed with a constant-current power supply. The negative electrode was in the donor compartment, while the positive electrode was in the receptor compartment. Reported voltages are average transdermal values, determined ~ 10 μs after the onset of each pulse. Because significant voltage drops occurred within donor and receptor solutions, applied voltages were significantly higher [Bose, 1994; Pliquett and Weaver, submitted, a; Prausnitz et al., 1993a].

# 6 In Vivo Skin[9]

The heterogeneous composition and complex geometry of tissues and the use of living animal models add new complexities not present in isolated-cell electroporation. For example: (a) concern for animal health and possible pain and nervous stimulation is required; (b) the use of multiple pulses increases the need to understand and control electrode properties and electrochemistry; and (c) heterogeneous and changing tissue electrical properties suggest the need for new pulse protocols and make interpreting experimental results more challenging. This chapter describes how we have addressed these methodological issues for our in vivo tissue electroporation studies.

## 6.1 Electroporation Protocol

### 6.1.1 Transdermal Delivery

Unlike other applications of tissue electroporation (e.g., cancer chemotherapy), electroporation of skin for transdermal drug delivery requires that a solution or gel containing drug be present between the electrode and the skin. Fig. 6-1 shows the apparatus we developed for this purpose, based in part on conventional in vivo transdermal drug delivery techniques and in part on the approach taken by Titomirov et al. [1991].

CD hairless rats were anesthetized with 75 mg/kg ketamine HCl (Ketaset, Aveco Co., Ft. Dodge, IA) and 10 mg/kg xylazine (Rompun, Mobay Corp., Shawnee, KS) by intraperitoneal injection. Animal care was in accordance with institutional guidelines. Depth of anesthesia was assessed using corneal and pedal reflexes. Additional 1/3 doses were given to maintain sedation (every 30 -

---

[9] These methods have also been described in [Prausnitz et al., in press, c].

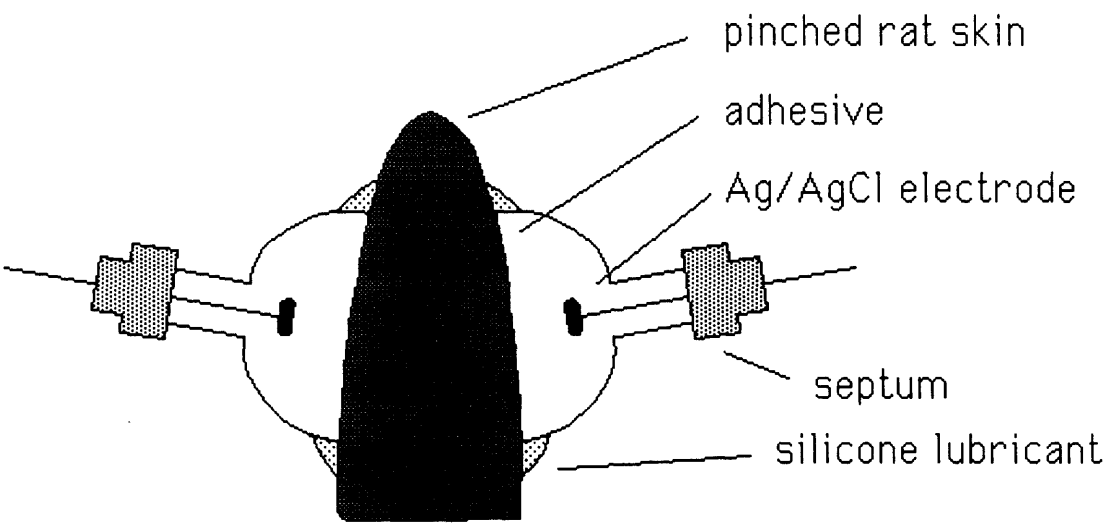


**Fig. 6-1.** Apparatus for in vivo transdermal drug delivery by skin electroporation: a schematic of the apparatus showing two glass bells, filled with saline solutions, adhered to a rat. On each, an electrode was inserted though a septum. Adhesive and a coating of silicone lubricant along the edge of the bell provided electrical insulation and prevented leakage. A non-conductive clamp held the apparatus in place (not shown).

45 min.). Lubricant ointment (Artificial Tears, Vedco, St. Joseph, MO) was placed on the eyes to prevent drying.

As shown in Fig. 6-1, two glass bells (~ 4 ml, 2.8 $cm^2$), fitted with rubber septa and Ag/AgCl electrodes (4 mm diameter disks, ~ 1 cm from skin, In Vivo Metrics, Healdsburg, CA), were affixed with cyanoacrylate adhesive (Permabond, Englewood, NJ) to pinched skin from the caudo-dorsal surface of the rat. Excess adhesive was added outside the bells to ensure a good seal. The area where the bells contacted the skin was then covered with silicone lubricant (Dow Corning, Midland, MI) to insure electrical insulation. The bells and pinched skin were held in place with a non-conductive pinch clamp. One bell was then filled with isotonic phosphate-buffered saline (PBS, pH 7.4), and the other with a saturated calcein solution in PBS. Calcein (Molecular Probes, Eugene, OR) is a fluorescent model for a moderate-size polar drug. Solutions were injected though each septum with a needle and syringe; during filling, a second needle was also inserted though the septum to avoid elevated pressure within the bells, which could cause leaks by breaking the adhesive seal at the skin. Care was taken to eliminate air bubbles. The anode was located on the "indifferent" PBS side of an exponential-decay pulse generator (ECM 600, BTX, San Diego, CA), while the cathode was on the "active" calcein-in-PBS side.

An electric pulse (exponential-decay constant, $\tau$ = 1.2 ms) was then applied once every 5 s for 1 h, a much longer electrical exposure than in previous in vivo tissue electroporation studies. Transtissue pulse voltages between 75 - 300 V were investigated. Rats were monitored visually throughout. The experiment was briefly suspended when administration of anesthetics was required to maintain deep sedation. After the end of 1 h of pulsing, the bells were drained, again using an extra needle to prevent pressure changes, and carefully removed

using Q-tips dipped in acetone to dissolve the adhesive. Some skin, probably the stratum corneum, generally remained adhered to the bells, leaving a thin ring of exposed pink tissue.

At a few time points between 15 - 120 min after pulsing, blood samples (~ 0.5 ml) were taken from the lateral tail vein with a pre-heparinized 25-gauge butterfly needle and transferred into a serum separator tube (Microtainer, Becton Dickinson, Rutherford, NJ). The tube was spun at 1000 g for 5 min. The plasma was then collected for analysis by spectrofluorimetry (Fluorolog-2, model F112AI, SPEX Industries, Edison, NJ). Samples were excited at 488 nm and emission spectra were obtained between 505 - 535 nm, as shown in Fig. 6-2. Background signal was subtracted, as determined with control plasma samples. Fluorescence was calibrated against known concentration standards.

The appropriate volume of distribution of calcein within the rat was determined by measuring plasma concentrations over time following intravenous and subcutaneous injections of known amounts of calcein. Maximum plasma concentrations were measured 30 - 60 min after injection, suggesting that significant metabolism or elimination of calcein did not occur over that period [Sontag, 1980; Suzuki and Mathews, 1966]. The volume of distribution determined from these measurements was 20 % of total rat volume [Wagner, 1975], which is equal to the volume of the extra-cellular aqueous compartment [Goldstein, 1977]. Given the very hydrophilic nature of calcein [Furry, 1985], distribution throughout all extracellular aqueous regions is a reasonable assumption.

Rats were kept comfortably warm with a heat lamp and under observation until they recovered from the anesthesia. They were then checked at least once daily to assess any adverse effects from the pulsing procedure. Mild, transient

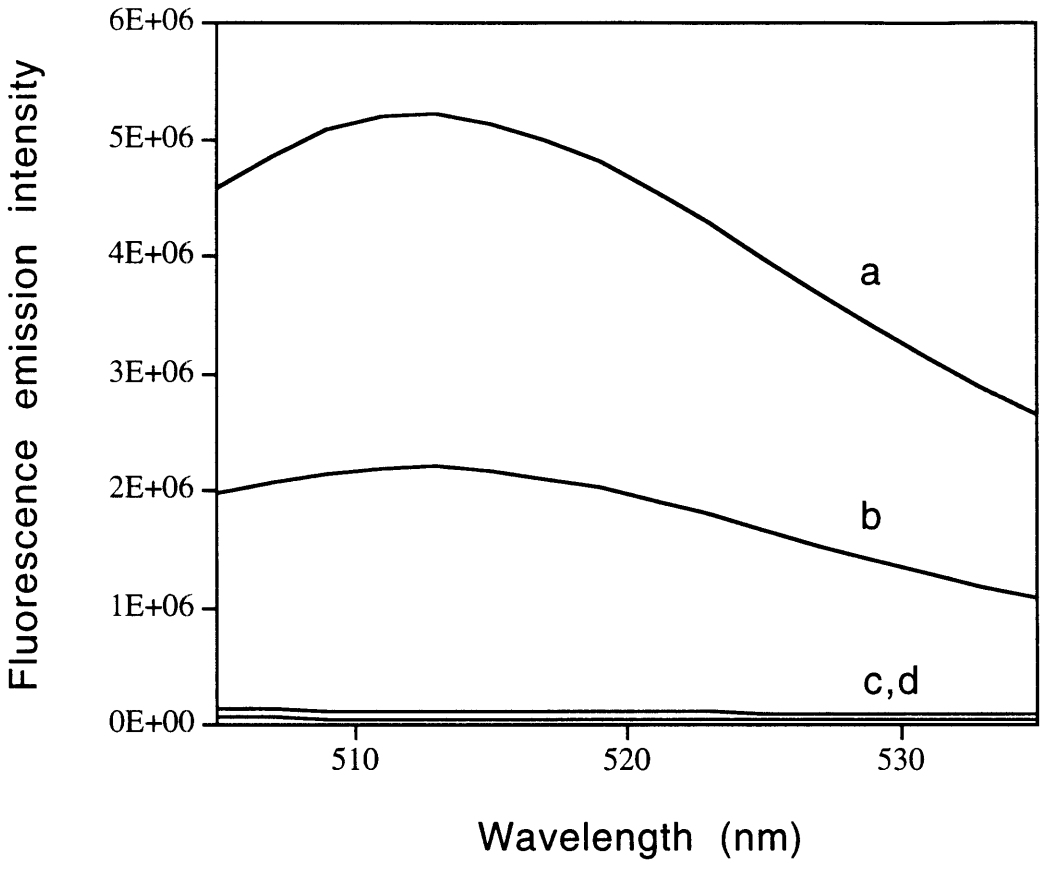


**Fig. 6-2.** Spectrofluorimetric analysis showing calcein fluorescence in hairless rat plasma collected 15 - 120 min after electroporating rat skin: (a) pulsed at 300 V, (b) pulsed at 75 V, (c) unpulsed control, (d) normal rat plasma (see text for pulsing protocols). Samples were excited at 488 nm; emission spectra are shown, with maxima between 510 - 515 nm. After calibration against known standards, absolute calcein plasma concentration was determined.

erythema and edema were generally seen over the area of electrical contact with the skin (i.e., where the solutions within the bell chambers touched the rat) immediately after pulsing for transdermal voltages below 150 V; more pronounced erythema and edema were observed at higher voltages. Deep tissue necrosis, evident from macroscopic examination, was observed in one rat two days after pulsing at the highest voltage used (300 V). No other rats responded to gentle prodding or protected the sites of pulsing, suggesting that they were not painful and that severe damage had not occurred.

### 6.1.2 Locally-Enhanced Delivery

Unlike the transdermal procedures, protocols used by us for locally-enhanced drug delivery were adapted from Mir et al. [Belehradek et al., 1991; Mir et al., 1991b]. Parallel-plane stainless steel electrodes, with a layer of conductive gel (Signa Gel, Parker Laboratories, Orange, NJ) coating the surfaces, were applied to a mouse's skin shortly after local or systemic injection of drug (Fig. 6-3). This fixed-spacing design was used in studies involving leishmaniasis, since the lesions being treated did not vary much in size. The electrodes were placed across the lesion at the base of the tail and held firmly in place.

## 6.2 Discussion

### 6.2.1 Electrode Material

We used homogeneously-mixed Ag/AgCl electrodes for the transdermal delivery studies, primarily for two reasons. First, these electrodes were able to pass the large instantaneous current densities associated with the high-voltage pulses applied. Using a current sampling resistor, we have measured peak instantaneous current densities up to 1 $A/cm^2$. In contrast, Ag wire electrodes

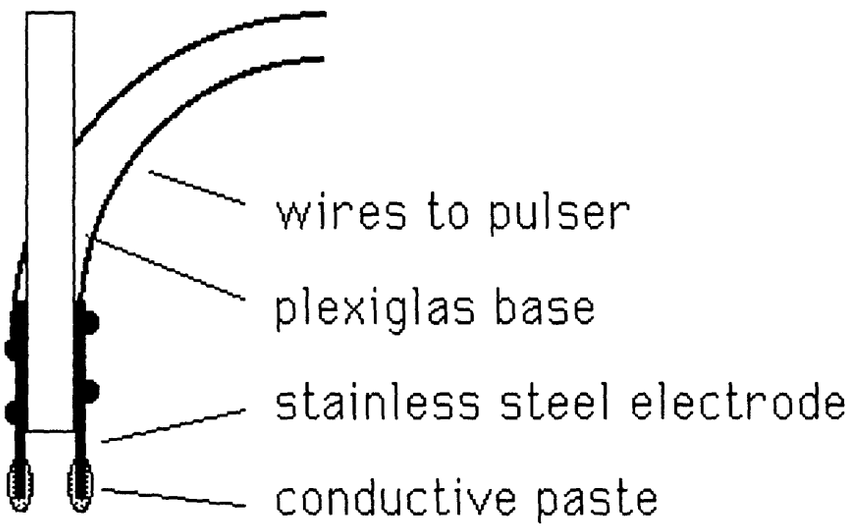


**Fig. 6-3.** Side view of parallel-plane electrodes used for tissue electroporation. This fixed-spacing electrode design was used in leishmaniasis studies, where lesions being treated did not vary much in size.

electrochemically plated with AgCl were problematic, as the outer, insulating layer of AgCl can detach during pulsing. Electrodes made of a homogeneous mixture of Ag and AgCl did not have this problem.

Second, Ag/AgCl electrodes reduced harmful electrochemical effects, such as pH changes due to hydrolysis, which are known to cause skin irritation [Ledger, 1992]. This is particularly important for transdermal delivery applications, where many pulses might be given over long periods of time. However, even the Ag/AgCl electrodes used appeared to hydrolyze water at the high current densities used, indicated by the formation of gas bubbles. Although pH changes were not observed in our buffered solutions, the formation of gas elevated the pressure within the bell chambers; occasional insertion of a needle through the septum alleviated the problem by returning the pressure to atmospheric.

### 6.2.2 Electrode Position

Our electrodes were place on pinched skin on the back for transdermal transport studies and across leishmaniasis lesions at the base of the tail for locally-enhanced delivery studies. Most investigators have placed electrodes at a single location and applied one or more pulses. However, we found that it may be advantageous to move the electrodes to different locations near the site being electroporated. Given the heterogeneities of tissue and the asymmetric shapes of cells, a pulse in one location may not electroporate a given cell, while a shift in field orientation may subsequently result in electroporation. However, when electrodes were moved, the skin had to be cleansed of any residual conductive paste to avoid electrical shorting. Also, to minimize cardiac risk, we placed electrodes away from the heart.

### 6.2.3 Electrical Parameter Selection

Mir et al. have based their selection of electrical parameters largely on work in vitro, coupled with further optimization in vivo [Belehradek et al., 1991; Mir et al., 1991b], while Okino et al. have studied pulse settings in vivo [Okino and Esato, 1990; Okino and Mohri, 1987; Okino et al., 1992]. Even for simpler in vitro systems, such as cells in suspension, choosing electrical parameters is highly empirical due to incomplete understanding of electroporation. Given the greater complexity of tissues, it is often difficult to translate such empirical in vitro parameters directly to in vivo applications. Nevertheless, in vitro results provide useful guides for optimization in vivo.

With this in mind, experimental results from single-cell electroporation in part motivated our work on locally-enhanced delivery to treat leishmaniasis. It is known that larger cells will electroporate at lower field strengths than smaller cells [Chang et al., 1992; Neumann et al., 1989; Orlowski and Mir, 1993; Tsong, 1991; Weaver, 1993b]. This should cause selective electroporation of macrophages, which are larger than most other cells [Sixou and Teissié, 1990]. Because leishmania are found predominantly in macrophages within the skin [Chang and Bray, 1985], drug delivery could be targeted to leishmania in macrophages by selection of appropriate electroporation protocols.

Determination of appropriate electrical parameters, however, was also dictated by concepts not evident from single cell electroporation. When using surface electrodes to electroporate cells deeper than the skin's outer layer, the stratum corneum, we chose to use multiple pulses. Since the stratum corneum normally has a resistance much greater than that of deeper tissues, the electric field concentrates at the stratum corneum. As a result, deeper cells experience much weaker fields, perhaps insufficient to electroporate. However, the stratum

corneum can also be electroporated, dramatically reducing its resistance after just one pulse, where significantly lowered resistance can persist for seconds to hours (see Chapter 10). Therefore, we used multiple pulses, whereby initial pulses were given to electroporate the stratum corneum, making subsequent pulses yield greater internal electric fields, more likely to electroporate deeper cells.

The heterogeneous electrical properties of tissues such as skin point to another difficulty associated with basing tissue protocols on single-cell results. For homogeneous cell suspension systems, pulse strengths are generally, and appropriately, described in units of field strength (e.g., kV/cm). However, the high resistance of the stratum corneum is an example of how tissue heterogeneity, and the resultant heterogeneity in field strength, make deceptive the use of nominal field strength (e.g., expressed as the voltage between the electrodes divided by electrode spacing) in tissue applications. We have found it most useful to record both voltages and electrode spacings. However, we have used comparisons involving assumptions that field strengths are uniform within a tissue as an initial approximation.

Finally, we also found it important to verify that the pulser used was capable of delivering square-wave pulses without overloading. During an electric pulse, the apparent resistance of tissue became very small due to electroporation, resulting in large instantaneous current densities. As an example, when we pulsed mouse legs at voltages between 1 - 2 kV (100 μs duration, 8 pulses, 1 pps, 3 - 10 mm electrode spacing, 1 $cm^2$ contact area) to enhance transport locally, the apparent resistance during the pulse was approximately 400 Ω, resulting in currents of a few amperes (unpublished data). Thus, to produce a square-wave pulse of 2 kV for this experiment, the pulser needed a power rating

of at least 10,000 W. Because most square-wave generators do not have such high power ratings, we used the Velonex (Santa Clara, CA) model 350 pulser with a V1743 output plug-in unit, which is capable of delivering 2 kV into a 200 Ω load. Only when an oscilloscope and appropriate sampling circuit were used, was it apparent that a square-wave pulser with an insufficient power rating had delivered a pulse of incorrect magnitude or waveform. A consequence of overloading a pulser is that the nominal electric field can be significantly smaller than estimated from the pulser setting and inter-electrode spacing.

### 6.2.4 Side-Effects During Pulsing

While animals insufficiently anesthetized responded to electroporation pulses, we also observed direct stimulation of motor nerves in fully anesthetized animals. This phenomenon is well known [Reilly, 1992]. Although the movement caused by such stimulation was not inherently problematic, we encountered two significant difficulties. First, in our transdermal experiments, involving application of multiple pulses to skin over the lower back, the rats' hind legs kicked in response to each pulse. The intensity of kicking varied with the applied voltage and electrode position. This effect lessened significantly within minutes, presumably due to muscle fatigue. However, the sustained kicking apparently caused some damage, evidenced by blood in the urine observed in some of the first rats used. Placement of subsequent rats on a cushioned surface alleviated this problem.

A second concern became apparent when pulsing leishmania lesions at the base of the tail in mice. Again, each pulse caused the mouse's hind leg muscles to contract. In this case, the electrodes (Fig. 6-3) were held by the experimenter firmly in contact with the mouse. Immediately after pulsing, a mild abrasion to the

skin under the electrodes was often evident. We believe it was due, at least in part, to the animal forcefully jumping into the thin metal electrodes. An apparatus using electrodes attached to the animal might have alleviated this problem, as would have securing the animal more firmly in place.

A final complication concerned anesthetized animals being awakened by pulsing. Sometimes animals which appeared to be fully anesthetized and remained so during a few pulses would start to wake up during subsequent pulses. Lack of deep anesthesia was demonstrated by animal vocalization and additional movement which followed the twitch caused directly by the pulse.

### 6.2.5 Damage To Tissue

At the membrane level, electroporation is a fundamentally gentle phenomenon, know to be reversible over a range of conditions [Chang et al., 1992; Neumann et al., 1989; Orlowski and Mir, 1993; Tsong, 1991; Weaver, 1993b]. However, the electroporation literature makes clear that secondary effects of electroporation are capable of killing cells in suspension, presumably affecting cells in tissues in a similar manner [Chang et al., 1992; Lee et al., 1992a; Neumann et al., 1989; Orlowski and Mir, 1993; Tsong, 1991; Weaver, 1993b]. Thermal and pH burns may also occur. Nevertheless, our work and that of others cited here suggest that severe tissue necrosis and other macroscopically visible damage due to electroporation do not occur over a useful range of conditions. However, careful biochemical and pathological studies of the effects of tissue electroporation are needed.

# ELECTROPORATION OF RED BLOOD CELL GHOST MEMBRANES

## 7 Plateau In Net Molecular Transport At Large Field Strength[10]

### 7.1 Introduction

Relatively few studies of electroporation have made quantitative measurements of molecular transport [Chakrabarti et al., 1989; Lambert et al., 1990; Mir et al., 1988], particularly on a "transport per cell" basis [Bartoletti et al., 1989; Poddevin et al., 1991]. However, if electroporation is to be better understood, more comprehensive, quantitative studies which determine the effects of basic parameters on molecular transport will be important. More specifically, quantitative determinations at the individual cell level should be important to: (1) suggesting and testing theoretical models, (2) providing a basis for comparing data for different molecules and experimental conditions, and (3) guiding applications of electroporation in research, biotechnology, and medicine.

### 7.2 Results

Flow cytometric measurements are displayed as two-dimensional contour plots and one-dimensional histograms for red blood cell ghost populations exposed to a single exponential-decay electric field pulse, of magnitude ranging from 0 - 8 kV/cm , and with a time constant between 1 - 2 ms. Fig. 7-1 contains typical log-log contour plots showing forward scatter (which is sensitive to ghost morphology) versus fluorescence (which provides a measure of the number of fluorescent molecules inside each ghost, after calibration). The lines on these contour plots represent iso-frequency-of-occurrence values for light scatter and fluorescence. Each plot represents data from approximately 20,000 ghosts.

---

[10] These results have also been reported in [Prausnitz et al., 1993d].

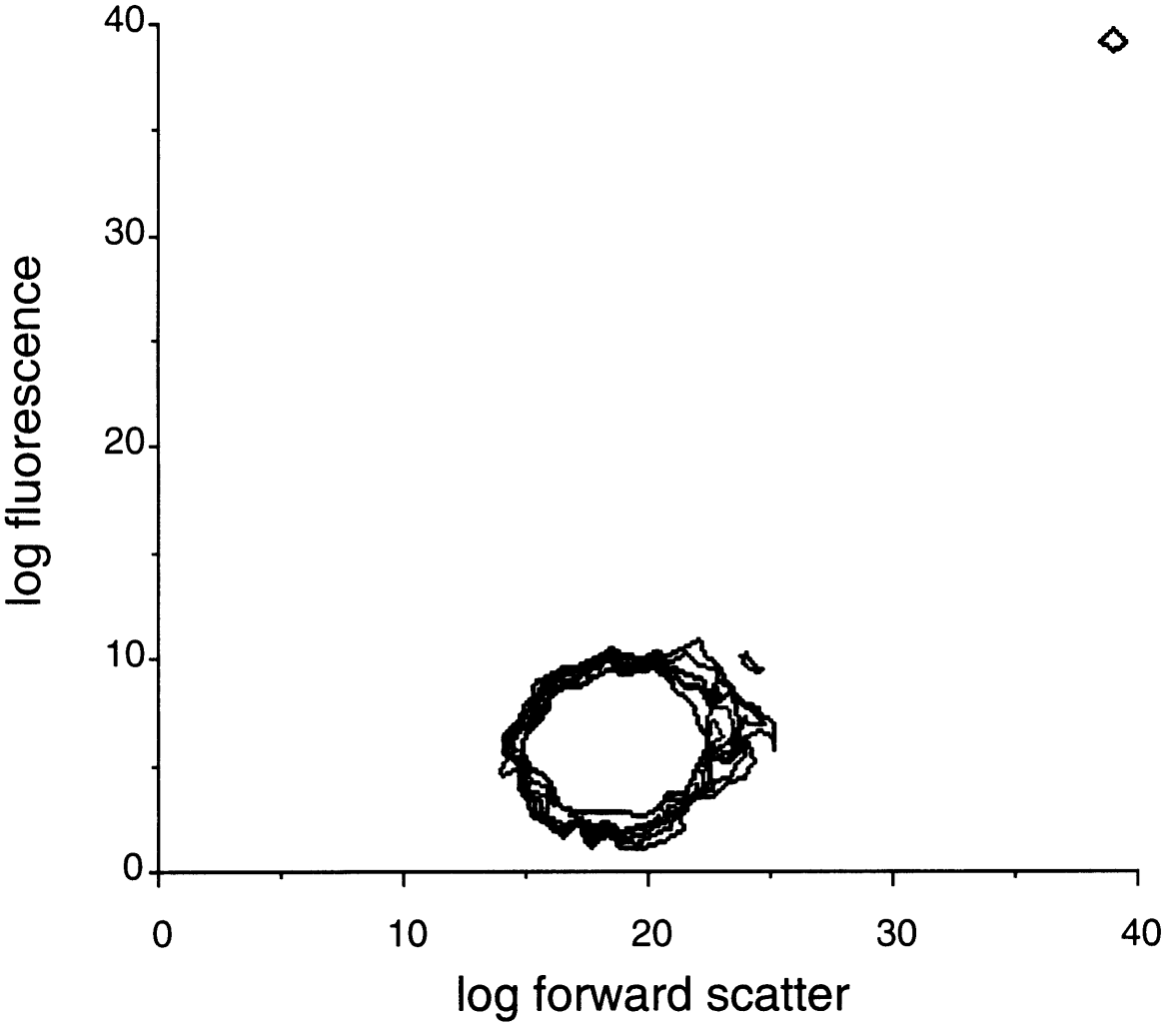


**Fig. 7-1A.** Typical log contour plot of fluorescence versus forward scatter, obtained from flow cytometry data. This graph shows a population of control (unpulsed) ghosts with low fluorescence, believed mainly due to a combination of autofluorescence, "background" surface binding of fluorescein-labeled BSA to ghosts, and flow cytometer noise. Reference beads comprise the population of events in the upper right corner; see text for discussion.

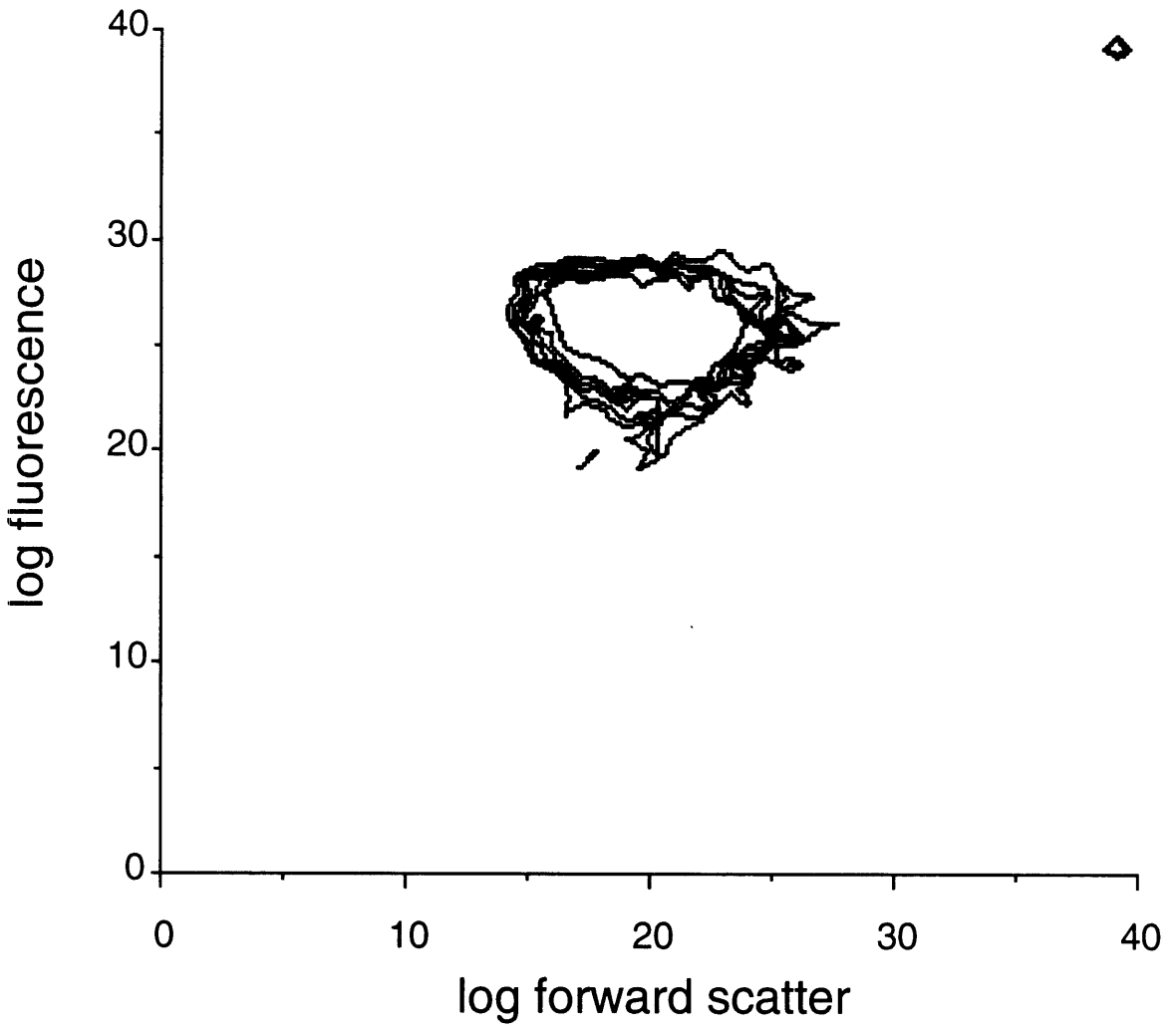


**Fig. 7-1B.** Typical log contour plot of fluorescence versus forward scatter, obtained from flow cytometry data. This graph shows a population of ghosts exposed to a 6 kV/cm pulse with high fluorescence, indicating uptake of fluorescein-labeled BSA molecules.

Fig. 7-1A shows a control (unpulsed) population of ghosts not subjected to an electric field pulse. Some background fluorescence is evident (autofluorescence, BSA surface binding, flow cytometer noise). Fig. 7-1B shows a population of ghosts with higher fluorescence, indicating uptake of BSA molecules by ghosts due to electroporation. Also, in the upper right corner is a tight population of co-suspended reference beads (large forward scatter and fluorescence), which are used to measure the loss of any ghosts as a result of electroporation or the washing procedure.

The distributions of net molecular transport per ghost are presented as one-dimensional log histograms. Fig. 7-2 shows representative histograms of ghost fluorescence (or molecular uptake) from three individual samples pulsed at different field strengths. While fluorescence/uptake increases at higher field strengths, the existence of a single population of ghosts is evident in each case. As expected for spherical membranes with a range of sizes, all ghosts appear to respond to a given pulse in a similar way: no subpopulations exist.

These distributions, however, exhibit a large range in fluorescence for both the control and pulsed ghosts (average coefficients of variation for electroporated ghosts are approximately 100%); heterogeneity of response is evident. Moreover, more pronounced heterogeneity is seen in other samples, particularly at lower field strengths. For example, sometimes (< 1%) two subpopulations are seen: one at lower fluorescence (similar to controls) and one at higher fluorescence. Broader distributions, including trailing edges at lower fluorescence, are also sometimes present. While these deviations are frequently observed, they are not consistent or reproducible; they do not support any identifiable trend. We interpret these data as meaning simply that there is

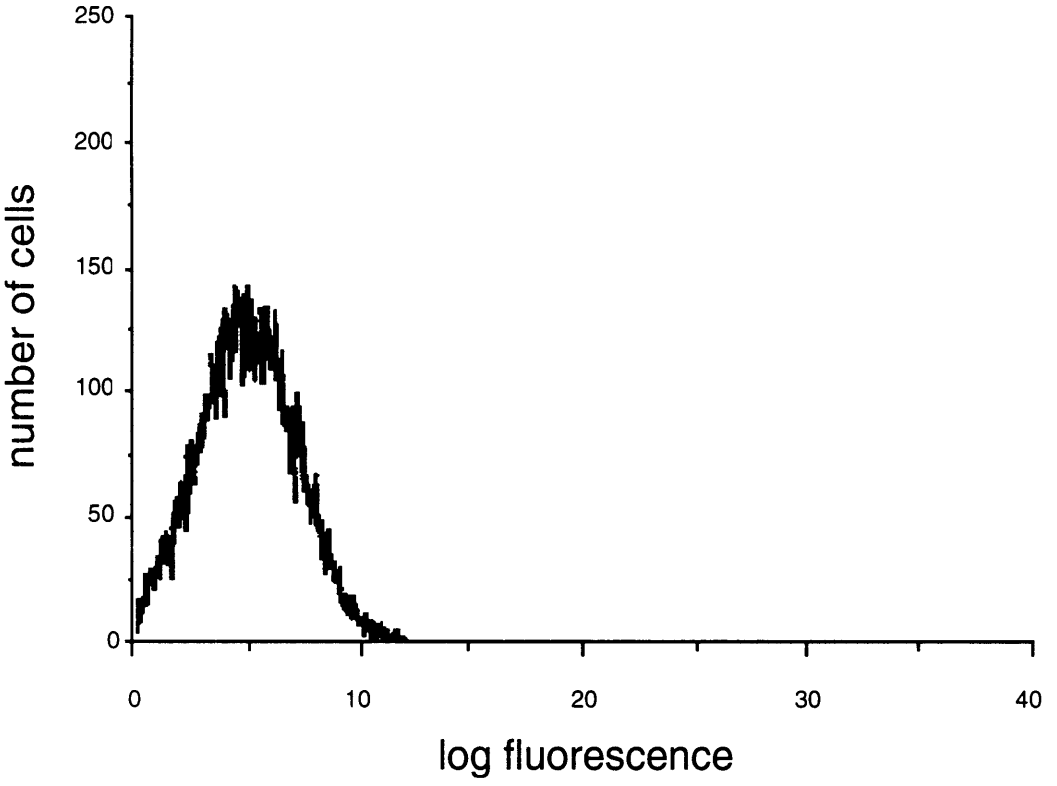


**Fig. 7-2A.** Fluorescence histogram showing uptake of fluorescein-labeled BSA by control (unpulsed) ghosts. The vertical axis gives the number of events (ghosts only; beads and debris have been edited out), while the horizontal axis gives fluorescein fluorescence (here arbitrary units). In Fig. 7-2, the existence of a single population of ghosts is evident in each case, although the amount of molecular transport varies widely within each population.

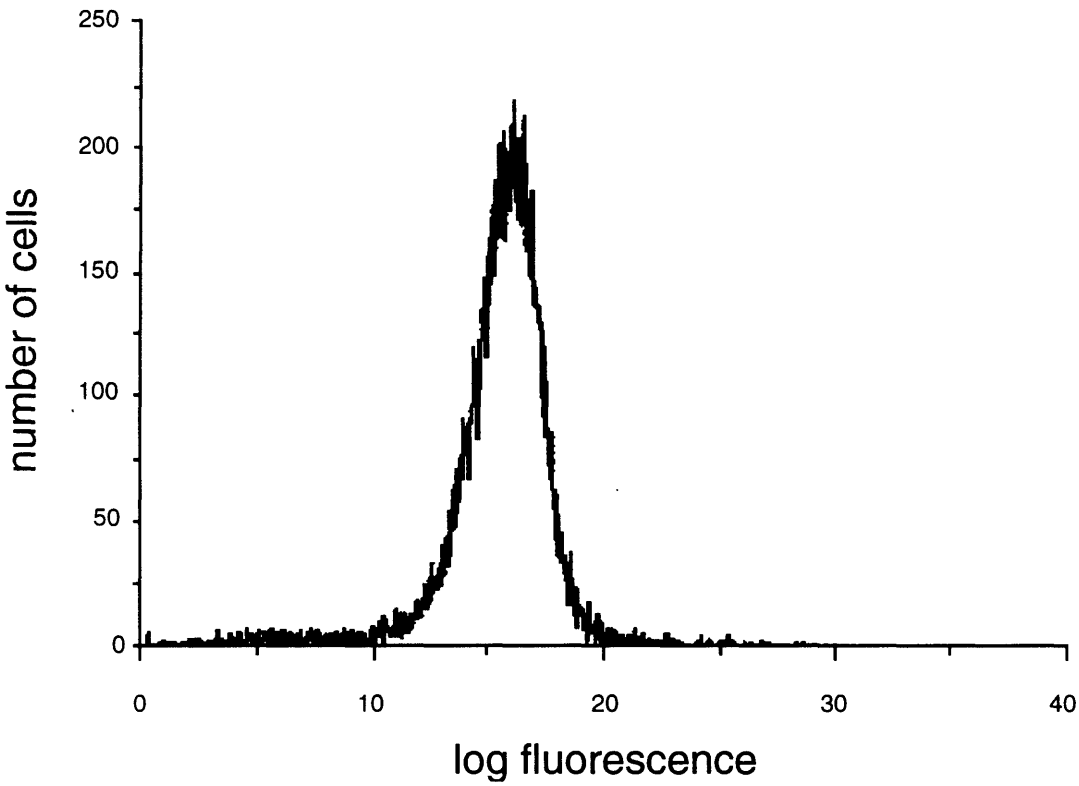


**Fig. 7-2B.** Fluorescence histogram showing uptake of fluorescein-labeled BSA by ghosts exposed to a small electric field (2 kV/cm).

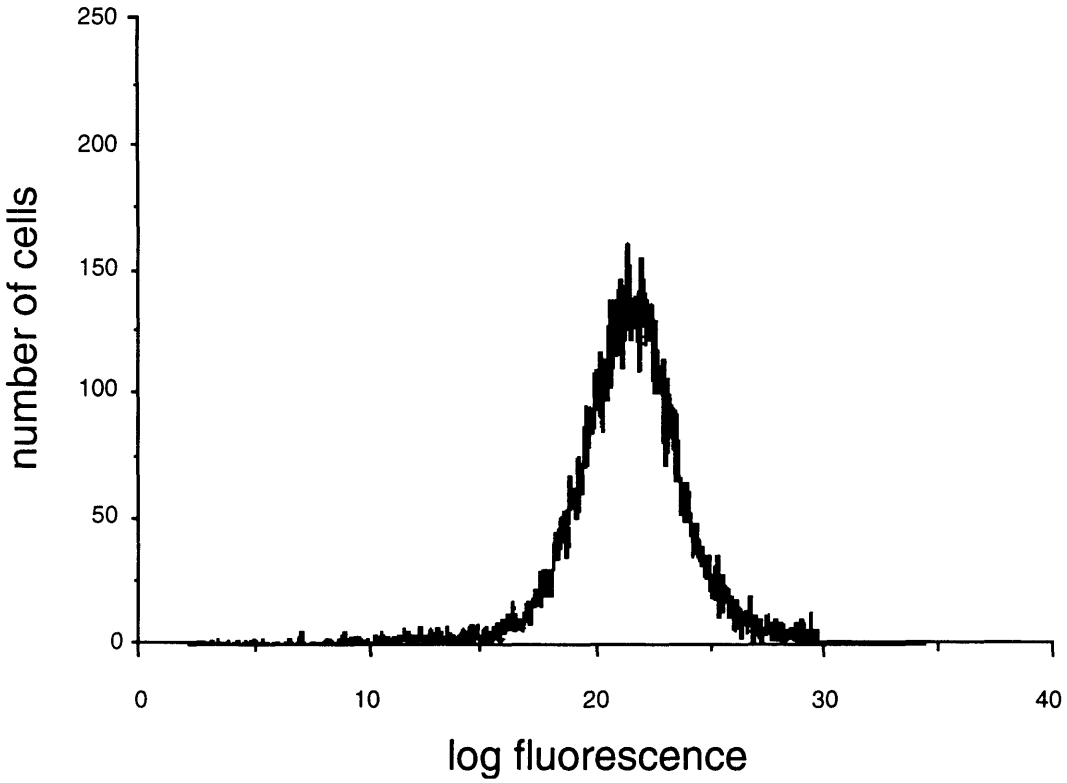


**Fig. 7-2C.** Fluorescence histograms showing uptake of fluorescein-labeled BSA by a large electric field (8 kV/cm).

heterogeneity in electroporation, both in the ghosts as well as in the experimental conditions. Sources of heterogeneity are discussed below.

Individual ghost fluorescence can be converted to an equivalent absolute number of fluorescent molecules associated with that ghost. Fig. 7-3 shows the average uptake of calcein versus field strength. The results of Fig. 7-3 indicate that significant calcein transport first occurred at 0.5 - 1 kV/cm, increased with increasing field strength, and plateaued at approximately 1.5 - 2 kV/cm. The plateau uptake value of approximately $6 \times 10^4$ molecules per ghost remained up to 8 kV/cm.

Fig. 7-4 shows a complimentary result, in which ghosts were each loaded with an average of approximately $8 \times 10^5$ calcein molecules before pulsing, so that release due to electroporation could be observed. As in Fig. 7-3, net calcein transport first occurred at approximately 1 kV/cm and achieved a maximum efflux at $\geq$ 2 kV/cm. In the plateau region, where fluorescence corresponds to an average of less than $4 \times 10^4$ calcein molecules, release is at least 95 % complete. The inability of progressively larger pulses to further reduce average ghost fluorescence is probably due to ghost autofluorescence, calcein surface binding, and flow cytometer noise.

Similar molecular transport behavior is found for fluorescence-labeled lactalbumin, BSA, and dextran (Figs. 7-5, 7-6, and 7-7). In these cases, however, the extracellular concentration was ten-fold lower ($10^{-4}$ M for calcein, $10^{-5}$ M otherwise). Nevertheless, for all cases, an initial region exists where uptake increased with field strength, which is followed by a plateau region where transport appears independent of field strength. However, there are significant quantitative differences (Table 7-1).

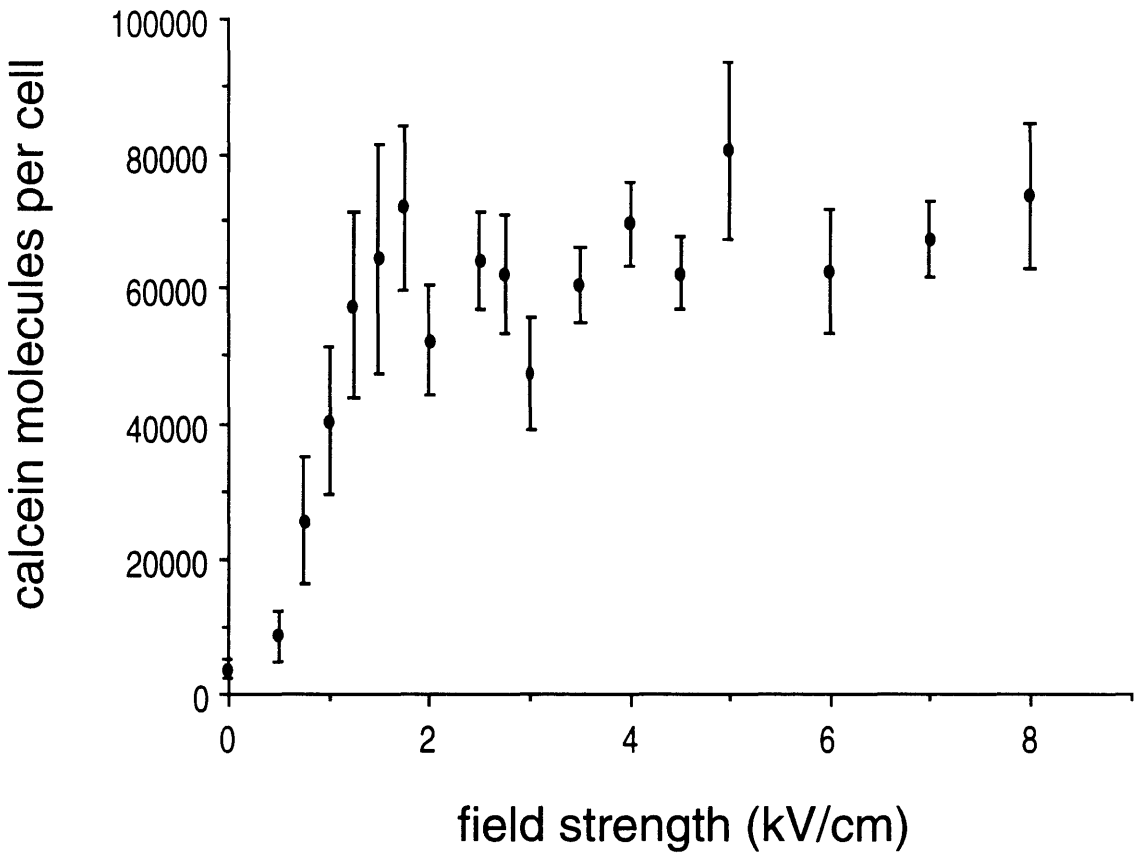


**Fig. 7-3.** Uptake of calcein by ghosts as a function of pulse magnitude. Above approximately 0.5 - 1 kV/cm, uptake increased with field strength, while above approximately 1.5 - 2 kV/cm, a plateau is observed. Graphs in Figs. 7-3 through 7-8 each include data from on the order of $10^6$ individual ghosts. Each point represents the average of between 4 - 30 samples collected during at least 3 different experiments. Standard error bars are shown.

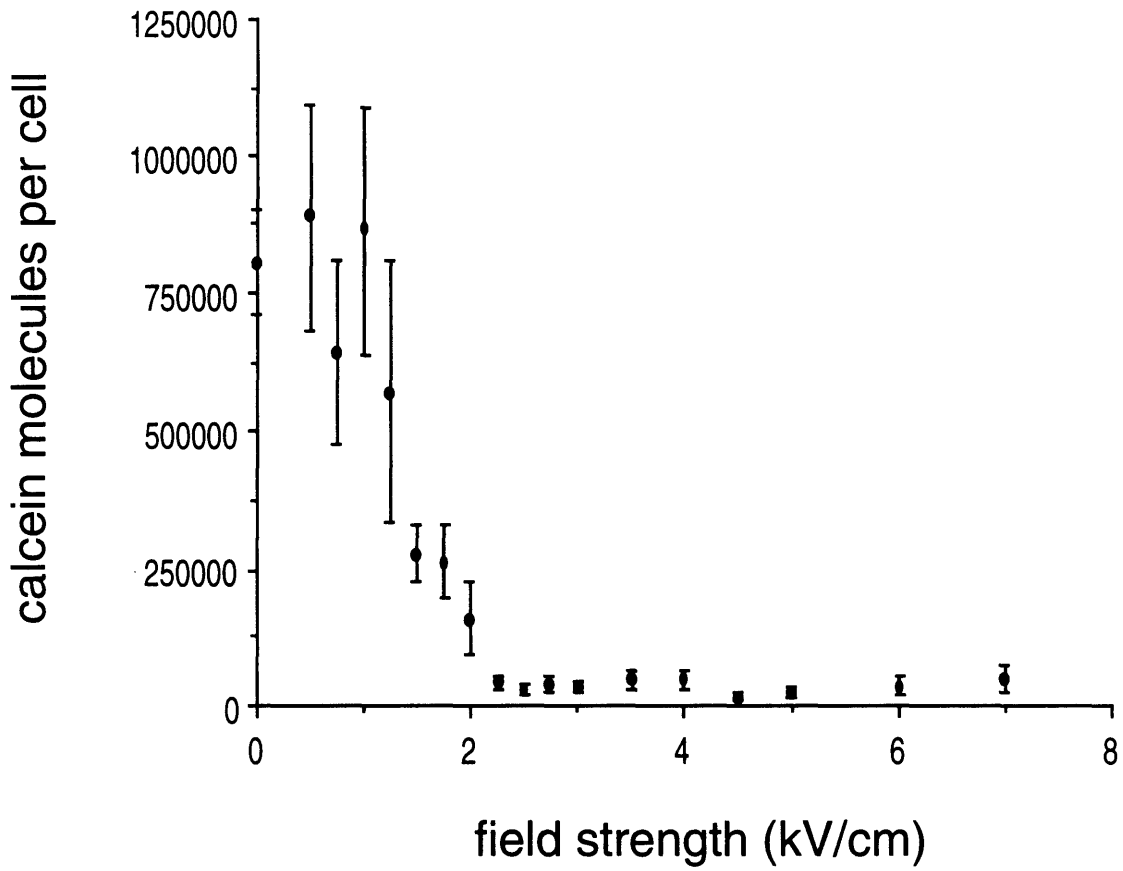


**Fig. 7-4.** Release of calcein from pre-loaded ghosts as a function of pulse magnitude. Calcein transport out of ghosts increased and then plateaued at approximately the same field strengths as calcein transport into ghosts (Fig. 7-3). Standard error bars are shown.

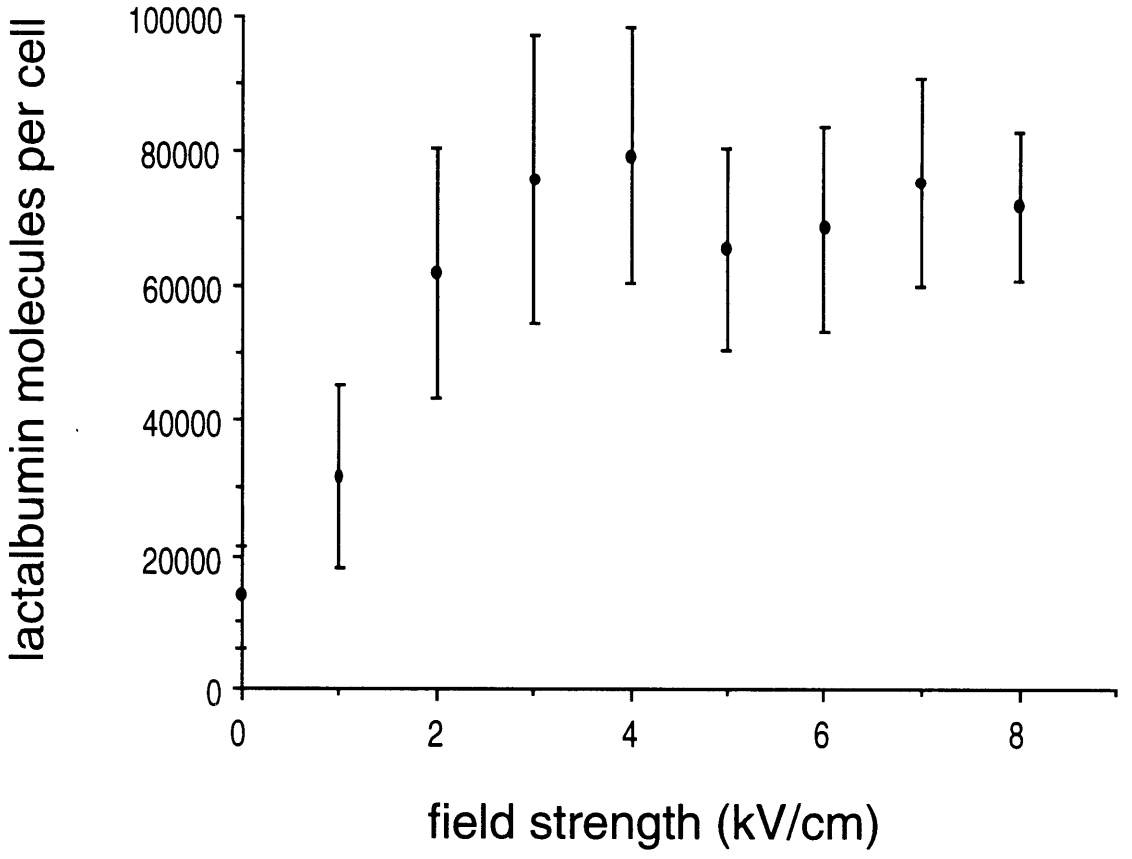


**Fig. 7-5.** Uptake of fluorescein-labeled lactalbumin by ghosts as a function of pulse magnitude. Above approximately 1 kV/cm, uptake increased with field strength, while above approximately 2 - 3 kV/cm, a plateau is observed. Standard error bars are shown.

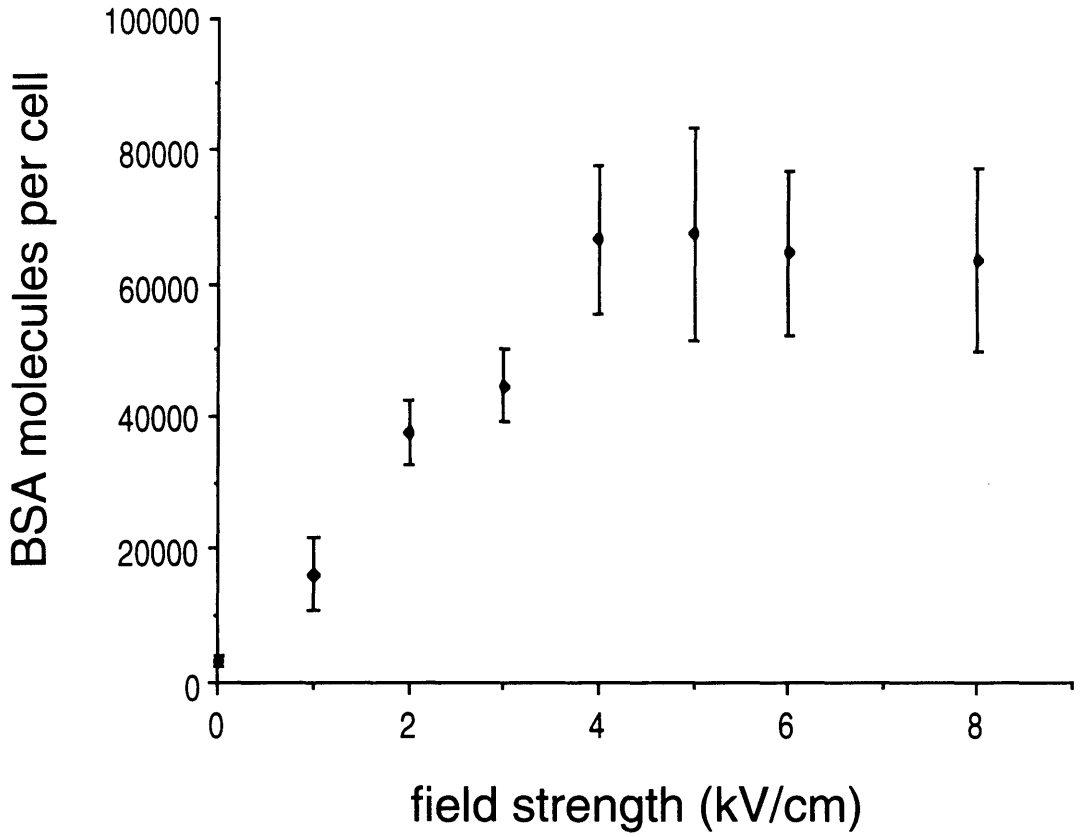


**Fig. 7-6.** Uptake of fluorescein-labeled BSA by ghosts as a function of pulse magnitude. Above approximately 1 kV/cm, uptake increased with field strength, while above approximately 4 kV/cm, a plateau is observed. Standard error bars are shown.

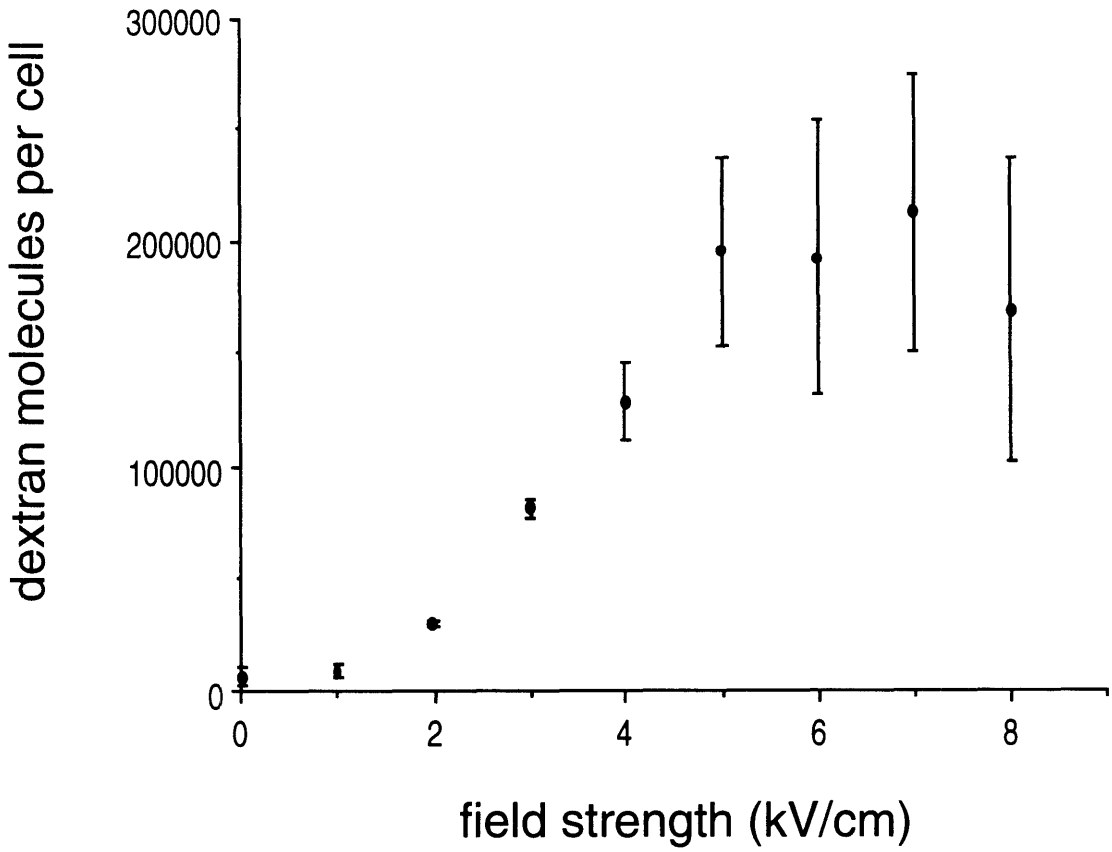


**Fig. 7-7.** Uptake of fluorescein-labeled dextran (71 kDa average MW) by ghosts as a function of pulse magnitude. Above approximately 1 - 2 kV/cm, uptake increased with field strength, while above approximately 5 kV/cm, a plateau is observed. Standard error bars are shown.

| MOLECULE | TRANSPORT THRESHOLD | PLATEAU CHARACTERISTICS | % "EQUILIBRIUM" AT PLATEAU |
|---|---|---|---|
| Calcein (623 Da, -4 charge) | 0.5 - 1 kV/cm | 1.5 - 2 kV/cm; $6 \times 10^4$ molec/cell | 0.7 |
| Lactalbumin (14.5 kDa, -15 charge) | < 1 kV/cm | 2 - 3 kV/cm; $6 \times 10^4$ molec/cell | 7 |
| BSA (68 kDa, ~-25 charge) | < 1 kV/cm | 4 kV/cm; $6 \times 10^4$ molec/cell | 7 |
| Dextran (71 kDa ave., -4 charge*) | 1 - 2 kV/cm | 5 kV/cm; $2 \times 10^5$ molec/cell | 20 |

* Associated with fluorescein label

**Table 7-1.** Summary of the basic features of molecular transport behavior. Plateau concentrations have been calculated by averaging the numbers of molecules per ghost in the plateau region and then subtracting the average number of molecules per ghost in controls. Percent "equilibrium" is a measure of how close the probe concentration inside the ghosts is to the supplied external concentration.

Finally, Fig. 7-8 shows the number of ghosts "lost" by the electroporation process. At field strengths > 1 kV/cm, approximately 30% of ghosts were "lost," determined as follows. Ghosts have known light scatter characteristics; by gating, only events which scatter like ghosts (or reference beads) were used in the analysis. A constant concentration of reference beads was present in each sample, so that the ratio of ghosts/bead was proportional to the ghost concentration. Since all samples had the same initial ghost concentration (and therefore the same ghosts/bead ratio), it is possible to identify what percent of ghosts were "lost" during the experimental protocol. Data for Fig. 7-8 come from the experiments shown in Figs. 7-3 though 7-7 and other similar experiments where fluorescent tracer molecules were present.

## 7.3 Discussion

### 7.3.1 Molecular Transport Plateau

For the single exponential pulse used, the uptake of four very different molecules exhibits qualitatively similar behavior. There appear to be two domains of transport: a sub-plateau domain at lower field strengths and a plateau domain at higher field strengths. In the sub-plateau domain, transport increased with increasing field strength, indicating that electrically-driven phenomena (e.g., electrical drift, electroosmosis, pore population characteristics) controlled the transport. In the plateau domain, transport occurred independent of field strength, suggesting that electrically-driven phenomena may not have controlled transport. The existence of such a plateau in uptake has not been reported before. This is not surprising, given that most previous studies have characterized transport as either occurring or not occurring; absolute amounts of transport have not been assessed.

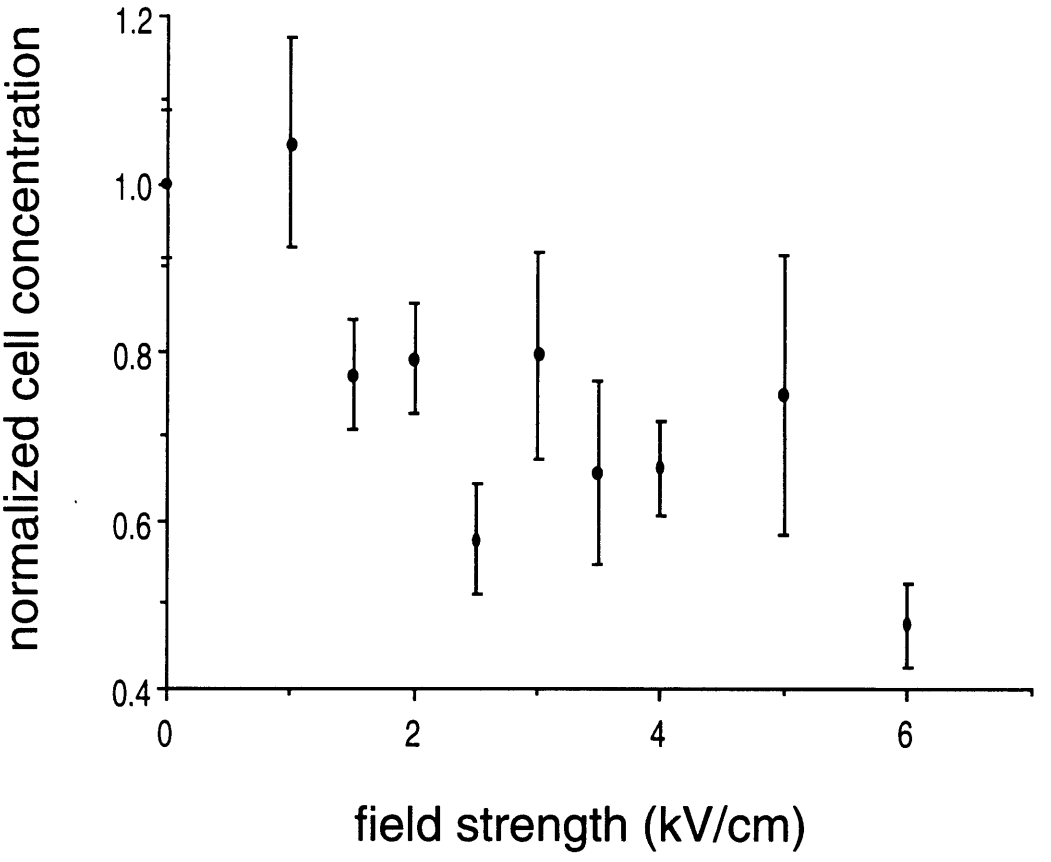


**Fig. 7-8.** Normalized ghost concentration versus pulse magnitude showing destruction or loss of ghosts due to electroporation. Significant numbers of ghosts were destroyed at field strengths > 1 kV/cm. See text for calculation methods and discussion. Standard error bars are shown.

We considered the possibility that artifact or error may have caused this transport plateau. However, (1) we have verified that the actual electric fields which the ghosts experienced were the fields selected on the pulser. Moreover, the plateau occurred at different pulse magnitudes for different molecules, also indicating that the pulser was not malfunctioning. (2) We have observed this trend with four different molecules. (3) Upon varying the time between pulsing and washing up to one hour, we found that the plateau still exists. This suggests that molecules were not coming back out of ghosts due to premature washing. (4) Finally, we continue to find pulse-amplitude plateaus in uptake under other conditions (e.g. multiple pulses, longer pulses, different external molecule concentrations), although the plateau transport value is different (see Chapter 8). For these reasons we believe that this plateau is real.

A plateau could be easily explained if the molecular concentration inside the ghost at the plateau were equal to its concentration outside the ghost, as there would be no net transport. However, plateau values of the intracellular fluorescent-molecule concentration (e.g., $6 \times 10^4$ molecules/ghost or $7 \times 10^{-7}$ M) correspond to between 0.7 and 20 % of the external concentration at the time of the pulse (Table 7-1). Since ghosts are believed to be essentially "empty" spherical membranes, with negligible cytoplasmic residue, an equilibrium altered by the content of the ghost's interior, such as a Donnan equilibrium associated with a negatively-charged cytoplasm, can be excluded. Moreover, microscopy showed that in most cases ghosts appeared as uniformly fluorescing solid circles, not fluorescent rings. This suggests that molecules are distributed within the interior of the ghosts and not binding to the membrane. Finally, other studies indicate that this uptake plateau can be exceeded by altering other electrical parameters (e.g., number of pulses; see Chapter 8). Therefore, this plateau is

not an absolute maximum in uptake by the ghost, but rather indicates a maximum effect of increasing field strength.

Considering mechanisms by which transport occurs, Dimitrov and Sowers [990] suggest that molecular efflux from erythrocyte ghosts is controlled by electroosmosis. Others argue that uptake of DNA by intact cells is controlled by DNA electrophoresis [Klenchin et al., 1991]. In either case, transport is governed by the electric field and increasing pulse magnitude is expected to increase transport. That a plateau in transport is observed at high field strengths suggests that molecular uptake may be a multistep process: at lower field strengths, an electric-field dependent step, such as electroosmosis or electrophoresis, is rate limiting. However, when this step becomes very fast at higher field strengths, a different step, which does not depend on electric field strength, becomes rate limiting. The exact nature of this second step is unclear, but could involve diffusion.

Observations presented by Abidor and Sowers [1992] on electrofusion, an electroporation-related phenomenon, also suggest a two-step process. They found that at lower electric field strengths, fusion rate increased strongly with increasing field magnitude, while at higher field strengths, fusion rate increased only moderately with increasing fields. Although they proposed a single step mechanism, it would instead appear that at lower field strengths a single voltage-dependent step was rate limiting and, after a sharp transition, at higher field strengths a different single weakly voltage-dependent step was rate limiting. Other possible hypotheses for the observed plateau behavior include: (1) diffusion controlled transport, (2) increased field strength did not alter pore population characteristics in ways which affected transport, (3) there was a limited effective volume inside the ghost available to entering molecules, and/or

(4) there was no net effect generated by the sum of a number of electrically-governed parameters.

We have considered hypotheses which could explain our results, but concluded that this data, even when combined with other information in the literature, is insufficient to conclusively support any one mechanism by which a plateau in transport was achieved. This plateau was probably a consequence of the detailed, interactive behavior of a dynamic pore population, the transmembrane voltage, and one or more molecular transport mechanisms. Presently the microscopic mechanisms by which molecules are transported across a cell membrane due to electroporation are poorly understood; they presumably include diffusion, electrophoresis of molecules and cells, and electroosmosis. Although some progress has been made, the ability to make complete quantitative predictions of molecular transport which are consistent with known electrical behavior of the cell membrane does not yet exist. With this in mind, the present results present a challenge to the development of models of electroporation and its associated molecular transport.

A final consideration concerns the quantitative differences in uptake between the four molecules investigated. These molecules can be ranked in order of decreasing charge density: calcein (-4 charge/623 Da = 6 x $10^{-3}$ e/Da) > lactalbumin (-15 charge/14.5 kDa = 1 x $10^{-3}$ e/Da) > BSA (~-25 charge/68 kDa = 4 x $10^{-4}$ e/Da) > dextran (-4 charge/71 kDa = 6 x $10^{-5}$ e/Da). Examination of the plateau characteristics summarized in Table 7-1 shows that the plateaus began at higher field strengths for molecules with lower charge densities; the field strength at which the plateau was achieved correlates inversely with molecule charge density. This suggests that the transition from electrically-controlled

transport to field-independent transport occurred at a lower field strength for a molecule with a higher charge density.

The different plateau concentrations of macromolecules inside ghosts also correlate inversely with charge density (see Table 7-1). Calcein was present at an external concentration of $10^{-4}$ M. It has an internal plateau concentration $\approx$ 6 x $10^4$ molecules / 150 $\mu m^3$ (erythrocyte ghost volume, [Sowers and Lieber, 1986]) $\approx$ 7 x $10^{-7}$ M, or approximately 0.7% of the external concentration. Lactalbumin and BSA, at external concentrations of $10^{-5}$ M, had internal plateaus at 7% of the external concentration. Finally dextran, at $10^{-5}$ M externally, plateaued at 20% of the external concentration. There appears to be a trend of increasing relative plateau concentration with decreasing charge density.

Even though present externally at different concentrations, the absolute number of molecules inside each cell was approximately the same for calcein and lactalbumin or BSA. This appears to be coincidental. Other studies indicate that internal plateau concentration is a function of external concentration and indicate that had calcein been present at $10^{-5}$ M, its uptake would have been significantly lower (unpublished data). Also, different transport plateau values have been found under a variety of different conditions (see Chapter 8). This argues against some sort of receptor binding limiting the plateau concentration to the order of 100,000 molecules per cell. Moreover, repeated examination under the microscope shows fluorescence throughout electroporated cells, indicating that uptake is not localized, for example, at the membrane.

### 7.3.2 Population Distributions

Fluorescence histograms, such as Fig. 7-2, show that no significant subpopulations of ghosts existed; all ghosts responded to a given electric-field

pulse in a similar manner. This is not surprising for spherically-symmetric ghosts, since many of the possible sources of variation in response are related to the relative size and orientation of asymmetric cells [Weaver and Barnett, 1992]. Exceptions, however, are sometimes observed where two subpopulations coexisted and/or where population distributions became much broader. These were especially evident at field strengths where transport due to electroporation began (e.g., 1 or 2 kV/cm). Sources of this heterogeneous behavior might include: (1) ghosts which were not spherical and/or were not the same size (both are supported by microscopy), and (2) possibly variable membrane properties due to ghost age (inherent to erythrocytes) and inter-ghost variability.

Despite these heterogeneities, in most cases only one population of ghosts was found, consistent with the widely-held view that electroporation occurs universally in lipid bilayer membranes if the transmembrane potential is raised to order 1 V; approximately 0.5 - 1 V for short pulses (~ 10 μs) and 0.2 - 0.5 V for longer pulses (> 100 μs) [Neumann, 1989]. The maximum change in transmembrane voltage, $\Delta U(t)$, across a spherical cell in an imposed uniform electric field, E(t), is well known at small field strengths to be [Foster and Schwann, 1986]

$$\Delta U(t) = 1.5\, E(t)\, R_{cell}$$

where $R_{cell}$ is the cell radius. In this study, molecular transport seems to first have occurred at less than 1 kV/cm. Using the above equation ($R_{ghost}$ = 3.3 μm, [Sowers and Lieber, 1986]), a 1 kV/cm electric field corresponds to a transmembrane voltage of approximately 0.5 V, in good agreement with the "universal" breakdown voltage of 0.2 - 0.5 V for longer pulses.

### 7.3.3 Direction Of Transport

Figs. 7-3 and 7-4 show transport of calcein into and out of ghosts. The finding that transport begins and plateaus at approximately the same field strengths indicates that the direction (influx/efflux) of transport across the membrane was not important in this case.

### 7.3.4 Destruction Of Ghosts

The results in Fig. 7-8 suggest that up to approximately 30% of the ghosts were destroyed by electroporation. However, these ghosts experienced more than just exposure to an electric-field pulse which may have contributed to their destruction. First, as erythrocyte ghosts, they were opened by osmotic swelling, released their hemoglobin, and then allowed to reseal. Although this is a well established procedure [Dodge et al., 1963; Sowers and Lieber, 1986], it is not a fully reversible process, leaving the membrane permanently altered [Lange et al., 1982; Lieber and Steck, 1982a; Lieber and Steck, 1982b]. Moreover, after electroporation, ghosts were washed, involving centrifugation twice at 10,000 g, which subjected the ghosts to mechanical stress. Nevertheless, the control preparations were subjected to these same procedures, which indicates that the exposure to the electric field pulse was responsible. From this study we conclude that significant losses of ghosts were observed at field strengths where electroporation occurs; further investigation is needed to establish whether these results showing ghost destruction can be generalized to other systems.

## 7.4 Conclusions

A quantitative study of molecular uptake due to electroporation was presented, including data on the transport of four different molecules from measurements of more than $10^6$ individual ghosts. Under the conditions of this study, the findings were: (A) A single population of ghosts generally existed, indicating that all ghosts responded to a given electric field pulse in a similar manner. However, the amount of transport per ghost within this population varied widely, indicated by average coefficients of variation of approximately 100 %. The onset of transport due to electroporation occurred at < 1 kV/cm, corresponding to a transmembrane voltage of approximately 0.5 V. (B) After the onset of electroporation, average uptake increased with increasing field strength and then plateaued at higher field strengths. Although a detailed mechanism was not proposed, it appears that transport was controlled by electric field-dependent processes at lower field strengths, but may have been controlled by electric field-independent processes at higher field strengths. Both the field strength at which the plateau was achieved and the relative internal plateau concentration appear to correlate inversely with the molecule's charge density. (C) The direction of transport (influx/efflux) did not appear to affect net molecular transport significantly. This result is based only on calcein transport data. (D) Up to ~30 % of ghosts were destroyed by the electroporation procedure. However, it is unclear whether these results can be generalized to intact cells.

# 8 Effects Of Other Parameters On Net Transport[11]

## 8.1 Introduction

Most applications of electroporation have the common goal of transporting useful numbers of molecules across cell membranes. However, few studies have measured the actual number of molecules transported, making efforts to advance both applications and basic modeling difficult. For example, the majority of published electroporation studies emphasize transfection and generally assess gene expression, not molecular transport into cells [Chang et al., 1992]. While transport across the cell membrane is a necessary part of transfection, it is not sufficient, because successful gene expression involves many other processes, including cell survival and correct incorporation of DNA into the cell's genetic material. Thus, determinations of gene expression are of limited use for characterizing molecular transport due to electroporation.

Some studies have directly measured indicators of molecular transport. However, most have not actually measured transport itself, but instead assess "percent of cells electroporated" or unitless "relative transport" [Berglund and Starkey, 1991; Brown et al., 1992; Dimitrov and Sowers, 1990; Escande-Geraud et al., 1988; Graziadei et al., 1991; Hashimoto et al., 1989; Kinosita and Tsong, 1977b; Kwee et al., 1990; Mishra and Singh, 1986; Rosemberg and Korenstein, 1990; Sixou and Teissié, 1990; Sowers and Lieber, 1986; Weaver et al., 1988]. A few studies have provided quantitative determinations (i.e. numbers of molecules transported) for one or a few electroporation conditions [Bartoletti et al., 1989; Casabiance-Pignède et al., 1991; Chakrabarti et al., 1989; Lambert et al., 1990; Michel et al., 1988]; others have systematically measured the number of molecules transported over a range of conditions [Bazile et al., 1989; Glogauer

---

[11] These results have also been reported in [Prausnitz et al., 1994] and [Lau et al., 1993].

and McCulloch, 1992; Mir et al., 1988; Poddevin et al., 1991; Rols and Teissié, 1990; Wilson et al., 1991].

To further assist applications and aid in understanding mechanisms, more studies which quantitatively measure molecular transport over a range of conditions are essential. In Chapter 7, we measured the number of molecules transported into erythrocyte ghosts as a function of applied field strength. We found that net molecular transport increased with field strength, but reached an apparently non-equilibrium plateau at higher field strengths, i.e., uptake saturated at higher field strengths, even though the internal concentration was less than the external concentration. This finding could not have been made without measurements of the numbers of molecules transported per cell. Here we examine the dependence of molecular transport on other electroporation conditions.

## 8.2 Results And Discussion

### 8.2.1 Multiple Pulses

Erythrocyte ghosts were exposed to different numbers of electric field pulses in the presence of fluorescein-labeled bovine serum albumin (BSA). Fig. 8-1A shows BSA uptake as a function of field strength, E, for different numbers of pulses, $N_{pulse}$, with inter-pulse spacing, $t_{inter}$ = 5 s. Uptake increased with both $N_{pulse}$ and E, but appeared to plateau at large E, as reported previously (see Chapter 7) and discussed further below. A related result is shown in Fig. 8-1B, for which multiple pulses were applied with $t_{inter}$ = 60 s.

Figs. 8-1C and 8-1D present the data from Figs. 8-1A and 8-1B, respectively, in another form to show the enhancement of uptake caused by additional pulses relative to the uptake due to one pulse at each E. For smaller E, multiple pulses

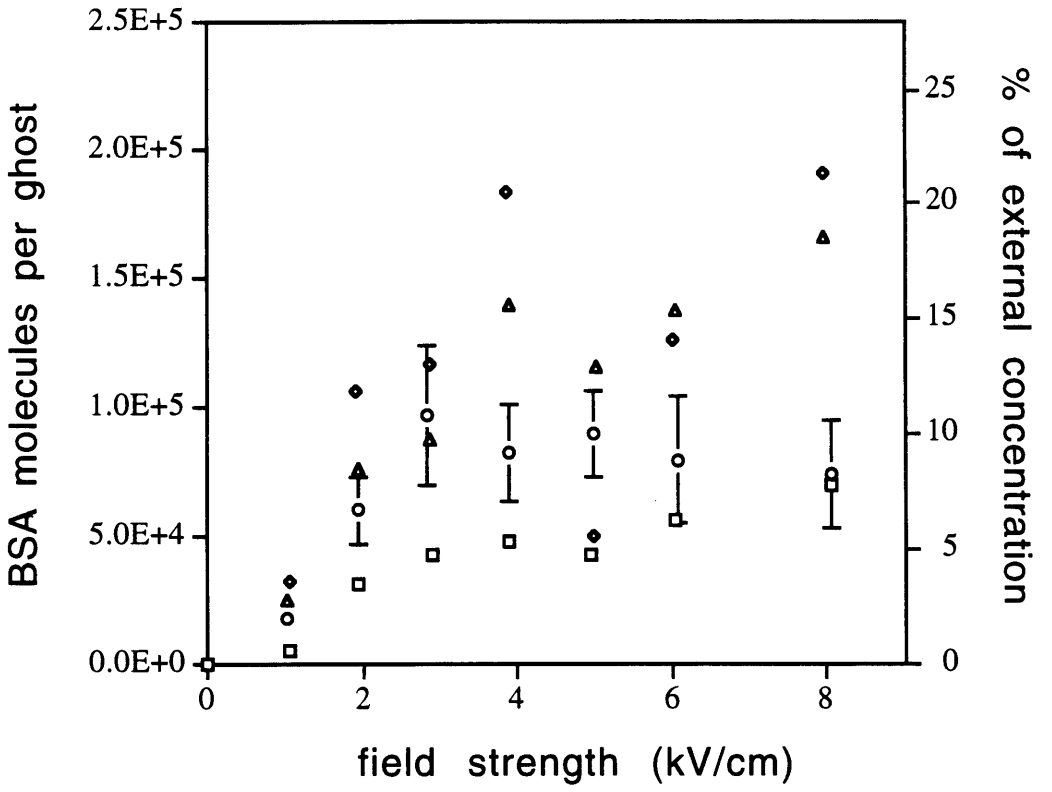


**Fig. 8-1A.** The effects of multiple pulses on uptake of fluorescein-labeled bovine serum albumin (BSA) by erythrocyte ghosts. Uptake of BSA (68 kDa, ~-25 charge) due to different numbers of exponential-decay pulses is plotted versus field strength. $N_{pulse}$ = (□) 1, (○) 2, (△) 3, (◇) 5. Inter-pulse spacing, $t_{inter}$ = 5 s. Figs. 8-1 through 8-6 each include data from $10^6$ - $10^7$ individual ghosts; each point represents the average of 3 - 12 samples collected during 2 - 6 different experiments. Representative standard error bars are shown. There was little difference in error magnitude between data sets.

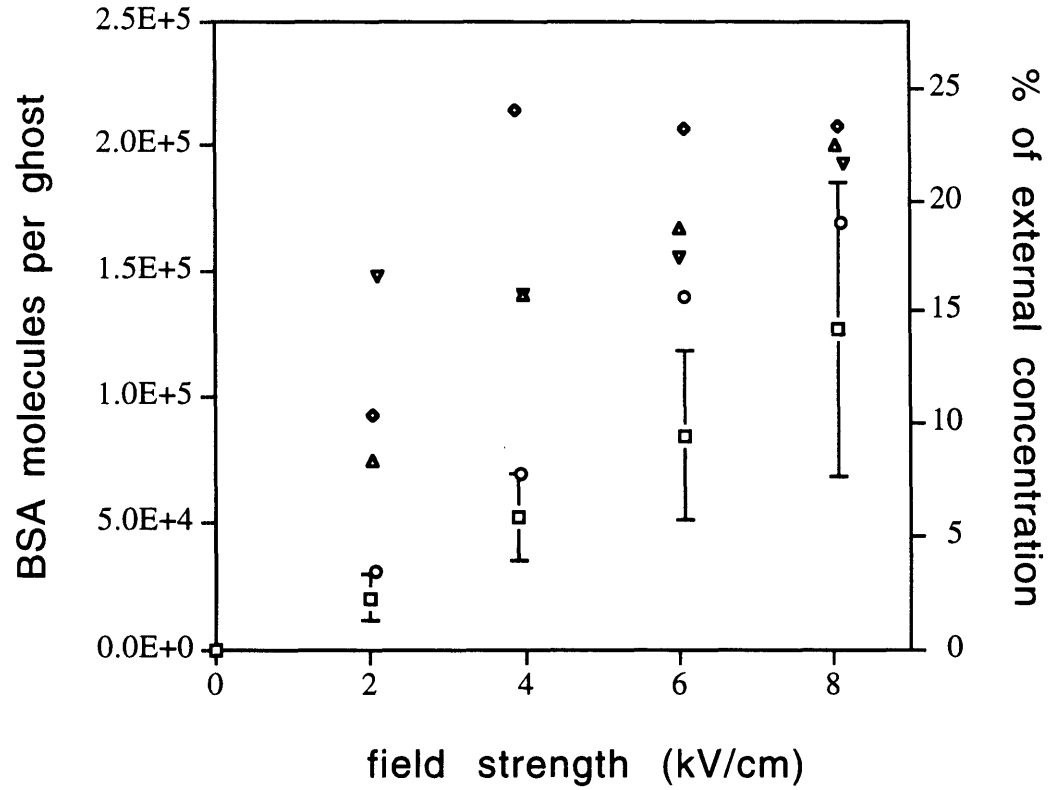


**Fig. 8-1B.** The effects of multiple pulses on uptake of BSA by erythrocyte ghosts. A result related to Fig. 8-1A is shown, for $t_{inter}$ = 60 s. $N_{pulse}$ = (□) 1, (○) 2, (△) 3, (◇) 5, (▽) 10. Representative standard error bars are shown. There was little difference in error magnitude between data sets.

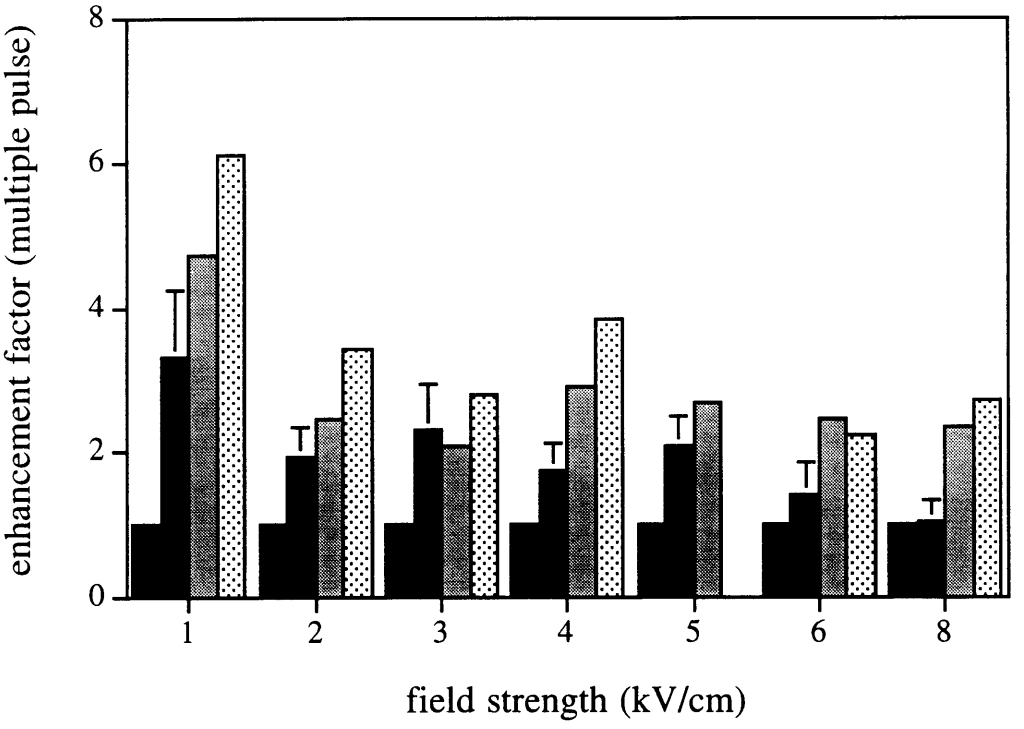


**Fig. 8-1C.** The effects of multiple pulses on uptake of BSA by erythrocyte ghosts. The increase in uptake relative to that of a single pulse is expressed as an enhancement factor for multiple pulses for $t_{inter}$ = 5 s. $N_{pulse}$ = (■) 1, (▩) 2, (▩) 3, (▩) 5. Representative standard error bars are shown. There was little difference in error magnitude between data sets.

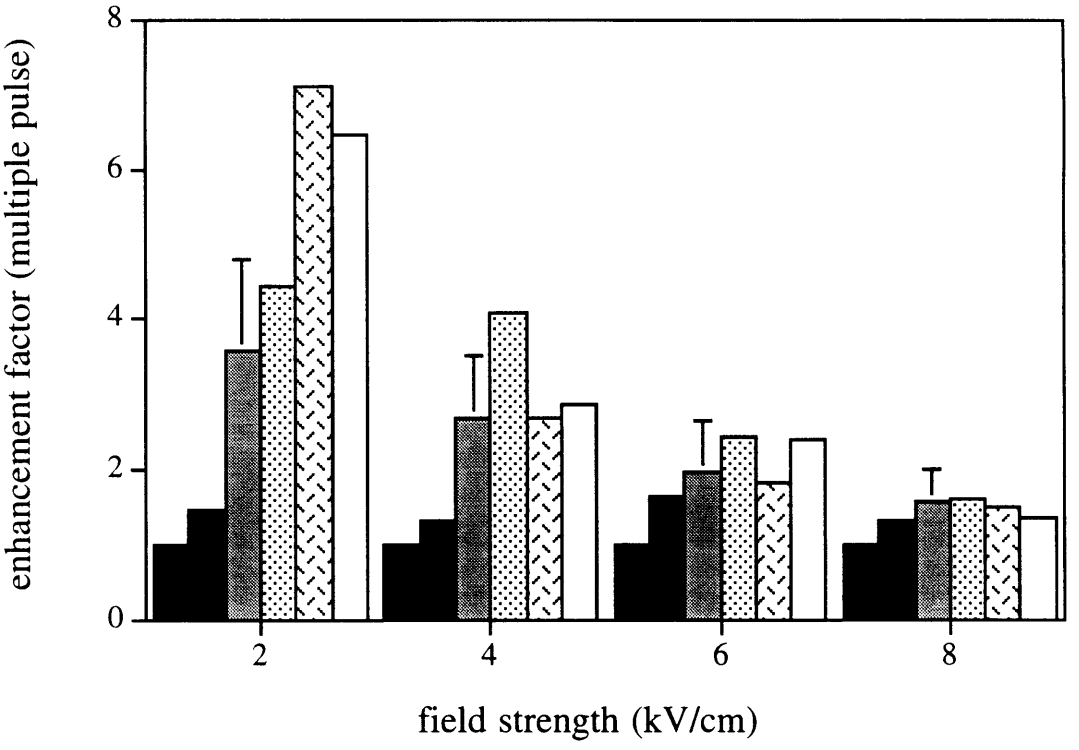


**Fig. 8-1D.** The effects of multiple pulses on uptake of BSA by erythrocyte ghosts. A result related to Fig. 8-1C is shown, for $t_{inter}$ = 60 s. $N_{pulse}$ = (■) 1, (▩) 2, (▨) 3, (▧) 5, (▨) 10, (□) 15. Representative standard error bars are shown. There was little difference in error magnitude between data sets.

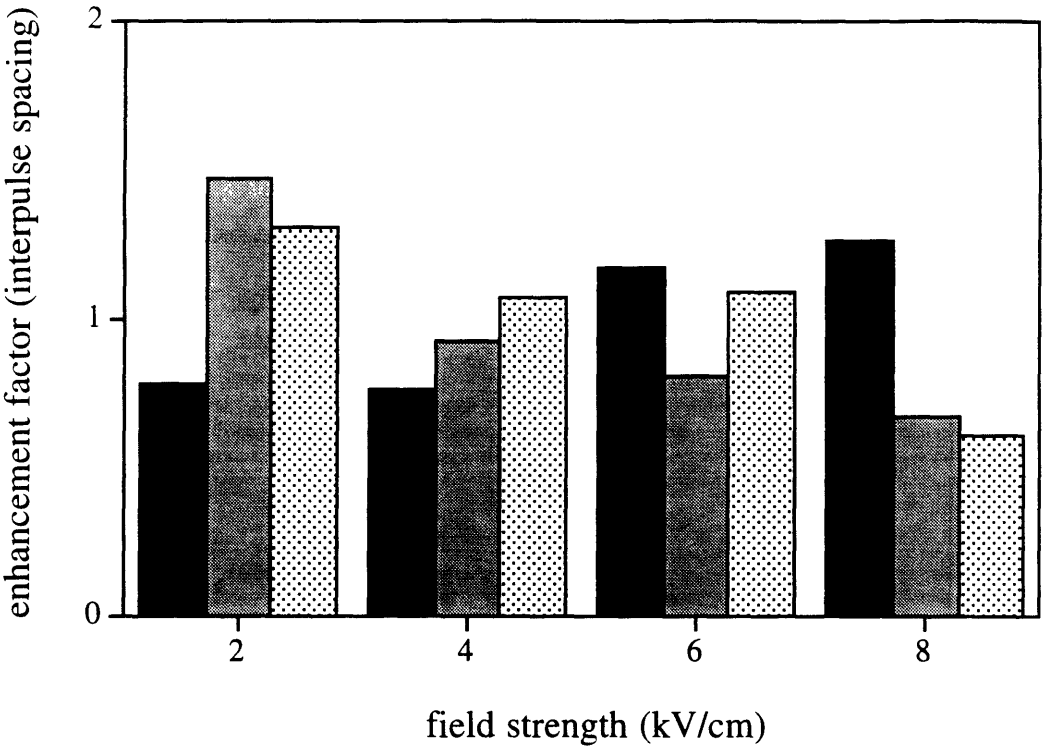


**Fig. 8-1E.** The effects of multiple pulses on uptake of BSA by erythrocyte ghosts. Enhancement of uptake due to pulses with $t_{inter}$ = 5 s relative to $t_{inter}$ = 60 s is shown: $N_{pulse}$ = (▩) 2, (▩) 3, (▩) 5. Fig 8-1 suggests that multiple pulsing enhanced uptake strongly at lower field strengths, but only weakly at higher field strengths. Moreover, no difference in effects on uptake were evident for $t_{inter}$ = 5 s versus 60 s.

resulted in up to seven times greater uptake than a single pulse. However, the relative enhancement of multiple pulses at larger E was progressively less. Finally, to assess the effect of $t_{inter}$ = 5 s versus 60 s, Fig. 8-1E shows ratios of uptake with $t_{inter}$ = 5 s to $t_{inter}$ = 60 s. In each case the ratio was approximately one.

This result shows that application of multiple pulses increased uptake, as reported previously [Dekeyser et al., 1990; Rols and Teissié, 1990]. However, the relationship between $N_{pulse}$ and uptake is not linear, i.e., the net effects of a series of pulses were not additive. The relative enhancement caused by additional pulses at small E was greater than at large E. This and other data (see below) suggest the existence of a transport maximum beyond which additional pulses could not increase uptake under the conditions of this study. For applications this suggests that more pulses at moderate E may lead to the same uptake as fewer pulses at larger E. However, pulses at larger E are generally associated with lower cell viability [Chang et al., 1992]. Multiple pulses at moderate E may maximize transport and cell viability. Finally, multiple pulses with $t_{inter}$ = 5 s and 60 s caused approximately the same uptake. Rols and Teissié [Rols and Teissié, 1990] have also reported that pulse rate ($\leq$ 0.1 Hz) did not affect net transport.

### 8.2.2 Longer Pulses

The uptake of BSA by ghosts due to single pulses having different time constants, $\tau$, was also assessed. Fig. 8-2A shows uptake as a function of E for $\tau \leq 2$ ms, while Fig. 8-2B shows uptake due to longer pulses, but only at small E. Longer pulses at large E were not used, because under those conditions, large (> 50 %) fractions of ghosts were destroyed (i.e., appear as many small particles

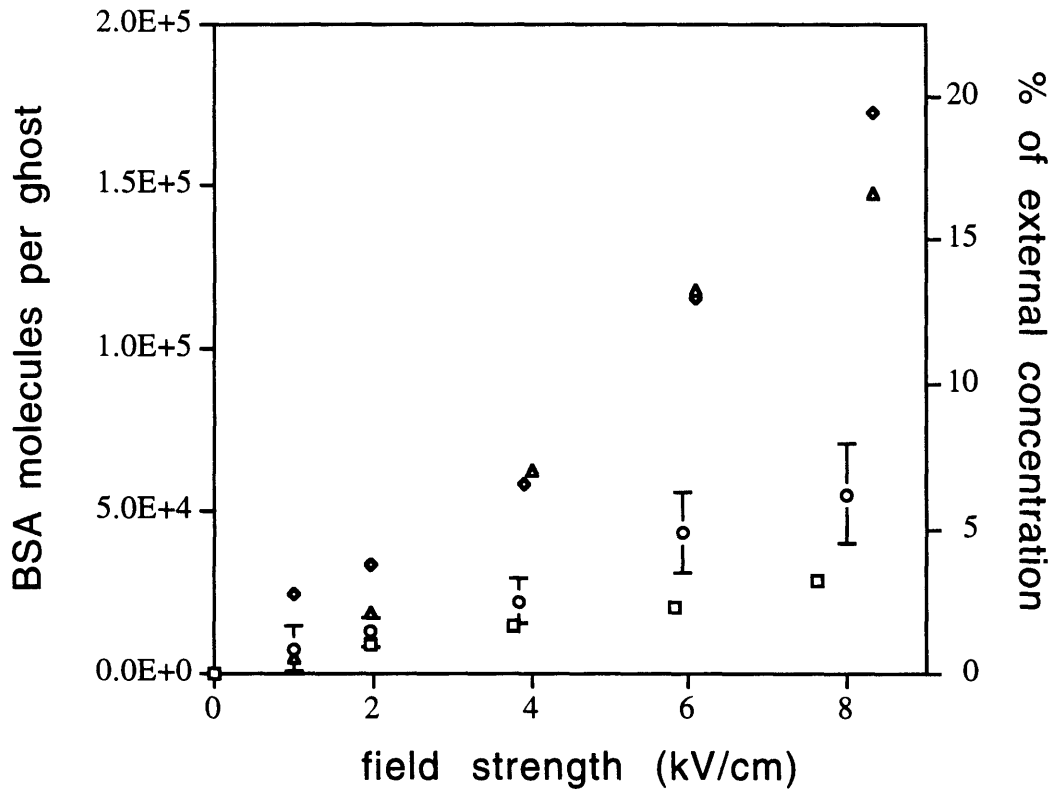


**Fig. 8-2A.** The effects of pulse time constant, $\tau$, on uptake. Uptake of BSA is plotted versus field strength for pulses of different length: $\tau$ = (□) 0.5 ms, (○) 1 ms, (△) 1.5 ms, (◇) 2 ms. Representative standard error bars are shown. There was little difference in error magnitude between data sets.

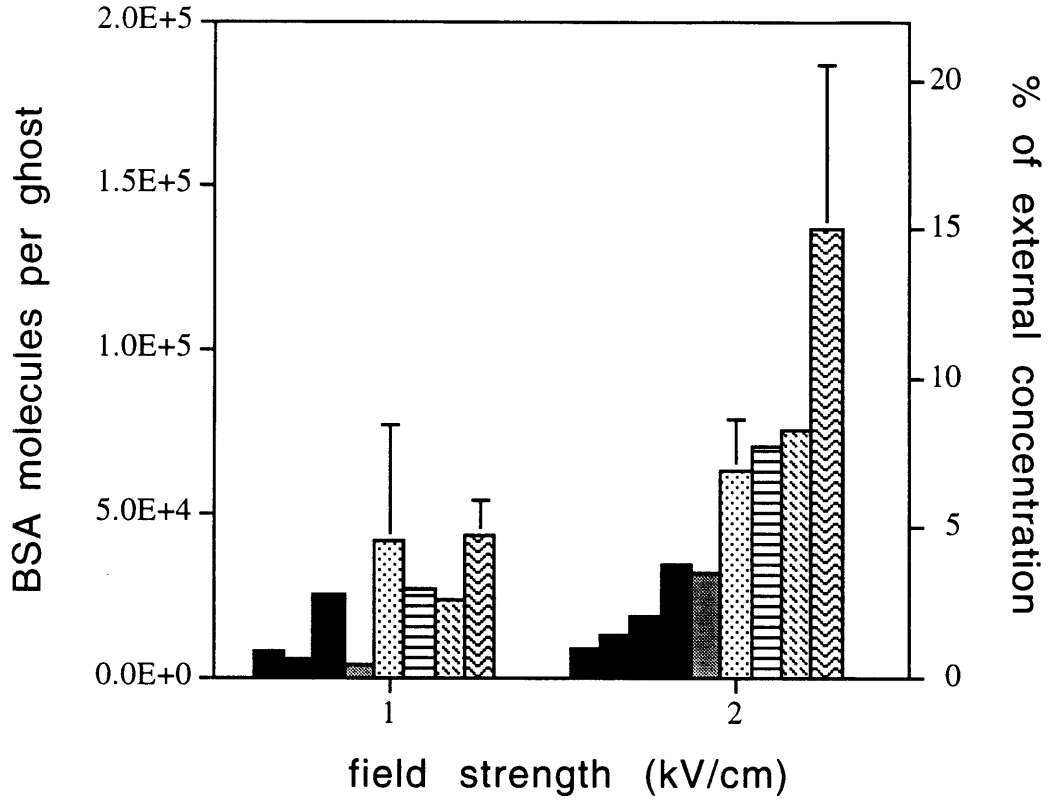


**Fig. 8-2B.** The effects of pulse time constant, $\tau$, on uptake. Uptake of BSA is plotted versus field strength for pulses of different length: $\tau$ = (■) 0.5 ms, (▩) 1 ms, (▩) 1.5 ms, (▩) 2 ms, (▩) 3 ms, (▩) 4 ms, (▤) 6 ms, (▨) 8 ms, (▨) 14 ms. These data suggest that uptake increased with $\tau$. Representative standard error bars are shown. There was little difference in error magnitude between data sets.

in the flow cytometer). Overall, uptake generally increased when longer pulses were used.

It has been widely reported that increasing pulse length increases transport [Dekeyser et al., 1990; Kinosita and Tsong, 1977b; Rols and Teissié, 1990; Rosemberg and Korenstein, 1990; Wilson et al., 1991], where longer pulses may be associated with larger pores [Kinosita and Tsong, 1977b; Rosemberg and Korenstein, 1990; Serpersu et al., 1985]. However, we found that our ghost preparation appeared to be destroyed when longer pulses with E > 2 kV/cm were used. For cell electroporation, this suggests that longer pulses may be less effective than multiple pulses for maximizing transport while minimizing damage.

### 8.2.3 Multiple Vs. Longer Pulses

A comparison is made of the effects of multiple pulses and single pulses having the same time integral of field strength (INT), defined as

$$INT = \int_0^\infty E_o\, e^{-t/\tau}\, dt = E_o\, \tau$$

where $E_o$ is the peak field strength, t is time, and $\tau$ is the decay time constant. In Fig. 8-3, uptake is plotted versus INT, where $INT = E_o\, \tau$ for a single pulse and $INT = \Sigma\, E_o\, \tau$ for multiple 1 ms pulses. Proportionality between transport and INT has been previously proposed [Jayaram et al., 1992; Liang et al., 1988; Schwister and Deuticke, 1985] and was therefore investigated here. Linear regressions are shown.

Fig. 8-3 addresses two issues: (a) whether INT correlates well with uptake and (b) whether multiple pulses and longer pulses with the same INT were

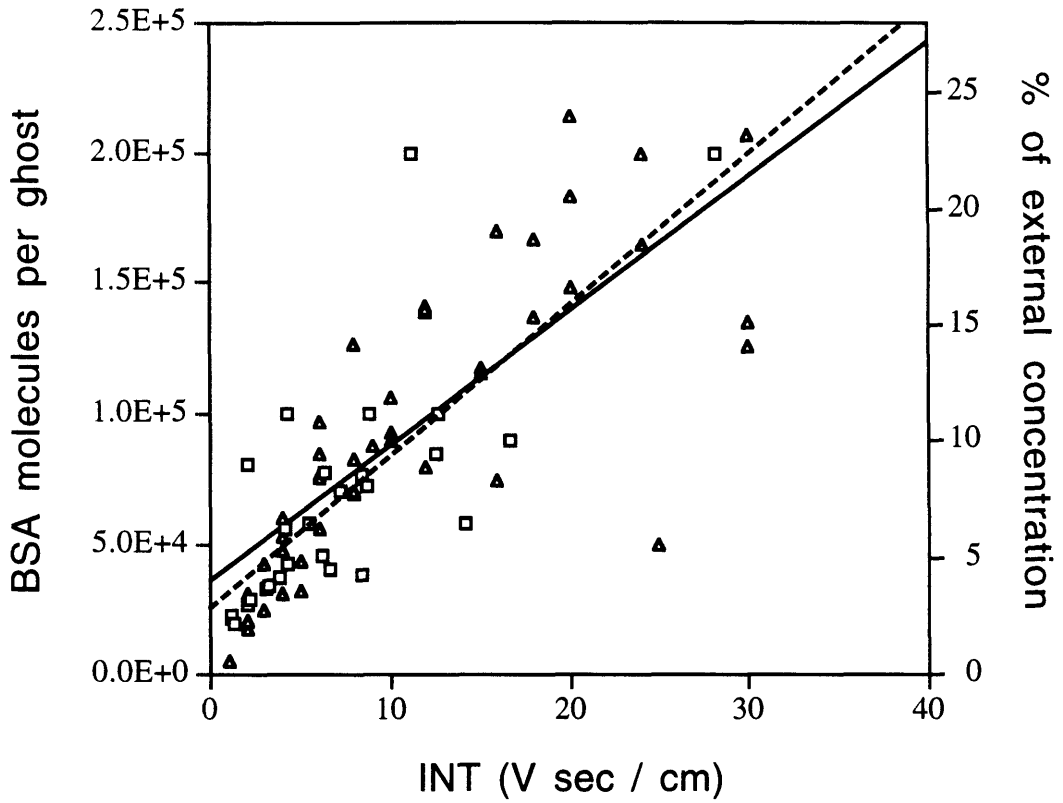


**Fig. 8-3.** Uptake as a function of the time integral of field strength, INT (see text). Uptake of BSA is plotted versus INT, where (□) INT = $E_0 \tau$ for a single pulse (data from Fig. 8-2) or (△) INT = $\Sigma E_0 \tau$ for multiple 1 ms pulses (data from Fig. 8-1). Least-squares linear regressions are shown: multiple pulse data (solid line, y = 5160 x + 36400, $r^2$ = 0.60) and single pulse data (dashed line, y = 5810 x + 25200, $r^2$ = 0.56). This graph suggests that (a) uptake can be approximately described by a linear function of INT and (b) multiple short pulses and single long pulses having the same INT result in similar uptake, over the range of conditions used.

equivalent. Addressing the first point, there is a relationship between INT and uptake, which seems to be roughly linear. Thus, the linear regressions for the multiple pulse data and the longer pulse data, each treated separately, may be useful for application-oriented estimations. However, for mechanistic understanding, a linear fit seems inappropriate. First, the $r^2$ correlation constants are approximately 0.6, indicating only a mediocre fit. Second, the y-axis intercepts (corresponding to no pulse) are approximately $3 \times 10^4$ molecules per ghost. However, this value should be zero, since "background" fluorescence of unpulsed controls was subtracted from all pulsed samples. Finally, the correlation consistently overpredicts the measured uptake for INT $< 10$ V s / cm and generally underpredicts at higher values. Such systematic deviations suggest that a non-linear model is appropriate.

The second issue concerns equivalency of multiple and single pulses of the same INT. The points corresponding to multiple and single pulses in Fig. 8-3 have approximately the same distribution. Moreover, their linear regressions are very similar. This suggests that different pulsing protocols having the same INT caused approximately the same uptake, over the range of conditions used. This has important mechanistic implications. First, it suggests that transport occurred primarily during pulses, since different $t_{inter}$ -- whether 60 s, 5 s, or 0 s (for longer single pulses) -- did not cause differences in transport. This point is discussed further below. Second, the non-linear dependence of uptake on INT is probably a result of the complex, time-dependent behavior of the pore population distribution and transmembrane voltage. Nevertheless, given the complexity of the phenomenon, it is remarkable that uptake can be approximated as a linear function of INT under the conditions used.

8.2.4 BSA Adsorption To Ghosts

To assess the possible role of BSA adsorption to ghost membranes, BSA was added to ghost suspensions at different times before pulsing. Fig. 8-4 shows that ~50 % more uptake resulted when BSA was added to ghost suspensions 1 h before pulsing than when added only 5 s before. This suggests that an interaction between BSA and ghosts occurred which affected uptake. It is reasonable to expect that an interaction might have occurred, such as non-specific binding (adsorption) of BSA to ghost membranes. Microscopy supports this, since we have observed weak fluorescence apparently associated with the ghost membrane of unpulsed control samples. However, no quantitative difference between fluorescence of unpulsed ghosts exposed to BSA for 5 s versus 1 h could be detected. Note that such "background" fluorescence has been subtracted from all data presented in this paper, since it does not represent uptake. Thus, higher fluorescence associated with longer co-incubation of ghosts and BSA before pulsing did not represent additional adsorption to the external surface, but represented increased uptake upon pulsing, probably due to BSA adsorption.

Similar results have been reported, where DNA expression following electroporation was enhanced up to three-fold by longer pre-pulse exposure of cells to DNA [Dekeyser et al., 1990; Klenchin et al., 1991]. Moreover, Xie et al. [1990] have demonstrated that enhanced DNA binding to cell membranes, caused by elevated divalent cation concentrations, increased DNA expression by up to almost two orders of magnitude. Finally, membrane interactions with molecules having surfactant properties have been shown to alter electropore growth kinetics [Klotz et al., 1993]. Although there are differences in experimental protocols, there appears to be evidence from a number of

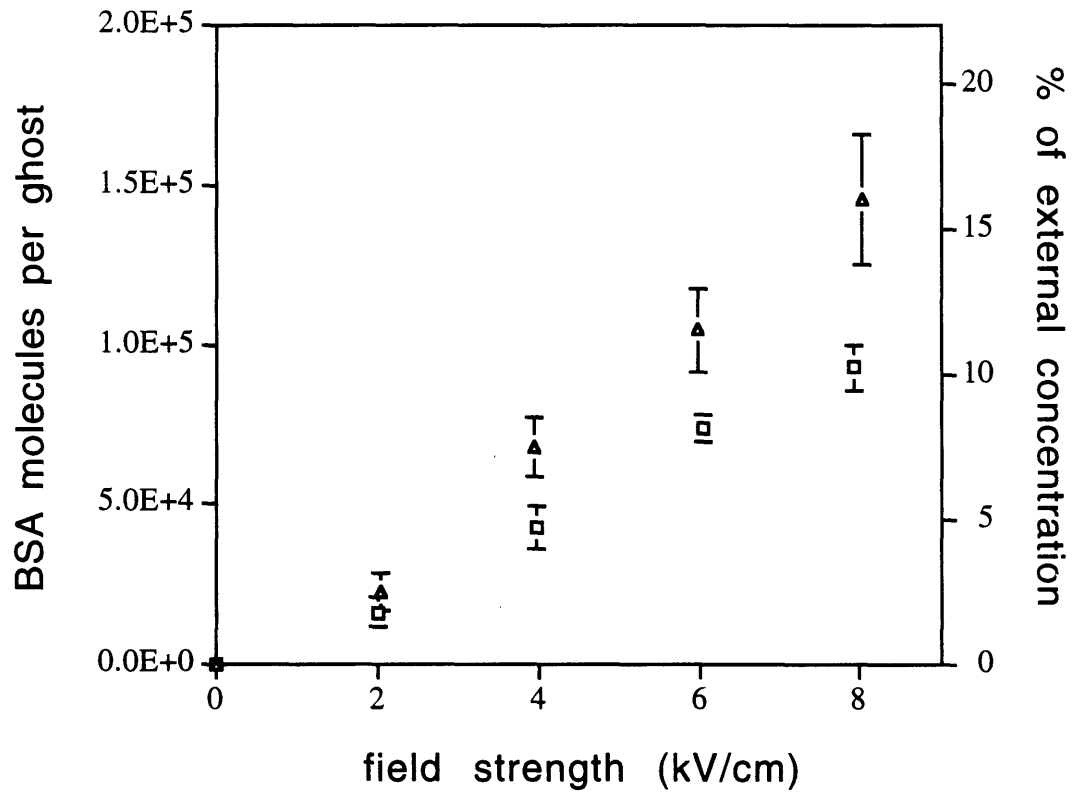


**Fig. 8-4.** The effects of BSA adsorption to ghosts before pulsing. Uptake is plotted versus field strength for cells exposed to BSA for different amounts of time before pulsing: (□) 5 s, (△) 1 h. This result suggests that increased BSA adsorption to ghost membranes increased uptake. Standard error bars are shown.

investigators that adsorption of a molecule to a cell membrane can increase transport of that molecule across the membrane.

### 8.2.5 Time Scale Of Transport

To distinguish between the relative importance of uptake during a pulse and that after a pulse though long-lived electropores, BSA was added to ghost suspensions either before pulsing or at various times after pulsing. Different waiting times (i.e., the time between pulsing and washing the ghosts) were also used. Fig. 8-5 shows these results and suggests that: (a) Although some uptake occurred when BSA was added after a pulse, much more occurred when BSA was added before. (b) The waiting time allowed after the pulse had only small effects on uptake. (c) The time of BSA addition, when added after the pulse, also had only small effects on uptake. This constrains possible mechanisms of transport.

Uptake is expected to occur by different mechanisms at different times: (a) Before, or in the absence of, a pulse, transport could in principle occur by diffusion though the intact lipid bilayer membrane. (b) During a pulse, transport could occur by diffusion and/or electrically-driven transport (e.g. electrical drift and electro-osmosis) though electropores. (c) After a pulse, transport could occur though electropores, as long as pores exist, by diffusion and/or low-voltage electrically-driven transport due to a small transmembrane diffusion potential [Weaver and Barnett, 1992]. Because no uptake was observed in unpulsed controls, it appears that significant diffusion of BSA across an intact membrane did not occur. Given the unfavorable energy cost to insert a charged species into the membrane [Parsegian, 1969], this result is expected. That uptake was observed even when BSA was added 5 min post-pulse suggests that long-lived

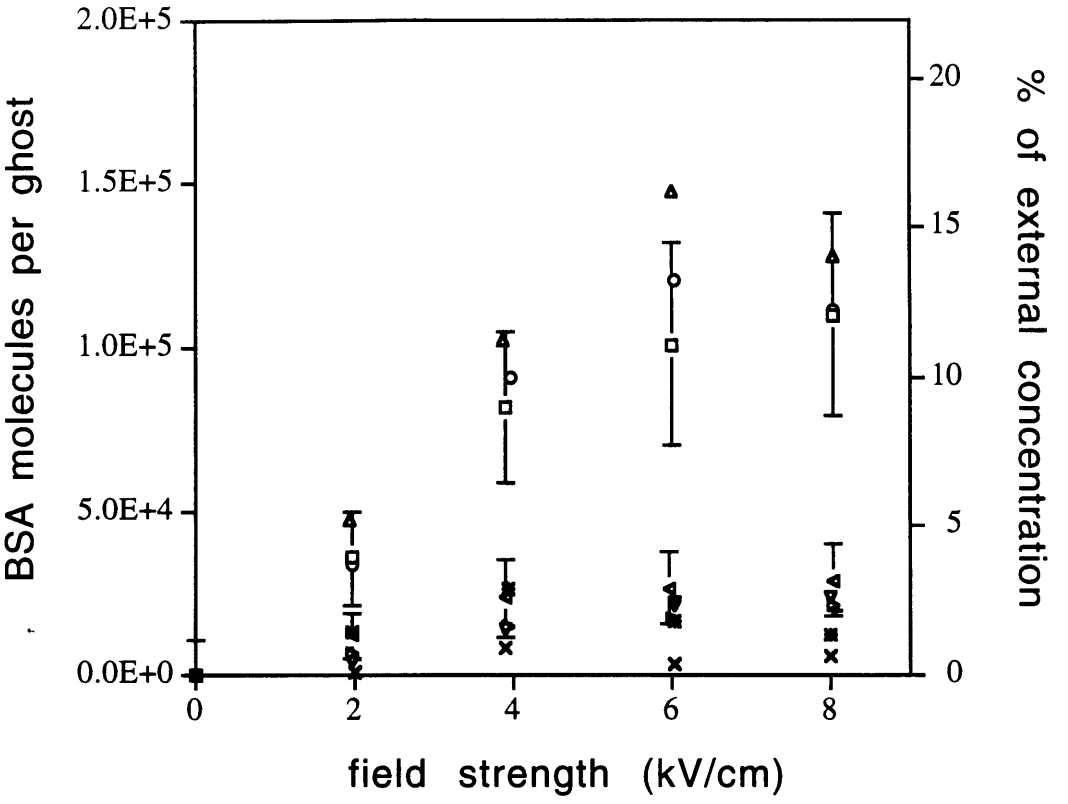


**Fig. 8-5A.** Uptake for pre-pulse and post-pulse addition of BSA. Uptake is presented as a function of field strength for ghosts exposed to BSA at different times. BSA was added to ghost suspensions either before pulsing or at various times after pulsing. Different waiting times (i.e., the time between pulsing and washing the ghosts) were also used. Conditions were as follows (see key below): (□) b,1m; (○) b,5m; (△) b,60m; (▷) a5s,1m; (▽) a5s,5m; (◁) a5s,60m; (×) a1m,5m; (+) a1m,60m; (✳) a5m, 60m. Representative standard error bars are shown. There was little difference in error magnitude between data sets.

Key: b = before pulsing; a = after pulsing; s = seconds; m = minutes. The first code represents when BSA was added, while the second code represents when ghosts were washed. For example, "a5s,1m" indicates that BSA was added to the ghost suspension 5 s after the pulse and that the ghosts were washed 1 min after the pulse.

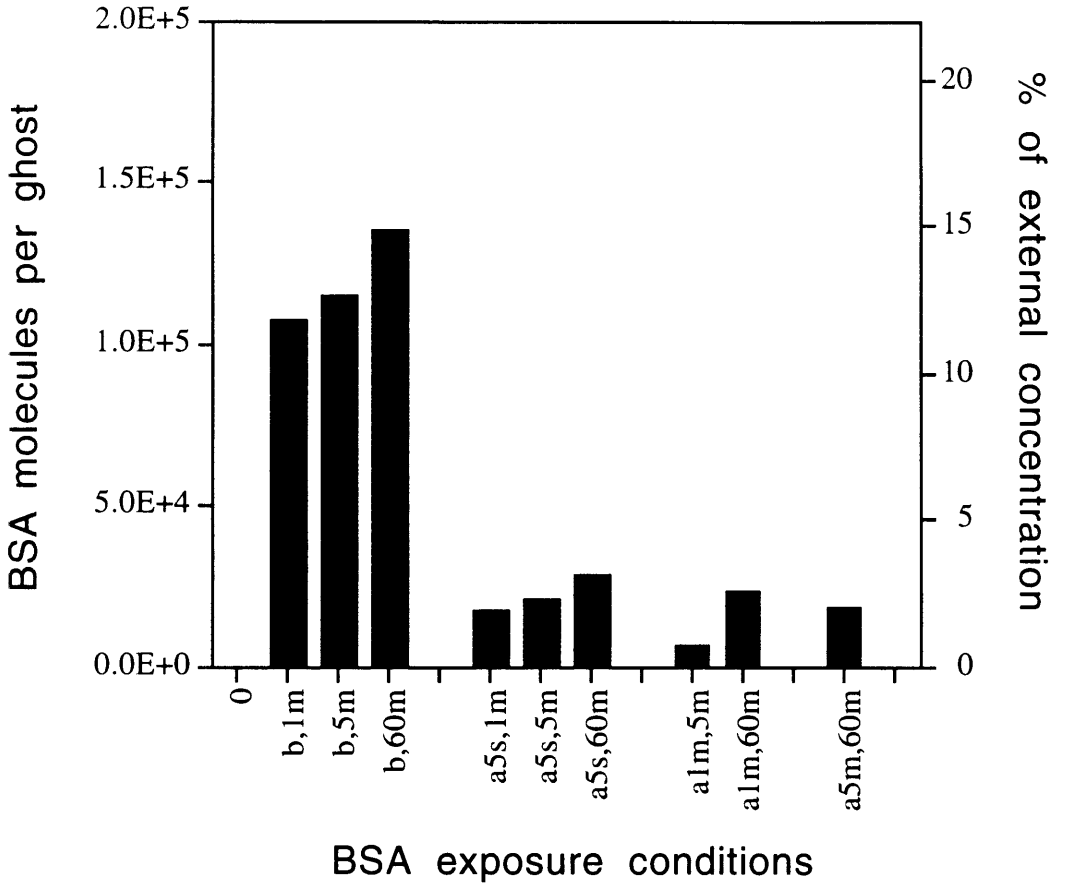


**Fig. 8-5B.** Uptake for pre-pulse and post-pulse addition of BSA. Average uptake in the plateau region (4-8 kV/cm, see text) is shown for each condition, described in Fig. 8-5A. This figure suggests that most uptake occurred during and/or within 5 s after a pulse, although some uptake occurred well after the pulse too.

electropores capable of allowing penetration of BSA by diffusion and/or low-voltage electrically-driven transport existed for at least minutes after a pulse. Finally, because uptake was much greater when BSA was added before a pulse suggests that: (a) a larger total effective pore area existed during and within 5 s after a pulse and/or (b) electrically-driven transport present during a pulse was significantly greater than post-pulse transport.

Additional results from the present study further suggest that the important events which affect transport occur during a pulse. First, Fig. 8-6 shows BSA uptake at three different temperatures (0, 23, and 37 °C). The results suggest that uptake was independent of temperature from 0 - 37 °C. Temperature has previously been shown to have little effect on pore formation, but strongly affect pore lifetime [Escande-Geraud et al., 1988; Kinosita and Tsong, 1977a; Michel et al., 1988; Serpersu et al., 1985]. If significant transport occurred post-pulse though long-lived pores, then elevated temperature would be expected to decrease pore lifetime and thereby decrease uptake. This was not the case, indicating that pore lifetime did not affect uptake. In this analysis, we have neglected changes in post-pulse transport due to increased diffusion and diffusion potentials at elevated temperature. However, these parameters are expected to vary less than an order of magnitude over the temperature range considered [Bockris and Reddy, 1970], while pores are believed to close orders of magnitude more quickly at 37 °C than at 0 °C.

Second, Fig. 8-1E suggests that multiple pulses applied every 5 s or 60 s result in the same uptake. Moreover, comparisons between multiple and single pulses suggests that transport approximately correlates with total INT, independent of $N_{pulse}$ (Fig. 8-3). If significant transport occurred between pulses, then, for the same INT, single long pulses should have resulted in the least

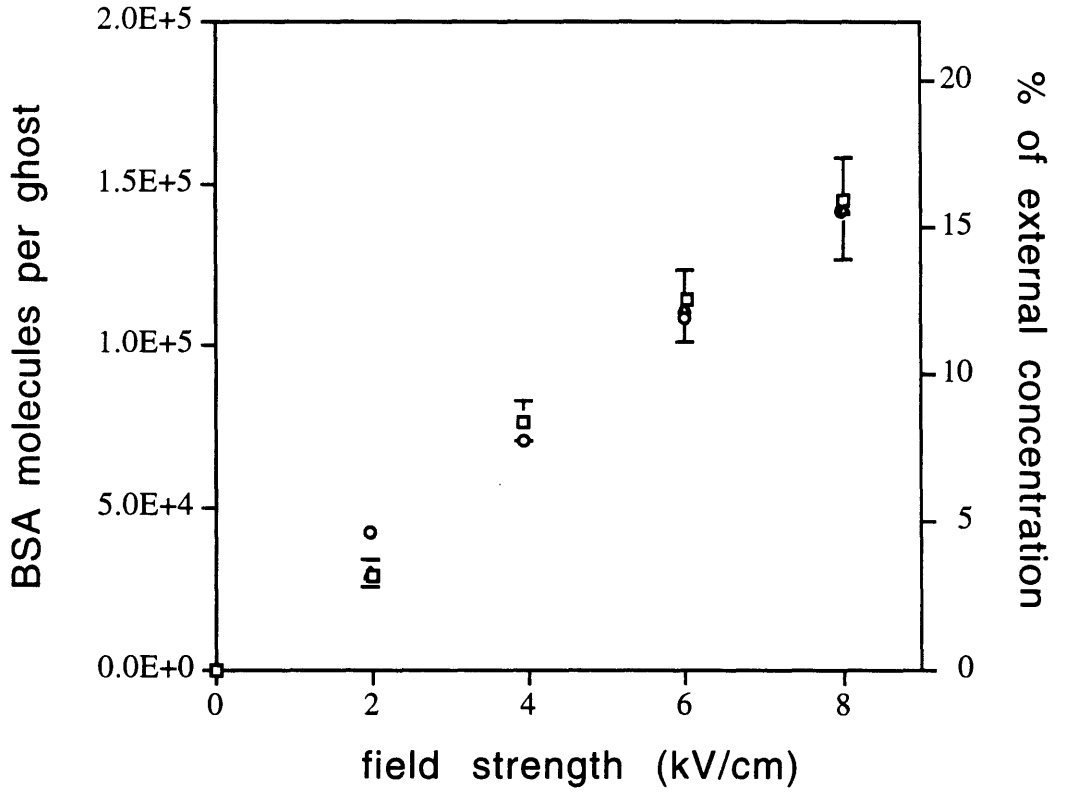


**Fig. 8-6.** The effects of temperature on uptake. BSA uptake versus field strength of a single pulse is shown at three different temperatures: (□) 0 °C, (△) 25 °C, (○) 37 °C. Samples were maintained at these temperatures before and after pulsing. Additional temperature rises due to the pulse itself have been shown to occur, but are not included in this analysis. However, this graph suggests that temperature had little effect on uptake. Standard error bars are shown.

uptake while pulsing every 60 s should have caused the most. However, if most transport occurred during pulses, then $t_{inter}$ (0, 5, or 60 s) should not have affected uptake, as was observed.

Additional evidence from the literature supports these findings. Although extensive transport of ions or molecules smaller than ~1 kDa has been shown to occur seconds to hours after electroporation [Kinosita and Tsong, 1977b; Rols and Teissié, 1990; Schwister and Deuticke, 1985; Serpersu et al., 1985], uptake of larger molecules, such as BSA, is not expected to occur extensively though long-lived electropores [Orlowski and Mir, 1993]. Many investigators have demonstrated this for DNA, where essentially no expression was observed in unpulsed controls, orders of magnitude more was seen when DNA was added within minutes post-pulse, and still orders of magnitude more expression was found when DNA was added before the pulse [Chang et al., 1992; Klenchin et al., 1991; Taketo, 1988; Xie et al., 1990]. Also, a number of investigators have argued that macromolecular uptake by electroporation occurs primarily by electrically-driven transport though electropores [Dimitrov and Sowers, 1990; Klenchin et al., 1991; Weaver and Barnett, 1992]. It is presently unclear whether transport is driven predominantly by electrical drift or electro-osmosis, although both appear to be important. An exception to this is found in the early electroporation literature, where release from erythrocytes of hemoglobin (67 kDa) occurred for hours post-pulse [Kinosita and Tsong, 1977a; Kinosita and Tsong, 1977b; Schwister and Deuticke, 1985]. However, in this case, hemoglobin release was a result of cell rupture caused by water uptake due to osmotic imbalances. This was not an example of hemoglobin transport though long-lived electropores, but represented a secondary irreversible effect of electroporation.

Thus, the present study, in combination with previous work, suggests that most uptake of macromolecules appears to occur by electrically-driven transport during a pulse, although transport, at a much slower rate, can also occur for at least minutes after a pulse.

### 8.2.6 Transport Plateau At High Field Strength

It was previously shown, with four molecules of different physical characteristics, that uptake into erythrocyte ghosts first increased with E, but reached an apparently non-equilibrium plateau at large E (Chapter 7). The onset of the plateau was different for each molecule, ranging from 2 - 5 kV/cm. To explain this result, it was proposed that transport may be controlled by E-dependent processes at small E, but could be controlled by E-independent processes at large E. The existence of a non-equilibrium large-E plateau has also recently been demonstrated in yeast cells for transport of calcein and BSA [Hui, 1994].

The present study provides additional examples of transport plateaus for BSA. Moreover, it gives further evidence that the amount of uptake at the plateau is not an absolute maximum in transport, but represents the maximum effect of increasing E, for a particular pulse protocol. Fig. 8-1 demonstrates this point most clearly. For a given $N_{pulse}$, a plateau was observed at large E, but the plateau amount of transport for each $N_{pulse}$ was different. For example, in Fig. 8-1A, application of a single pulse for E > 3 - 4 kV/cm did little to further increase uptake. In contrast, application of additional pulses increased uptake up to four-fold above the single-pulse large-E plateau. Thus, our interpretation is that the plateau represents the maximum effect of increasing E for a particular pulse protocol, rather than the maximum uptake possible under any condition.

In some experiments, a plateau was not clearly observed (e.g., Figs. 8-4 and 8-6). Instead, uptake appeared to continue to increase for larger E over the range investigated. While sometimes the large error bars associated with this inherently-heterogeneous biological preparation allow a plateau, in other cases a plateau is excluded. The most notable exceptions are seen in Figs. 8-4 and 8-6. However, the data in these two figures come from the same set of experiments, suggesting that they may represent an isolated result. Nevertheless, it is evident that although plateaus are usually observed, they are not always observed.

Plateaus are probably a consequence of the interactive behavior of a dynamic pore population, the transmembrane voltage, and one or more molecular transport mechanisms. A number of potential explanations have been proposed: (a) We previously suggested that transport may be controlled by E-independent processes at large E; (b) Wang et al. [1993] recently demonstrated that a detailed computer simulation of electroporation predicted transmembrane voltage and molecular transport which featured an approximate plateau in transport at large E. This result was based on a dynamic, heterogeneous pore population and local electrophoretic transport though the transient pores; (c) Non-equilibrium steady-state transport could be achieved at large E by a mechanism which in part involves molecules which may enter a cell and then exit it on the other side, by electrophoresis and/or electro-osmosis. This could also result in a plateau in net uptake.

### 8.2.7 Transport Maximum

While the maximum uptake which was achieved by increasing E alone was apparently not an absolute maximum, there does appear to be a maximum amount of BSA which could be transported into a ghost in this study. Under any

condition used, uptake never exceeded approximately 2.5 x $10^5$ BSA molecules per ghost. Assuming a spherical ghost with an internal volume of 150 $um^3$ [Sowers and Lieber, 1986], this corresponds to an internal BSA concentration of approximately 2.8 x $10^{-6}$ M. Given that the supplied external BSA concentration was $10^{-5}$ M, then the maximum BSA internal concentration corresponds to only one fourth of the external concentration, an apparently non-equilibrium state, assuming no partition coefficients or binding sites.

Determination of apparent equilibrium requires correct assessment of ghost volume. We have used the volume determined by Sowers and Lieber [1986] for ghosts prepared and used under conditions similar to those of the present study. Examination by microscopy showed that our ghost preparation appeared spherical and had average diameters of 6 - 7 μm, in good agreement with Sowers and Lieber. To explain the apparent non-equilibrium presented here, our estimate of ghost volume would have to be a factor of four too large, which we believe is unlikely.

Apparent non-equilibrium uptake has precedent in the literature. Uptake of molecules ranging from antibodies to oligonucleotides to simple carbohydrates has corresponded to internal concentrations from 0.1 - 60% of external concentration [Bartoletti et al., 1989; Bazile et al., 1989; Casabiance-Pignède et al., 1991; Mir et al., 1988; Poddevin et al., 1991; Serpersu et al., 1985]. In contrast, other studies have reported uptake of proteins where internal concentrations appear to correspond to as much as 1 - 2 orders of magnitude above external concentrations [Glogauer and McCulloch, 1992; Wilson et al., 1991], according to our calculations. Although direct assessment of relative concentrations was not discussed by these authors, our calculations were made using cell dimensions and molecular uptakes given in the papers. These higher

internal concentrations suggest that protein binding within cells may have occurred. In contrast to studies with macromolecules, uptake corresponding to equilibrium or Donnan equilibrium has been reported for Lucifer Yellow (450 Da) [Mir et al., 1988] and small ions [Kinosita and Tsong, 1977b; Schwister and Deuticke, 1985; Serpersu et al., 1985].

To summarize, the literature reports equilibrium uptake only for small molecules; macromolecules were transported at sub-equilibrium levels, except when internal binding appeared to occur. However, experiments in the literature differ significantly from the present study; non-equilibrium uptake did not represent the maximum possible uptake, but simply represented uptake observed under the particular conditions used. Nevertheless, to our knowledge, uptake of a macromolecule corresponding to apparent equilibrium has not been reported under any experimental conditions, including ours. This poses an intriguing problem relevant to mechanistic understanding. Explanations may involve the mechanisms proposed above to explain plateaus and/or other mechanisms, such as an electric field-altered equilibrium or a Donnan equilibrium.

### 8.2.8 Approaches To Increase Transport

The findings of this study may aid approaches to increase transport of molecules across lipid bilayer membranes in cells and in tissues, relevant to many existing electroporation protocols. These findings are summarized below. Note that issues of cell viability are beyond the scope of this study and therefore not considered.

- Increasing E may not always increase transport. The E above which transport plateaus is expected to be a function of cell size and orientation, as well as the molecule being transported.
- Using longer and/or multiple pulses can increase transport, even beyond the large-E plateau. INT appears to be the most important parameter, where $t_{inter}$ is less important. The added constraint of cell viability issues may determine the best pulsing protocol.
- It may not be possible to transport macromolecules to apparent equilibrium, although transport to well within an order of magnitude of apparent equilibrium has been demonstrated with macromolecules here and previously. Binding within cells may affect maximum possible transport.
- Because molecule-membrane interaction may be important, longer pre-pulse exposure times could increase transport.
- Most transport appears to occur primarily during pulses and is electrically driven. Transport after pulsing may be limited by lack of a powerful driving force to transport molecules though long-lived pores. Additional driving forces, such as pressure gradients or weak electric fields (e.g. electrophoresis), could be applied after pulsing to enhance post-pulse transport.
- Temperature does not appear to have substantial effects on transport.

## 8.3 Conclusions

Results have been presented for a quantitative study of the number of bovine serum albumin (BSA) molecules transported into erythrocyte ghosts caused by electroporation: 1) Uptake of BSA was found to plateau at high field strength. However, this was not necessarily an absolute maximum in transport. Instead, it

represented the maximum effect of increasing field strength, for a particular pulse protocol. 2) Maximum uptake under any conditions used in this study corresponded to approximately one fourth of apparent equilibrium with the external solution. 3) Multiple and longer pulses each increased uptake of BSA, where the total time integral of field strength correlated with uptake, independent of inter-pulse spacing. 4) Pre-pulse adsorption of BSA to ghost membranes appears to have increased transport. 5) Most transport of BSA probably occurred by electrically-driven transport during pulses; post-pulse uptake occurred, but to a much lesser extent. Finally, approaches to increasing transport were discussed.

# 9 Kinetics Of Transport[12]

## 9.1 Introduction

Electroporation involves the creation of transient aqueous pathways in lipid bilayer membranes by the application of a short (μs, ms) electric field pulse [Chang et al., 1992; Neumann et al., 1989; Orlowski and Mir, 1993; Tsong, 1991; Weaver, 1993b]. Well established in cell membranes and artificial bilayer systems, permeability and electrical conductance of lipid bilayers are increased by orders of magnitude, where membrane changes can be reversible or irreversible, depending mainly on pulse magnitude and duration. Electrical exposures typically involve electric field pulses which generate transmembrane potentials of approximately 1 V and last 10 μs to 10 ms [Chang et al., 1992; Neumann et al., 1989].

Electropores are thought to be created on the sub-microsecond time scale [Benz et al., 1979; Hibino et al., 1991; Kinosita and Tsong, 1977c; Neumann et al., 1992] and continue growing in size for the duration of the electrical exposure [Barnett and Weaver, 1991; Freeman et al., in press; Kinosita and Tsong, 1977a]. After the pulse, pores are believed to shrink to a metastable state, over a characteristic time of milliseconds [Chernomordik et al., 1983; Glaser et al., 1988] and, under reversible conditions, disappear completely over lifetimes from sub-second to hours [Abidor et al., 1979; Chang and Reese, 1990; Hibino et al., 1991; Zhelev and Needham, 1993; Zimmermann et al., 1975].

Transport due to electroporation is expected to occur by different mechanisms at different times. During a pulse, transport could occur by diffusion and/or electrically-driven transport (e.g. electrical drift and electroosmosis) through electropores. After a pulse, transport could occur through electropores, as long

---

[12] These results have also been reported in [Prausnitz et al., submitted, a].

as pores exist, by diffusion and/or low-voltage electrically-driven transport due to a small transmembrane diffusion potential [Weaver and Barnett, 1992].

While a number of studies have shown that molecular transport through electropores can occur seconds to hours post-pulse [Lambert et al., 1990; Lee et al., 1992b; Mishra and Singh, 1986; Rols and Teissié, 1990; Tekle et al., 1991], it has been proposed that most transport occurs during a pulse, driven by electrical drift or electroosmosis [Dimitrov and Sowers, 1990; Klenchin et al., 1991; Orlowski and Mir, 1993; Prausnitz et al., 1994; Weaver and Barnett, 1992]. However, until now, the kinetics of transport due to electroporation have not been measured on a time scale the same as or faster than that of the pulse, making it difficult to compare transport rates during and after the pulse. Such information could give direct insight into transport mechanisms. This need motivated the following study, which measured transport across erythrocyte ghost membranes on the sub-millisecond time scale during and after electroporation pulses of a few milliseconds duration.

## 9.2 Results

Erythrocyte ghosts were preloaded with calcein, a small (M = 623 Da), highly charged (z = -4), fluorescent molecule, which is unable to cross resealed erythrocyte ghost membranes. Then, fluorescence of individual ghosts was measured during and up to 10 s after single exponential-decay electric field pulses. Rates and time scales of calcein transport across ghost membranes were assessed with time resolution as short as 200 μs. Representative results are shown in Figs. 9-1 to 9-3.

Due to a single pulse, extensive transport of calcein out of a ghost occurred, where the ghost was partially (Fig. 9-1A) or fully (Fig. 9-1B) emptied, over the

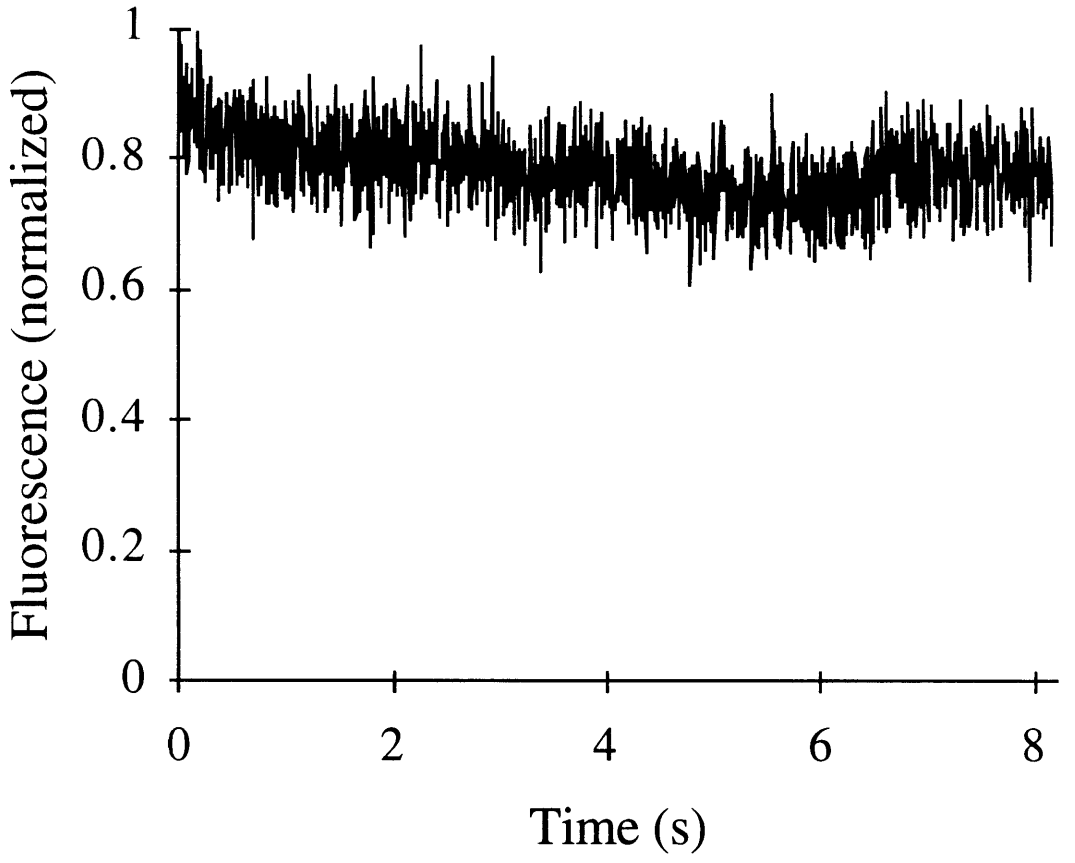


**Fig. 9-1A**. Normalized fluorescence of a calcein-loaded erythrocyte ghost during and after an exponential-decay electric field pulse (5 ms resolution). Calcein is a small (M = 623 Da) fluorescent molecule which is unable to cross resealed erythrocyte ghost membranes. Fluorescence has been normalized to prepulse values. Approximately 25 % of the calcein was transported out of the ghost over the time scale of the experiment. Electric field strength, E = 1.0 kV/cm; exponential decay time constant of pulse, $\tau$ = 2.3 ms.

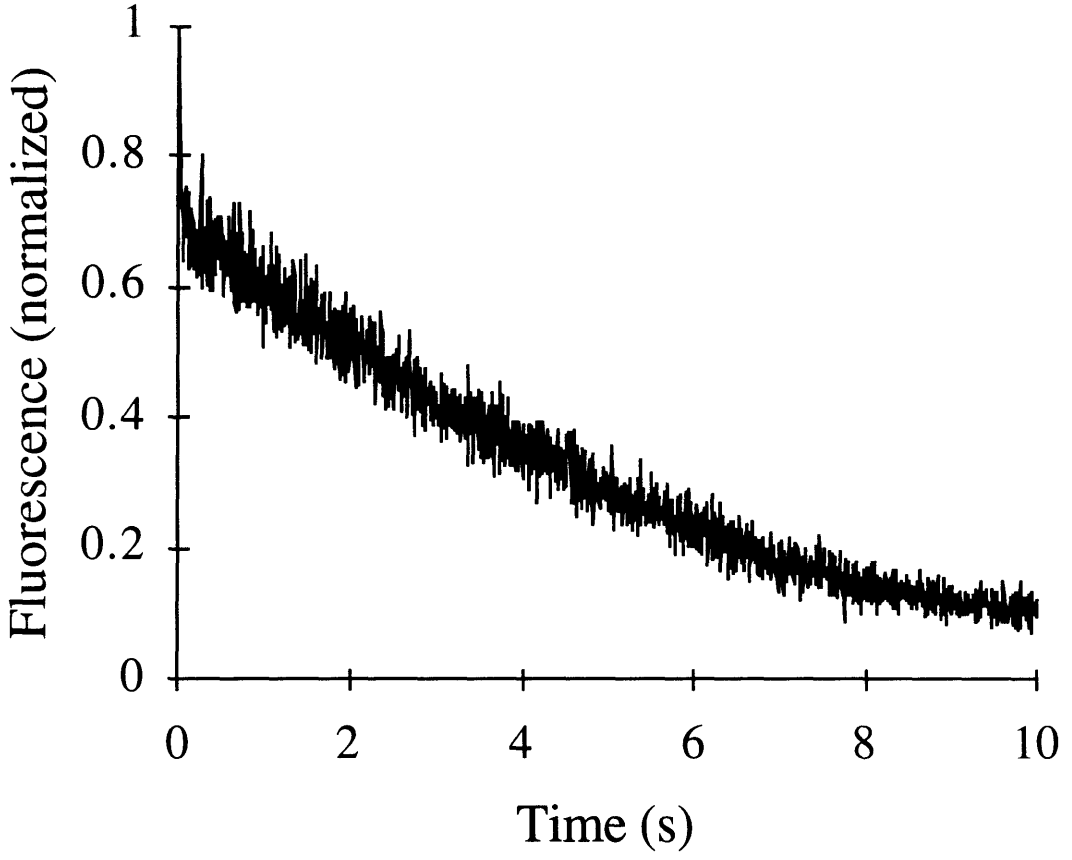


**Fig. 9-1B**. Normalized fluorescence of a calcein-loaded erythrocyte ghost during and after an exponential-decay electric field pulse (5 ms resolution). At least 90 % of the calcein was transported out of the ghost over the time scale of the experiment. E = 1.5 kV/cm, $\tau$ = 2.7 ms.

time scale of the experiment. When a ghost was only partially emptied, additional transport may have occurred after the experiment concluded, possibly emptying the ghost completely over a longer time scale.

To distinguish between transport during and after a pulse, measurements over shorter times with greater time resolution were made. Generally, one of four possible outcomes was observed, where the ghost was: (1) partially emptied of calcein, involving transport primarily after the pulse (Figs. 9-2A and 9-2B); (2) completely emptied of calcein, involving transport primarily after the pulse (Figs. 9-2C and 9-2D); (3) completely emptied of calcein, involving transport both during and after the pulse (Figs. 9-2E and 9-2F); or (4) completely emptied of calcein, involving transport primarily during the pulse (Figs. 9-2G and 9-2H). For cases where transport occurred largely during the pulse, transport kinetics are shown with still greater time resolution in Fig. 9-3 .

Data from 97 experiments like those shown above are summarized in Fig. 9-4. Significant transport occurred both during and after a pulse. This point is further illustrated in Table 9-1, which suggests that post-pulse transport accounted for 30 - 75 % of the transport which occurred over the time scale of the experiment.

## 9.3 Discussion

Some experimental studies have assessed membrane structural changes due to electroporation with sub-millisecond time resolution by electrical [Coster and Zimmermann, 1975; Hibino et al., 1991; Kinosita and Tsong, 1977c; O'Neill and Tung, 1991] and optical [Neumann et al., 1992] techniques. However, measurements of the molecular transport associated with these changes have not been performed on time scales faster than the applied pulse length, making

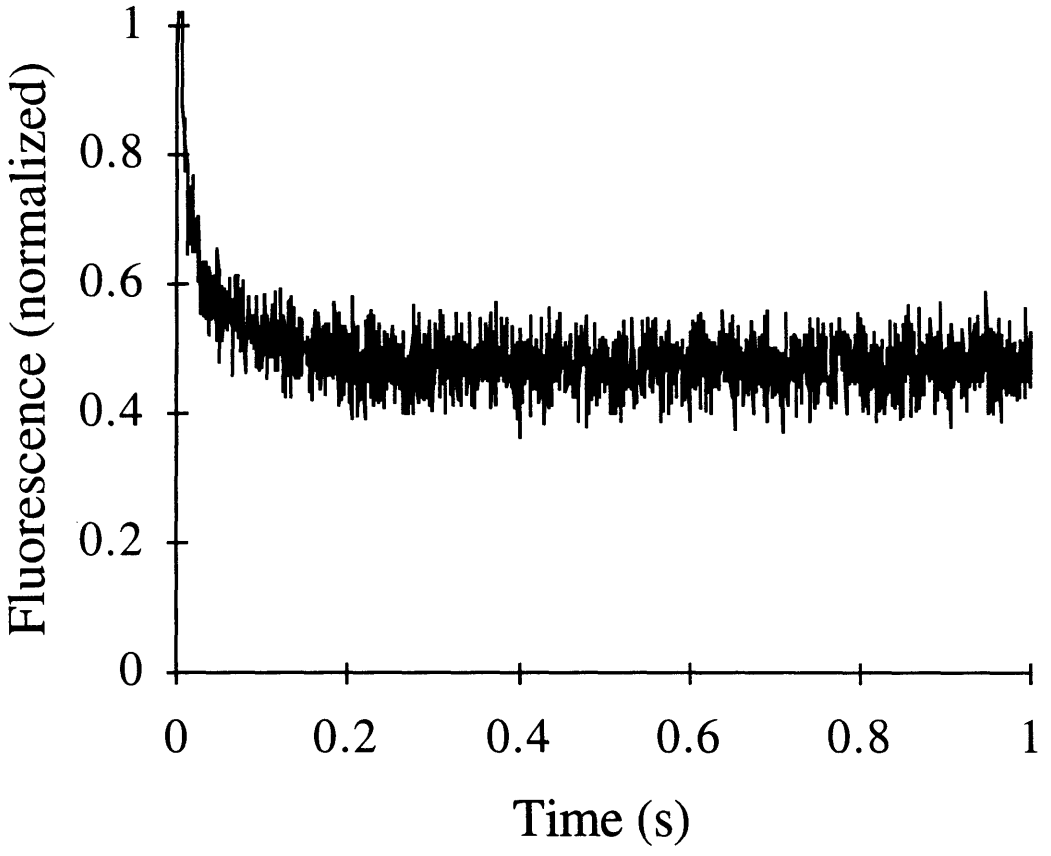


**Fig. 9-2A**. Normalized fluorescence of a calcein-loaded erythrocyte ghost during and after an exponential-decay electric field pulse (0.5 ms resolution). The ghost was only partially emptied of calcein, where most transport occurred after the pulse. E = 2.5 kV/cm, $\tau$ = 3.4 ms.

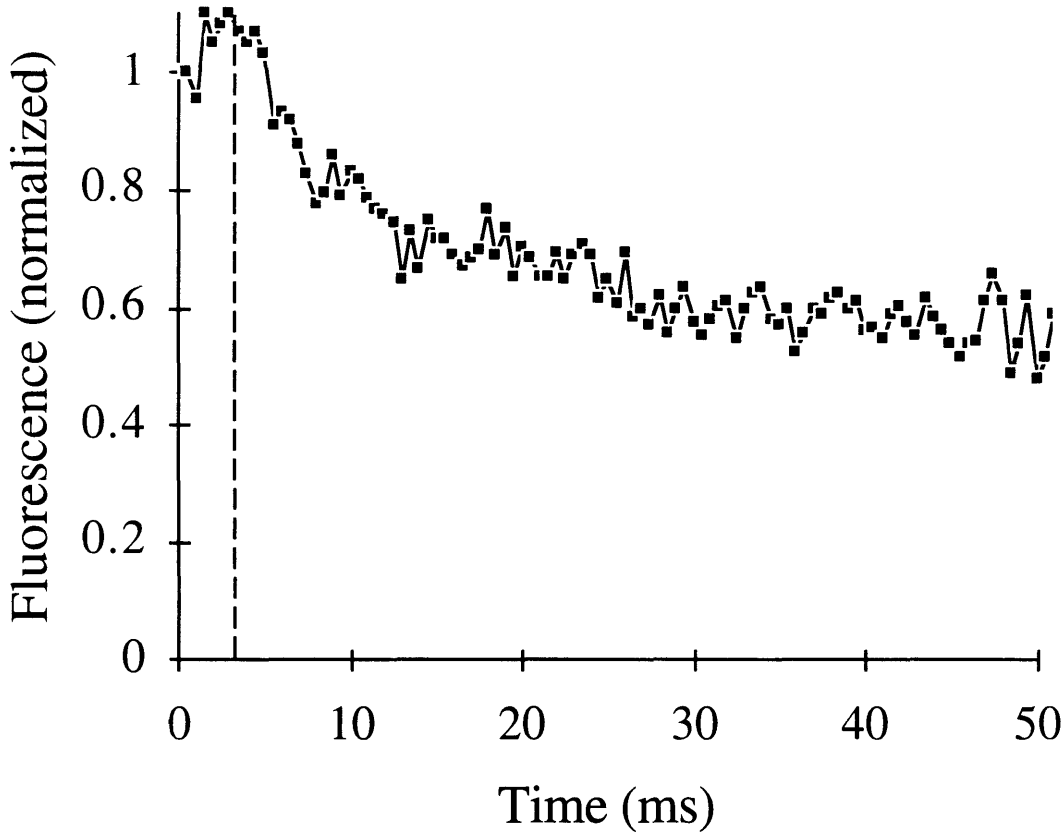


**Fig. 9-2B**. Normalized fluorescence of a calcein-loaded erythrocyte ghost during and an single exponential-decay electric field pulse (0.5 ms resolution). The ghost was only partially emptied of calcein, where most transport occurred after the pulse. E = 2.5 kV/cm, $\tau$ = 3.4 ms. This figure contains the same data as Fig. 9-2A shown on a different time scale. The dashed line indicates the time constant, $\tau$, of the pulse.

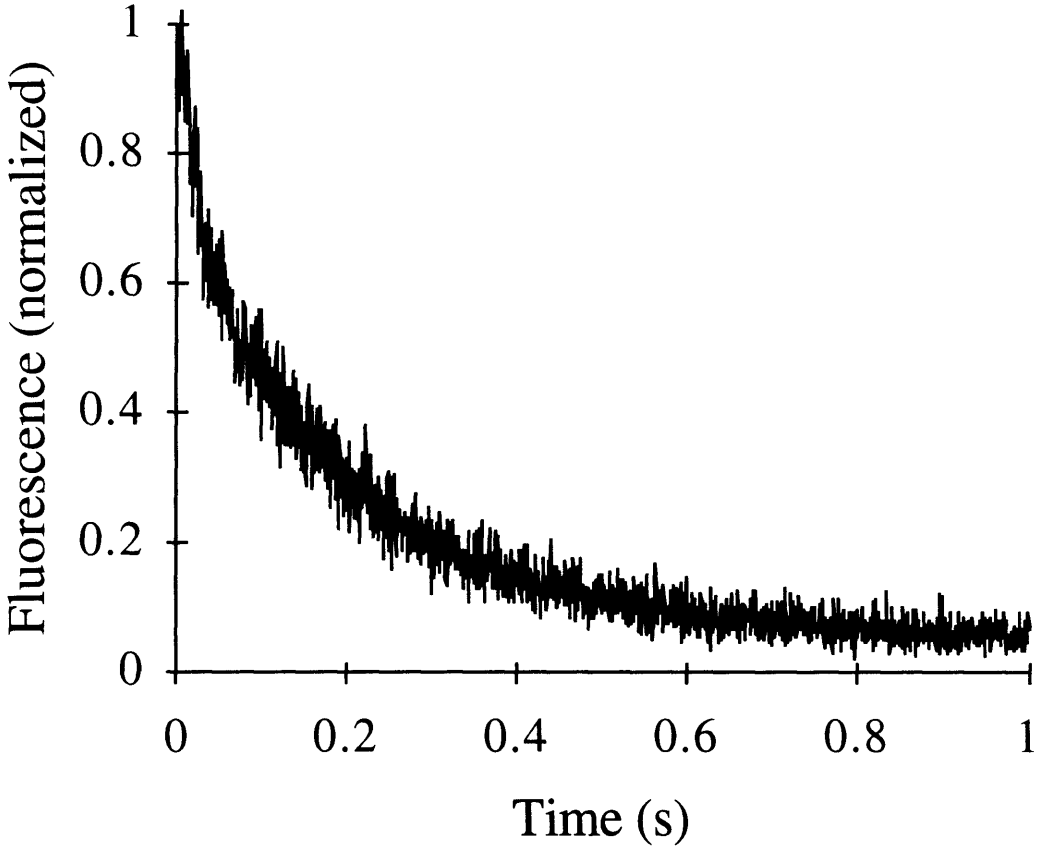


**Fig. 9-2C**. Normalized fluorescence of a calcein-loaded erythrocyte ghost during and after an exponential-decay electric field pulse (0.5 ms resolution). The ghost was completely emptied of calcein, where most transport occurred after the pulse. E = 2.5 kV/cm, $\tau$ = 2.6 ms.

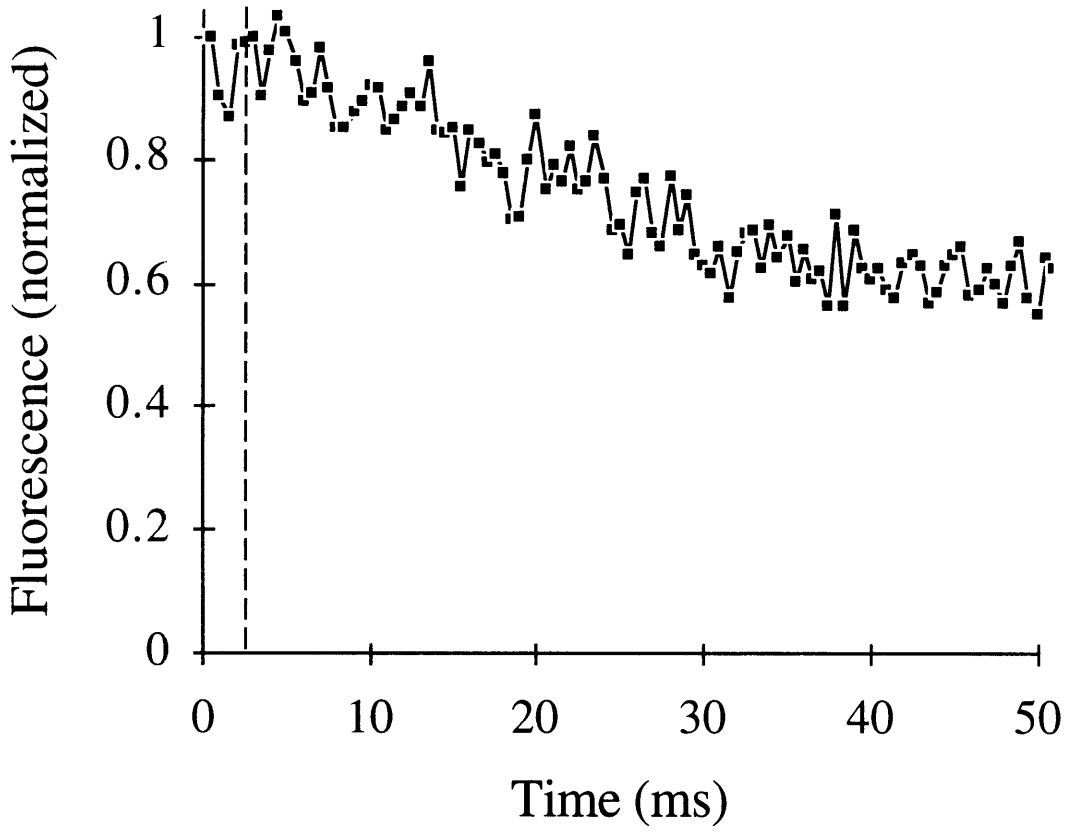


**Fig. 9-2D**. Normalized fluorescence of a calcein-loaded erythrocyte ghost during and an single exponential-decay electric field pulse (0.5 ms resolution). The ghost was completely emptied of calcein, where most transport occurred after the pulse. E = 2.5 kV/cm, $\tau$ = 2.6 ms. This figure contains the same data as Fig. 9-2C shown on a different time scale. The dashed line indicates the time constant, $\tau$, of the pulse.

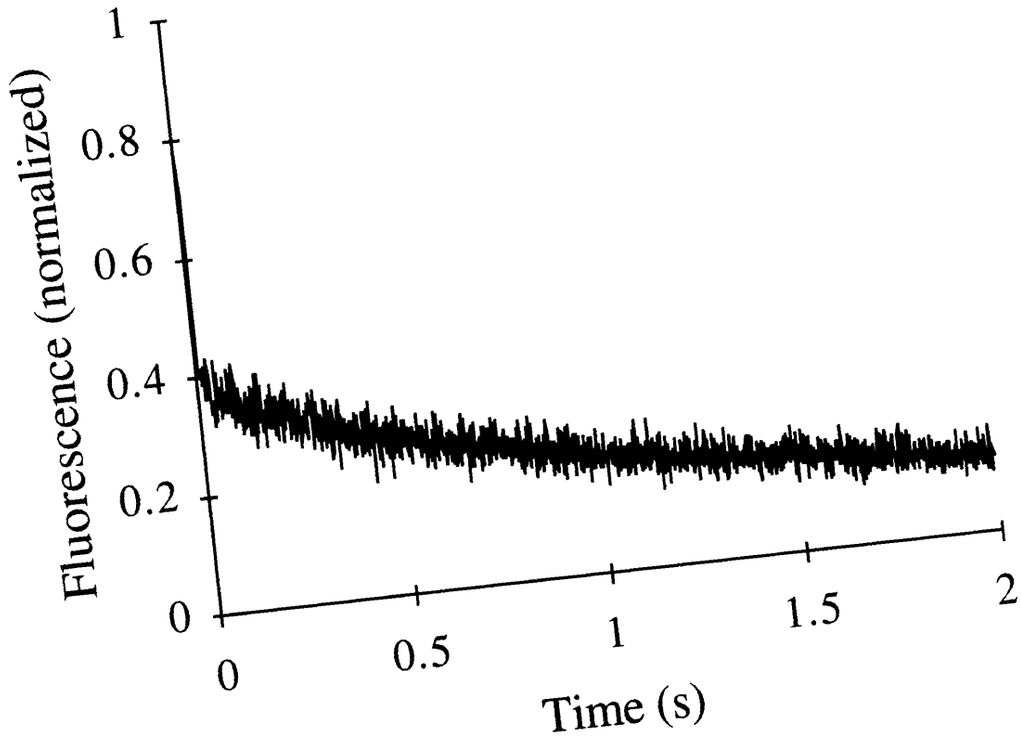


**Fig. 9-2E**. Normalized fluorescence of a calcein-loaded erythrocyte ghost during and after an exponential-decay electric field pulse (1 ms resolution). The ghost was completely emptied of calcein, where extensive transport occurred both during and after the pulse. E = 2.5 kV/cm, $\tau$ = 3.4 ms.

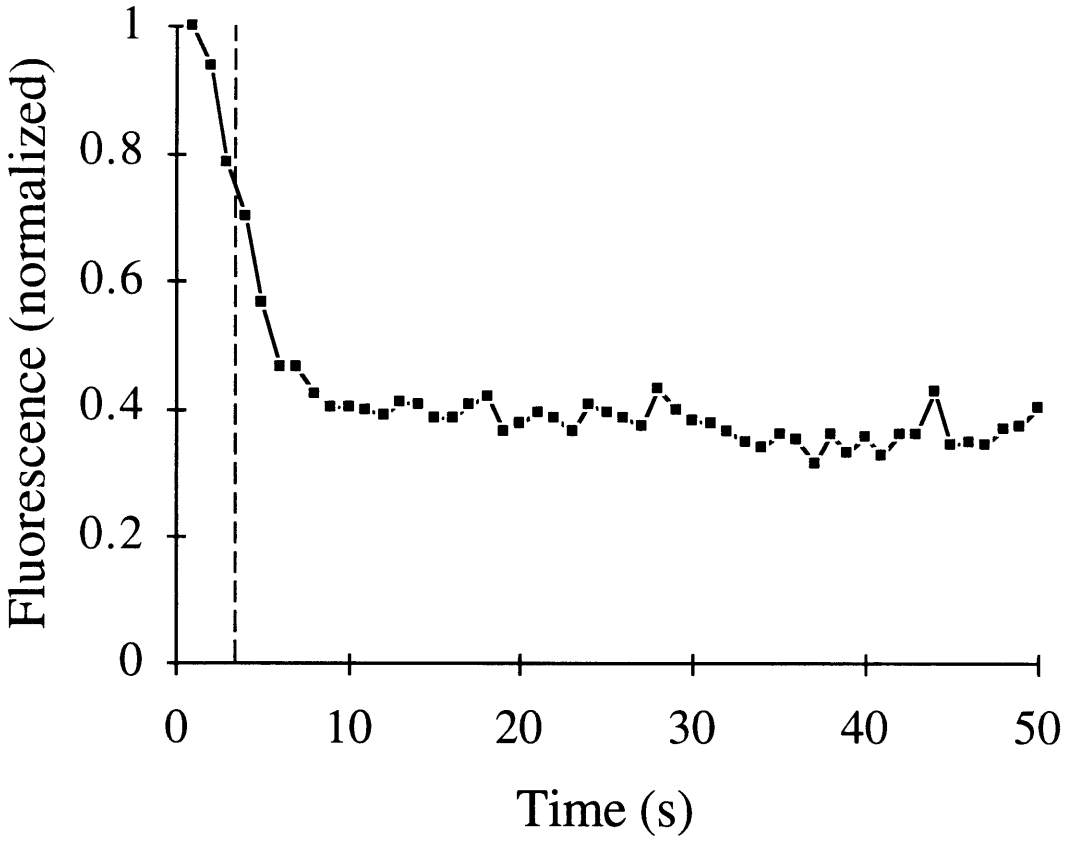


**Fig. 9-2F**. Normalized fluorescence of a calcein-loaded erythrocyte ghost during and after an exponential-decay electric field pulse (1 ms resolution). The ghost was completely emptied of calcein, where extensive transport occurred both during and after the pulse. E = 2.5 kV/cm, $\tau$ = 3.4 ms. This figure contains the same data as Fig. 9-2E shown on a different time scale. The dashed line indicates the time constant, $\tau$, of the pulse.

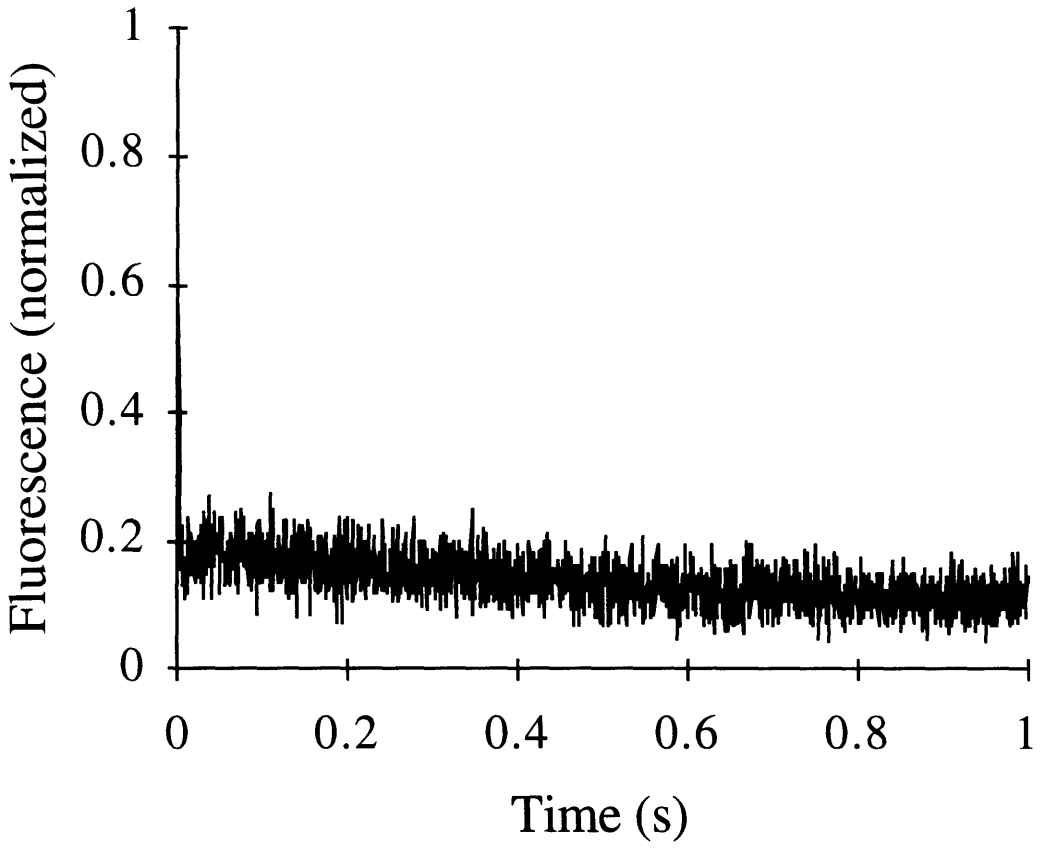


**Fig. 9-2G.** Normalized fluorescence of a calcein-loaded erythrocyte ghost during and after an exponential-decay electric field pulse (0.5 ms resolution). The ghost was completely emptied of calcein, where most transport occurred during the pulse. E = 2.5 kV/cm, $\tau$ = 2.4 ms.

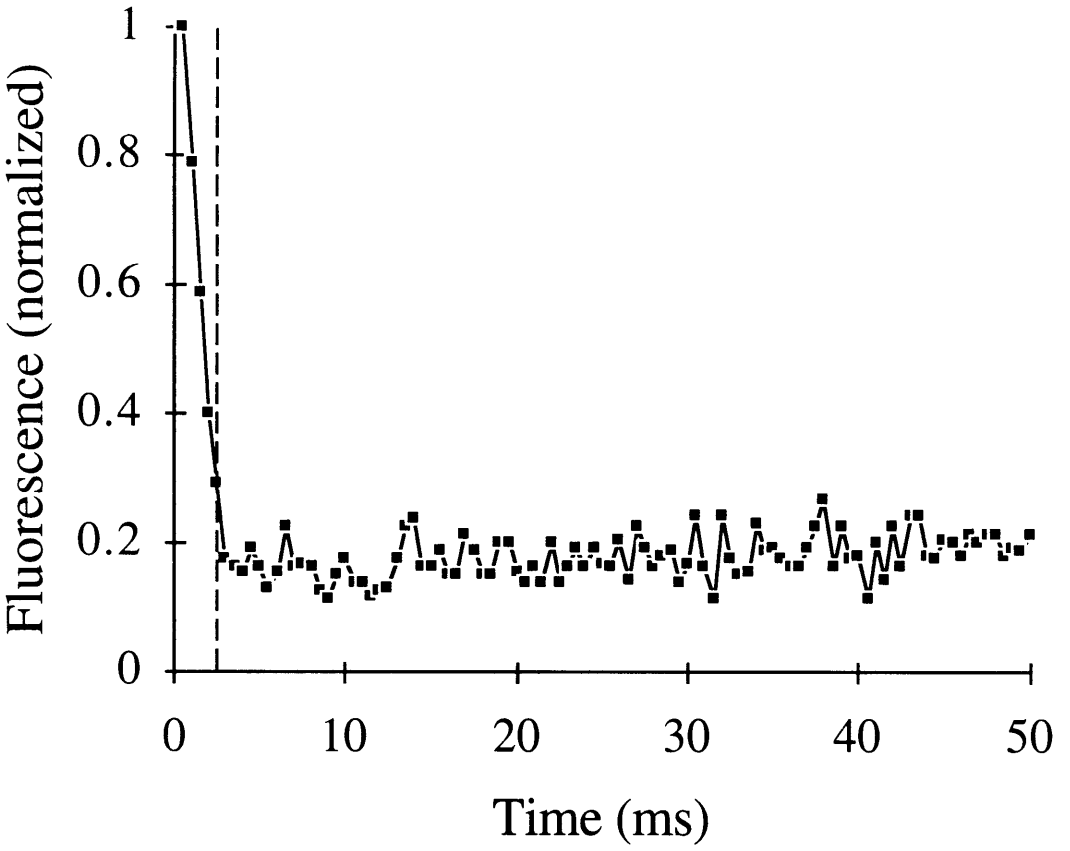


**Fig. 9-2H**. Normalized fluorescence of a calcein-loaded erythrocyte ghost during and after an exponential-decay electric field pulse (0.5 ms resolution). The ghost was completely emptied of calcein, where most transport occurred during the pulse. E = 2.5 kV/cm, $\tau$ = 2.4 ms. This figure contains the same data as Fig. 9-2G shown on a different time scale. The dashed line indicates the time constant, $\tau$, of the pulse.

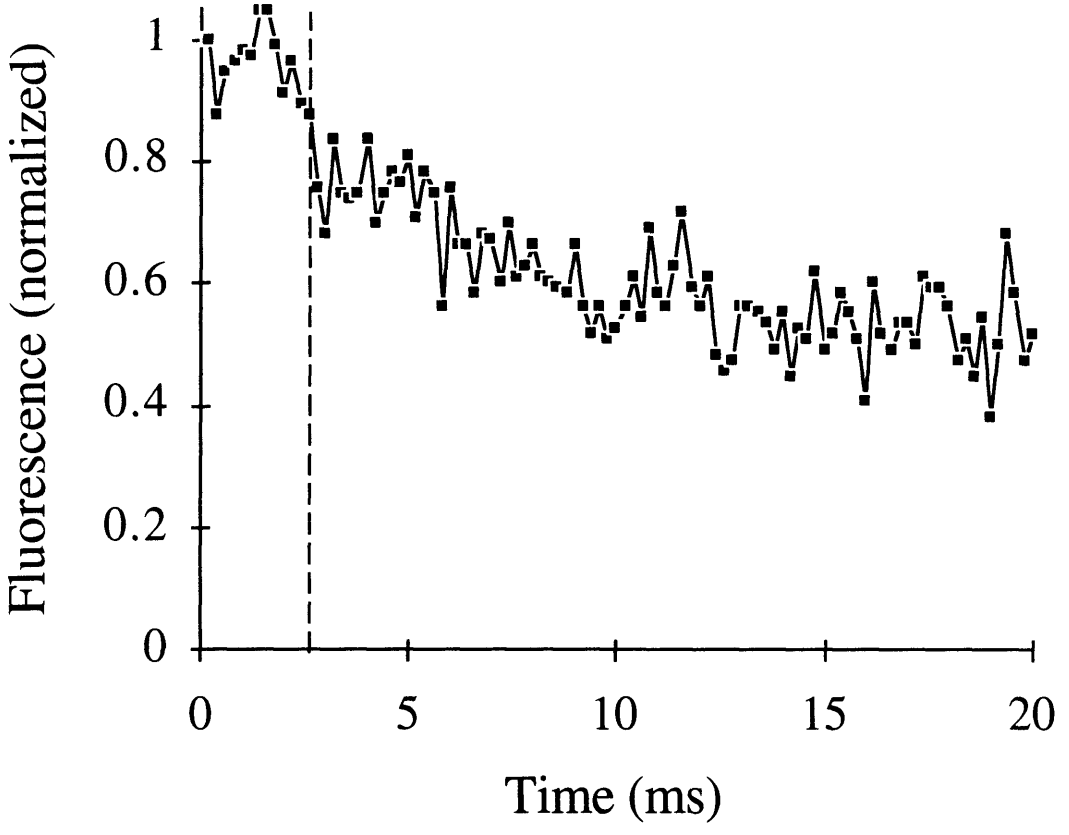


**Fig. 9-3A**. Normalized fluorescence of a calcein-loaded erythrocyte ghost during and after an exponential-decay electric field pulse (0.2 ms resolution). Most transport occurred on a time scale on the order of 10 ms. E = 2.5 kV/cm, $\tau$ = 2.6 ms. The dashed line indicates the time constant, $\tau$, of the pulse.

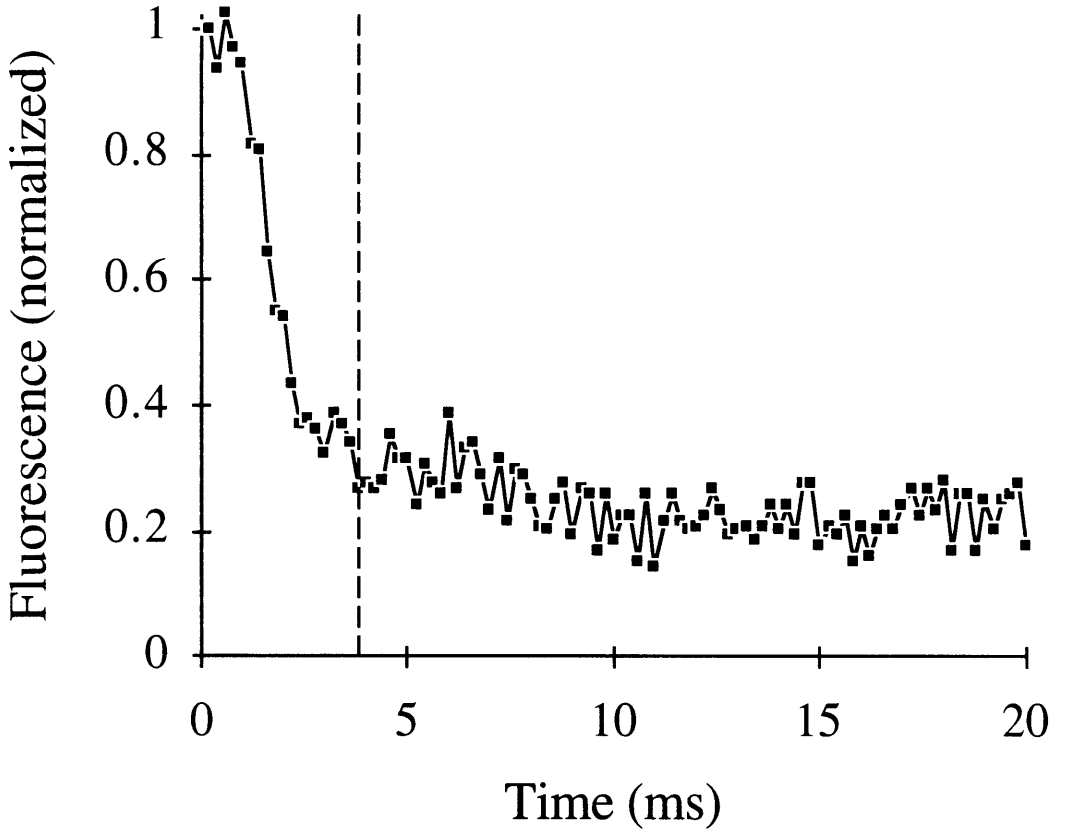


**Fig. 9-3B**. Normalized fluorescence of a calcein-loaded erythrocyte ghost during and after an exponential-decay electric field pulse (0.2 ms resolution). Most transport occurred on a time scale on the order of 1 ms. E = 3.8 kV/cm, $\tau$ = 3.8 ms. The dashed line indicates the time constant, $\tau$, of the pulse.

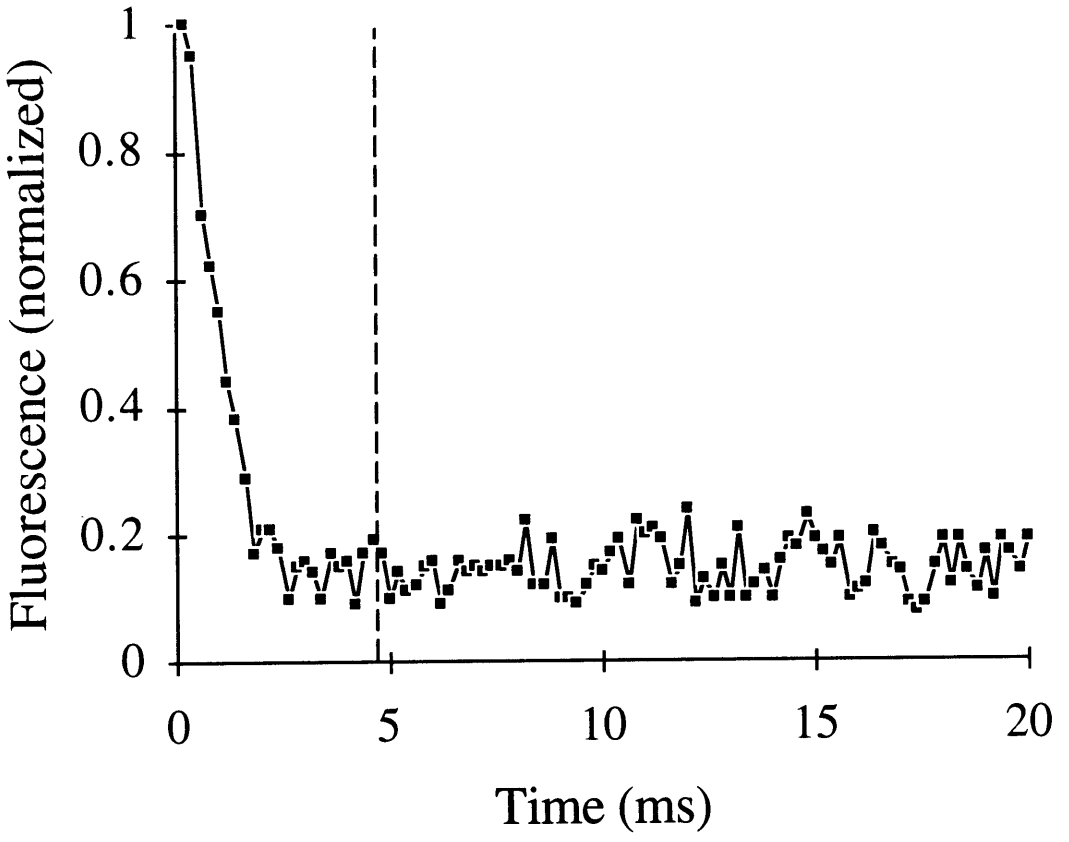


**Fig. 9-3C**. Normalized fluorescence of a calcein-loaded erythrocyte ghost during and after an exponential-decay electric field pulse (0.2 ms resolution). Most transport occurred on a time scale on the order of 1 ms. E = 3.8 kV/cm, $\tau$ = 4.7 ms. The dashed line indicates the time constant, $\tau$, of the pulse.

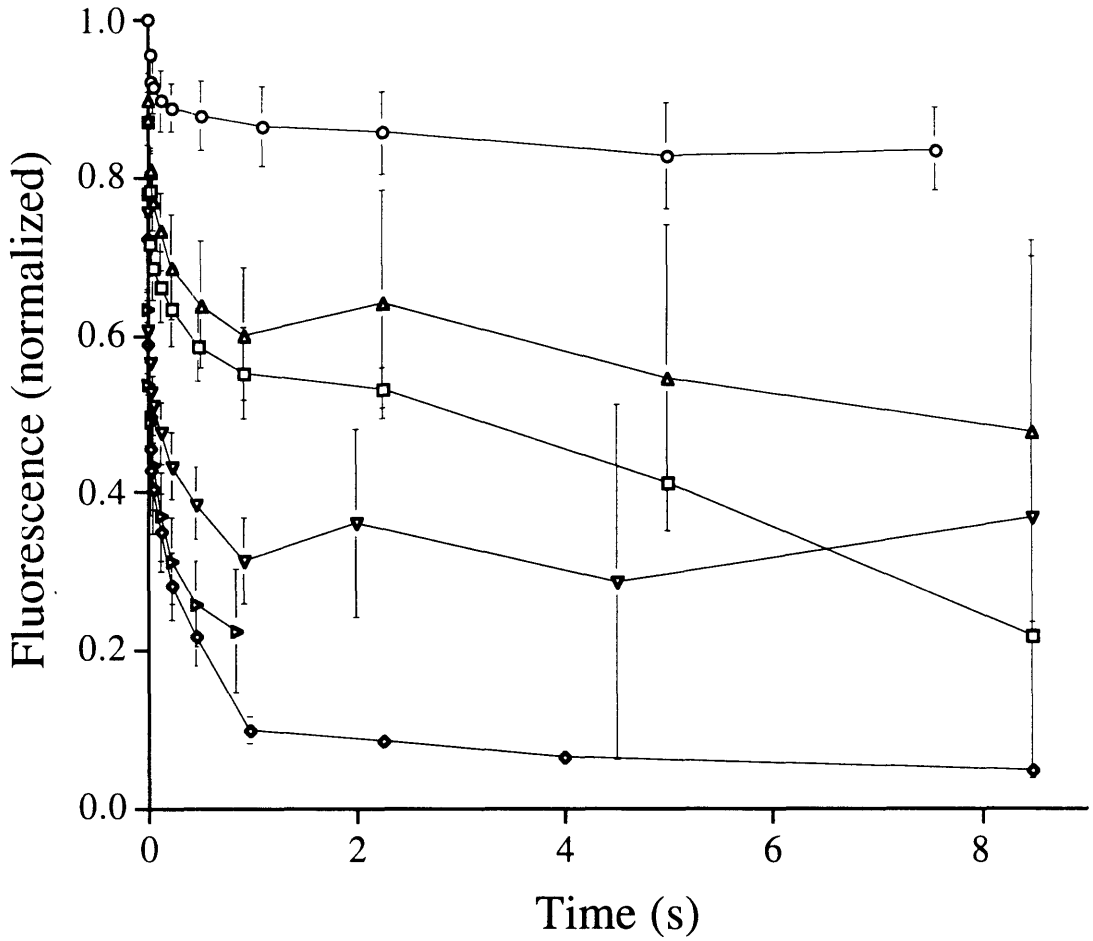


**Fig. 9-4A**. Average normalized fluorescence of individual calcein-loaded erythrocyte ghosts during and after single exponential-decay electric field pulses. E = 1.0 kV/cm (○), 1.5 kV/cm (△), 1.9 kV/cm (□), 2.5 kV/cm (▽), 3.1 kV/cm (◇), 3.8 kV/cm (▷); $\tau = 3.6 \pm 1.1$ ms (mean ± standard deviation). This figure contains data from 97 different experiments like those shown in Figs. 9-1 to 9-3. Each point represents the average fluorescence of ghosts from 2 - 40 different experiments. Standard error bars are shown.

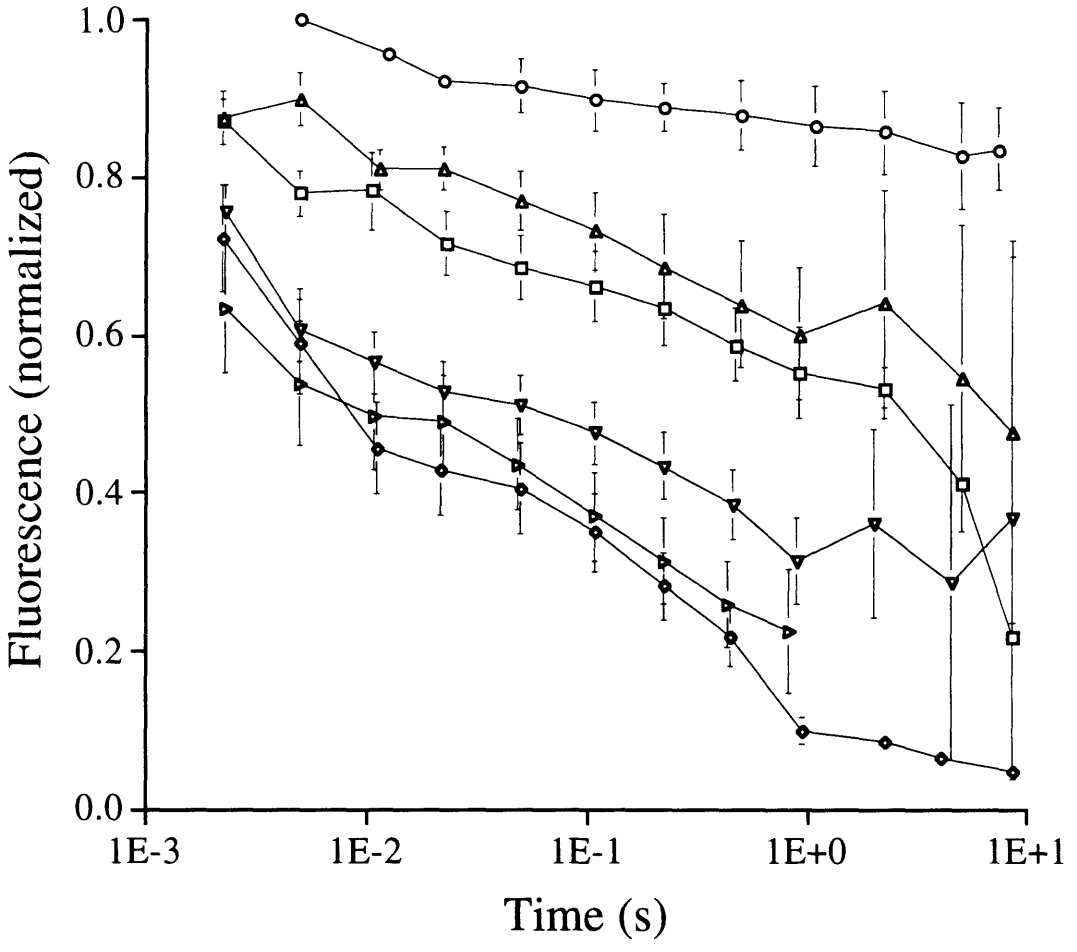


**Fig. 9-4B**. Average normalized fluorescence of individual calcein-loaded erythrocyte ghosts during and after single exponential-decay electric field pulses. E = 1.0 kV/cm (○), 1.5 kV/cm (△), 1.9 kV/cm (□), 2.5 kV/cm (▽), 3.1 kV/cm (◇), 3.8 kV/cm (▷); $\tau = 3.6 \pm 1.1$ ms (mean ± standard deviation). This figure contains the same data as Fig. 9-2C shown on a different time scale.

| NOMINAL FIELD STRENGTH (kV/cm) | FRACTION RELEASED "DURING" PULSE | FRACTION RELEASED TOTAL | RATIO (DURING/TOTAL) |
|---|---|---|---|
| 1.0 | 0.04 | 0.16 | 0.25 |
| 1.5 | 0.19 | 0.52 | 0.37 |
| 1.9 | 0.22 | 0.78 | 0.28 |
| 2.5 | 0.44 | 0.63 | 0.70 |
| 3.1 | 0.54 | 0.95 | 0.57 |
| 3.8 | 0.50 | --- | --- |

**Table 9-1.** Comparison of transport during and after a pulse. Using data from Fig. 9-4, the fraction of calcein transported out of the ghost "during" the pulse and the total fraction transported out over the time scale of the experiment are shown. Transport "during" the pulse corresponded to the amount transported within the first 10 ms of the exponential-decay pulse (~ 3 time constants). Total transport represents calcein transported after approximately 8 s. However, additional transport may have occurred at later times in some cases. These data suggest that although transport generally occurred during the pulse, significant transport also occurred after the pulse, probably by passive diffusion through long-lived pores.

separate assessment of transport during and after the pulse difficult. Until now, the fastest electroporation transport measurements had 17 ms time resolution [Dimitrov and Sowers, 1990]. Here, data have been collected which have time resolution as short as 0.2 ms.

Moreover, some previous studies of electroporation transport kinetics have used molecules which fluoresce upon binding to a substrate (i.e., ethidium bromide binding to DNA) [Marszalek et al., 1990; Sixou and Teissié, 1993; Tekle et al., 1991], thereby coupling transport and binding rates. In contrast, we measured calcein fluorescence, which should be directly related to transport kinetics.

### 9.3.1 Mechanisms Of Transport

To aid in the interpretation of data presented here, we can consider the mechanisms by which transport might have occurred. During a pulse, transport could have occurred through electropores by diffusion and/or electrically-driven transport, such as electroosmosis and electrical drift. To compare the relative importance of diffusion to electroosmosis, calculation of a Peclet number, Pe, yields a ratio of the characteristic times of diffusion to electroosmotic convection:

$$Pe = \frac{u\,r}{D}$$

$$u = \mu\,E$$

where u is electroosmotic velocity, r is ghost radius ($4 \times 10^{-4}$ cm [Prausnitz et al., 1993d]), D is calcein diffusivity ($3.5 \times 10^{-6}$ cm$^2$/s [Prausnitz et al., submitted, b]), $\mu$ is electrophoretic velocity of the mobile cations, assumed to be sodium ($5 \times 10^{-4}$ cm$^2$/V s [Atkins, 1986]), and E is electric field strength (2.5 kV/cm, as a representative value).

To compare diffusion to electrical drift, a modified Peclet number, $Pe^*$, can be defined, which has the same form as Pe, except the electrophoretic velocity of calcein, $u^*$, is used and calculated utilizing the electrophoretic mobility of calcein, $\mu^*$ ($-6 \times 10^{-4}$ $cm^2/V$ s [Prausnitz et al., submitted, b]). Employing the values given above, Pe = 143 and $Pe^* = 171$. Such large Peclet numbers indicate that during a pulse electrically-driven transport, by either electroosmosis or electrical drift, is much faster than diffusion, in agreement with previous calculations [Dimitrov and Sowers, 1990; Weaver and Barnett, 1992].

In contrast, after a pulse, no electric fields were applied, suggesting that transport occurred only by diffusion. Low-voltage electrically-driven transport due to a small transmembrane diffusion potential has also been proposed [Weaver and Barnett, 1992]. However, with the exception of calcein, the composition of solutes inside and outside the ghosts used in this study was the same, making diffusion potentials unlikely.

With these mechanisms in mind, this suggests that when ghosts were completely emptied of calcein during the pulse (e.g., Figs 9-2G and 9-2H), transport was driven predominantly by electrophoresis and/or electroosmosis, in agreement with previous studies [Dimitrov and Sowers, 1990; Klenchin et al., 1991; Orlowski and Mir, 1993; Prausnitz et al., 1994; Weaver and Barnett, 1992]. However, when significant transport occurred after the pulse (Figs. 9-2A to 9-2F), transport occurred in part or almost completely by diffusion. Although rates of electrically-driven transport were generally faster than diffusion, electrophoresis and electroosmosis only occurred for the duration of a pulse (milliseconds), while transmembrane diffusion occurred orders of magnitude longer (as long as pores

exist). Thus, the net, time-integrated contribution of diffusion was often greater than that of electrically-driven transport[13].

Some previous studies have concluded that most transport due to electroporation occurs during the pulse and is electrically driven [Dimitrov and Sowers, 1990; Klenchin et al., 1991; Prausnitz et al., 1994; Taketo, 1988; Weaver and Barnett, 1992]. However, most studies which have compared transport during and after a pulse have involved experiments where the molecules to be transported were added to cell suspensions either before or seconds to minutes after pulsing [Chang et al., 1992; Klenchin et al., 1991; Prausnitz et al., 1994; Taketo, 1988]. Using this approach, post-pulse transport may not have been detected because molecules were added too late. Evidence suggests that post-pulse diffusion may often occur predominantly within a few seconds after the pulse: (a) significant transport by post-pulse diffusion was observed here to occur on a time scale of seconds or less (Figs. 9-1 to 9-2) and (b) pore closure kinetics have also been determined to occur often over seconds or less [Chang and Reese, 1990; Chernomordik et al., 1987; Hibino et al., 1991; Zhelev and Needham, 1993; Zimmermann et al., 1975].

Kinetic studies have suggested that rates of transport are greater during a pulse than after [Dimitrov and Sowers, 1990; Sixou and Teissié, 1993], in agreement with results reported here. However, given the vastly different time scales over which diffusion and electrically-driven transport occur, this does not exclude a significant net contribution of diffusion to transport. Finally, studies which indicate transport predominantly in a single direction oriented parallel to

---

[13] In this study, transport by diffusion after a pulse may have been facilitated by calcein's realtively small size (Stokes-Einstein radius, r = 0.6 nm [Edwards et al., submitted]). In contrast, the contribution of post-pulse diffusion of macromolecules, such as proteins or DNA, may be significantly smaller, since long-lived electropores are thought to be ~ 1 nm in radius [Abidor et al., 1979; Glaser et al., 1988b].

the applied electric field [Dimitrov and Sowers, 1990; Klenchin et al., 1991] more strongly suggest transport by electrophoresis and/or electroosmosis.

Thus, based on our data and that in the literature, we conclude that under some conditions transport due to electroporation is predominantly electrically-driven, in agreement with others. However, we also conclude that under other conditions transport can occur in part or almost completely by diffusion within seconds after a pulse.

### 9.3.2 Functional Dependence Of Transport Kinetics

The functional dependence of rates of transport can give additional insight into transport mechanisms and electropore closure kinetics. Fig. 9-4B suggests a reasonable correlation with a logarithmic dependence of concentration on time ($C \sim \log t$; $r^2 = 0.93 \pm 0.04$, mean correlation constant $\pm$ standard deviation). Moreover, a reasonable fit with a power function dependence was also found ($C \sim t^a$; $0.02 < a < 0.34$; $r^2 = 0.90 \pm 0.08$). However, no mechanistic basis for these correlations is evident.

One-dimensional transport by electrical drift would be proportional to the electric field strength [Bockris and Reddy, 1970], but correlation with an exponential decay was poor ($C \sim e^{-t}$; $r^2 = 0.65 \pm 0.22$). For one-dimensional diffusion from a point source, which would show a linear dependence of concentration on the inverse of the square root of time [Crank, 1975], the data correlated better ($C \sim t^{-1/2}$; $r^2 = 0.80 \pm 0.13$). For one-dimensional diffusion from a source of finite thickness, linear correlation with the error function is expected [Crank, 1975],

$$C = \mathrm{erf}\left(\frac{x}{2\sqrt{D\,t}}\right)$$

where C is the concentration at the center of the ghost, x is ghost radius ($4 \times 10^{-4}$ cm [Prausnitz et al., 1993d]), D is calcein diffusivity ($3.5 \times 10^{-6}$ $cm^2/s$ [Prausnitz et al., submitted, b]) and t is time. In this case, correlation was better ($r^2 = 0.89 \pm 0.08$), where deviation from linearity was primarily observed at short times (i.e., during the pulse).

To more fully capture the physics of the problem, diffusion from concentric spheres having different diffusivities (representing the ghost membrane and interior) could be used. For time-independent diffusivities, the solution takes the form of an infinite sum of exponentials ($C = \sum e^{-t}$) [Bell, 1945]. However, to reflect the time-dependent nature of electropores, the derivation would need to be modified to include an outer sphere with time-dependent diffusivity. Moreover, electrically-driven transport during a pulse should be included. Analysis at this level of complexity is beyond the scope this study.

## 9.4 Conclusions

Electroporation involves the application of an electric field pulse which creates transient aqueous pathways in lipid bilayer membranes. Transport through these pathways can occur by different mechanisms during and after a pulse. To determine the time scale of transport and the mechanism(s) by which it occurred, transport of a fluorescent molecule, calcein, across erythrocyte ghost membranes was measured with a fluorescence imaging apparatus with sub-millisecond time resolution during and after electroporation pulses of a few milliseconds duration. Generally, one of four possible outcomes was observed, where the ghost was: (a) partially emptied of calcein, involving transport primarily after the pulse; (b) completely emptied of calcein, involving transport primarily after the pulse; (c) completely emptied of calcein, involving transport both during and after the pulse;

or (d) completely emptied of calcein, involving transport primarily during the pulse. We conclude that under some conditions transport due to electroporation occurs predominantly by electrophoresis and/or electroosmosis during a pulse, while under other conditions transport occurs in part or almost completely by diffusion within seconds after a pulse.

# ELECTROPORATION OF SKIN

## 10 Electroporation Of Mammalian Skin[14]

### 10.1 Introduction

Transdermal drug delivery offers a number of potential advantages compared to conventional methods, such as pills and injections: 1) no degradation due to stomach, intestine, or first pass of the liver, 2) likely improved patient compliance because of a user-friendly method, and 3) potential for steady or time-varying controlled delivery [Bronaugh and Maibach, 1989; Champion et al., 1992; Cullander and Guy, 1992; Hadgraft and Guy, 1989]. Nevertheless, very few drugs can be administered transdermally at therapeutic levels, due to the low permeability and lipophilic nature of human skin. As a result, fewer than ten drugs are now clinically administered transdermally. However, the market for these drugs exceeds one billion dollars in the United States alone, indicating the importance of this delivery method. Therefore, significant enhancement of transdermal drug delivery has the potential for major impact on medicine.

A number of approaches have been taken to increase transdermal transport [Bronaugh and Maibach, 1989; Cullander and Guy, 1992; Hadgraft and Guy, 1989]. Most common is the addition of chemical enhancers, compounds which are believed to increase the partitioning of drugs into the skin. Another approach is chemical modification of a drug into a "prodrug," which penetrates the skin well, but is subsequently converted by epidermal enzymes into the original pharmacologically-active drug. Application of ultrasound has been used as well to increase transdermal flux and to reduce transport lag times. Yet another approach is iontophoresis, the movement of drugs across the skin by an electric

[14] These results have also been reported in [Prausnitz et al., 1992], [Prausnitz et al., 1993a], [Prausnitz et al., 1993b] and [Prausnitz et al., in press, a].

field. Mechanistically similar to electrophoresis, iontophoresis is believed to act primarily by moving charged species across the skin by an electrical force.

The barrier properties of skin are attributed primarily to the stratum corneum, the skin's outer layer. The stratum corneum is a dead tissue composed of flattened cells filled with cross-linked keratin and intercellular spaces made up of lipids arranged largely in bilayers [Bouwstra et al., 1991; Elias, 1991]. Unlike the unilamellar phospholipid bilayers of cell membranes, these multilamellar, intercellular bilayers contain no phospholipids, being composed primarily of ceramides, cholesterol, and fatty acids [Bronaugh and Maibach, 1989; Champion et al., 1992; Hadgraft and Guy, 1989]. Intercellular pathways are generally the most important routes for transdermal transport [Bronaugh and Maibach, 1989; Champion et al., 1992; Hadgraft and Guy, 1989]. Therefore, permeabilization of the lipid bilayers filling these intercellular pathways would be expected to increase transdermal transport.

Electroporation is a method of reversibly permeabilizing lipid bilayers, involving the creation of transient aqueous pores by the application of an electric pulse [Chang et al., 1992; Neumann et al., 1989]. Dramatically reduced electrical resistance and extensive transport of molecules, including macromolecules, are generally associated with electroporation of lipid bilayers, including membranes of artificial planar and spherical systems, as well as those of living cells. Electric field exposures causing electroporation typically generate transmembrane potentials of ~ 1 V and last 10 μs to 10 ms. Electroporation of isolated single cells is well established, but electroporation of cells that are part of an intact tissue has received little attention [Belehradek et al., 1994; Dev and Hofmann, 1994; Okino and Mohri, 1987; Titomirov et al., 1991]. To our knowledge,

electroporation of multilamellar or non-phospholipid systems has not been previously demonstrated.

In this study, we examine the possibility of electroporating the multilamellar, non-phospholipid, intercellular lipid bilayers of the stratum corneum as a mechanism to enhance transdermal drug delivery. Although both electroporation and iontophoresis involve electric fields, the two approaches are fundamentally different. While iontophoresis acts primarily on the drug, involving skin structural changes as a secondary effect [Bronaugh and Maibach, 1989; Hadgraft and Guy, 1989], electroporation is expected to act directly on the skin, making transient changes in tissue permeability. Because electroporation of cells has been shown to increase transmembrane fluxes dramatically and reversibly, electroporation of skin could make possible transdermal delivery of many more drugs at therapeutic levels.

## 10.2 Results

Quantitative measurements of transdermal molecular fluxes and electrical measurements are compared with the three characteristic features of electroporation [Chang et al., 1992; Neumann et al., 1989; Orlowski and Mir, 1993; Tsong, 1991; Weaver, 1993b]: 1) large increases in molecular flux and ionic conductance, 2) reversibility over a range of voltages, where recovery has two time constants (ms and min), and 3) structural changes in the membrane barrier.

First, transdermal fluxes of calcein (623 Da, -4 charge), a moderate-sized, highly polar, fluorescent molecule which does not normally cross skin in detectable quantities, were measured during application of low-duty-cycle electric-field pulses. Fig. 10-1 shows average transdermal flux of calcein

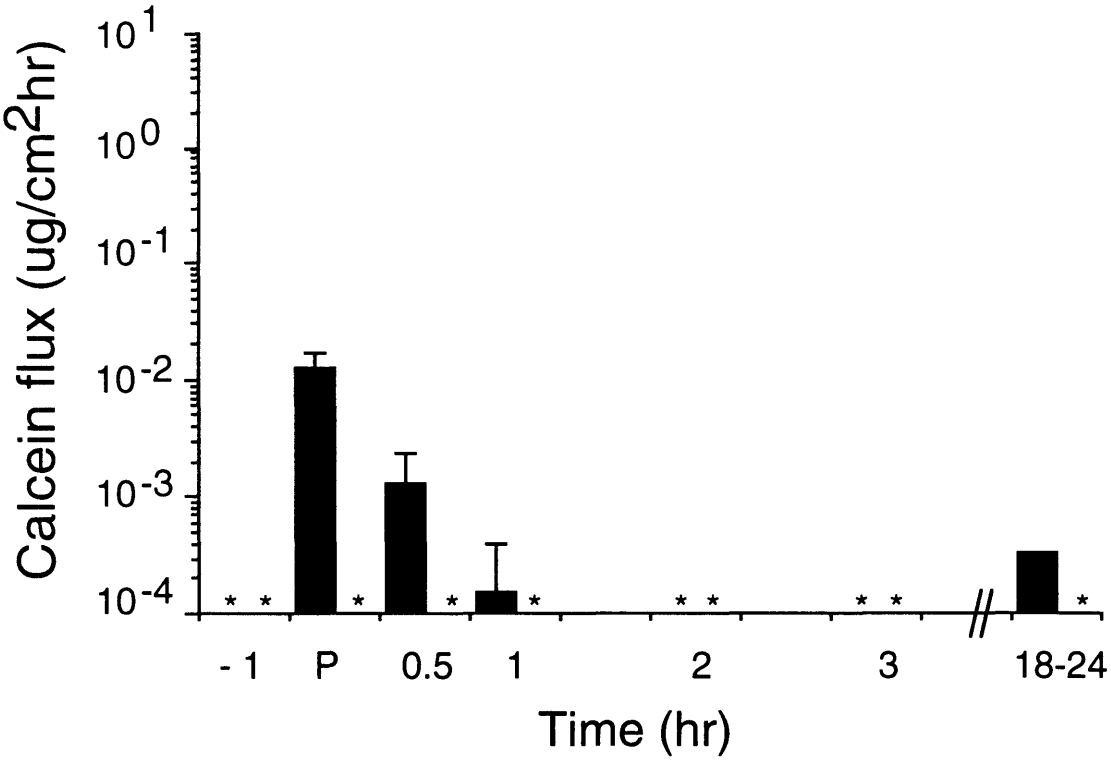


**Fig. 10-1A.** Transdermal flux of calcein (623 Da, -4 charge) before, during, and after "forward" pulsing (■) and "reverse" pulsing (▨) at 55 V. In Fig. 10-1, flux increases up to four orders of magnitude are observed under "forward" pulsing conditions (see text). These increases are at least partially reversible. "Reverse" pulsing facilitates independent assessment of changes in skin permeability due to electroporation (see text), suggesting that skin electroporation may be fully reversible below approximately 100 V, under the conditions used. Fluxes are shown one hour before pulsing, during pulsing (indicated by a "P"), and at times after pulsing. Pulsing was performed for 1 h (see text). Elevated fluxes at 18 - 24 h could be caused be skin deterioration. Each point represents the average of 3 - 7 skin samples, from 2 - 4 different subjects. Standard deviation bars are shown. The (*) symbol indicates a flux below the detection limit of order $10^{-4}$ $\mu g/cm^2$ h.

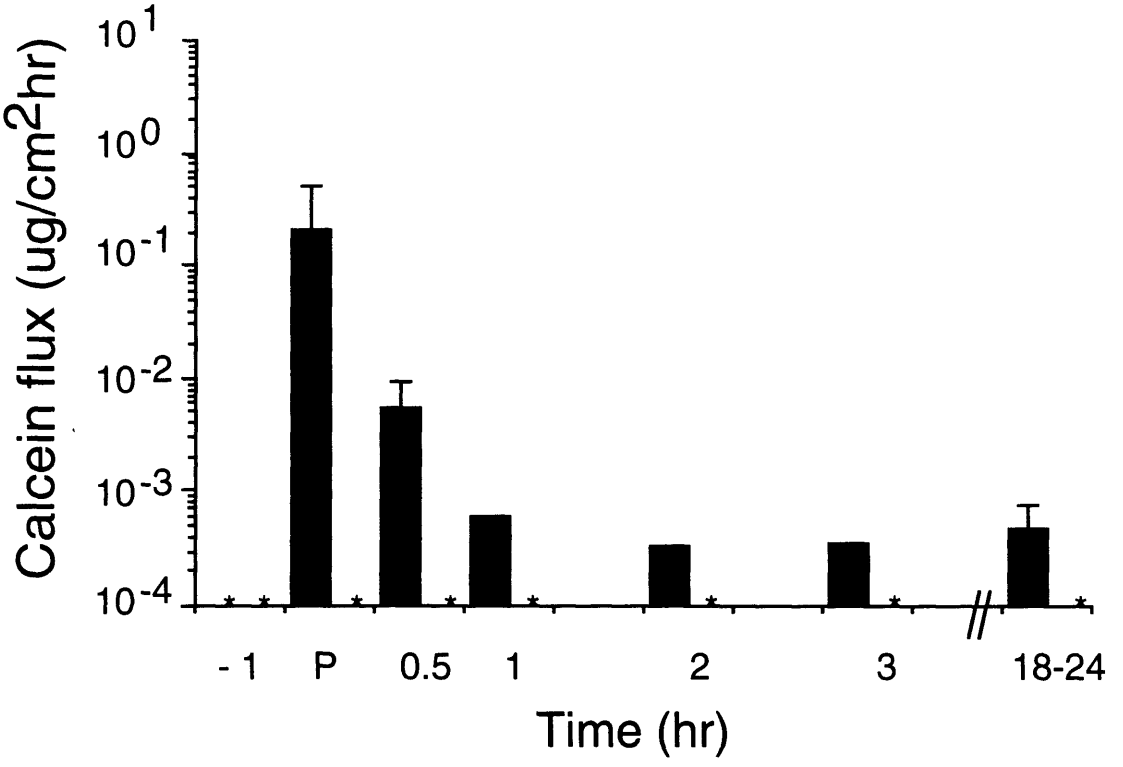


**Fig. 10-1B.** Transdermal flux of calcein before, during, and after "forward" pulsing (■) and "reverse" pulsing (▨) at 90 V. See caption for Fig. 10-1A for explanation and discussion.

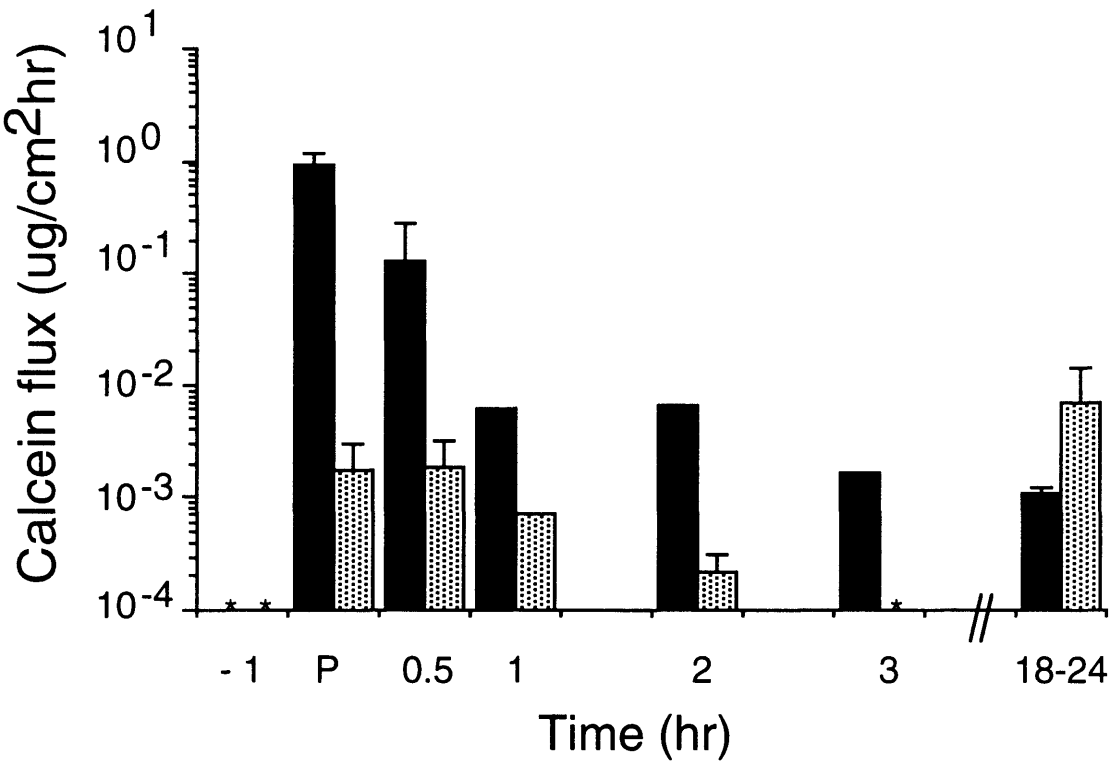


**Fig. 10-1C.** Transdermal flux of calcein before, during, and after "forward" pulsing (■) and "reverse" pulsing (▨) at 165 V. See caption for Fig. 10-1A for explanation and discussion.

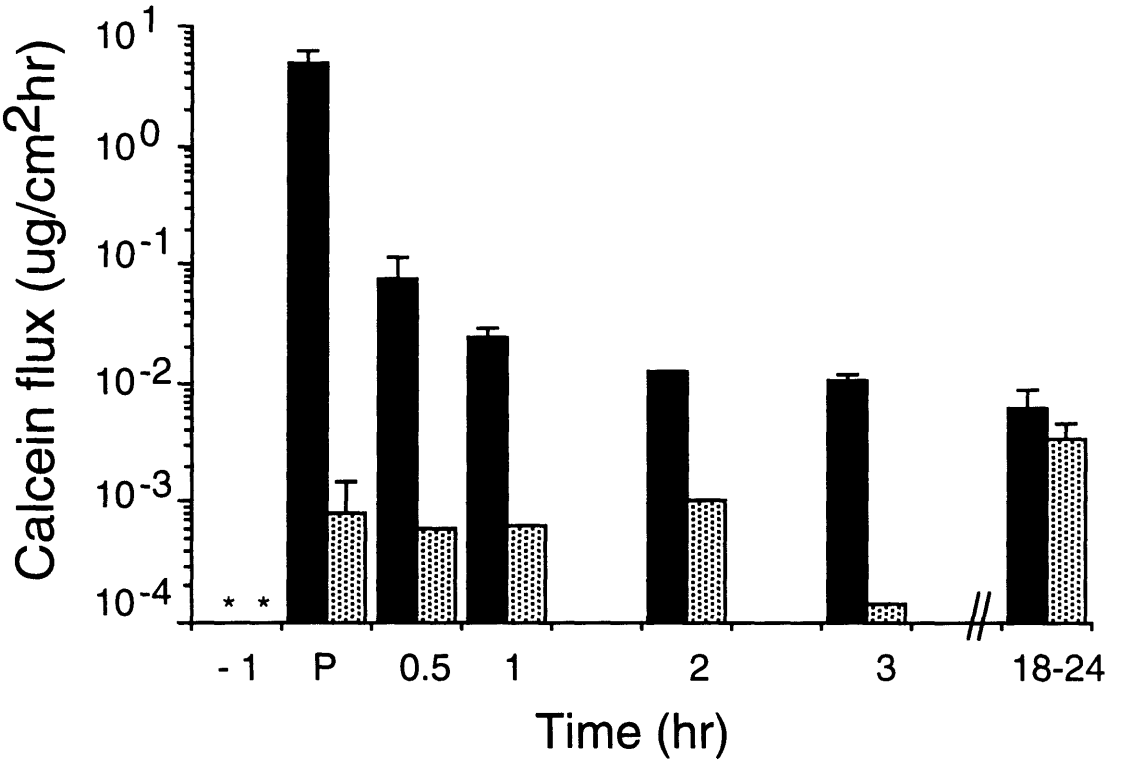


**Fig. 10-1D.** Transdermal flux of calcein before, during, and after "forward" pulsing (■) and "reverse" pulsing (▨) at 300 V. See caption for Fig. 10-1A for explanation and discussion.

before, during, and after pulsing at representative voltages. Fluxes before pulsing were below the detection limit (imposed by background fluorescence), while fluxes during pulsing were up to 10,000-fold greater. Fig. 10-2 shows that flux increased nonlinearly with increasing pulse voltage, i.e. the flux increased strongly with increasing voltage below ~100 V and increased weakly with increasing voltage at higher voltages. Supporting electrical measurements also showed increases in skin conductance of one to three orders of magnitude [Bose, 1994; Pliquett and Weaver, submitted, a].

Second, reversibility was assessed. Following electrical pulsing for 1 h, transdermal fluxes generally decreased by ~90 % within 30 min. and > 99 % within 1 - 2 h, consistent with significant reversibility. Electrical conductance measurements also showed recovery [Bose, 1994; Pliquett and Weaver, submitted, a]. However, elevated post-pulsing fluxes could be caused not only by irreversible alterations of skin structure, but also by the efflux of calcein "loaded" into the skin during high fluxes caused by pulsing.

The results of an additional, and possibly better, test of reversibility are also shown in Figs. 10-1 and 10-2: skin was pulsed with the electrode polarity reversed, leaving the transtissue voltage magnitude during pulsing the same. However, the reverse-polarity electrophoretic driving force associated with the pulse should have moved calcein away from the skin, significantly reducing transdermal transport during pulsing. By measuring fluxes ~1 h after such reverse-pulsing, long-lived changes in skin permeability can be assessed independently (Fig. 10-2). These data suggest that pulses ≤100 V caused no detectable long-lived changes in skin permeability. However, higher voltage pulses appear to have caused lasting changes. Fig. 10-2 also suggests that a transition region may exist at ~100 V, below which flux increased as a strong

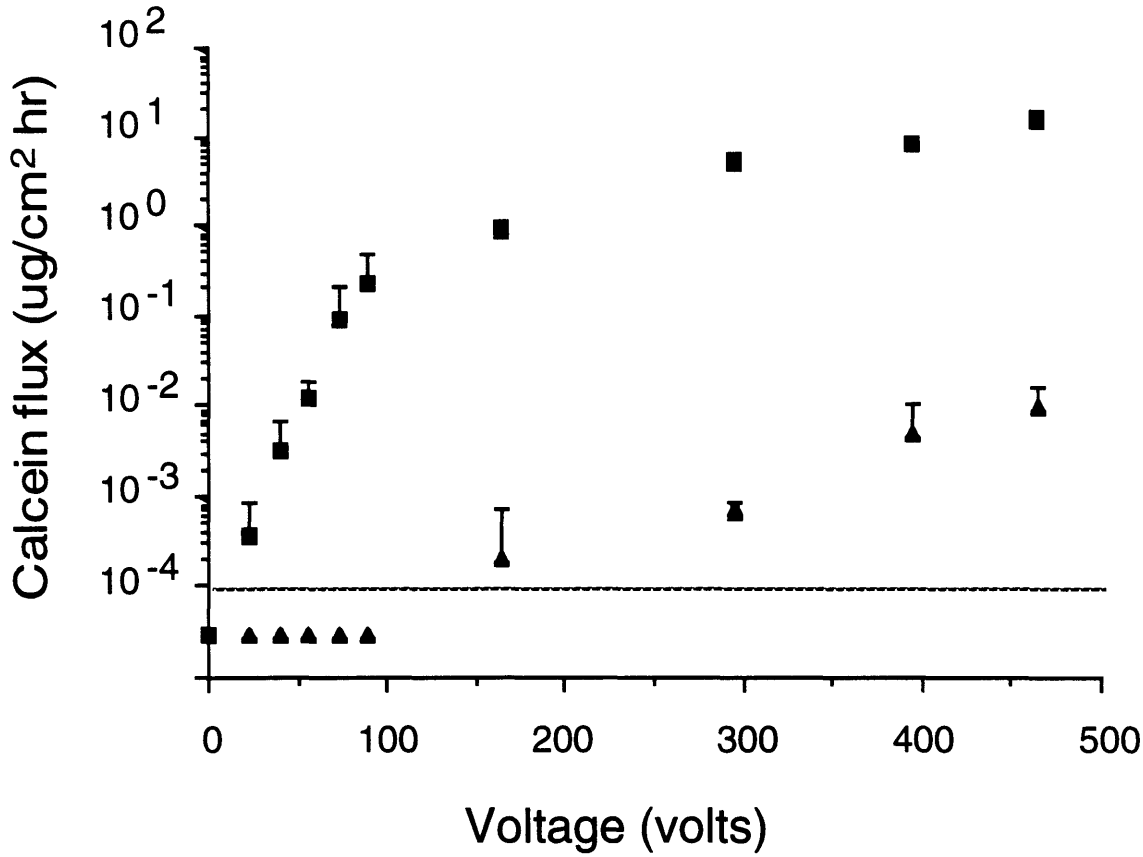


**Fig. 10-2.** Transdermal flux of calcein due to exposure of human skin to different electrical conditions. Calcein flux during application of "forward-polarity" pulses (■) and approximately 1 h after pulsing in the "reverse" direction (see text) (▲). This figure suggests that a transition point may exist at approximately 100 V, below which flux increases as a strong function of voltage and flux increases are reversible, and above which flux increases only weakly with voltage and effects are only partially reversible. Each point represents the average of 3 - 7 skin samples, from 2 - 4 different subjects. Standard deviation bars are shown. Fluxes below the calcein flux detection limit are indicated below the dashed line.

function of voltage and flux increases were reversible, and above which flux increased only weakly with voltage and effects were only partially reversible. The exact mechanism underlying this transition is presently unclear. However, for medical applications, it is potentially important that up to 1000-fold flux increases which appear to be fully reversible can be achieved using pulses below ~100 V. The longer-lived changes associated with up to 10,000-fold flux increases may limit application of higher-voltage electroporation.

Third, changes in skin structure cannot be expected to be revealed by microscopy, for reasons discussed below. However, demonstrating that increased fluxes caused by pulsing cannot be explained by electrophoresis alone suggests that changes in skin structure are necessary to explain our results. We therefore compared fluxes caused by low-duty-cycle high-voltage pulsing to fluxes caused by the continuous low-voltage dc current which would provide the same total electrophoretic transport contribution if no changes in skin structure occurred. For example, if the skin were unaltered (i.e., same conductance), then constant application of 0.1 V would transfer the same amount of charge across the skin as the pulsed application of 500 V for 1 ms every 5 s, making these conditions "equivalent" electrophoretically. As seen in Fig. 10-3, application of continuous voltages caused fluxes three orders of magnitude smaller than pulsing under "equivalent" conditions, suggesting that skin structural changes are needed to explain these results. Moreover, Fig. 10-1 indicates that during reverse-pulsing, transdermal flux increased, even though the electrophoretic driving force should have moved calcein away from the skin. This also suggests that structural alterations in the skin occurred.

To appropriately characterize electroporation, we believe that measurement of changes in molecular flux and electrical properties is the best approach,

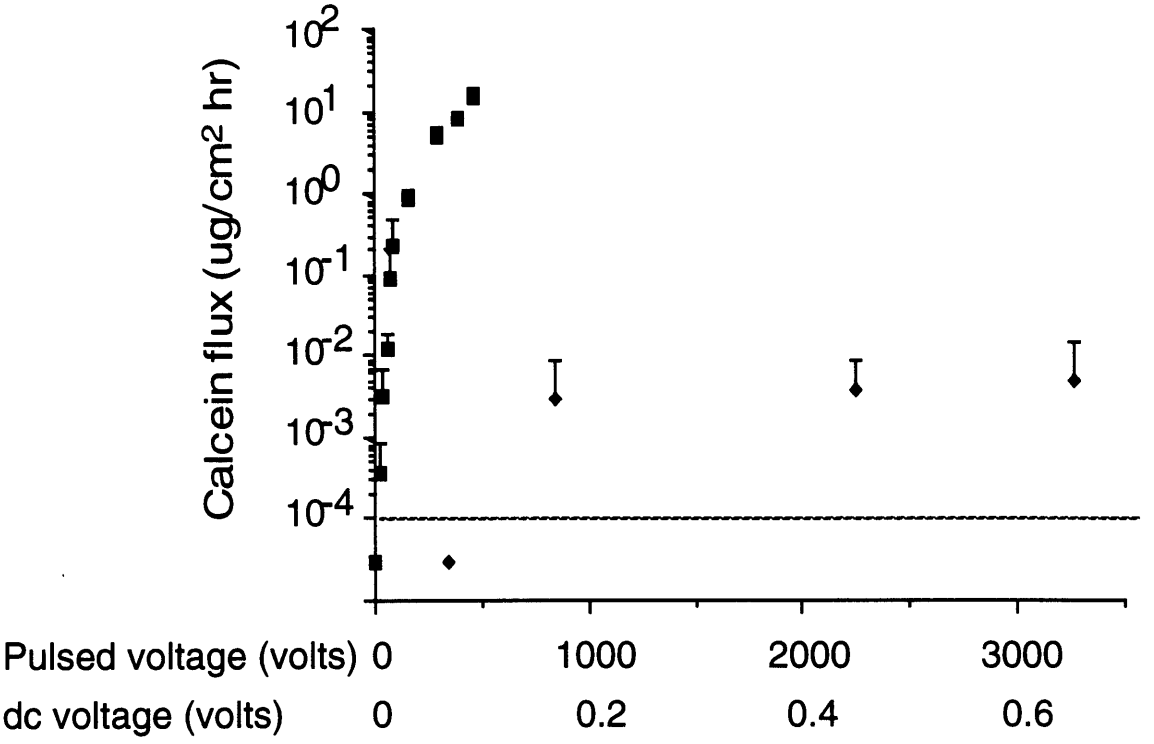


**Fig. 10-3.** Transdermal flux of calcein during pulsing (■) and during application of dc iontophoresis (◆). Upper axis indicates pulsing voltages electrically "equivalent" to continuous dc voltages on lower axis (see text), suggesting that skin structural changes may be needed to explain the high fluxes caused by electroporation. Each point represents the average of 3 - 7 skin samples, from 2 - 4 different subjects. Standard deviation bars are shown. Fluxes below the calcein flux detection limit are indicated below the dashed line.

because these measures are widely used in the electroporation literature. Upon initial consideration, electron microscopy might also appear to be an appropriate tool for visualizing the pores created by electroporation. However, there currently exist no satisfactory electron micrographs of electropores in any membrane, primarily because electropores are believed to be small (< 10 nm), sparse (< 0.1% of surface area), and generally short-lived (μs to s). Thus, visualization of electropores by any form of microscopy is not expected [Weaver, 1993a]. Moreover, although the name electroporation suggests the creation of physical pores, all that has been experimentally established is that transiently elevated transport and electrical conductance occur. We therefore did not employ electron microscopy to look for pores in the complex multilaminate structures of the skin, as they have not been imaged in simpler systems.

Enhanced transport of two other polar molecules across the skin was achieved by electroporation: Lucifer Yellow (457 Da, -2 charge) and an erythrosin derivative (1025 Da, -1 charge), a small macromolecule, neither of which normally crosses skin at detectable levels. These molecules were selected because they are fluorescent and have different physical properties than calcein. As seen in Fig. 10-4, pulsing can cause fluxes of both molecules similar to those caused for calcein under the same conditions. This suggests that electroporation-enhanced transport may be broadly applicable to many molecules, possibly including those of larger molecular weights.

Finally, electroporation in vivo was performed on anesthetized hairless rats. Using protocols similar to those employed in vitro, electroporation at voltages ranging from 30 to 300 V caused transport of 10 - 20 $\mu g/cm^2h$ (Fig. 10-5). No calcein was detected in the serum of unpulsed rats. That the in vivo fluxes did not increase with voltage suggests that a rate-limiting step other than transport

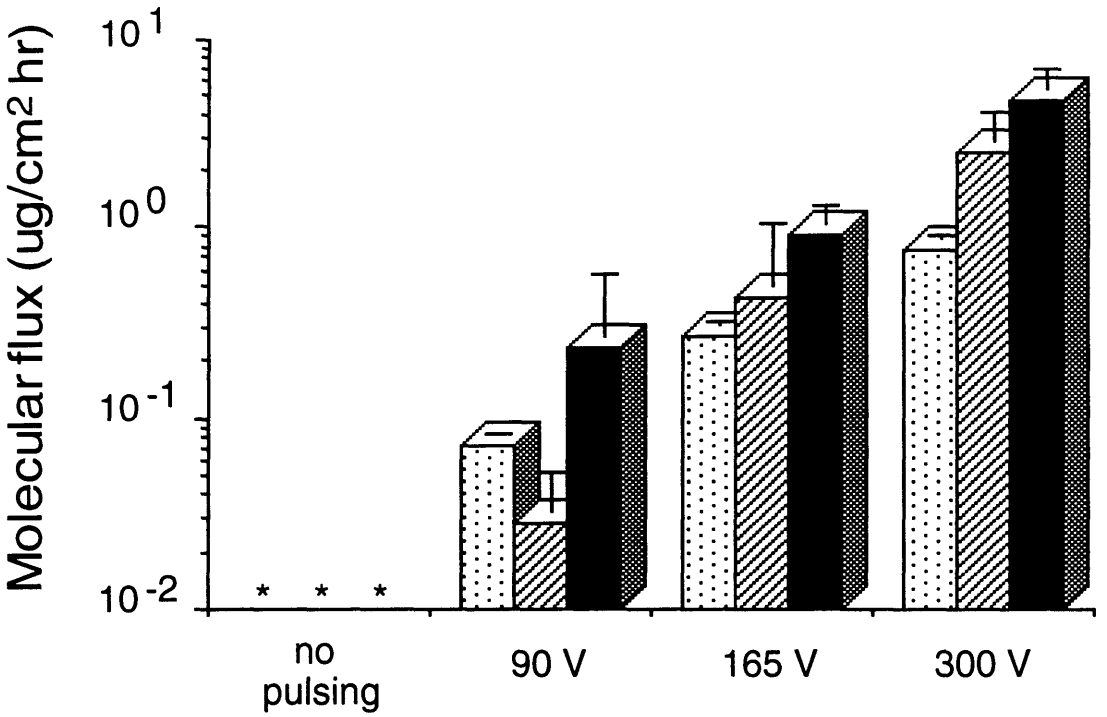


**Fig. 10-4.** Transdermal flux of (▨) an erythrosin derivative (1025 Da, -1 charge), (▨) Lucifer Yellow (457 Da, -2 charge), and (■) calcein across human skin. This figure demonstrates that electroporation increases the flux of a number of polar molecules having different molecular characteristics. Each point represents the average of 3 - 7 skin samples, from 2 - 4 different subjects. Standard deviation bars are shown. The (*) symbol indicates a flux below the detection limit: order $10^{-2}$ μg/cm$^2$ h for the erythrosin derivative and order $10^{-3}$ μg/cm$^2$ h for Lucifer Yellow.

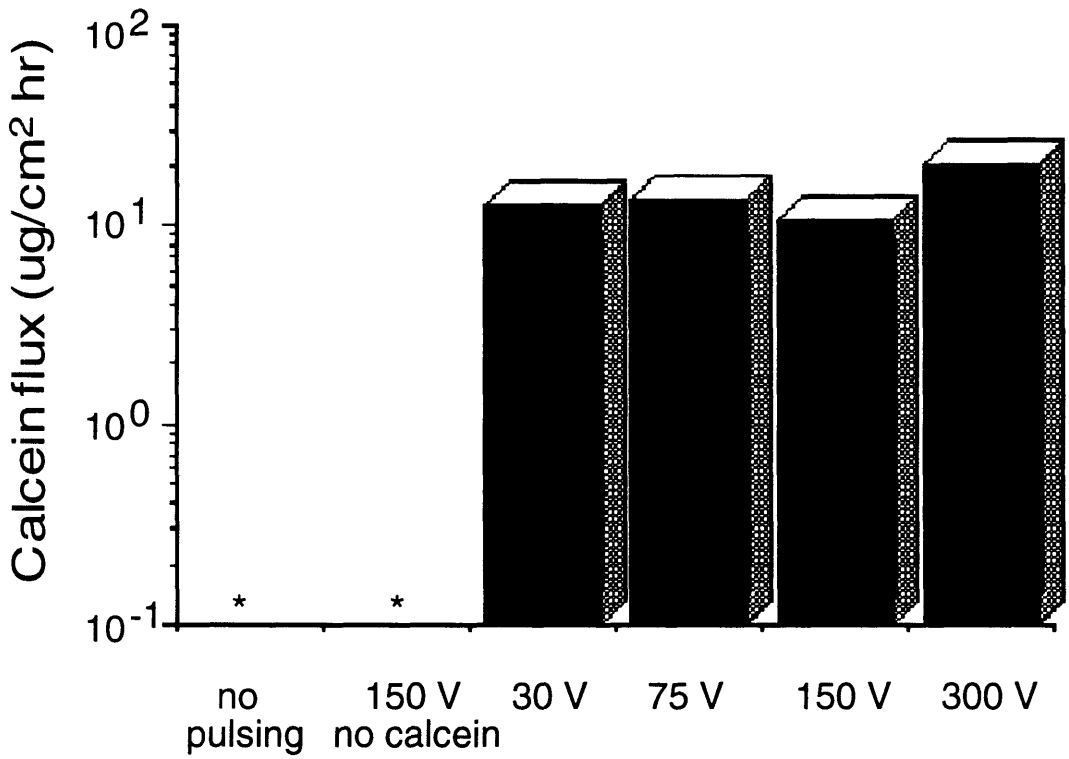


**Fig. 10-5.** Transdermal flux of calcein across hairless rat skin *in vivo*, which suggests that electroporation can increase transdermal flux in a living animal. Each point represents the average result from 1 - 2 rats. The (*) symbol indicates a flux below the detection limit of order $10^{-1}$ $\mu g/cm^2$ h.

across the stratum corneum existed, perhaps uptake of calcein from a skin depot into the bloodstream. No visible skin damage was observed after pulsing at voltages below 150 V; erythema and edema were evident at higher voltages (see Chapter 6). Long term biochemical and pathological studies are needed.

Together these results have implications for understanding mechanisms and for applications to transdermal drug delivery. First, the three characteristic features of electroporation were found in pulsed skin, suggesting that electroporation is the mechanism of flux enhancement. Moreover, for applications, the marked flux increases which are reversible over a range of voltages could make possible the therapeutic delivery of many drugs across skin.

## 10.3 Discussion

### 10.3.1 Mechanisms And Interpretations

It is well established that the stratum corneum is the primary barrier to transdermal transport [Bronaugh and Maibach, 1989; Champion et al., 1992; Cullander and Guy, 1992; Hadgraft and Guy, 1989]; thus, our interpretation is that changes in the stratum corneum account for the observed increases in flux due to electroporation. Although studied mainly in the context of living cells, electroporation has also been widely investigated in artificial planar bilayer membranes and liposomes [Abidor et al., 1979; Chang et al., 1992; Neumann et al., 1989; Orlowski and Mir, 1993; Tsong, 1991; Weaver, 1993b]. Because electroporation is a physical process based on electrostatic interactions and thermal fluctuations within fluid membranes, no active transport processes are involved [Chang et al., 1992; Neumann et al., 1989; Orlowski and Mir, 1993; Tsong, 1991; Weaver, 1993b]. Thus, electroporation could occur in the stratum corneum, even though it does not contain living cells.

"Proving" that electroporation occurs in skin is difficult. In the literature, electroporation has been described experimentally as (1) characteristic behavior (e.g., very large increases in molecular transport and conductance in lipid bilayers) (2) occurring at characteristic voltages (e.g., approximately 1 V across a bilayer) and (3) over characteristic times (e.g., sub-microsecond onset and biphasic recovery over milliseconds and minutes). Although there are plausible mechanisms by which these events occur (e.g., creation of aqueous pores, called electropores), these mechanisms are hypotheses; electropores have not been experimentally observed by imaging. Therefore, an experimental investigation of skin electroporation should establish whether phenomena similar to those observed in cell electroporation occur in skin as well.

The above experiments demonstrate very large increases in transdermal flux, which are reversible over a range of conditions and appear to be associated with structural changes. These results were seen with three different molecules having molecular masses up to slightly more than 1000 Da. Similar results were observed in vivo with animal skin. Electrical analysis has shown dramatic electrical changes occurring within 1 μs and recovery with millisecond and second to minute time constants [Bose, 1994; Pliquett and Weaver, submitted, a]. Our interpretation is that these experimental results exhibit the characteristic behavior of electroporation. We therefore conclude that electroporation of skin has occurred.

### 10.3.2 Applications

Although electroporation causes large flux increases across stratum corneum, deeper viable tissue may be essentially unaffected. This localization is expected because the stratum corneum has a much higher electrical resistance than other

regions of the skin. As a result, an electric field applied to the skin will concentrate in the stratum corneum, resulting in other, viable tissues being exposed to much lower fields. Therefore, an electric field sufficient to cause electroporation could exist in the stratum corneum, while a significantly lower field exists in viable tissues, insufficient to cause electroporation. An implicit targeting mechanism results, where the greatest electric fields are generated where the largest resistivities exist, thereby protecting the already-permeable viable parts of the skin and deeper tissues.

It is presently difficult to state with certainty which electrical conditions will be acceptable for clinical use. Many features, including pulse voltage/current/energy, pulse length, pulse frequency, duration of total exposure, and electrode size, site, and design, will be important. A complete consideration of the safety of electroporation of skin is beyond the scope of this study. However, that the electrical exposures used were fully reversible over a range of voltages is a strong indication that the procedure is not damaging and may be safe. Moreover, there exists a clinical precedent for safely applying electric pulses to skin with voltages up to hundreds of volts and durations up to milliseconds. Such diagnostic and therapeutic applications include transcutaneous electrical nerve stimulation, functional electrical stimulation, electromyography, and somatosensory evoked potential testing [Reilly, 1992; Webster, 1988].

Because of the stratum corneum's overall hydrophobic character and net negative charge, transdermal transport of negatively-charged hydrophilic molecules is especially challenging [Bronaugh and Maibach, 1989; Champion et al., 1992; Cullander and Guy, 1992; Hadgraft and Guy, 1989]. Calcein, with eight charge sites and a net charge of -4 [Furry, 1985], is therefore considerably more

difficult to transport across the skin than many other molecules. Approaches to transdermal flux enhancement involving chemical enhancers have been successful with some lipophilic and moderately polar molecules, but limited in applicability to highly polar and charged molecules. Iontophoresis has been successfully employed with some polar and charged molecules. For many drugs, delivery rates in the $\mu g/cm^2h$ range could be therapeutic, while significantly higher rates of delivery may be required for other drugs. In general, a 10-fold increase in flux caused by an enhancement method is impressive, while a 100-fold increase is of great interest. Thousand-fold increases are rarely found. The up to ten thousand-fold increases in flux caused by electroporation are therefore potentially very significant and could make possible transdermal delivery of many drugs at therapeutic levels.

Finally, transdermal flux enhancement has been demonstrated with other techniques, including chemical, iontophoretic, and ultrasonic methods. Because electroporation is mechanistically different, involving temporary alterations of skin structure, it could be used in combination with these or other enhancers. Together, these results suggest that electroporation of skin occurs and may be useful to enhance transdermal drug delivery.

## 10.4 Conclusions

Mammalian skin owes its remarkable barrier function to its outer-most and dead layer, the stratum corneum. Transdermal transport through this region occurs predominantly through intercellular lipids, organized largely in bilayers. Electroporation is the creation of aqueous pores in lipid bilayers by the application of a short (μs, ms) electric pulse. Our measurements suggest that electroporation occurs in the intercellular lipid bilayers of the stratum corneum by

a mechanism involving transient structural changes. Flux increases up to four orders of magnitude are observed with human skin in vitro for three polar molecules having charges between -1 and -4 and molecular weights up to more than 1000 Da. Similar flux increases have been observed in vivo with animal skin. Moreover, theoretical consideration suggests that a mechanism involving electroporation may be responsive for these effects. These results may have significance for drug delivery and other medical applications.

# 11 Theoretical Analysis of Enhanced Transdermal Transport By Skin Electroporation [15]

## 11.1 Introduction

The oral administration of many drugs is prevented by significant degradation in the stomach, intestine and liver [Langer, 1990]. While injections may reduce these effects, parenteral delivery is invasive and generally unpleasant. An attractive alternative to conventional methods is drug delivery across the skin, a noninvasive, user-friendly approach which reduces degradation by the stomach, intestine and liver [Bronaugh and Maibach, 1989; Hadgraft and Guy, 1989]. However, transdermal drug delivery is presently limited. Few drugs are able to cross the skin at therapeutic rates, due to the remarkable barrier properties of the skin's outermost, dead layer, the stratum corneum. The stratum corneum is composed of flattened cells (corneocytes) separated by narrow regions of intercellular lipids, arranged largely in bilayers [Bouwstra et al., 1991; Elias, 1991]. Corneocytes are usually considered to be impenetrable, forcing drugs to cross the stratum corneum through the intercellular lipids.

Recently, a novel transdermal drug delivery approach, believed to involve electroporation of stratum corneum lipids, has been shown [Bommannan et al., 1993; Prausnitz et al., 1992; Prausnitz et al., 1993a] to dramatically increase drug transport across the skin. This phenomenon is believed to be distinct from the more commonly observed phenomenon of skin iontophoresis [Bronaugh and Maibach, 1989; Cullander and Guy, 1992; Hadgraft and Guy, 1989], whereby molecules are forced by application of an electric field through existing aqueous pathways of the skin.

---

[15] This chapter was written in collaboraion with David Edwards and has also been reported in [Edwards et al., submitted].

Electroporation involves the formation of transient aqueous pathways in lipid bilayers by the application of a brief electric field pulse [Chang et al., 1992; Neumann et al., 1989; Orlowski and Mir, 1993; Weaver, 1993b]. This phenomenon occurs when the voltage across a lipid bilayer reaches approximately 0.5 to 1 V for short pulses [Abidor et al., 1979; Weaver and Barnett, 1992]. Typical electrical exposures last 10 $\mu$s to 10 ms. Electropores are thought to be created on the sub-microsecond time scale and, under reversible conditions, to disappear over time scales ranging from milliseconds to hours. Electroporation has been demonstrated in many different mammalian, plant, yeast, bacterial and other cells, as well as in artificial planar and spherical membranes [Chang et al., 1992; Neumann et al., 1989]. It has found application as a method of introducing DNA into cells for gene transfection in vitro [Chang et al., 1992; Neumann et al., 1989] and, more recently, for transporting drugs into tumor cells for improved chemotherapy in vivo [Mir et al., 1991b; Okino and Mohri, 1987; Salford et al., 1993].

This study seeks to determine if there is theoretical evidence supporting the electropore origin of skin electroporation. Transport of charged species through the skin is described on the basis of a recently derived theory [Edwards and Langer, in press], by considering three routes of transport through the skin (i.e., 'intercellular', 'shunt' and 'transcorneocyte' pathways). Predictions based upon the shunt route of transport are found to agree with iontophoretic data at low electric field strengths, whereas transcorneocyte route predictions agree with experimental data at high electric field strengths. These results are shown to be consistent (qualitatively as well as quantitatively) with single lipid bilayer electroporation at high electric field strengths.

## 11.2 Theory

### 11.2.1 Iontophoresis Vs. Electroporation

Experimental evidence [Cullander, 1992; Phipps and Gyory, 1992] suggests that the transport of charged molecules through the stratum corneum in the presence of electric fields typical of iontophoresis occurs via pre-existing pathways, viz. either a 'shunt' (hair follicle and sweat duct) route or an intercellular route between corneocytes. This conclusion is supported by theoretical considerations as well [Edwards and Langer, in press; Kasting, 1992]. However, if a suitably large electric field is applied across the skin, new, perforating pathways through the intercellular lipid bilayers (and possibly through the corneocytes as well) may be created via bilayer electroporation.

An estimation of the transdermal voltage $\Delta\bar{V}$ necessary to electroporate lipid bilayers within the stratum corneum may be made upon assuming lipid bilayers to be simple voltage dividers. That is, the voltage $\Delta\bar{V}$ across the skin is taken to be the sum total of the individual voltage drops across the stratum corneum's lipid bilayers. Given that there exist approximately 100 lipid bilayers between the upper and lower surfaces of the stratum corneum [Elias, 1991], and that electroporation of single bilayers occurs at a transbilayer voltage of approximately 1V [Abidor et al., 1979; Weaver and Barnett, 1992], we have that

$$\Delta\bar{V} << 100 \text{ V} \qquad \text{skin iontophoresis} \tag{1}$$

typifies the transdermal voltage for which charged molecules may be expected to follow the standard intercellular and/or shunt routes of transport through the skin, whereas

$$\Delta\bar{V} > 100 \text{ V} \qquad \text{skin electroporation} \tag{2}$$

characterizes the conditions for which electroporation of lipid bilayers may be expected to occur, possibly resulting in a transcorneocyte route of transport.

In the remainder of this paper, theoretical expressions are developed for the transdermal flux of charged solute molecules in the low field-strength conditions of standard skin iontophoresis [cf. Eq. (1)] and in the high field-strength conditions of skin electroporation [cf. Eq. (2)]. We begin by presenting general expressions for transdermal solute flux in terms of effective transport properties of the skin.

### 11.2.2 Transdermal Flux Formulas

The steady-state, time-average, one-dimensional solute flux across the stratum corneum may be expressed as [Edwards and Langer, in press]

$$\langle \bar{J} \rangle = \frac{1}{T} \int_0^T \bar{J} dt \approx \bar{K}_1 \langle \bar{U}^* \rangle \bar{C}_1, \tag{3}$$

assuming transport by diffusion is negligible. These conditions are typical of electric-field mediated transport of charged molecules across the skin [Phipps and Gyory, 1992; Kasting, 1992]. Here, $\bar{J}$ is the solute flux normal to the skin surface, $T$ the time period of any oscillatory process, $\bar{K}_1$ the skin/donor-solution equilibrium partition coefficient, $\bar{U}^*$ the mean solute velocity component normal to the skin surface (with $\langle \bar{U}^* \rangle$ its time average), and $\bar{C}_1$ the time-independent solute concentration in the donor compartment. The receptor solute concentration is taken to be zero.

In the absence of convection (i.e. mean, electric-field drift),

$$\langle \bar{U}^* \rangle = 0, \tag{4}$$

the diffusive contribution to $\langle \bar{J} \rangle$, which is neglected in Eq. (6), predominates, and the time-average, steady-state flux of solute is given by

$$\langle \bar{J} \rangle = \frac{1}{h} \bar{K}_1 \langle \bar{D}^* \rangle \bar{C}_1, \tag{5}$$

with $\bar{D}^*$ the effective dispersivity of the solute in the stratum corneum and *h* the stratum corneum thickness.

The formulas (3) and (5) may be used to offer predictions of steady-state, transdermal solute flux $\langle \bar{J} \rangle$ data in the presence of an electric field given expressions for the mean solute velocity $\bar{U}^*$ and dispersivity $\bar{D}^*$ in terms of the geometrical and physicochemical properties of the specific transdermal pathways. These expressions are summarized below for the cases of skin iontophoresis (intercellular/shunt pathway) and skin electroporation (transcorneocyte pathway).

### 11.2.3 Iontophoretic Transport Through Unaltered Tissue

At low electric fields [cf. Eq. (4)], the structure of intercellular lipids is assumed to be unaltered, and the transport pathways of charged molecules through the skin are taken to be the standard pre-existing intercellular and/or shunt routes. These pathways of transport have been discussed previously [Edwards and Langer, in press], where it was predicted that the mean, transdermal velocity of charged solute in the presence of an electric field appropriate to the combined intercellular and shunt routes of transport is given by[16]

$$\bar{U}^* \approx 0.02594 \left( \phi_{SH} + 0.042 H_W^1 \right) z \, \Delta\bar{V} \qquad (6)$$

Here, $\bar{U}^*$ is given in units of cm/s, $\phi_{SH}$ denotes the area fraction of shunt pathways relative to the total skin surface area (for the abdomen region of human skin, $\phi_{SH} \approx 2.7 \times 10^{-4}$: see [Edwards and Langer, in press]), and $H_W^1$ is a hydrodynamic hindrance factor characterizing hydrodynamic interactions

[16] It is important to emphasize that the numerical values appearing in Eq. (6) have been obtained [Edwards and Langer, in press] by use of estimates [principally those reported following Eq. (10)] for geometrical and physicochemical properties of the stratum corneum. They have not been fitted to the data in this study.

between the convecting molecule (of valence $z$) and the lipid head groups between which it convects in an applied electrical field. The transdermal voltage $\Delta\bar{V}$ is expressed in units of volts.

Intercellular and shunt routes are jointly considered in the preceding flux expression because both involve transport through the skin via aqueous pathways and each are accessed over a similarly small skin surface area fraction. The first term in Eq. (6) characterizes the flux through shunts. This route exhibits relatively large ($\mu$m-size) pathways. Thus, hydrodynamic hindrance is negligible; this is reflected implicitly in the first term of Eq. (6) by a hydrodynamic hindrance coefficient of unity. The second term accounts for hindered transport through the lipid head group channels of the intercellular route. The factor 0.042 appearing in the second term in parenthesis in Eq. (6) represents an inverse tortuosity for intercellular transport [Edwards and Langer, in press]. The tortuous pathway between corneocytes is only slightly reduced by the creation of pores in intercellular lipid bilayers, owing to the fact that the lateral corneocyte dimension (≈23 $\mu$m [Rougier et al., 1988]) is much larger than the spacing between corneocytes (≈0.05 $\mu$m [Scheuplein, 1978]). Thus, Eq. (6) can be used to describe intercellular transport during electroporation as well (as described in the next subsection).

A characteristic value for the thickness ($l_W$) of the bound-water layers between lipid head groups is 0.7 nm [Bouwstra et al., 1991]. Because the molecules (i.e., calcein) considered in comparisons with experimental data (presented below) possess a Stokes-Einstein diameter $2a$>0.7 nm [cf. the discussion following Eq. (13)], the hindrance coefficient $H_W^1$ appearing in Eq. (6) is expected to be negligibly small. Thus Eq. (6), with $\phi_{SH}$ =2.7×10–4, simplifies to

$$\bar{U}^* \approx 7.00 \times 10^{-6} z\, \Delta\bar{V}, \qquad (7)$$

characterizing the mean iontophoretic velocity of solute species through the hair follicles and/or sweat ducts. In this case, the solute partition coefficient, which accounts for area exclusion effects, is simply

$$\bar{K}_1 \equiv \phi_{SH} = 2.7 \times 10^{-4}. \tag{8}$$

Thus, Eq. (3) may be expressed as

$$\langle \bar{J} \rangle \approx 6.8 z \langle \Delta \bar{V} \rangle \bar{C}_1 \qquad (\text{nmol / cm}^2\text{ / h}), \tag{9}$$

with $\bar{C}_1$ given in units of mol/l.

### 11.2.4 Electrophoretic Transport Through Porated Tissue

For the electric-field conditions of Eq. (2), electroporation of intercellular lipid bilayers is assumed to permit transport of charged molecules across lipid bilayers and through the corneocytes of the stratum corneum. This pathway of transport is expected to predominate over the intercellular and shunt pathways since it is characterized by a significantly greater exposed surface area fraction than the latter pathways, which are essentially unaffected by the creation of electropores. Owing to the thinness of the intercellular regions relative to the thickness of corneocyte layers, electrophoretic transport of charged molecules is expected to be rate-limited by transport through the corneocytes, whence [Edwards and Langer, in press]

$$\begin{aligned} U^* &= \left[ \frac{(l_C + l_L)^2 (l_W + l_O)}{l_L (l_O + l_W \phi_L)\phi_C + l_C (l_W + l_O)\phi_L} \right] \\ &\quad \times \left[ \frac{(l_O + l_W \phi_L)\phi_L \phi_C H_L^{\dagger} H_C^{\dagger}}{l_C H_L^{\dagger} (l_O + l_W \phi_L)\phi_C + l_L H_C^{\dagger} (l_W + l_O)\phi_L} \right] \frac{zFD_W}{RT} \left( \frac{\Delta \bar{V}}{h} \right) \\ &\approx 0.012 H_C^{\dagger} z \, \Delta \bar{V}. \end{aligned} \tag{10}$$

Here, $l_L$ (≈0.05 $\mu$m [Scheuplein, 1978]) is the thickness of a single stratum corneum lamella, $l_C$ (≈1.0 $\mu$m [Scheuplein, 1978]) is the characteristic thickness

of a corneocyte, $l_O$ (≈ 5.8 nm [Bouwstra et al., 1991]) and $l_W$ (≈ 0.7 nm [Bouwstra et al., 1991]) are the respective thicknesses of the lipid bilayer and bound-water layers within intercellular lamellae, $\phi_C$ (≈0.5 [Campbell et al., 1977]) is the lateral area fraction of aqueous channels within the corneocytes, $\phi_L$ (≈$10^{-3}$ (see Chapter 12)) is the net area fraction of the lamellar layers accessible to ion transfer, $h$ (≈15 $\mu$m [Bouwstra et al., 1991]) is the thickness of the stratum corneum, $R$ is the gas constant, $T$ is the absolute temperature and $D_w \approx 10^{-5}$ cm$^2$/s is the free-volume diffusion coefficient of the transporting substance. The hindrance factors $H_C^1$, $H_L^1$ respectively characterize hydrodynamic hindrance coefficients in the aqueous channels of the corneocytes, and in the aqueous electropores in the lipid bilayers.

The effective dispersivity for the transcorneocyte route is given by [Edwards and Langer, in press]

$$\bar{D}^* = \left(\frac{zFR_C\Delta\bar{V}}{RTh}\right)^2 D_w H_W^3 \left(\frac{(l_w + l_o)(l_c + l_L)\phi_L}{l_L\phi_C(l_o + l_w\phi_L) + l_c\phi_L(l_w + l_o)}\right)^2$$
$$\approx \left[H_C^1 + 7.42 \times 10^{-6} H_C^3 (R_C z \Delta\bar{V})^2\right] \times 10^{-5}, \qquad (11)$$

in units of cm$^2$/s. Here, $R_C$ is the radius of corneocyte channels (see below) expressed in units of nm, $H_C^3$ is a convective-dispersion transport coefficient, which depends upon molecular size and shape and the dimensions of the aqueous channels of the corneocytes.

Aqueous channels within corneocytes can be characterized as circular cylinders of radius $R_C$. This idealization has frequently been used [Deen, 1987; Malone and Anderson, 1978; Frenkel, 1944] to characterize pore spaces within biological porous media as it allows explicit analytical expressions to be developed for the hindrance coefficients $H_C^1$, $H_C^3$. Characterizing solute

molecules as hard spheres (of radius *a*), allows the calculation of the hindrance factors introduced above by [Brenner and Edwards, 1993]

$$H_C^1 \approx \frac{1 - \frac{9}{8}\left(\frac{a}{R_C}\right)\ln\frac{R_C}{a} - 1.539\frac{a}{R_C}}{\left(1 - \frac{a}{R_C}\right)^2} \qquad (12\,a)$$

for small $a/R_C$,

$$H_C^1 \approx \left(\frac{1 - \frac{a}{R_C}}{\frac{a}{R_C}}\right)^{5/2} \qquad \left(\frac{a}{R_C} \to 1\right) \qquad (12\,b)$$

for large $a/R_C$, and

$$H_C^3 \approx \frac{\left(\frac{a}{R_C}\right)^2\left[0.158\ln^2\left(\frac{R_C}{a}\right) - 0.901\ln\left(\frac{R_C}{a}\right) + 1.385\right]}{\left(1 - \frac{a}{R_C}\right)^6}. \qquad (13)$$

For intermediate ratios of $a/R_C$ (i.e., $0.2 < a/R_C < 0.8$), $H_C^1$ can be determined by extrapolation, as shown in Fig. 2 of Mavrovouniotis and Brenner [1988].

The characteristic radius $R_C$ can be estimated upon noting that corneocytes are composed of cross-linked keratin fibers of radius ≈ 7 nm [Scheuplein, 1978] and contain approximately 50 % water when fully hydrated [Campbell et al., 1977]. Assuming a uniform distribution of keratin fibers within the corneocytes, $R_C \approx 1.8$ nm is found from the geometric relationship $[7\text{ nm} / (R_C + 7\text{nm})]^3 \approx 0.5$.

The Stokes-Einstein radius of calcein (the molecule principally examined in subsequent comparisons with experiments) is estimated[17] as $a \approx 0.6$nm. Assuming calcein molecules to be hydrated by a uniform layer of water

[17] Use of Lyderson's method [Lyderson, 1955] for estimating critical volumes suggests an estimate for the critical volume of calcein of $V_c \approx 1260$ cm$^3$/gmol. Combination of the Stokes-Einstein equation for a spherical particle together with the Wilke-Chang and Tyn-Calmus relations [Reid et al., 1977] permits the hydrodynamic radius *a* (in nm) to be related to the critical volume as, $a \approx 0.00683 V_c^{0.6288}$.

molecules (molecular diameter $\approx$ 0.2 nm), suggests a hydrated calcein radius of $a \approx 0.8$ nm. Thus, $a/R_C \approx 0.44$ and Eqs. (12) and (13) give

$$H_C^1 \approx 0.20, \qquad H_C^3 \approx 5.09,$$

such that Eqs. (10) and (11) furnish

$$\bar{U}^* \approx 0.0024\, z\, \Delta\bar{V}, \tag{14}$$

$$\bar{D}^* \approx \left[0.20 + 0.0001\left(z\,\Delta\bar{V}\right)^2\right] \times 10^{-5}. \tag{15}$$

The skin/donor compartment partition coefficient characterizing the transcorneocyte route is equivalent to the skin area fraction accessible to charged molecular transport during skin electroporation. Recent experiments involving skin electroporation (see Chapter 12) suggest a steady-state value for this calcein area fraction of

$$\bar{K}_1 \approx 10^{-3}, \tag{16}$$

for skin voltages satisfying Eq. (2). For transdermal voltages on the order of 100V or less, this value has been observed (Chapter 12) to diminish sharply with skin voltage, and to depend strongly on the size of the transporting substance.

It is interesting to observe that the partition coefficient (16) is consistent with theoretical predictions made for single bilayer electroporation [Freeman et al., in press]. These calculations suggest a maximum aqueous area fraction of $10^{-3}$, though the aqueous area fraction may be many orders of magnitude smaller than $10^{-3}$, depending upon factors such as voltage pulse duration and magnitude. However, given that direct experimental evidence of aqueous pore area fraction in single lipid bilayers is presently lacking, and that experimental studies of multilipid bilayer electroporation have not been reported in the literature, the precise physical state and kinetics of stratum corneum lipid bilayers during skin electroporation is not well enough understood to make a clear physical

interpretation of the partition coefficient value experimentally observed in Chapter 12 and shown in Eq. (16).

Upon combining Eqs. (14)–(16) with Eqs. (3) and (5) we have

$$\langle \bar{J} \rangle \approx 8.64 \times 10^3 z \langle \Delta\bar{V} \rangle \bar{C}_1 \qquad (\text{nmol} / \text{cm}^2 / \text{h}) \tag{17}$$

for convectively-dominated transdermal transport, and

$$\langle \bar{J} \rangle \approx 2.4 \times 10^4 \left[0.20 + 0.0001 \left\langle (z\,\Delta\bar{V})^2 \right\rangle\right] \bar{C}_1 \qquad (\text{nmol} / \text{cm}^2 / \text{h}) \tag{18}$$

in the conditions (4) of zero time-average convection.

For voltages characteristic of electroporation [cf. Eq. (2)], the dispersive flux (18) is much smaller in magnitude than the purely convective (i.e., electric-field drift) flux (17). This explains our neglect of the diffusional contribution in Eq. (17). Similarly, the diffusion contribution to the iontophoretic flux (9) is also negligible in conventional iontophoretic conditions.

## 11.3 Results

Here we compare theoretical predictions and experimental data for both small and large electric field strengths.

### 11.3.1 Small $\Delta\bar{V}$ : Iontophoresis.

In the experiments of Chapter 10, a continuous dc voltage was applied across human epidermis. In these conditions,

$$\langle \Delta\bar{V} \rangle = \Delta\bar{V} .$$

Calcein molecules (MW=623, $z$=–4) were placed in the donor compartment of an in vitro diffusion-cell apparatus at a concentration of $\bar{C}_1$ =1 mM. The transdermal flux of calcein was measured for 'small' transdermal voltages ( $\Delta\bar{V}$ <2V). For iontophoretic transport through unaltered tissue, Eq. (9) yields

$$\langle \bar{J} \rangle \approx 1.7 \times 10^{-2} \Delta \bar{V} \qquad (\mu \text{ g / cm}^2 \text{ / h}), \tag{19}$$

whereas for electrophoretic transport through porated tissue Eq. (17) gives

$$\langle \bar{J} \rangle \approx 2.5 \times 10^{1} \Delta \bar{V} \qquad (\mu \text{ g / cm}^2 \text{ / h}). \tag{20}$$

A comparison of the experimental data with the theoretical estimates based upon Eqs. (19) and (20) is made in Fig. 11-1. The shunt-route (nonporated) prediction (19) nearly matches the experimental data over most of the voltage range considered. In contrast, the porated (transcorneocyte) formula (20) overpredicts the transport of calcein by several orders of magnitude. This suggests that the hair follicle/sweat duct route is the most likely pathway for charged calcein transport through the skin, at least for $\Delta \bar{V} \leq 1$V. The poor correspondence between the shunt-route prediction (19) and the experimental data at the largest voltages examined (i.e., 2V), and, particularly, the nonlinear dependence of the experimental flux values versus voltage, might be explained by an increase in the number of shunt pathways accessible by the iontophoresed molecules with increasing voltage, as described by Scott *et al.* [1993].

### 11.3.2 Large $\Delta \bar{V}$ : Electroporation.

Transdermal calcein flux values were measured in a second set of experiments (Chapter 10) at significantly larger pulsed voltages (40V< $\Delta \bar{V}$ <500V) across human epidermis. The electric field pulses exponentially decayed with a time constant , $\tau$, of approximately 1 ms. One pulse was applied every $T$ = 5 s for one hour (corresponding to a duty cycle of 0.02%). In the present notation, these conditions correspond to

$$\langle \Delta \bar{V} \rangle = 2 \times 10^{-4} \Delta \bar{V} .$$

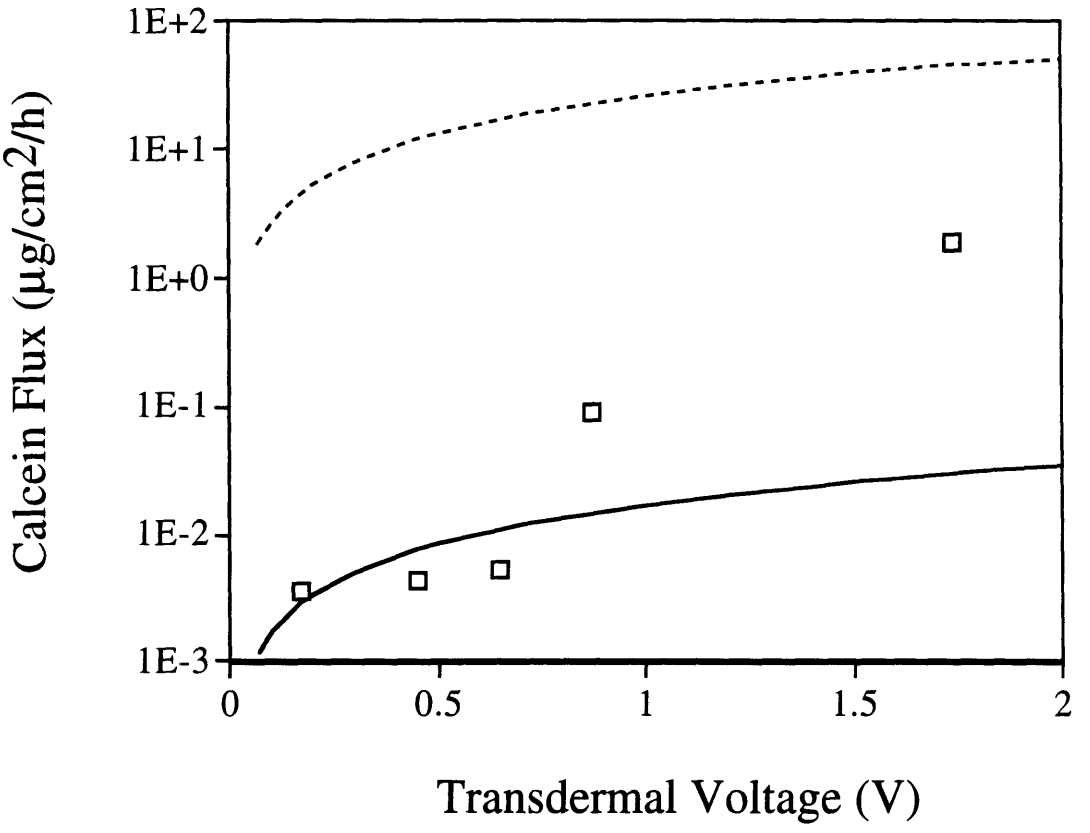


**Fig. 11-1.** Calcein flux versus transdermal voltage due to standard skin iontophoresis. Experimental data (□, from Fig. 10-3) are compared with theoretical predictions based on shunt-route (—, from Eq. 19) and transcorneocyte (- - - , from Eq. 20) formulas.

Equation (9) adopts the form

$$\langle \bar{J} \rangle \approx 3.4 \times 10^{-6} \Delta \bar{V} \qquad (\mu \text{ g / cm}^2 \text{ / h}) \qquad (21)$$

characterizing the flux of calcein associated with the shunt-route (nonporated) route of transport, whereas, Eq. (17) gives

$$\langle \bar{J} \rangle \approx 4.4 \times 10^{-3} \Delta \bar{V} \qquad (\mu \text{ g / cm}^2 \text{ / h}) \qquad (22)$$

characterizing transport through electroporated skin (transcorneocyte route).

Figure 11-2 provides a comparison of the theoretical estimates (21) and (22) with the experimental data. At the lowest voltages examined ( $\Delta \bar{V}$ <100 V), the data fall between the predictions based upon the shunt (nonporated) formula (21) and the porated (transcorneocyte) formula (22). However, as $\Delta \bar{V}$ increases beyond 100 V, predictions based upon the porated-route formula (22) match the experimental data. At the highest voltages, the transcorneocyte route underpredicts the experimental data. While this discrepancy may owe to many factors, as discussed in the following section, it may be significant that for transdermal voltages exceeding 100 V, irreversible damage to the skin was observed (Chapter 10). In general, however, the severalfold enhancement of charged molecule transport associated with the porated, transcorneocyte route of transport appears to offer evidence that pores were created in the intercellular bilayers and that a transcorneocyte (rather than an intercellular or shunt) route of transport is followed by the calcein molecules at the highest voltage drops shown in Fig. 11-2.

Further support of transcorneocyte transport through bilayers at high electric field strengths is provided by the comparisons made in Fig. 11-3. This figure supplements the calcein data of Fig. 11-2 with experimental data (shown in Chapter 10, collected under identical conditions) for Lucifer yellow (MW = 457, $z$ = -2) and an erythrosin derivative (MW = 1025, $z$ = -1). Attributing to each

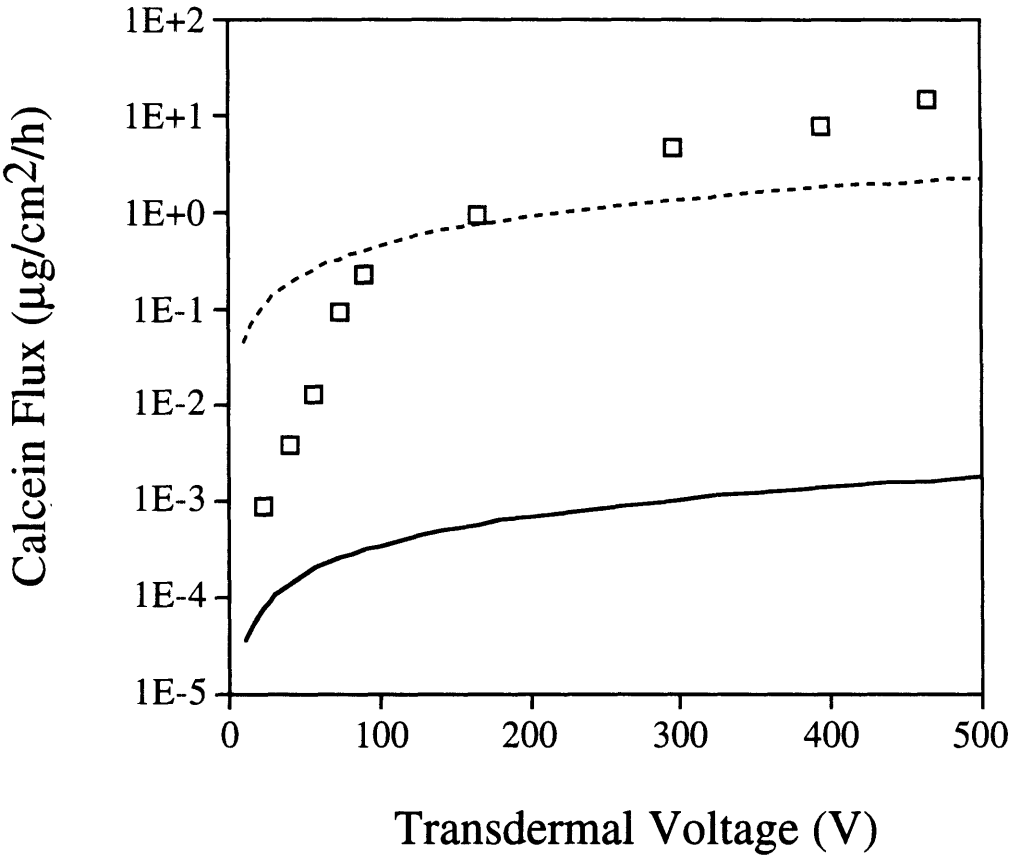


**Fig. 11-2.** Calcein flux versus transdermal voltage due to high field strength pulses believed to cause skin electroporation. Experimental data (□, from Fig. 10-2) are compared with theoretical predictions based on shunt-route (— , from Eq. 21) and transcorneocyte (- - - , from Eq. 22) formulas.

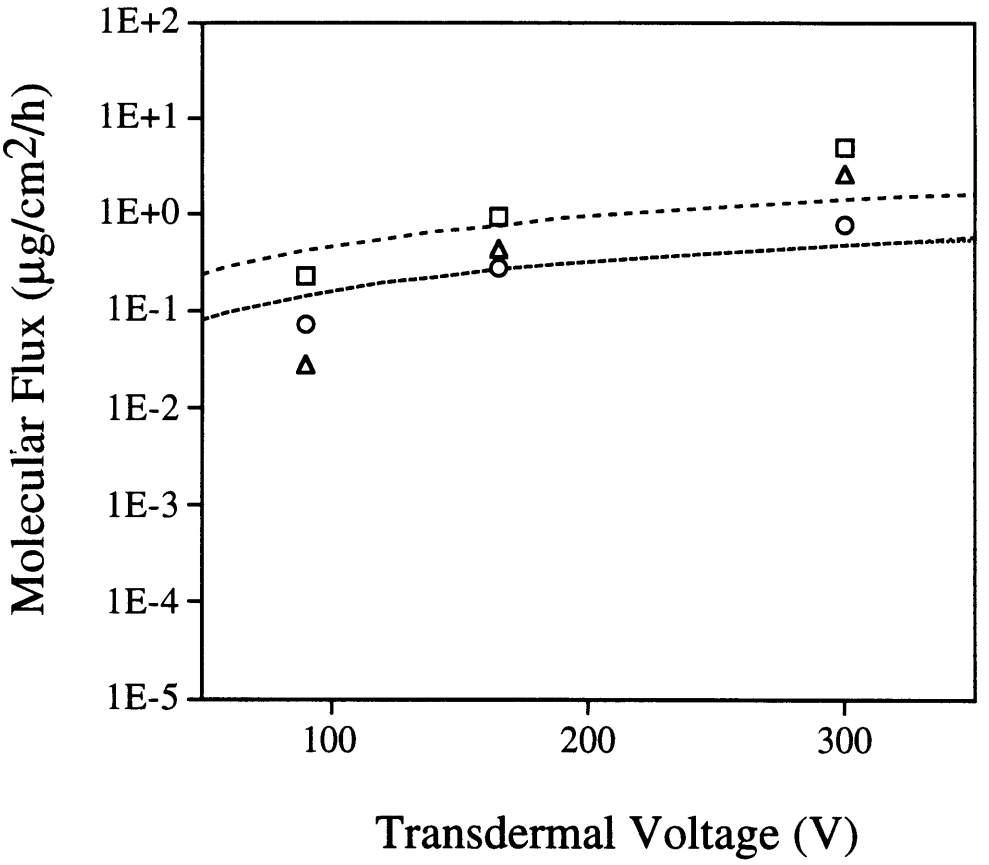


**Fig. 11-3.** Molecular flux for three different compounds versus transdermal voltage due to high field strength pulses believed to cause skin electroporation. Experimental data (from Fig. 10-4) are compared with theoretical predictions based on the transcorneocyte formula (from Eq. 23): calcein (□, - - -), Lucifer yellow (△, -·-·), and erythrosin derivative (○, ·····).

molecule its respective hindrance coefficient via Eq. (12) [for Lucifer yellow, $H_C^1 \approx 0.2$ ($a \approx 0.78$ nm); for the erythrosin derivative, $H_C^1 \approx 0.17$ ($a \approx 0.90$ nm)], Eqs. (3), (10) and (16) may be combined to give

$$\langle \bar{J} \rangle \approx \begin{cases} 4.4 \times 10^{-3} \Delta\bar{V} & \text{(calcein)} \\ 1.6 \times 10^{-3} \Delta\bar{V} & \text{(Lucifer yellow)} \\ 1.5 \times 10^{-3} \Delta\bar{V} & \text{(erythrosin derivative)} \end{cases} \quad (\mu \text{ g/cm}^2\text{/h}) \qquad (23)$$

characterizing the transport rates for the three different molecules according to the porated route through the stratum corneum. Predictions based upon the above equations are shown with the experimental data in Fig. 11-3. The convergence of experimental and theoretical results as $\Delta\bar{V}$ increases above 100 V is consistent with the comparisons made between theory and experiment in Fig. 11-2.

### 11.3.3 Large $\Delta\bar{V}$ (Alternating Polarity): Electroporation.

In Chapter 12, calcein flux was measured during skin electroporation due to electric field pulses, with $\tau \approx 1$ ms, $T = 5$ s, and $\bar{C}_1 = 1$mM, but with the polarity alternating from one pulse to the next (Fig. 12-1); thus,

$$\langle \Delta\bar{V} \rangle = 0.$$

These are the conditions of validity of Eq. (18); i.e., there is zero net convection [cf. Eq. (4)] across the skin. Even in the absence of net solute convection, a significant enhancement of transport was experimentally observed (see Fig. 11-4). This phenomenon cannot be explained in the standard electrophoresis (or electroosmosis) terms by which electric field enhancement of charged molecule transport across the skin has been explained in the past, since, on average, there is no net forced diffusion or convection.

For zero net skin convection, Eq. (18) gives

$$\langle \bar{J} \rangle \approx 3.0 \times 10^{-3} \left[ 0.20 + 0.0008 \Delta\bar{V}^2 \right] \quad (\mu \text{ g/cm}^2\text{/h}). \qquad (24)$$

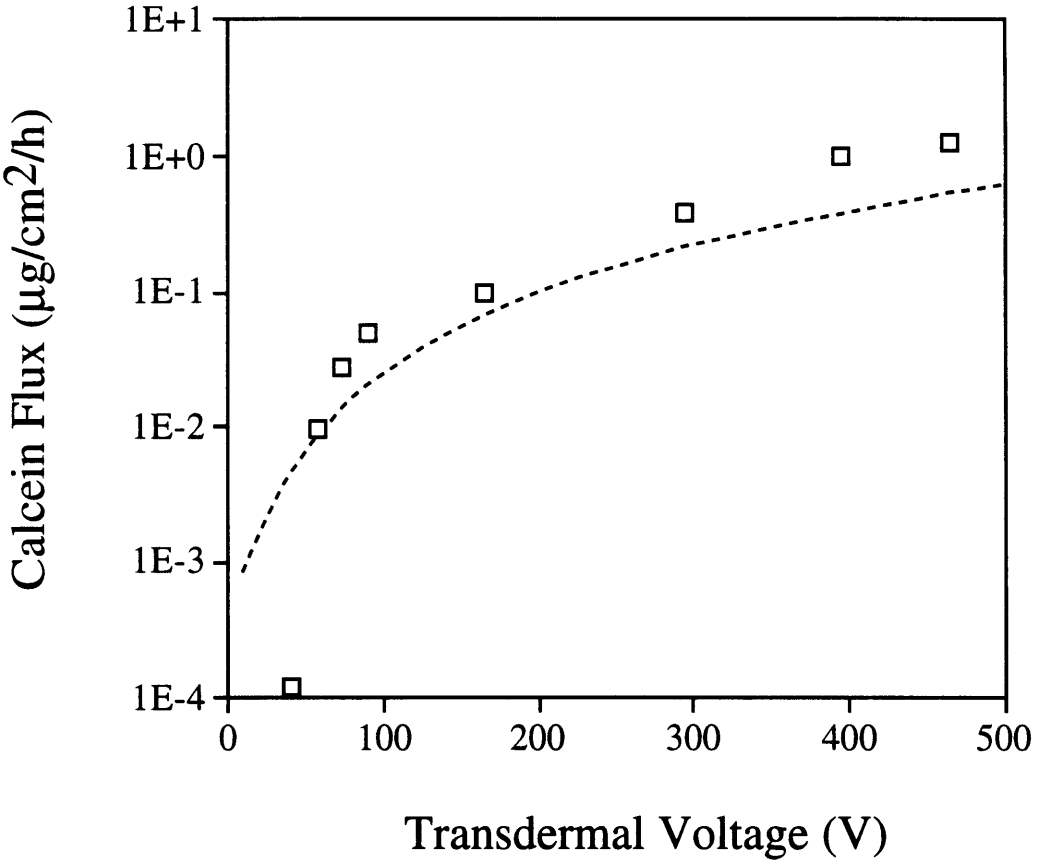


**Fig. 11-4.** Calcein flux versus transdermal voltage due to alternating-polarity, high field strength pulses believed to cause skin electroporation. Experimental data (□, from Fig. 12-1) are compared with theoretical predictions based on the transcorneocyte formula (- - - , from Eq. 24).

The first term in brackets identifies the contribution arising from the purely diffusive transport of calcein in the conditions of skin electroporation. This term is seen to be of order $10^{-4}$ $\mu g/cm^2/h$, the order of the sensitivity of the experimental measurements. The second term in brackets identifies a convective-dispersive contribution, quantifying the (oscillatory) convective enhancement of net solute 'diffusion'. This contribution remains even in an alternating electric field because it depends upon the square of the transdermal voltage. The physical origin of convective dispersion is further discussed in the following section.

Predictions based upon Eq. (24) are shown in Fig. 11-4 together with the experimental data. Very good agreement is found between the experimental data and the theoretical predictions for $\Delta\bar{V}$ >100 V. This appears to be strong evidence both for the validity of a porated, transcorneocyte route of transport in the conditions of Eq. (2) and for the occurrence of convective dispersion in the skin.

## 11.4 Discussion

The theoretical/experimental comparisons made in Figs. 11-1 to 11-4 strongly suggest that charged molecules follow different pathways through the stratum corneum below and above a transdermal voltage of approximately 100 V. At transdermal voltages significantly less than 100 V, transport of charged calcein appears to occur through nonporated skin via a shunt route (Fig. 11-1). However, for $\Delta\bar{V}$ >100 V, the comparisons made in Figs. 11-2 to 11-4 indicate that transport through porated intercellular bilayers and corneocytes is preferred, consistent with the known characteristics [cf. Eqs. (2) as well as Eq. (16)] of lipid bilayer electroporation.

Additional evidence for the electroporation of stratum corneum bilayers can be offered on the basis of the electrical properties of skin. It has been found [Edelberg, 1967; Inada et al., 1994; Kasting and Bowman, 1990; Stephens, 1963] that the specific electrical resistance of the skin exhibits a steady-state value of approximately 1,000–10,000 $\Omega$-cm$^2$ following application of a low-strength electric field for about one hour. In the high-strength conditions of Eq. (2), the skin's electrical resistance can diminish up to three orders of magnitude, to a value of approximately 10–100 $\Omega$-cm$^2$ [Bose, 1994; Pliquett and Weaver, submitted, a]. This drop in resistance is found to be consistent with the current analysis.

Thus, the electrical resistance of unaltered skin has been estimated as [Edwards and Langer, in press]

$$\bar{\rho} \approx 4000 \quad \Omega - \mathrm{cm}^2, \tag{25}$$

with ions transporting through intercellular and shunt routes. As previously [cf. Eq. (10)], if we assume $\phi_L = 10^{-3}$ for the stratum corneum area fraction accessible to ion transfer in electroporation conditions, a value that has been experimentally observed (Chapter 12), it follows that the transport of ions through electropores and corneocytes causes a reduction of the skin's electrical resistance to approximately [cf. Eq. (31b) of Edwards and Langer [in press]]

$$\bar{\rho} \approx 6 \quad \Omega - \mathrm{cm}^2. \tag{26}$$

Ths latter result is substantially lower than the experimental skin resistance data [Bose, 1994; Pliquett and Weaver, submitted, a] at high electric field strengths. A potential explanation for this underprediction is that the result (26) does not include hindrance effects arising in the transport of ions through electropores. However, the predicted diminution of skin resistance by several orders of

magnitude appears to lend further support to a transcorneocyte route of transport in skin electroporation circumstances.

The results of this study indicate that multiple lipid bilayers within the stratum corneum electroporate at conditions similar to those for which electroporation has been observed or predicted in single bilayer systems [Abidor et al., 1979; Chang et al., 1992; Neumann et al., 1989; Orlowski and Mir, 1993; Weaver, 1993b; Weaver and Barnett, 1992]. As in single bilayer systems, whether planar or spherical, electroporation of skin appears to give rise to a dramatic enhancement of transbilayer molecular flux, leading to pathways for molecular transport through the aqueous channels of the corneocytes.

The successful description of key features of electric-field mediated transdermal transport, based upon the physical characteristics of the stratum corneum and the transporting molecules, constitutes an essential step toward understanding the mechanisms of transport and optimizing experimental protocols. However, the physical and geometrical complexity of the stratum corneum, including its possible dependence upon applied (e.g., electric) fields, limits the scope of conclusions that may be drawn via each set of theoretical predictions until a broad range of experimental observations have been confirmed.

In the current study, experimental flux data at relatively low transdermal voltages ($\leq$ 1V) have been fairly well predicted (Fig. 11-1) on the basis of a shunt route of charged-molecule transport. Yet, the observed nonlinear dependence of molecular flux upon voltage is not predicted by the current theory. This may reflect the creation of new transport pathways through the skin with increasing applied voltage (as observed by Scott et al. [1993]). Nonlinear electrical

properties of skin above 1 V is well documented [Edelberg, 1967; Inada et al., 1994; Kasting and Bowman, 1990; Stephens, 1963].

Experimental transdermal flux values have been found (Fig. 11-2) to be approximated by theoretical predictions based upon an electroporated, transcorneocyte route of transport through the stratum corneum. However, the strong nonlinearities exhibited by the data over the entire range of voltages shown in Fig. 11-2 suggest a significant dependence of electropore area fraction upon voltage (a dependence not accounted for here), and perhaps irreversible skin damage at the very highest voltages. Moreover, Eqs. (10) and (11), which describe the transcorneocyte route of transport, apply to circumstances where transport across the intercellular lipids occurs relatively fast in comparison to transport across the corneocytes. It may occur, however, that at the intermediate voltages shown in Fig. 11-2, significant hindrance of transport across the intercellular lipids occurs, requiring modification of Eqs. (10) and (11).

Other approximations made in the theory, such as the idealization of circular cylindrical aqueous pores within corneocytes, may give rise to significant errors in conditions other than have been examined here. For example, very large molecules (i.e., $R_C > 1.8$ nm), may potentially transport across corneocytes during electroporation. However, our assumption of a uniform pore size in the corneocytes [see following Eq. (13)] would wrongly preclude this possibility because it does not account for the heterogeneous distribution of aqueous pathway dimensions within corneocytes.

One of the striking features of skin electroporation is the observation (Fig. 11-4) that a dramatic enhancement of charged species is possible even in the absence of a net transdermal voltage. This has been explained here by the convective dispersion of charged molecules within corneocytes—a phenomenon

that appears not to have been discussed previously in the context of transdermal transport.

Convective dispersion resulting from oscillating flow conditions have been observed in numerous practical capillary and porous media problems [Brenner and Edwards, 1993], such as human lungs (i.e., high-frequency ventilation schemes) [Fung and Sabin, 1977], abdominal cavities [Rudoy et al., 1987] and river estuaries [Fisher et al., 1979]. Physically, these phenomena occur because solute molecules instantaneously transport through porous media at significantly different rates depending upon their individual 'local' trajectories through the medium. In the case of skin, a charged molecule may transport (under the action of an oscillatory electric field) predominately along the centerline through aqueous channels of the corneocytes, avoiding contact with keratin fibers, and thereby maximizing its speed through the skin. However, diffusion may cause another molecule to follow a trajectory that frequently brings it into contact with keratin fibers, so that it moves much more slowly through the skin than the 'centerline' molecule. On average, all molecules will move with a mean speed through the skin. In the case of oscillatory flow, this mean speed may even be zero. However, the *dispersion*—or spatial spread—of the solute molecules about this mean speed will be significantly enhanced (over that enhancement which normal molecular diffusion provides) owing to the interaction between convection and diffusion.

## 11.5 Conclusions

The transport of charged molecules across human skin can be dramatically enhanced by application of high-strength, pulsed electric fields. This phenomenon is theoretically characterized here in terms of the electroporation of

lipid bilayers within the stratum corneum above the transbilayer voltage for which electropores have been observed in single bilayer membranes. Accounting for the size, shape and charge of the transporting molecules, predictions of transdermal molecular flux are made in two electric field conditions. At small field strengths (transdermal voltage <<100 V), representative of standard skin iontophoresis, charged molecules are modeled as transporting through the pre-existing shunt routes of the skin. At electric field strengths sufficiently large (transdermal voltage >>100 V) to electroporate lipid bilayers, a transcorneocyte pathway is accessible to charged molecules, with transbilayer transport occurring through electropores within the lipid bilayers. Experimental data of transdermal molecular flux compared favorably with the respective theoretical predictions in the small and large electric field strength limits. Predictions of the skin's electrical resistance are also found to be consistent with experimental data at small and large electric field strengths. In both limits, electrophoretic transport is shown to be predominately convective (i.e., dominated by electric-field drift); however, a form of transport enhancement involving convective dispersion may also be significant during skin electroporation.

# 12 Effects Of Pulse Parameters On Transport[18]

## 12.1 Introduction

Although transdermal drug delivery has the potential to be a noninvasive, user-friendly method of delivering drugs, its clinical use has found limited application due to the remarkable barrier properties of skin's outermost layer, the stratum corneum [Hadgraft and Guy, 1989]. As a result, chemical, iontophoretic, ultrasonic, and other methods of enhancement have been studied as approaches to increase rates of transport. Recently, application of low duty cycle, high-voltage pulses has been shown to cause largely or completely reversible transdermal flux increases up to four orders of magnitude [Bommannan et al., submitted; Bose, 1994; Pliquett and Weaver, submitted, a; Prausnitz et al., 1992; Prausnitz et al., 1993a; Prausnitz et al., submitted, c; Prausnitz et al., in press, a]. These large increases in transport may be explained by electroporation, a mechanism involving transient structural changes in the intercellular lipid bilayers of the stratum corneum.

Well established in cell membranes and artificial bilayer systems, electroporation is believed to involve the creation of transient aqueous pathways in lipid bilayers by the application of a short (μs, ms) electric field pulse [Chang et al., 1992; Orlowski and Mir, 1993; Weaver, 1993b]. Permeability and electrical conductance of lipid bilayers are increased by many orders of magnitude, where membrane changes can be reversible or irreversible, depending mainly on pulse magnitude and duration. Electroporation has also been demonstrated in cells in monolayers [Kwee et al., 1990], as well as in cells part of intact tissues [Belehradek et al., 1994; Dev and Hofmann, 1994].

---

[18] These results have also been reported in [Prausnitz et al., submitted, b], [Prausnitz et al., 1993c], and [Prausnitz et al., in press, b].

Electroporation occurs when the transmembrane voltage reaches ~ 1 V for electric field pulses typically of 10 μs to 10 ms duration. During electroporation, the following sequence of events is believed to take place: (1) within nanoseconds to microseconds, electropores are created, (2) molecules are moved through electropores primarily by electrophoresis and/or electroosmosis due to the local electric field, and (3) after the pulse, pores close over characteristic times ranging from milliseconds to hours [Chang et al., 1992; Orlowski and Mir, 1993; Weaver, 1993b].

Recent theoretical estimates suggest that some features of ionic transport across the multilamellar system of bilayers in human stratum corneum might be accounted for by electroporation at transdermal voltages of approximately 100 V [Chizmadzhev et al., submitted; Edwards et al., submitted]. This study seeks to better characterize the effects of higher-voltage pulsed electric field conditions on transdermal transport and to use these results to better understand possible mechanisms for flux enhancement, especially as compared to conventional lower-voltage iontophoresis.

## 12.2 Results

Calcein transport across human epidermis was studied due to the effects of lower-voltage continuous electric fields (iontophoresis) and higher-voltage pulsed electric fields (electroporation). The dependence of transport on electric field parameters was evaluated and transport numbers were calculated to facilitate mechanistically-oriented comparisons.

In Fig. 12-1, transdermal calcein transport due to electric field pulses of forward polarity and of alternating polarity is shown. According to our terminology, forward-polarity pulses were applied with the positive electrode in

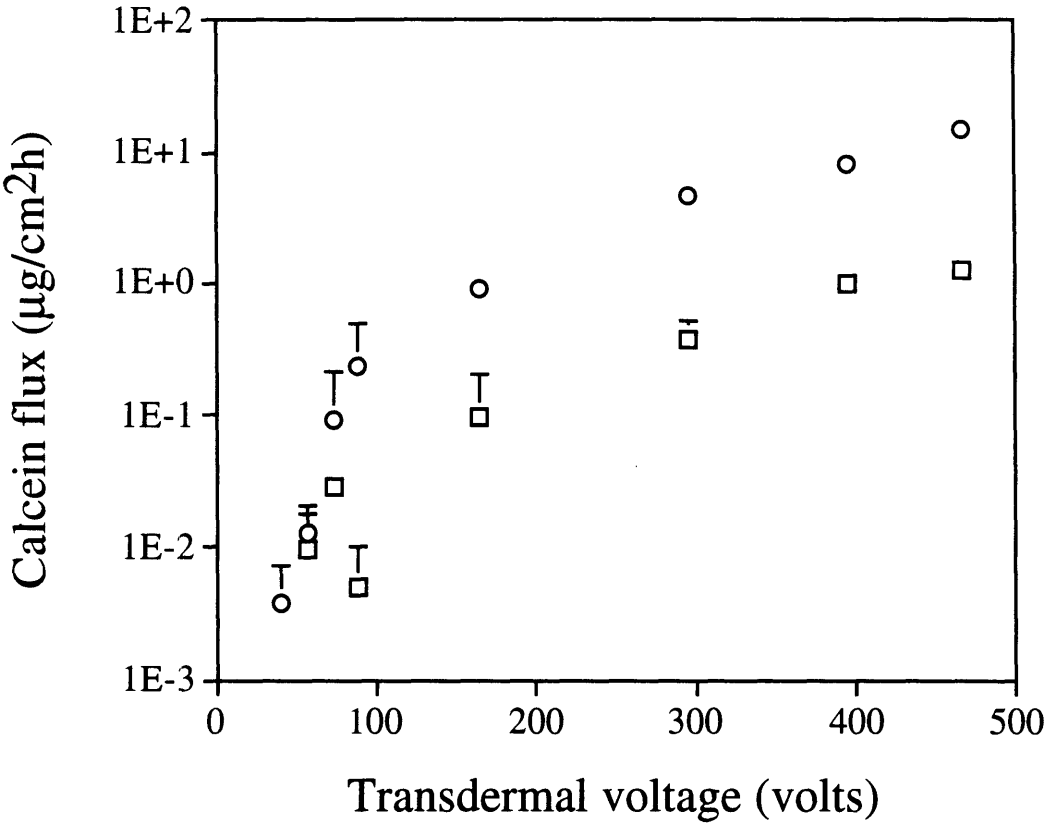


**Fig. 12-1.** Average calcein flux across human epidermis due to forward-polarity and alternating-polarity exponential-decay electric-field pulses (exponential-decay time constant, $\tau$ = 1.0 - 1.3 ms; pulse rate, r = 12 pulses per minute (ppm)). Forward-polarity pulsing (O) could cause both creation of electropores and electrophoresis through electropores. Data from Fig. 10-2. Alternating-polarity pulsing (□) could cause creation of electropores, but should result in no net electrophoretic movement. See text for discussion. Each point represents the average of 2 - 5 different skin samples. Standard deviation bars are shown.

the receptor compartment and the negative electrode in the donor compartment. For this configuration, electric field pulses could (a) cause structural changes in the skin due to electroporation and (b) move calcein across the skin by electrophoresis through both previously-existing and newly-created transport pathways. Forward-polarity pulsing resulted in flux increases of up to four orders of magnitude. In contrast, alternating-polarity pulses were applied such that the electrode polarity alternated with each pulse. In this way, the pulses could cause electroporation, but should cause no net ion transport by electrophoresis (see Discussion). However, under these conditions, flux increases of up to three orders of magnitude were observed. In contrast, application of continuous sinusoidal ac voltages up to 5 $V_{rms}$ at 1 kHz for 1 h caused insignificant enhancement of transdermal calcein transport (data not shown).

The effects of pulse rate and pulse time constant of exponential-decay electric field pulses were assessed in Fig. 12-2. We previously reported that there appeared to be a transition at 100 - 150 V, below which flux increases were fully reversible, and above which they were only partially reversible [Prausnitz et al., 1993a]. We therefore studied the effects of pulse rate and pulse time constant both below (75 V) and above (300 V) the transition region. Over the range of conditions studied, there appears to be approximate proportionality between calcein flux and total pulse "on" time (i.e., the product of pulse time constant multiplied by pulse rate).

Previous studies of skin electroporation [Bommannan et al., submitted; Prausnitz et al., 1992; Prausnitz et al., 1993a] and results presented here measured transdermal transport due to electrical exposures of 1 h or less. Fig. 12-3 shows the effects of pulsing for 7 h continuously, where steady state transport was achieved within ~ 10 min and maintained throughout.

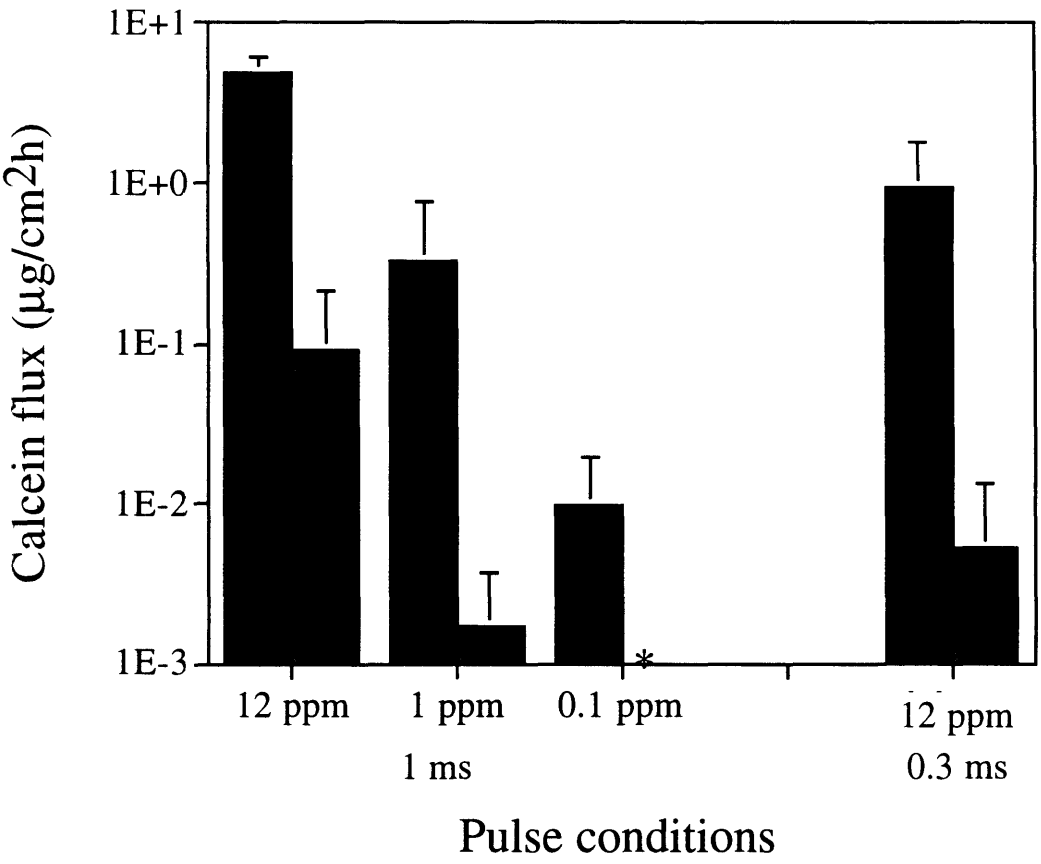


**Fig. 12-2.** Average transdermal calcein flux due to exponential-decay pulses at different rates and pulse lengths. Pulses were applied at 300 V (■) and 75 V (▩). Pulse rates and time constants are shown. Asterisk indicates a flux below the detection limit, of order $10^{-4}$ μg/cm$^2$h. Each point represents the average of 3 - 6 different skin samples. Standard deviation bars are shown.

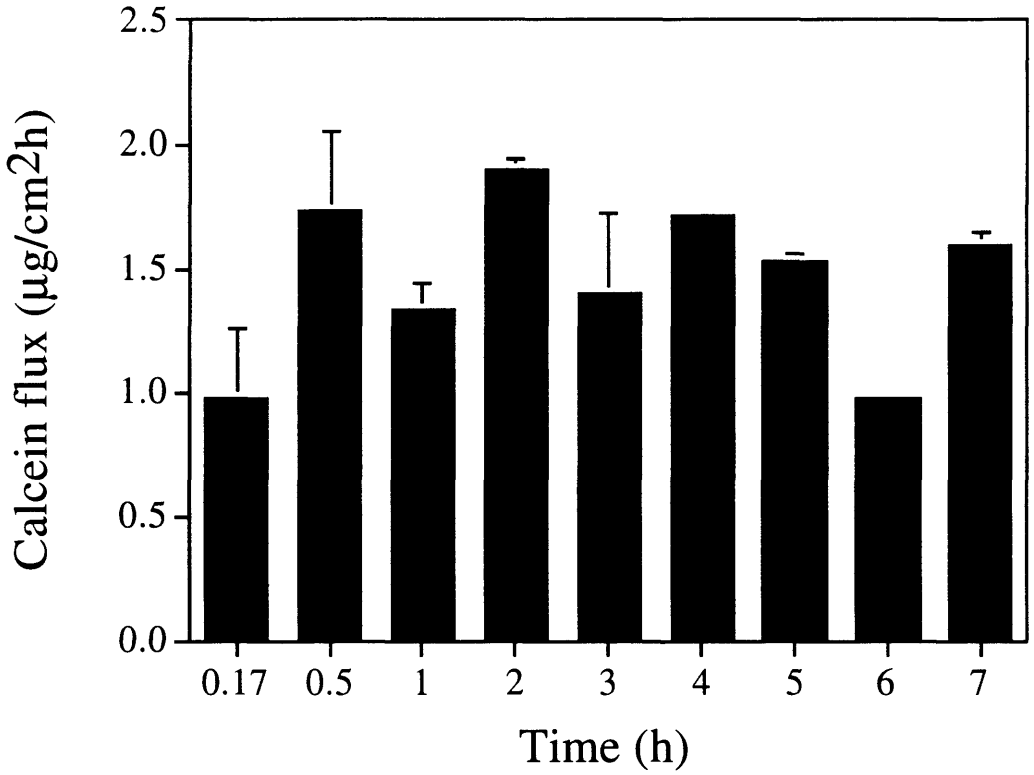


**Fig. 12-3.** Average transdermal calcein flux due to exponential-decay pulses (transdermal voltage, v = 300 V; $\tau$ = 1.1 ms; r = 12 ppm) applied for 7 h. The flux remained approximately constant throughout. Each point represents the average of 2 different skin samples. Standard deviation bars are shown.

In Fig. 12-4, the effects of pulse rate and pulse length were examined for square-wave pulses. Only voltages below the reversible-irreversible transition region were studied, since fully-reversible conditions may be more relevant for drug delivery applications. In Fig. 12-4A, the dependence of flux on pulse length was examined. For pulses longer than 10 μs, flux increased approximately in proportion with pulse length. However, 10 μs pulses caused a disproportionately low flux. Fig. 12-4B shows the effects of pulse rate on transdermal calcein flux. There also appears to be approximate proportionality between pulse rate and flux, except at 3 pps, where flux appears to be disproportionately low.

Fig. 12-4C further addresses the proportionality between flux and total "on" time. Five different pulsing protocols are compared, where the product of pulse length multiplied by pulse rate was held constant. In each case, the resulting flux was approximately the same, except for 10 μs pulses applied at 200 pps. This is in agreement with Fig. 12-4A, which also suggests that 10 μs pulses cause disproportionately small increases in transport.

To assess changes in skin electrical properties under conditions examined in this study, time traces of current and voltage during a pulse were collected. Fig. 12-5A shows the voltage across a permeation chamber during a 200 V, 10 μs square-wave pulse. The corresponding current through the chamber is shown in Fig. 12-5B. While time-varying effects were seen for the first 1 - 2 μs of the pulse, no further changes in electrical properties were observed during the remainder of the pulse. Although the initial time-varying behavior could be due to changes in skin properties, it is more likely to be associated with the electrical properties of the pulse application system. Thus, any changes in skin electrical properties occurred on a time scale of microseconds or less.

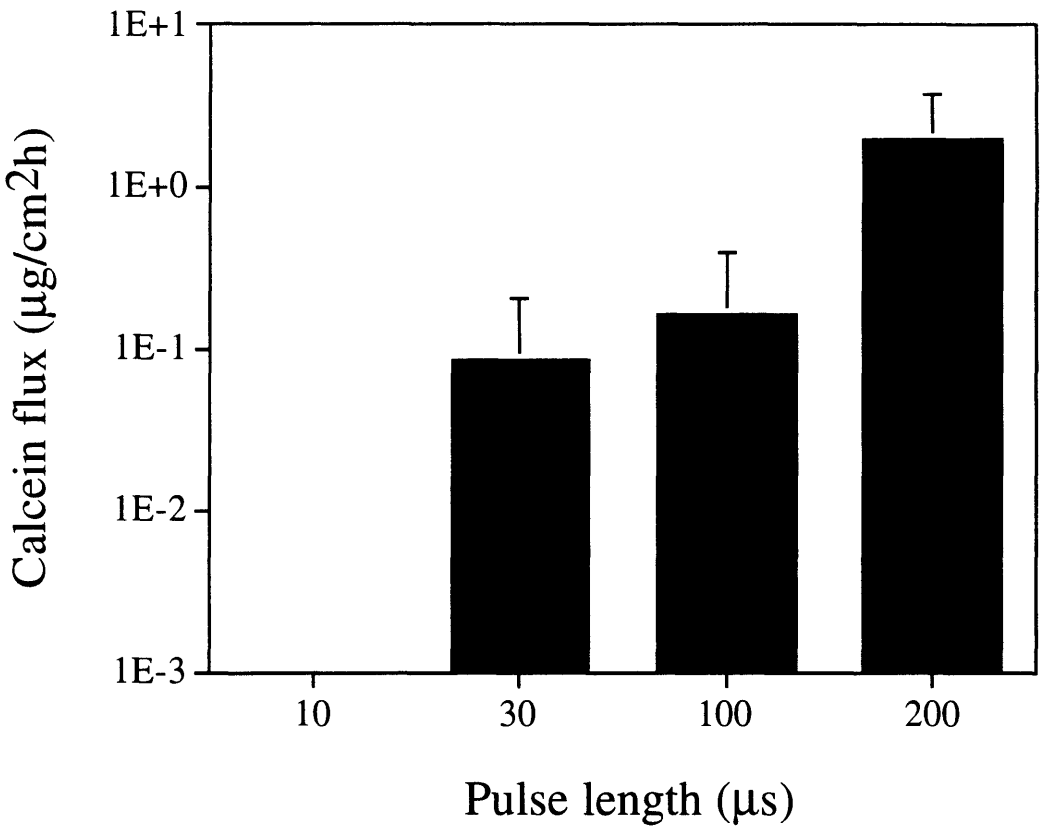


**Fig. 12-4A.** Average transdermal calcein flux due to square-wave electric-field pulses (v = 40 V; r = 30 pulses per second, pps) of different pulse lengths. The shortest (10 μs) pulses caused a disproportionately low flux. Asterisk indicates a flux below the detection limit, of order $10^{-4}$ μg/cm$^2$h. Each point represents the average of 6 different skin samples.

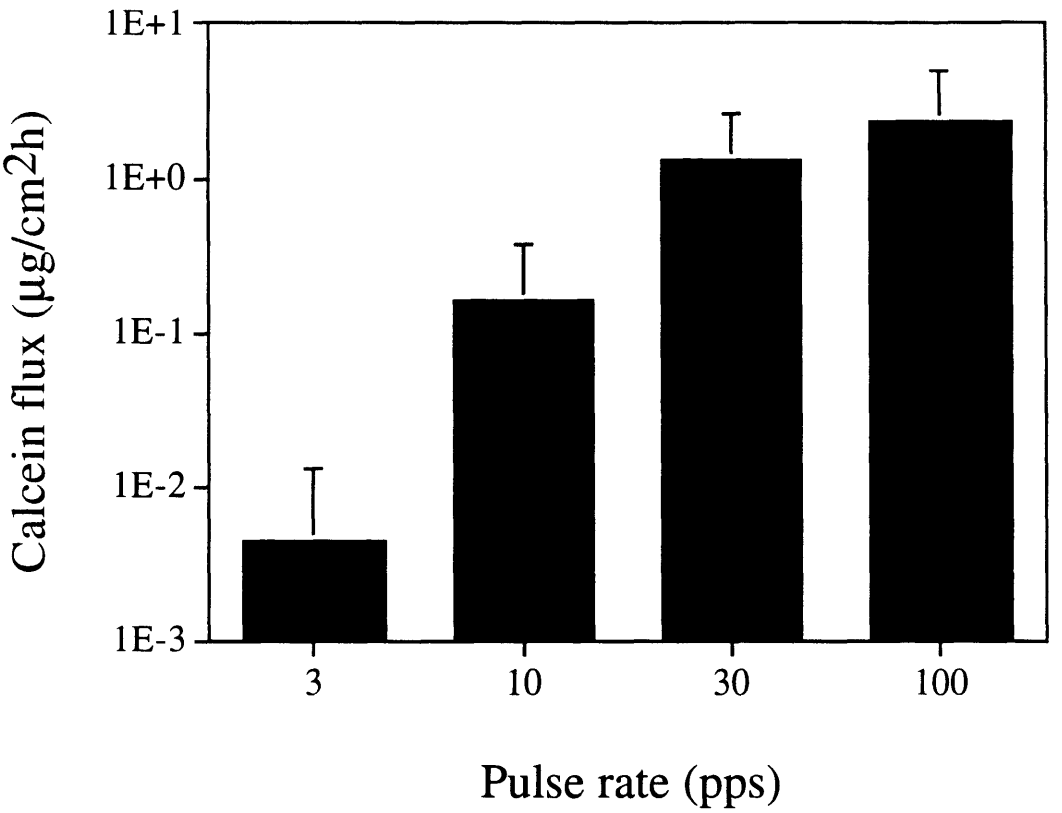


**Fig. 12-4B.** Average transdermal calcein flux due to square-wave electric-field pulsing (v = 75 V; pulse length, t = 30 μs) at different pulse rates. Each point represents the average of 4 - 11 different skin samples.

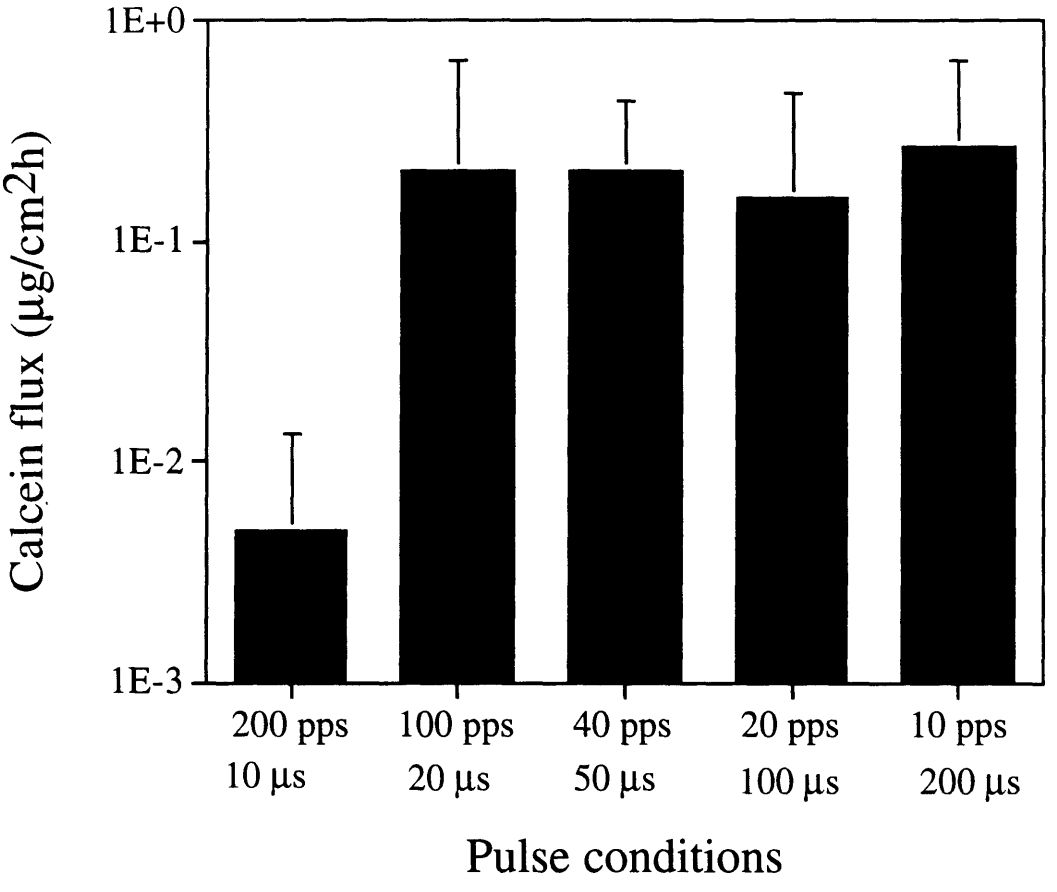


**Fig. 12-4C.** Average transdermal calcein flux due to square-wave electric-field pulsing (v = 75 V) at different pulse rates and pulse lengths. The product of pulse rate multiplied by pulse length was kept constant (2000 μs pps), so that the average total "on" time was the same in each case. Each point represents the average of 6 - 9 different skin samples. Standard deviation bars are shown.

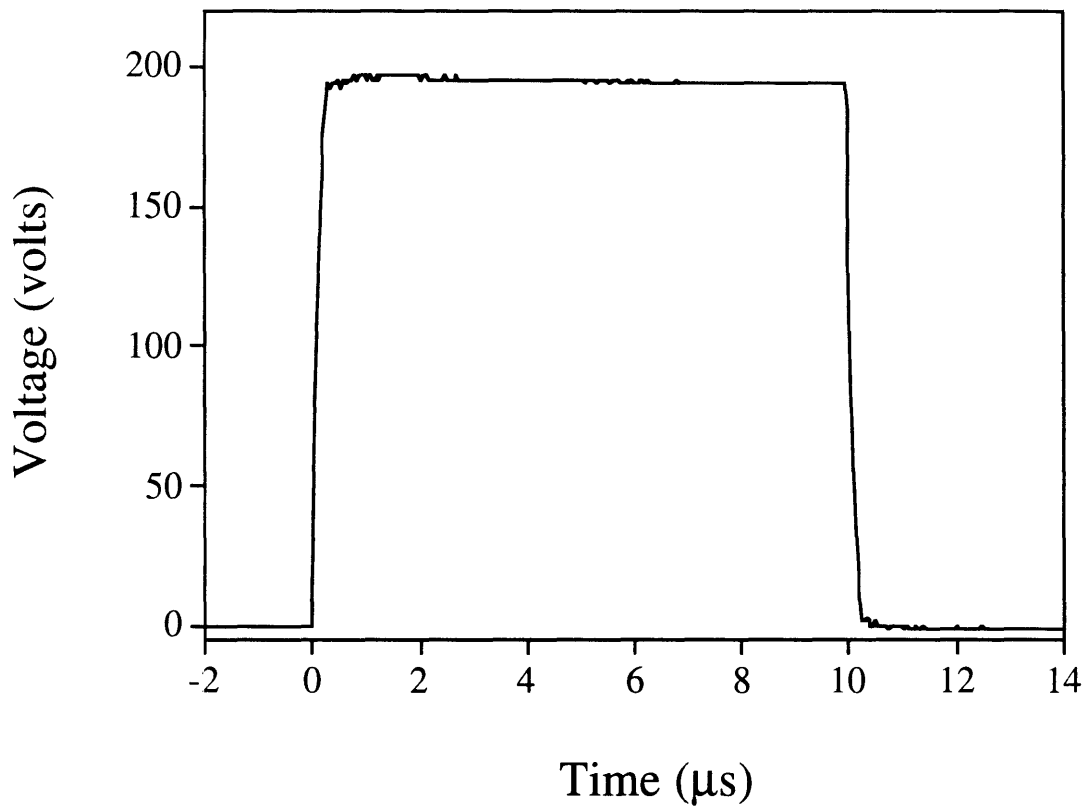


**Fig. 12-5A.** Characterization of changes in skin electrical properties due to higher-voltage electrical exposures. Voltage across a permeation chamber containing skin (i.e., not the voltage across the skin) due to a 200 V square-wave electric-field pulse of 10 μs duration.

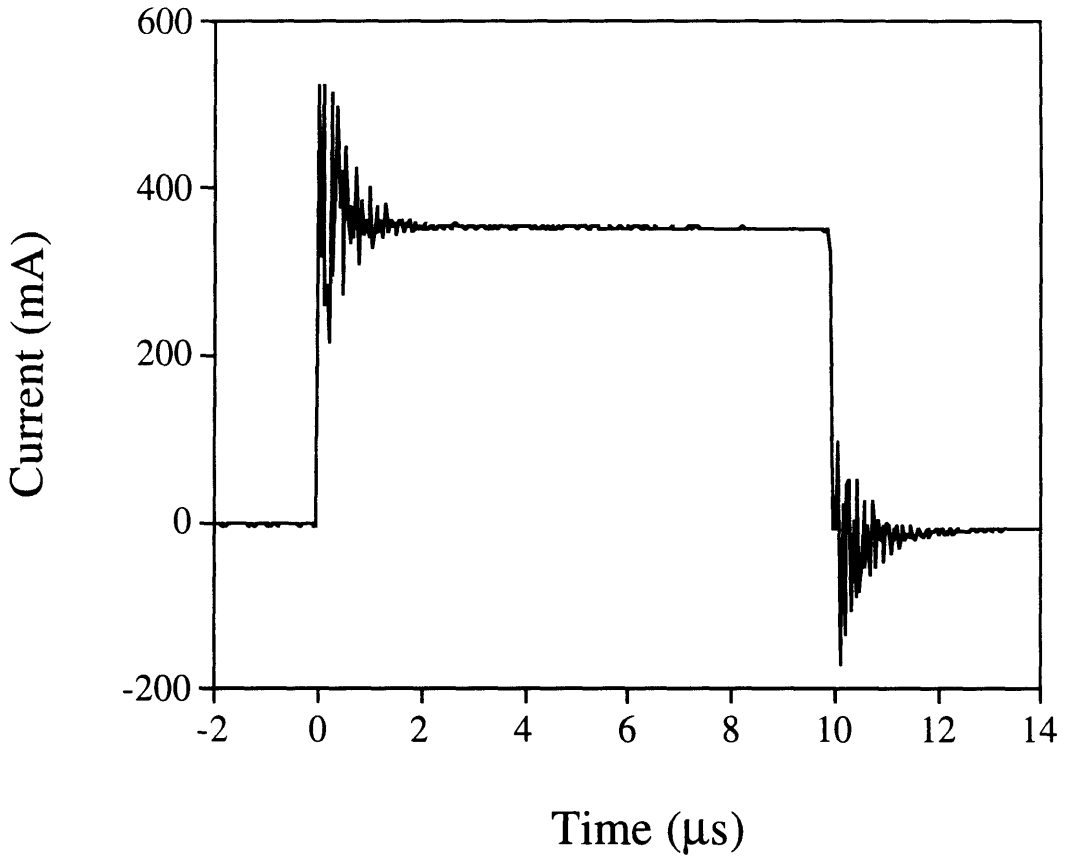


**Fig. 12-5B.** Characterization of changes in skin electrical properties due to higher-voltage electrical exposures. Current measured through the permeation chamber during the voltage pulse shown in Fig. 12-5A. This figure suggests that the skin resistance dropped from ~ 100,000 Ω to ~ 90 Ω on a time scale of ≤ 2 μs (see text).

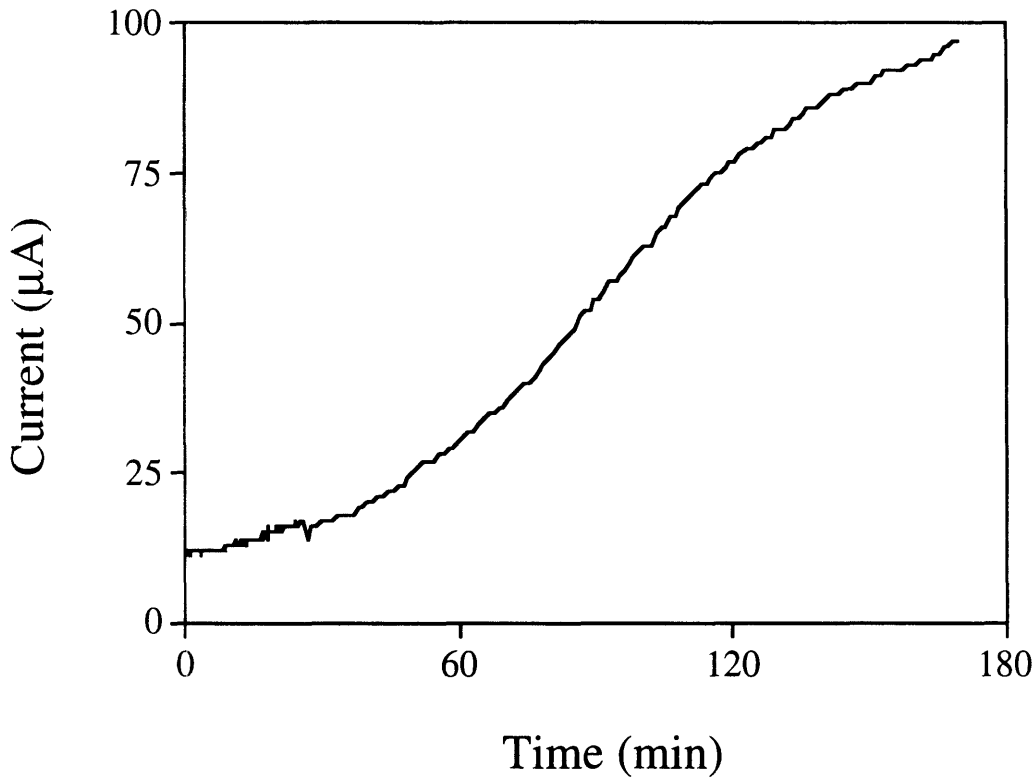


**Fig. 12-5C.** Characterization of changes in skin electrical properties due to lower-voltage electrical exposures. Current measured through the permeation chamber during continuous application of 1 V iontophoresis. This curve suggests that the skin resistance dropped from ~ 100,000 Ω to ~ 10,000 Ω on a time scale of an hour (see text).

During the time-invariant, purely resistive portion of the pulse, the voltage was ~ 200 V and the current was ~ 350 mA. Using Ohm's Law, the apparent resistance of the system was ~ 570 Ω. The apparent resistance of the permeation chamber without skin (but including electrodes, saline, and interfacial resistances) was measured during a pulse to be 480 Ω, independent of voltage [Bose, 1994; Prausnitz et al., 1993a]. Therefore, the apparent resistance of the skin, $R_{skin}$, fell to ~ 90 Ω within 2 μs after the onset of the pulse. Since $R_{skin}$ was on the order of 100,000 Ω before pulsing, $R_{skin}$ dropped three orders of magnitude on a time scale of microseconds or less.

In contrast, changes in skin electrical properties due to lower-voltage iontophoresis are less dramatic and much slower. In Fig. 12-5C, transdermal voltage was maintained at 1 V for 3 h and the resulting current is shown. Using Ohm's Law, $R_{skin}$ can be calculated. Under these conditions, which are representative of typical iontophoresis, $R_{skin}$ decreased from ~ 100,000 Ω to ~ 10,000 Ω over a characteristic time on the order of an hour. This resistance drop was two orders of magnitude less than that seen during the higher-voltage pulse. Moreover, it occurred over a time scale at least nine orders of magnitude slower. The vastly different magnitudes and times scales suggest that different mechanisms are responsible for the changes in skin electrical properties observed during lower-voltage and higher-voltage electrical exposures.

To further explore mechanisms of transport enhancement, transport numbers were calculated for fluxes associated with different electrical exposures. The transport number is the fraction of total current carried by a given ionic species, which can be thought of as the efficiency of electrophoretic transport of that species [Bockris and Reddy, 1970; Bommannan et al., submitted; Phipps and Gyory, 1992]. The transport number, $t_i$, of ionic species, i, is defined as

$$t_i = \frac{J_i \, z_i \, F}{I}$$

where $J_i$ is the transdermal flux of i, $z_i$ is the valence (charge) of i, F is Faraday's constant, and I is the total current passed across the skin [Bockris and Reddy, 1970]. In transdermal transport, current can be carried across the skin by any ion present, such as sodium, chloride, or charged drug. Thus, in this study, the transport number gives the efficiency with which current transported calcein across the skin, compared to competing ions, such as sodium or chloride.

To perform an analysis involving transport numbers, we used exponential-decay pulse, square-wave pulse, and constant-voltage iontophoresis data shown above and presented previously [Prausnitz et al., 1993a]. This was supplemented with constant-current iontophoresis data, shown in Fig. 12-6.

Transport numbers for transdermal calcein transport, $t_{calcein}$, are shown in Fig. 12-7 during constant-voltage and constant-current iontophoresis. Here, $t_{calcein}$ increased with increasing voltage and current. This suggests that (a) the transport properties of skin were altered by the electric field and (b) the nature of these alterations were functions of voltage and current.

Fig. 12-8 shows $t_{calcein}$ under exponential-decay and square-wave pulsed conditions. Fig. 12-8A indicates that $t_{calcein}$ increased with increasing voltage. However, Figs. 12-8B and 12-8C suggest that $t_{calcein}$ was not a function of pulse length or pulse rate. Moreover, no clear difference between exponential-decay and square-wave electric field pulses is evident.

Finally, direct comparison between continuous lower-voltage electric field exposures (Fig. 12-7) and pulsed higher-voltage electric field exposures (Fig 12-8) requires evaluation on a common basis. Fig. 12-9 contains all these data,

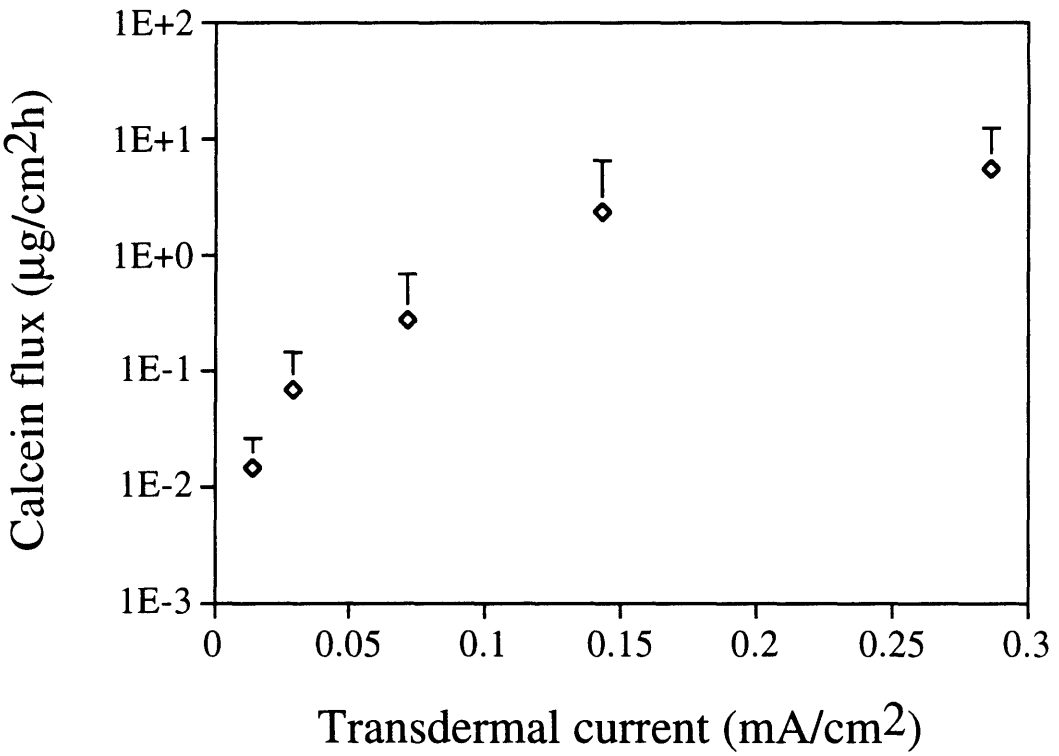


**Fig. 12-6.** Average transdermal calcein flux due to continuous constant-current iontophoresis. The iontophoretic flux was not directly proportional to current. Each point represents the average of 5 - 17 different skin samples. Standard deviation bars are shown.

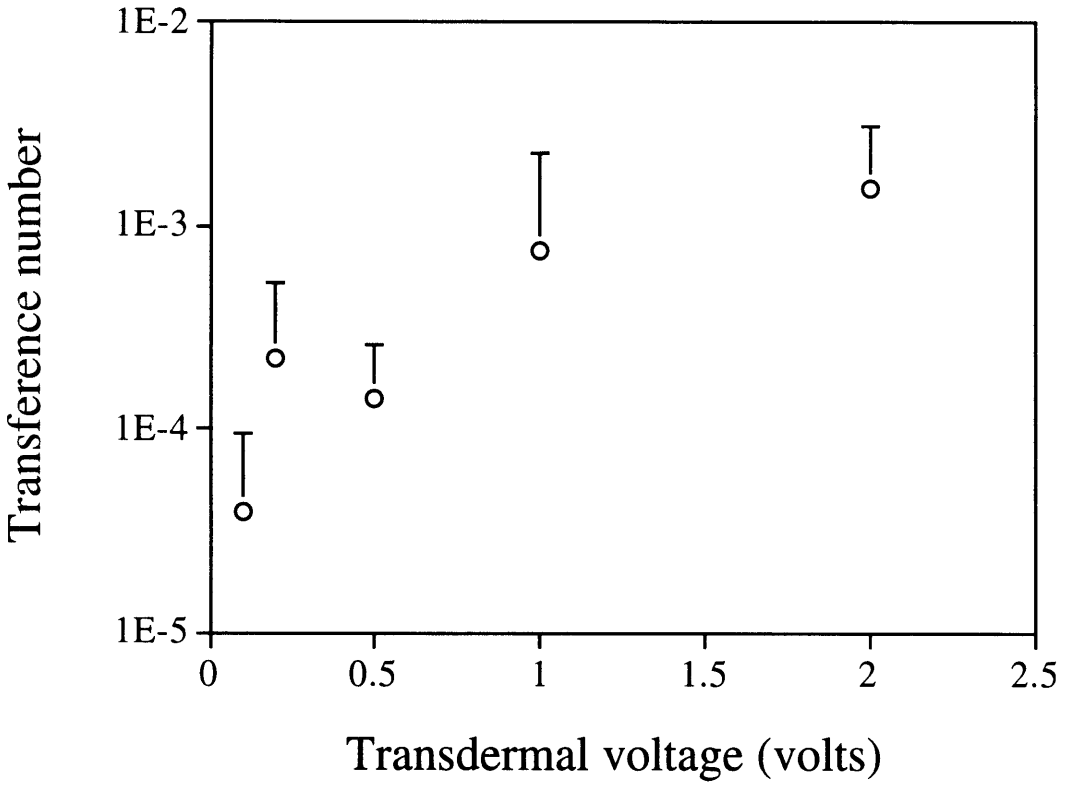


**Fig. 12-7A.** Average transport number for transdermal calcein transport by continuous constant-voltage iontophoresis. Transport number, which is a measure of transport efficiency, increased with increasing voltage. Data are from Fig. 10-3. Standard deviation bars are shown.

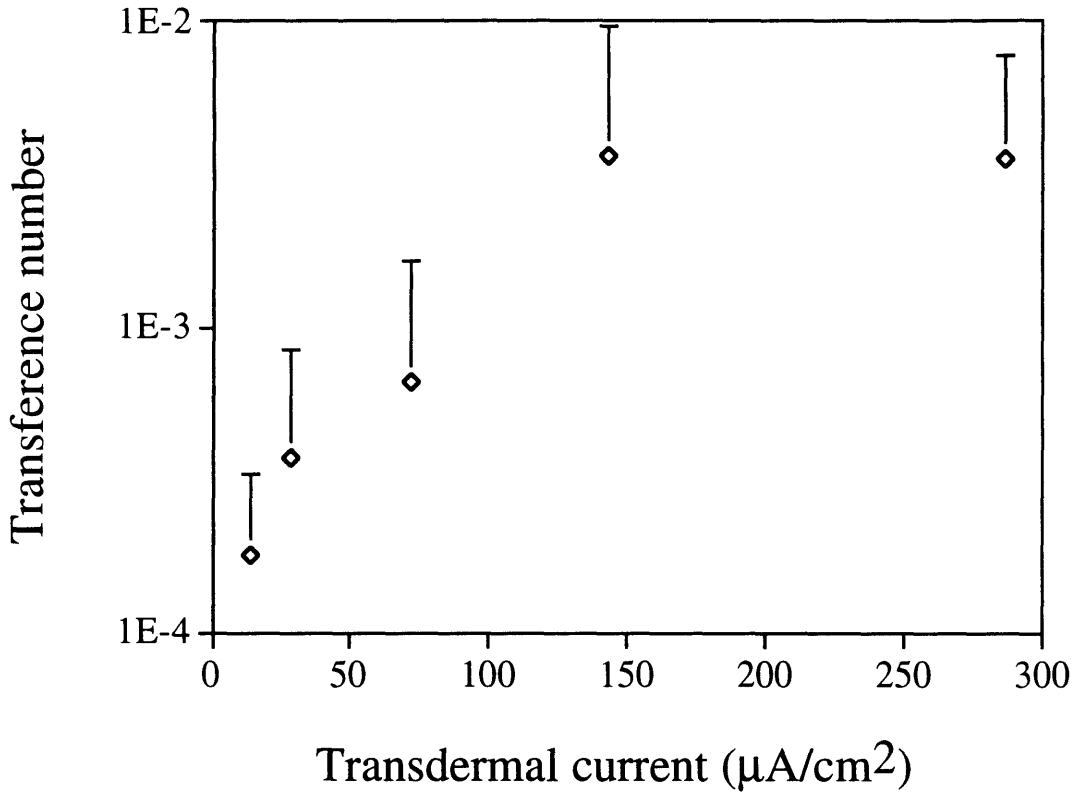


**Fig. 12-7B.** Average transport number for transdermal calcein transport by continuous constant-current iontophoresis. Transport number, which is a measure of transport efficiency, increased with increasing current. Data are from Fig. 12-6. Standard deviation bars are shown.

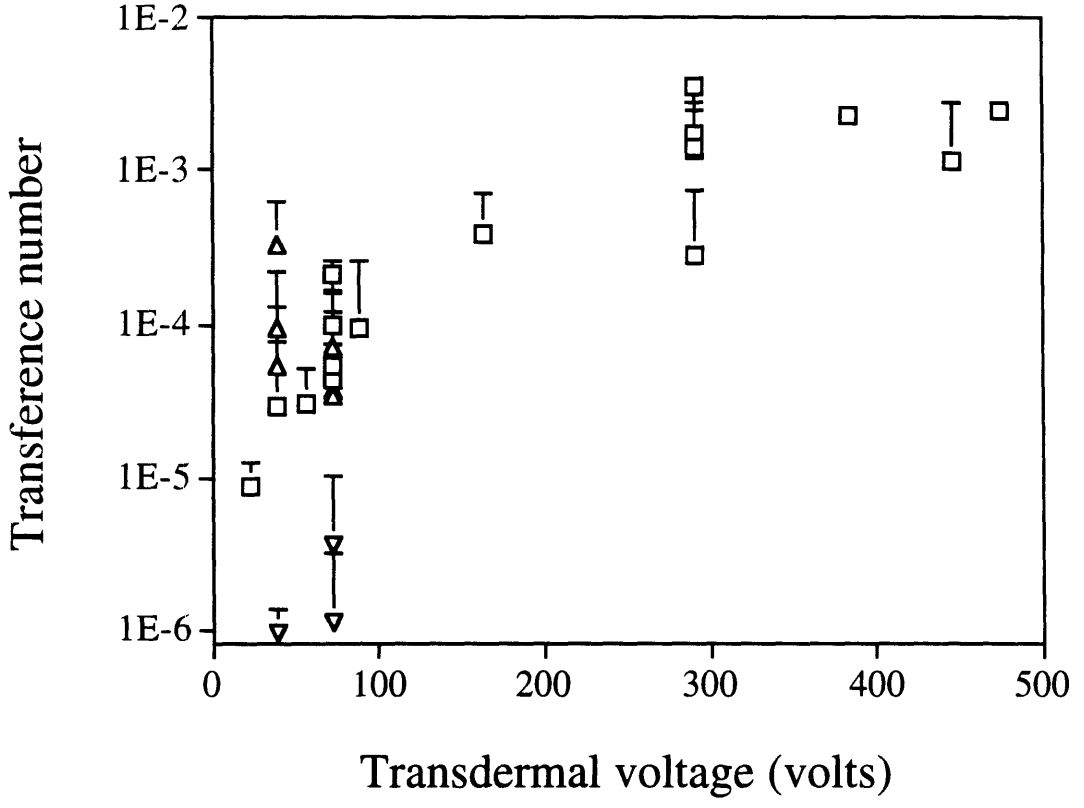


**Fig. 12-8A.** Average transport number for transdermal calcein transport by exponential-decay and square-wave electric-field pulses as a function of pulse voltage. Transport number increased with increasing voltage. Square-wave pulse data (△,▽) are from Fig. 12-4. Exponential-decay pulse data (□) are from Figs. 10-2, 12-1 and 12-2. Standard deviation bars are shown. The three up-side-down triangle data points (▽) were calculated from the anomalous 10 μs (Figs. 12-4A and 12-4C) and 3 pps (Fig. 12-4B) data (see text).

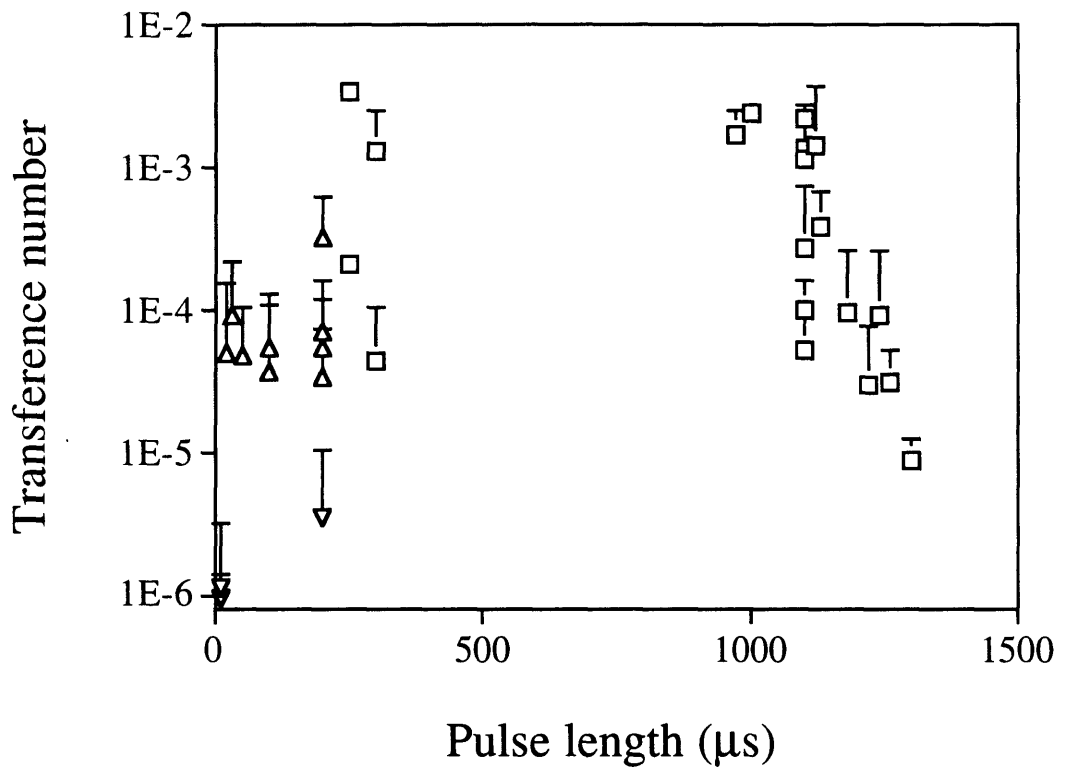


**Fig. 12-8B.** Average transport number for transdermal calcein transport by exponential-decay and square-wave electric-field pulses as a function of pulse length. Transport number showed no significant dependence on pulse length. See caption for Fig. 12-8A for explanation.

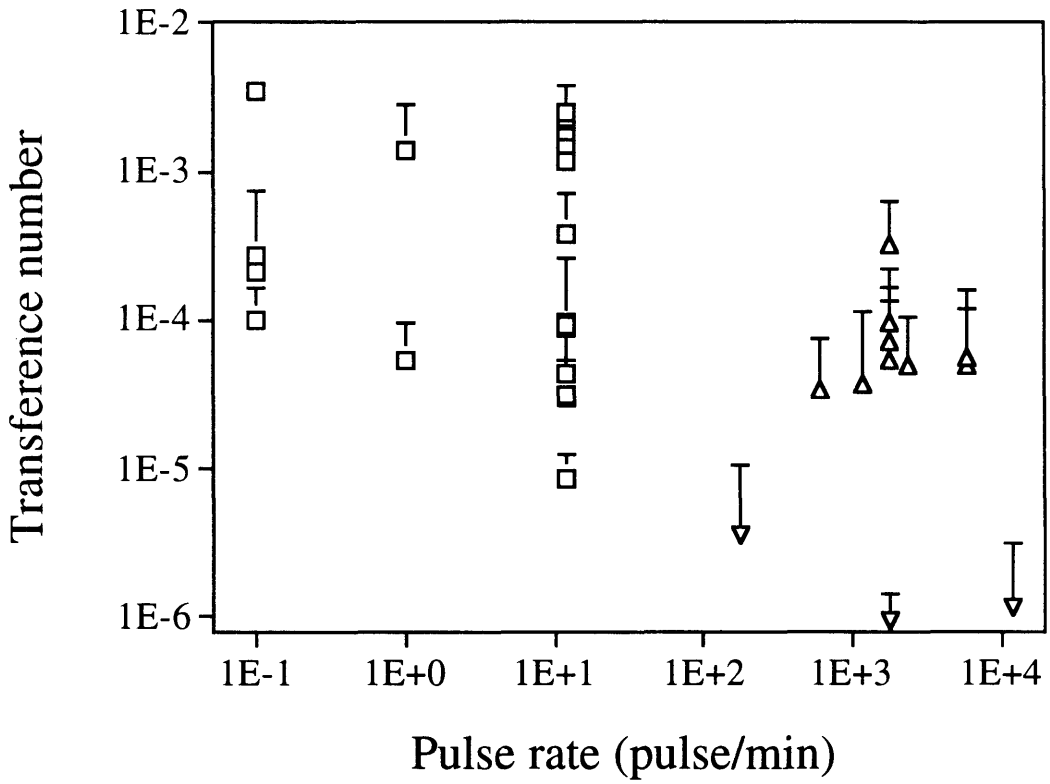


**Fig. 12-8C.** Average transport number for transdermal calcein transport by exponential-decay and square-wave electric-field pulses as a function of pulse rate. Transport number showed no significant dependence on pulse rate. See caption for Fig. 12-8A for explanation.

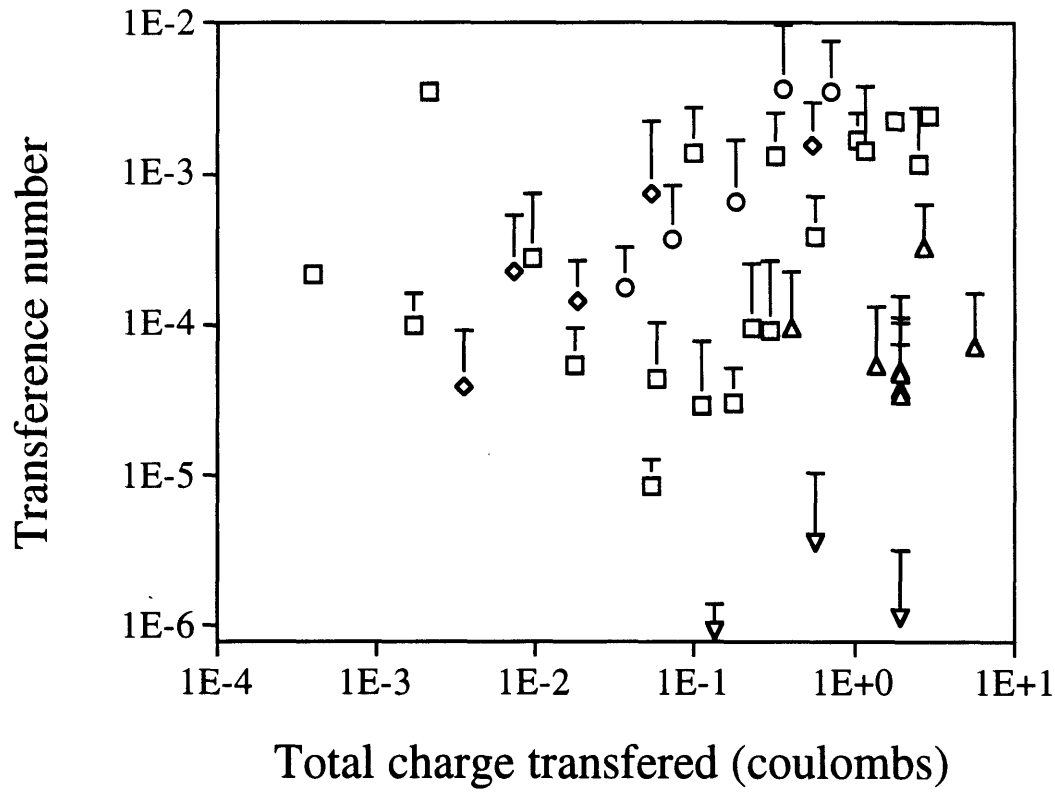


**Fig. 12-9.** Average transport number for transdermal calcein transport by different electric-field exposures as a function of total charge transferred across the skin: (△,▽) square-wave pulses, (□) exponential-decay pulses, (○) constant-voltage iontophoresis, and (◇) constant-current iontophoresis. Pulsed and continuous electrical exposures can be compared directly when evaluated on the basis of total charge transferred.

expressed on the basis of total charge transferred. No clear dependence of $t_{calcein}$ on total charge transferred is evident. However, the range in $t_{calcein}$ seen for both lower-voltage and higher-voltage protocols is approximately the same ($10^{-5}$ - $10^{-2}$).

## 12.3 Discussion

### 12.3.1 Alternating-Polarity Pulses

Higher-voltage forward-polarity pulses are expected to increase transdermal transport by first creating structural changes in the skin and then transporting molecules across the skin by electrophoresis [Prausnitz et al., 1993a]. Because structural changes due to electroporation are believed to occur independent of electric field polarity [Chang et al., 1992; Orlowski and Mir, 1993; Weaver, 1993b], alternating-polarity pulses should also cause skin structural changes, but result in no net ion electrophoresis. Evidence for these structural changes is given in Fig. 12-1, where alternating-polarity higher-voltage pulses increased calcein transport by up to three orders of magnitude. In contrast, no enhancement was provided by electrically "equivalent" continuous lower-voltage ac fields, which also provide no net electrophoresis, but are not expected to cause electroporation.

We now explain what is meant by electrically "equivalent" pulsed and continuous electric fields. Although they provide no net ion electrophoresis, alternating-polarity electric fields can enhance transport of a given ionic species (e.g., calcein) by electrophoresis and/or by convective dispersion [Brenner and Edwards, 1993; Edwards et al., submitted]. Considering transport enhancement by electrophoresis, which is proportional to the time integral of the voltage applied [Bockris and Reddy, 1970], continuous application of 5 V should provide

the same electrophoretic contribution to transport as 25,000 V applied at a 1:5000 duty cycle (a 1 ms pulse every 5 s). Considering transport enhancement by convective dispersion, which is proportional to the time integral of the square of the applied voltage [Brenner and Edwards, 1993], continuous application of 5 V should provide the same convective dispersive contribution to transport as exponential-decay pulsing at 177 V. Therefore, iontophoresis at $\leq$ 5 V is electrically "equivalent" to pulses on the order of 100 V. For this reason, we used continuous sinusoidal ac voltages up to 5 $V_{rms}$ at a frequency of 1 kHz, selected because its period, 1 ms, is the same as the time constant of the alternating pulses used.

### 12.3.2 Effects of Pulsed Electrical Conditions on Transport

Understanding the dependence of transport on electrical conditions can guide applications and provide insight into transport mechanisms. Transport showed a highly non-linear dependence on pulse voltage, as discussed previously [Prausnitz et al., 1993a]. However, Figs. 12-2 and 12-4 suggest that over a range of conditions transport was approximately proportional to total pulse "on" time (i.e., the product of pulse length multiplied by pulse rate). Transport associated with electroporation of single bilayer membranes has also been shown to depend non-linearly on pulse voltage, but vary linearly with total pulse "on" time (Chapter 8).

There were two anomalous cases where transport was apparently not proportional to total "on" time. First, in Fig. 12-4B, pulsing at 3 Hz was disproportionately low when compared to pulsing at faster rates. Although it is presently unclear, an explanation could involve pores which close between pulses at 3 Hz but do not close when pulsing more rapidly ($\geq$ 10 Hz).

Second, Figs. 12-4A and 12-4C suggest that 10 μs pulses also caused a disproportionately low flux. Possible explanations relating to skin electrical behavior include: (a) if the capacitive charging time of the skin were longer than 10 μs, then current would have gone to charging the skin, rather than causing transport across the skin and (b) if skin electroporation occurred on a time scale slower than 10 μs, then new pathways would not have been created to enhance transport. However, after 1 - 2 μs of a 10 μs pulse, transdermal current was constant (skin acted like a resistor) and skin resistance had dropped by three orders of magnitude (Fig. 12-5). This suggests that at the beginning of the pulse (a) the skin was charged and (b) skin electroporation had occurred. This result was expected, since (a) for this apparatus, the capacitive charging time of skin, $\tau_{skin}$, should be on the order of 1 μs ($\tau_{skin} = R_{chamber}$ (chamber resistance, $10^{-2}$ Ω) x $C_{skin}$ (skin capacitance, $10^{-8}$ F/cm$^2$ [Bose, 1994; Pliquett and Weaver, submitted, a]) and (b) electropores are believed to be created in single-bilayer systems on a time scale of nanoseconds to microseconds [Chang et al., 1992; Orlowski and Mir, 1993; Weaver, 1993b].

Thus, although skin electroporation occurred and small ion transport (current) increased by orders of magnitude within 2 μs, calcein transport did not increase dramatically until after 10 μs. This suggests that during the first 10 μs of a pulse, pathways too small for calcein transport may have existed, while larger pathways were created at later times. This agrees with studies of electroporation in single bilayer membranes, which suggest that longer pulses may be associated with larger pores [Chang et al., 1992; Freeman et al., in press; Orlowski and Mir, 1993; Weaver, 1993b].

12.3.3 Transport Number Functionality

By calculating the transport number, or transport efficiency, associated with transport under different electrical conditions, we can partially characterize the pathways available to ion transport. In this study, $t_{calcein}$ is a measure of the ease with which calcein can transport through ion transport pathways relative to small ions, such as sodium or chloride. Thus, transport numbers can give information about the effective average size of transport pathways.

Figs. 12-7 and 12-8 show that $t_{calcein}$ increased with increasing current and voltage during iontophoresis and skin electroporation. This suggests that larger currents and voltages altered the skin's transport properties in ways that favored calcein transport over small ion transport, perhaps due to creation of larger transport pathways. At the lowest voltages and currents ($t_{calcein} = 10^{-5}$), transport pathways may have dimensions of the same order of magnitude as calcein (Stokes-Einstein radius, $r_{calcein} = 0.6$ nm[19] [Edwards et al., submitted]). In this case, sodium or chloride (crystal ionic radius, $r_{Na+} = 0.1$ nm and $r_{Cl-} = 0.2$ nm[19] [Weast, 1985]) transport would be less hindered, while calcein would find considerable steric hindrance. At higher-voltages or currents ($t_{calcein} = 10^{-3}$ to $10^{-2}$), larger pathways could exist, having dimensions much larger than calcein. In this case, small ion transport would remain unhindered while calcein transport would become less hindered, thereby increasing $t_{calcein}$ by increasing its transport relative to small ions.

The predicted maximum value of $t_{calcein}$ would occur if calcein and small ion transport were both completely unhindered. In this case, their transport numbers would scale with the product of electrophoretic mobility multiplied by concentration multiplied by valence [Bockris and Reddy, 1970]. Since their

---

[19] Hydration shells have not been considered and could make effective molecular dimensions larger.

mobilities were approximately equal (in water at 25 °C: $\mu_{sodium} = 5.2 \times 10^{-4}$ $cm^2/V\ s$ [Atkins, 1986], $\mu_{chloride} = -7.9 \times 10^{-4}\ cm^2/V\ s$ [Atkins, 1986], $\mu_{calcein} = -5.7 \times 10^{-4}\ cm^2/V\ s$ [20]), their relative concentrations were 1:300 (1 mM calcein and ~ 300 mM small ions), and their relative valences were 4:1 ($z_{calcein} = -4$ and generally $z_{ion} = -1$ or +1), then $t_{calcein,\ max}$ would be approximately $10^{-2}$ if all transport were unhindered. However, at pH 7.4 the skin carries a negative charge, showing permselectivity for cations [Hadgraft and Guy, 1989], suggesting that $t_{calcein,\ max}$ may be somewhat lower, between $10^{-3}$ and $10^{-2}$.

Reexamining the transport number data in this light suggests that at the lowest voltages and currents used during iontophoresis and skin electroporation, on a relative scale, small ion transport was favored over calcein transport by a factor of 100 to 1000 ($t_{calcein} \approx 10^{-5}$). Pathways which might show this selectivity could include transport between head-groups of the stratum corneum intercellular lipid bilayers (r = 0.7 nm [Bouwstra et al., 1991]) or through intercellular junctions in the lining of shunt pathways. Another possibility is that many pathways exist which only allow small ion transport, such as Angstrom-size "holes" in lipid bilayers created by random thermal motion [Hamilton and Kaler, 1990], along with a few much larger routes which readily permit passage of calcein, perhaps associated with appendages.

At the highest voltages and currents, $t_{calcein}$ appeared to reach its predicted maximum value ($t_{calcein,\ max} = 10^{-3}$ to $10^{-2}$). Under these conditions, calcein transport appears to have been unhindered, suggesting that transport pathways

---

[20] Calcein mobility was calculated using the relation [Bockris and Reddy, 1970], $\mu_{calcein} = \frac{DzF}{RT}$, where z is valence (-4 [Prausnitz et al., 1993a]), F is Faraday's constant, R is the gas constant, T is temperature (298 K), and D is diffusivity, calculated using the Stokes-Einstein relation [Bockris and Reddy, 1970], $D = \frac{kT}{6\pi r \eta}$, where k is Boltzman's constant, T is temperature, r is molecular radius (0.6 nm (Chapter 11)), and $\eta$ is viscosity (1 cp [Weast, 1985]).

were significantly larger than calcein. However, with this data alone we cannot assess (a) how much larger than calcein these pathways were or (b) whether these were newly-created pathways or enlargements of pre-existing pathways.

Finally, $t_{calcein}$ showed no clear dependence on pulse length, pulse rate, pulse waveform, or total charge transferred. This is consistent with known mechanisms for single-bilayer electroporation, where pore characteristics are believed to be determined largely by voltage [Chang et al., 1992; Orlowski and Mir, 1993; Weaver, 1993b]. It is also consistent with known changes in skin electrical properties due to iontophoresis, where reduction of skin resistance is a function of voltage [Edelberg, 1967].

There are some similarities between changes caused by iontophoresis and skin electroporation. Both showed a dependence on voltage and led to the creation of transport pathways significantly larger than calcein. However, as discussed below, electrical characterization indicates that different mechanisms are involved.

### 12.3.4 Electrical Characterization of Skin Electroporation and Iontophoresis

The mechanistic insight provided by transport data can be supplemented by characterization of changes in skin electrical properties due to different electric field exposures. First, we can calculate what fraction of the skin is available to ion transport. Second, we can determine over what characteristic times these transport pathways become accessible.

By measuring skin resistance and assuming that ion transport pathways are filled with saline, we can calculate the area fraction of skin made up of these pathways, $F_{ion}$. After minutes to hours of conventional iontophoresis (up to a few volts), human skin resistance can drop to 1,000 - 10,000 $\Omega$ cm$^2$ [Hadgraft and

Guy, 1989; Inada et al., 1994; Kasting, 1992], in agreement with Fig. 12-5C. This corresponds to ion transport pathways occupying 0.01 - 0.001 % of the skin's surface area ($F_{ion} = 10^{-5} - 10^{-4}$) for stratum corneum of 17 μm thickness [Hadgraft and Guy, 1989] and saline resistivity of 72 Ω cm [Weast, 1985].

Making the same calculation during higher-voltage pulses, where skin resistance drops to ~ 100 Ω $cm^2$ (see Fig. 12-5 and references [Bose, 1994] and [Pliquett and Weaver, submitted, a]), suggests that 0.1 % of skin surface area is available to ion transport ($F_{ion} = 10^{-3}$). Electroporation in single bilayer systems is also believed to cause up to 0.1 % of membrane area to contain pores, although areas are often much smaller [Freeman et al., in press]. Therefore, 10 - 100 times more skin area is available for ion transport during skin electroporation than during conventional iontophoresis. This may correspond to a shift from iontophoretic transport largely through shunt routes to transport through electropores within the bulk of the stratum corneum.

We can also consider differences between pathways available to small ions and those available to calcein. Since $F_{ion}$ gives the fraction of skin area containing ion pathways and $t_{calcein} / t_{calcein,\,max}$ gives the fraction of ion pathways available to calcein transport, then the fraction of skin area available to calcein transport is

$$F_{calcein} = F_{ion} \times \frac{t_{calcein}}{t_{calcein,\,max}}.$$

Using this relationship, $F_{calcein} = 10^{-6}$ to $10^{-3}$ during skin electroporation and $F_{calcein} = 10^{-8}$ to $10^{-4}$ during iontophoresis.

Finally, we consider the time scale over which these transport pathways become accessible. Changes in skin resistance due to conventional

iontophoretic exposures occur over a characteristic time of at least minutes [Hadgraft and Guy, 1989; Inada et al., 1994; Kasting, 1992], in agreement with Fig. 12-5C. In contrast, ion transport pathways created by skin electroporation become accessible at least eight orders of magnitude more quickly, over a characteristic time of microseconds or faster (see Fig. 12-5 and references [Bose, 1994] and [Pliquett and Weaver, submitted, a]). Electroporation in single bilayer systems is also known to occur on a time scale of microseconds or faster [Chang et al., 1992; Orlowski and Mir, 1993; Weaver, 1993b]. Given that skin electroporation causes 1 to 2 orders of magnitude greater resistance drops which occur at least 8 orders of magnitude more quickly than those associated with iontophoresis, it seems unlikely that the mechanistic bases for changes associated with these two phenomena are the same.

There is little reason to expect electroporation of stratum corneum lipids to occur at typical iontophoresis voltages (i.e., up to a few volts across the skin). Electroporation is known to occur when the voltage across a single lipid bilayer membrane reaches ~ 1 V, which corresponds to an electric field within the membrane (~ 10 nm thick) on the order of $10^6$ V/cm [Chang et al., 1992; Orlowski and Mir, 1993; Weaver, 1993b]. To achieve a field strength of $10^6$ V/cm within the membrane, bulk electric fields of $10^4$ V/cm are often used for electroporation of bacteria cells in suspension (~ 1 μm diameter), $10^3$ V/cm for yeast (~ 10 μm diameter) and $10^2$ V/cm for sea urchin eggs (~ 100 μm diameter) [Chang et al., 1992]. This is because the electric field concentrates within the membranes of spherical cells in suspension, due to their large resistance, following the well-known relationship [Foster and Schwann, 1986]

$$\Delta V_{membrane} = 1.5\, E_{bulk}\, r_{cell}$$

where $\Delta V_{membrane}$ is the maximum transmembrane voltage, $E_{bulk}$ is the imposed uniform electric field strength, $r_{cell}$ is the cell radius, and the factor 1.5 is introduced due to local distortion of the electric field by the cell. Thus, typical iontophoretic exposures might be sufficient to electroporate a few bilayers, perhaps affecting the lining of appendages [Kasting, 1992]. However, to electroporate the approximately 100 bilayers in series found in a pathway across human stratum corneum, transdermal voltages on the order of 100 V should be required [Chizmadzhev et al., submitted; Edwards et al., submitted; Prausnitz et al., 1993a].

### 12.3.5 Implications for Applications

These results may give insight into how protocols could be designed to optimize transdermal transport by electroporation. First, steady-state flux can be reached within minutes and maintained for many hours (Fig. 12-3), as discussed previously [Prausnitz et al., submitted, c]. This short lag time may aid applications requiring rapid onset of therapeutic action and/or complex drug delivery profiles. Moreover, the long-term maintenance of steady state suggests that results obtained from experiments for 1 h could be generalized for longer times.

Higher-voltage protocols appear to be more efficient, as they increase transport number for both electroporation and iontophoresis (Figs. 12-7 and 12-8). However, higher-voltage pulses may be associated with nerve stimulation and unpleasant sensation. Thresholds for nerve stimulation are non-linear functions of pulse current, pulse length, and contact area, where threshold currents increase exponentially with decreasing pulse length for short pulses (< 1

ms) [Reilly, 1992]. Therefore, shorter pulses at higher-voltage may provide increased transport efficiency without sensation or pain. However, Fig. 12-4 indicates that pulses longer than 10 μs may be required for dramatic flux enhancement, suggesting that pulses between 10 μs and 1 ms may be most useful.

Transdermal delivery by pulsed protocols described here may reduce sensation, compared to conventional iontophoresis. In a recent review, Ledger identified three sources of unwanted cutaneous effects of iontophoresis: direct nerve stimulation, high current densities associated with skin appendages, and transfer of ions into the skin [Ledger, 1992]. First, as discussed above, short pulses (≤ 1 ms) significantly reduce direct nerve stimulation, thereby potentially causing less irritation in vivo than continuous electric fields. Pulsed iontophoresis has previously received considerable attention [Bagniefski and Burnette, 1990; Chien et al., 1987].

Second, irritation during iontophoresis caused by high current densities concentrated within skin appendages may be reduced by skin electroporation. Because the area for ion transport was dramatically increased during higher-voltage pulses ($F_{ion} = 10^{-3}$), irritation may be reduced by distributing current more evenly across the stratum corneum through new pathways.

The third potential cause of irritation involves introduction of ions into skin, resulting in pH changes or electrical polarization of the skin [Ledger, 1992]. Because no net current (or ion transfer) occurs in an alternating-polarity protocol, pH changes may be reduced or eliminated and electrical polarization of the skin should not occur. As shown in Fig. 12-1, an alternating-polarity pulsed protocol can dramatically increase transport across the skin. In contrast, lower-voltage (≤ 5 V) alternating-polarity iontophoresis did not enhance transport.

In conclusion, higher-voltage pulsed electric fields appear to make dramatic changes in skin transport properties, probably by a mechanism involving electroporation. It is already evident that potential advantages of this approach include dramatically increased flux, short transport lag times, and the possibility to reduce irritation. However, the present challenge is to gain a deeper understanding of skin electroporation and thereby assess more fully how this mechanism might best be used for drug delivery and other applications.

## 12.4 Conclusions

Transdermal transport of calcein was measured during lower-voltage, continuous electric fields (iontophoresis) and higher-voltage pulsed electric fields (electroporation). Transport due to pulsing showed a nonlinear dependence on pulse voltage, but was proportional to total "on" time (the product of pulse length multiplied by pulse rate), except at the shortest pulse length (10 μs) and at the slowest pulse rate (3 Hz). Alternating-polarity pulses increased transport by up to three orders of magnitude, while electrically "equivalent" continuous alternating-current fields provided no enhancement. For both iontophoresis and skin electroporation, calcein transport number, or transport efficiency, (a) ranged from $10^{-5}$ to $10^{-2}$, (b) was a function of voltage and current, and (c) did not show dependence on pulse length, pulse rate, pulse waveform, or total charge transferred. The area fraction of skin available to small ion transport was $10^{-5}$ to $10^{-4}$ during iontophoresis and $10^{-3}$ during skin electroporation, while that available to calcein transport ranged from $10^{-8}$ to $10^{-4}$ during iontophoresis and $10^{-6}$ to $10^{-3}$ during skin electroporation. Skin transport properties changed due to electroporation over a time scale of microseconds or faster. Potential strengths of transdermal drug delivery by skin electroporation include dramatically

increased flux, short transport lag times, and the possibility of reduced irritation compared to iontophoresis.

# 13 Rapid Temporal Control Of Transport[21]

## 13.1 Introduction

Transdermal drug delivery has the potential to be a noninvasive, user-friendly method of delivering drugs at steady or time-varying rates [Bronaugh and Maibach, 1989; Hadgraft and Guy, 1989]. However, to date it has found limited clinical application, largely because transport of most drugs across human skin is very slow, exhibiting lag times of hours to days and steady-state rates which are often subtherapeutic. Recently, evidence for electroporation of skin has been demonstrated and proposed as a mechanism to enhance transdermal drug delivery [Bommannan et al., 1993; Bose, 1994; Prausnitz et al., 1992; Prausnitz et al., 1993a; Prausnitz et al., in press, a].

Electroporation involves the application of a brief electric field pulse which creates aqueous pathways in lipid bilayers, such as cell membranes [Chang et al., 1992; Neumann et al., 1989; Orlowski and Mir, 1993; Weaver, 1993b]. During electroporation, the electric field is believed to dramatically increase molecular transport by a combination of two mechanisms: 1) electropores are created and 2) as pores appear, molecules are rapidly moved through the pores by electrophoresis and/or electroosmosis due to the local field.

Electroporation of skin could have significance for drug delivery, having been shown to cause transdermal flux increases up to four orders of magnitude which are largely or fully reversible, possibly involving transient structural changes in the intercellular lipid bilayers of the stratum corneum [Prausnitz et al., 1993a; Prausnitz et al., in press, a]. This study focuses on the rapid kinetics of transdermal transport by electroporation, which may allow rapid onset of

---

[21] These results have also been reported in [Prausnitz et al., submitted, c].

therapeutic action and/or complex drug delivery profiles during transdermal drug delivery.

## 13.2 Results

### 13.2.1 Time Scale Of Transport

Transdermal transport by electroporation of calcein across human epidermis was continuously measured (Figure 13-1). Figure 13-1A shows calcein flux versus time due to pulsing at three different voltages at the same pulse rate (1 pulse per minute, ppm) for 1 h. At each voltage, flux reached a steady state within minutes and then decreased below background levels within seconds after pulsing stopped.

At first, the curves in Figure 13-1A may appear to contain a lot of noise. However, the same data shown with an expanded time axis in Figure 13-1B, indicates that flux varied with a regular period of approximately 1 peak per minute. This is the same rate at which pulses were applied. Our interpretation is that these variations show the effects on transport of individual pulses. This is also supported by results seen during pulsing at other rates (data not shown). After each pulse, the flux initially increased, but then decayed as the effects of the pulse decreased. Although the time over which the flux decayed after each pulse appears to be tens of seconds, it may be shorter, as discussed previously [Pliquett et al., submitted].

Figure 13-1C shows this data replotted as cumulative calcein transported. From the graph, steady-state lag times (the characteristic time for flux to reach steady state) can be calculated by extending the linear portion of the graph to the time axis. The intercept is the steady-state lag time, determined to be approximately 10 min, independent of voltage. Figure 13-1D, which shows the

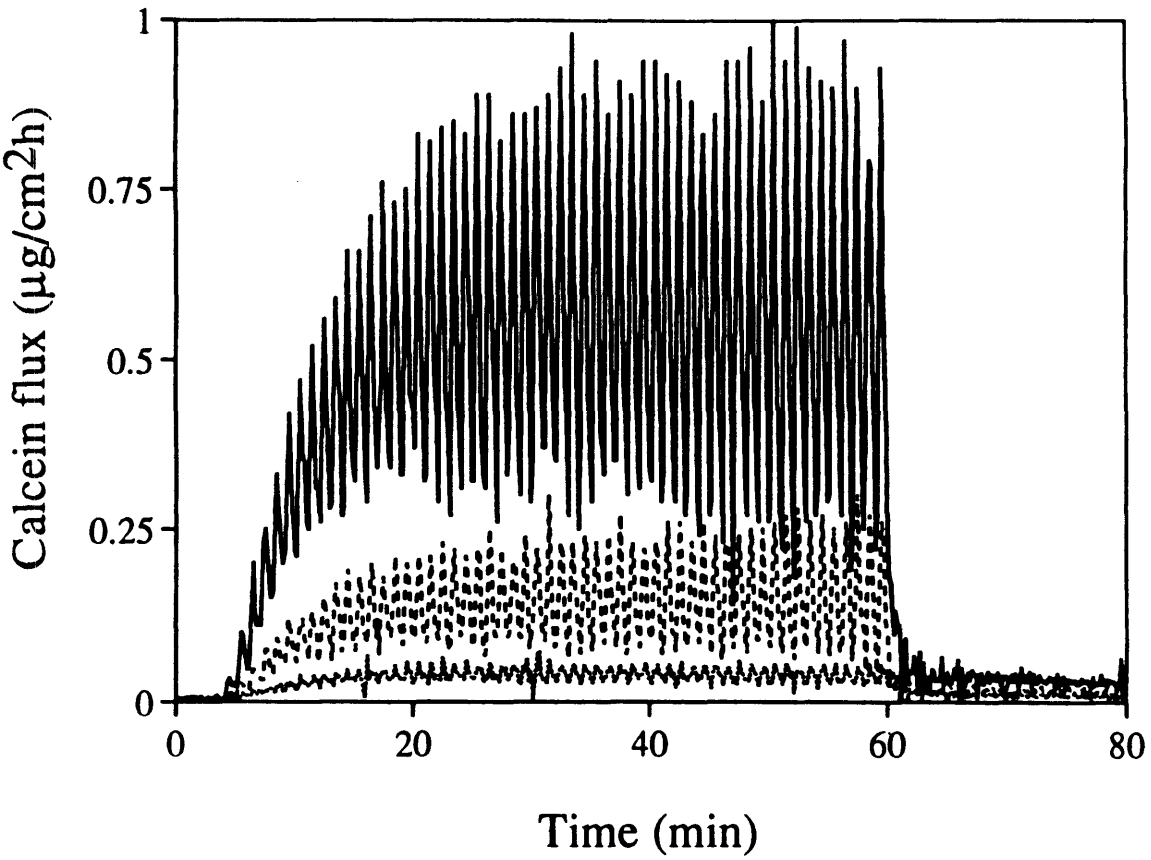


**Fig. 13-1A.** Time profiles of transdermal transport of calcein due to electroporation at different voltages. Transdermal flux due to pulsing at 1 pulse per minute (ppm) for 1 h: 270 V (solid line), 135 V (dashed line), 115 V (dotted line) (Data from [Pliquett et al., submitted, b]). This graph demonstrates that transdermal flux was rapidly responsive to electrical conditions, over characteristic times of seconds to minutes (see Table 13-1).

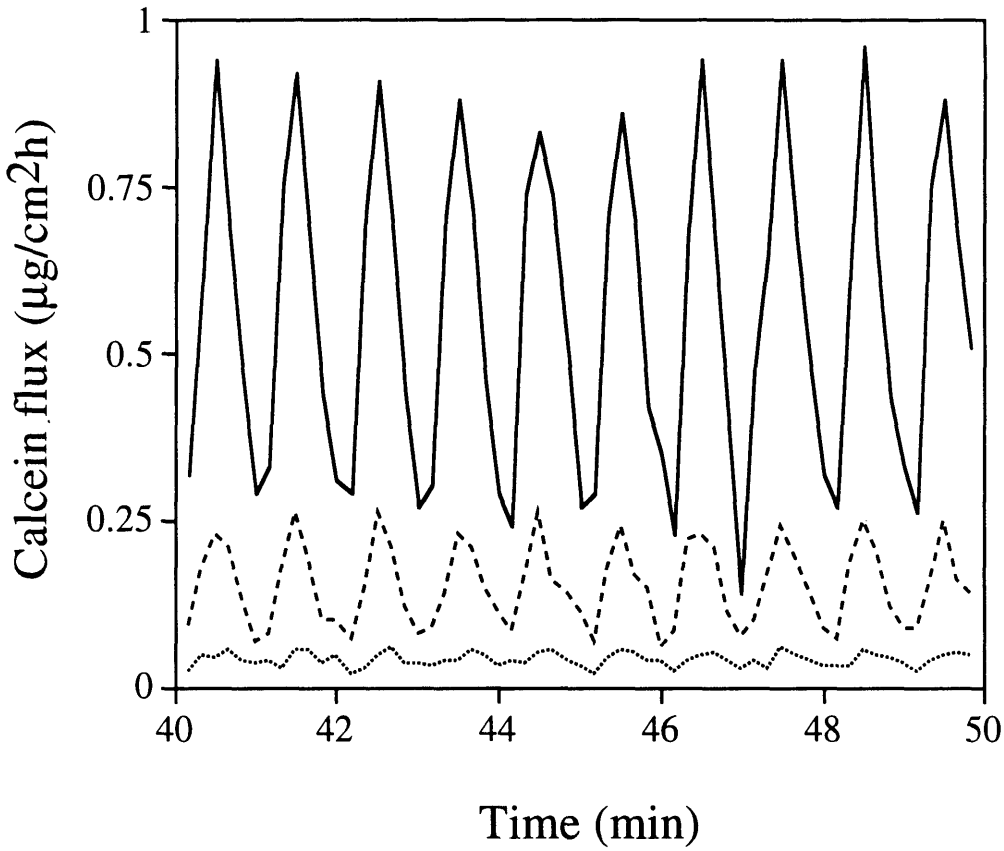


**Fig. 13-1B.** Time profiles of transdermal transport of calcein due to electroporation at different voltages. This figure contains data in Fig. 13-1A replotted with the time axis expanded.

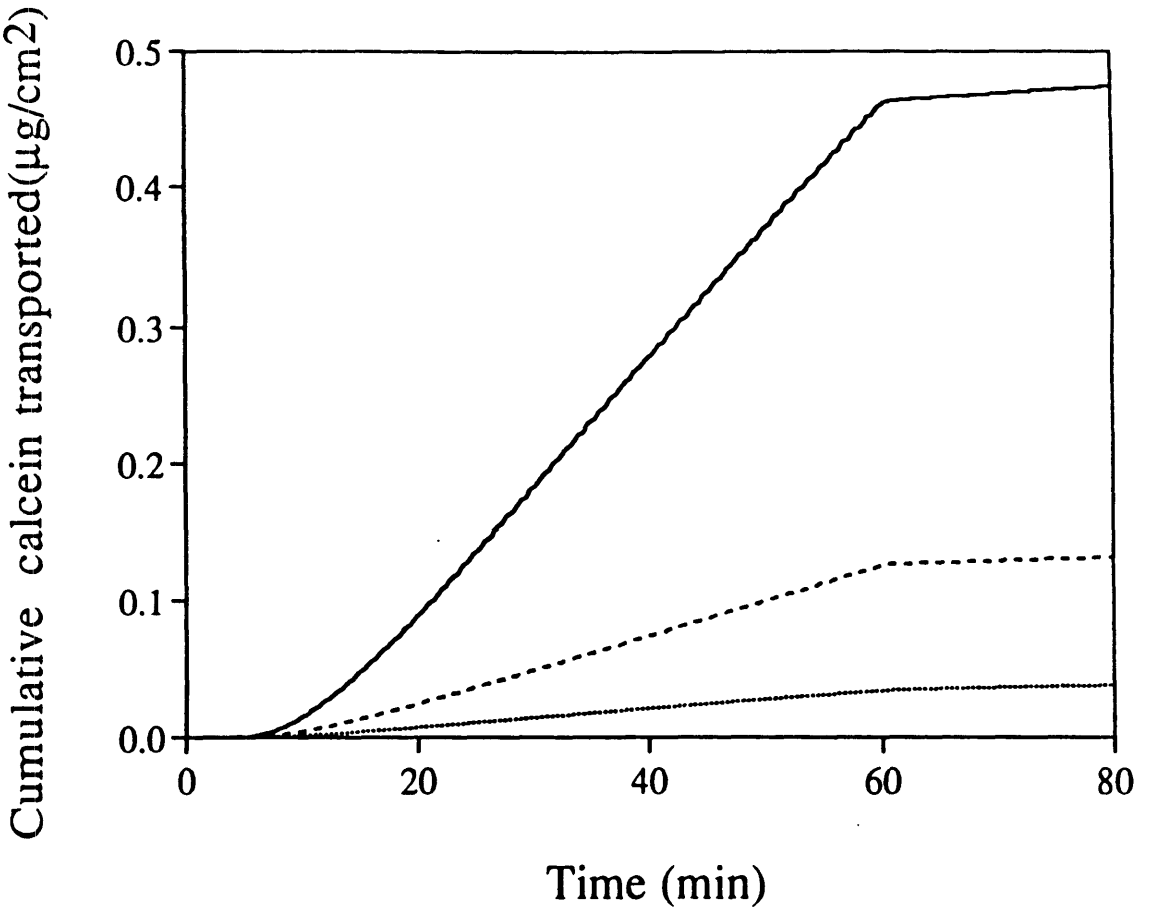


**Fig. 13-1C.** Time profiles of transdermal transport of calcein due to electroporation at different voltages. This figures contains data from Fig. 13-1A replotted as cumulative calcein transported, for calculation of steady-state lag times, indicated by the time-axis intercept.

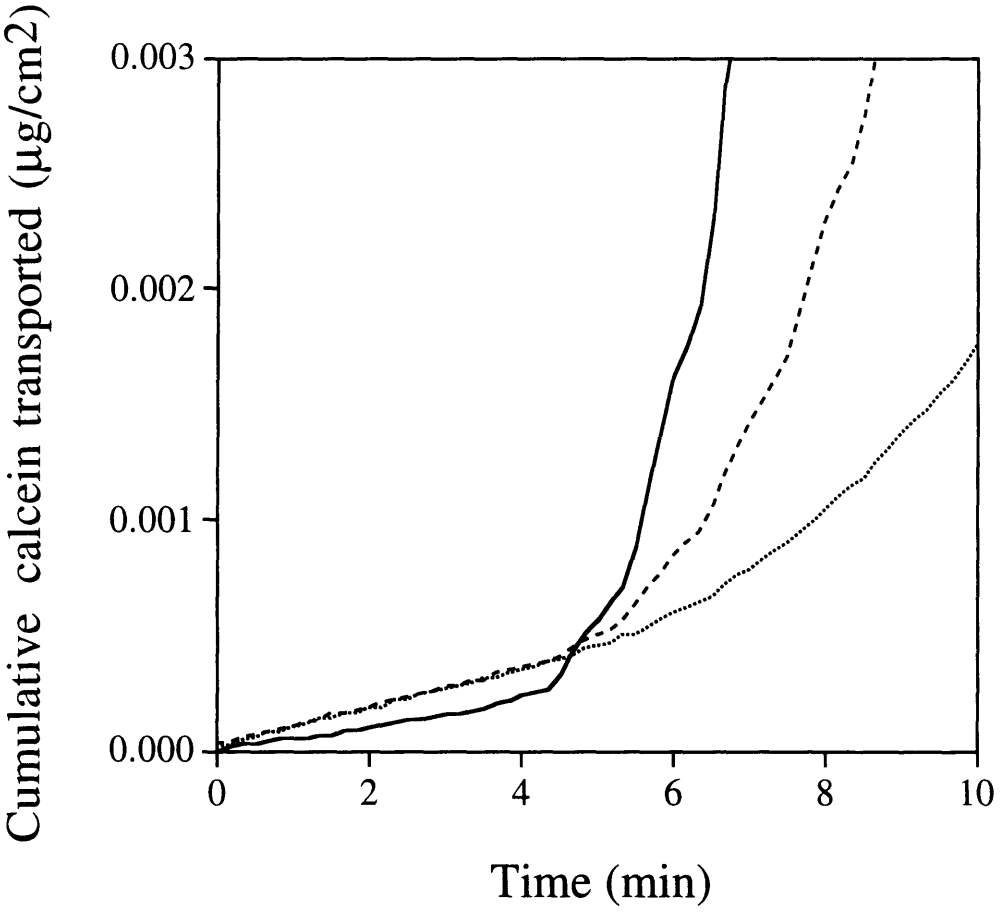


**Fig. 13-1D.** Time profiles of transdermal transport of calcein due to electroporation at different voltages. This figure contains data in Fig. 13-1C replotted with the time axis expanded, to show transport onset time.

same data with an expanded time axis, indicates that the onset time for transport was 3 min, independent of voltage: pulsing was started at 3 min and the first detectable transdermal transport was measured at 6 min.

### 13.2.2 Empirical Characterization Of Flux Vs. Time Profiles

Data similar to that of Figure 13-1 have been collected over a range of pulsing conditions by Pliquett and Weaver [submitted, b]. Characteristic values describing these data are summarized in Table 13-1. They indicate that while flux depended on both pulse voltage and pulse rate, the steady-state lag time and onset time depended only on pulse rate. Decay time was independent of both pulse voltage and pulse rate.

Using the data in Table 13-1, flux as a function of time was empirically fit using the following equations:

$$J = J_{ss}\left[1 - e^{\frac{-(t - T)}{\tau}}\right] \quad (1)$$

$$J_{ss} = k_1 V R \quad (2)$$

$$\tau = \frac{k_2}{R} \quad (3)$$

$$T = \frac{k_3}{R} \quad (4)$$

where J = calcein flux ($\mu g/cm^2h$), $J_{ss}$ = steady-state calcein flux ($\mu g/cm^2h$), t = time (min), T = onset time (min), $\tau$ = steady-state lag time (min), V = pulse voltage (V), R = pulse rate (ppm), and $k_1$, $k_2$, and $k_3$, are empirical constants equal to $8 \times 10^{-4}$ $\mu g/(cm^2hVppm)$, 10, and 4 respectively.

| Pulse voltage (V) | Pulse rate (ppm) | Steady-state flux (μg/cm$^2$hr) | Steady-state lag time (min) |
|---|---|---|---|
| 63 | 1 | 0.055 | 13 |
| 63 | 3 | 0.074 | |
| 63 | 6 | 0.11 | |
| 63 | 12 | 0.14 | |
| 86 | 1 | 0.073 | 10 |
| 86 | 3 | 0.13 | |
| 86 | 6 | 0.25 | |
| 86 | 12 | 0.49 | |
| 134 | 1 | 0.16 | 12 |
| 134 | 3 | 0.30 | |
| 134 | 6 | 0.47 | |
| 134 | 12 | 0.74 | |
| 191 | 1 | 0.1 | 11 |
| 191 | 3 | 0.43 | 5 |
| 191 | 6 | 1.1 | 3 |
| 191 | 12 | 2.1 | 2 |
| 231 | 1 | 0.24 | 11 |
| 231 | 3 | 0.64 | 6 |
| 231 | 6 | | 1 |
| 231 | 12 | | 1 |

**Table 13-1.** Characteristic values of transdermal transport of calcein due to electroporation. These data have been obtained and summarized from [Pliquett et al, submitted, b]. Each data point is the average of 1 - 2 experimental values, including results from a total of 15 different skin samples. Steady-state lag time (the characteristic time for flux to reach steady state) corresponds to the time-axis intercept of graphs of cumulative calcein transported versus time (see Fig. 13-1C). Onset time, which indicates the time at which an increased flux was first measured (see Fig 13-1D), generally corresponded to the time required to give 3 - 5 pulses (e.g., 3 - 5 min for 1 ppm or 15 - 25 s for 12 ppm). Decay time, which corresponds to the characteristic time over which flux decayed after pulsing was stopped, was < 10 s under all conditions investigated (determined by fitting to an exponential decay).

The three empirical constants were determined using the data in Table 13-1. To calculate $k_1$, steady-state flux was plotted versus the product of pulse voltage time pulse rate and a least-squares linear regression was performed (correlation constant, $r^2 = 0.83$) yielding a slope equal to $k_1$. Similarly, $k_2$ equaled the slope of a linear fit of steady-state lag time versus the inverse of pulse rate ($r^2 = 0.95$). Average onset time corresponded to the time required to give 4 pulses, which determined the value for $k_3$.

The form of these flux equations does not yet have a mechanistic basis. Instead, their form was suggested by (a) the shape of the curves (see Figure 13-1), which appear to exponentially approach a steady-state value after an onset time (eq. 1), and (b) the observation that steady-state flux appeared to be proportional to pulse rate and voltage (eq. 2), while lag time (eq. 3) and onset time (eq. 4) appeared to be inversely proportional to pulse rate (see Table 13-1).

The flux equations can predict the time profile of transdermal flux for a given pulse rate and voltage. Similarly, pulsing parameters can be determined for a desired delivery schedule. However, these equations are only valid under the conditions of this study and only over a limited range of electrical parameters. Given the large variability in flux across different skin samples from different donors, these equations should only be used in their present form for order of magnitude estimates.

### 13.2.3 Rapid Temporal Control Of Transport

Figures 13-2 and 13-3 show how the rapidly responsive behavior of transdermal drug delivery by electroporation can be used to achieve desired delivery profiles. For example, continuous low-level delivery of a drug with intermittent boluses may be a desirable delivery schedule for some drugs. To

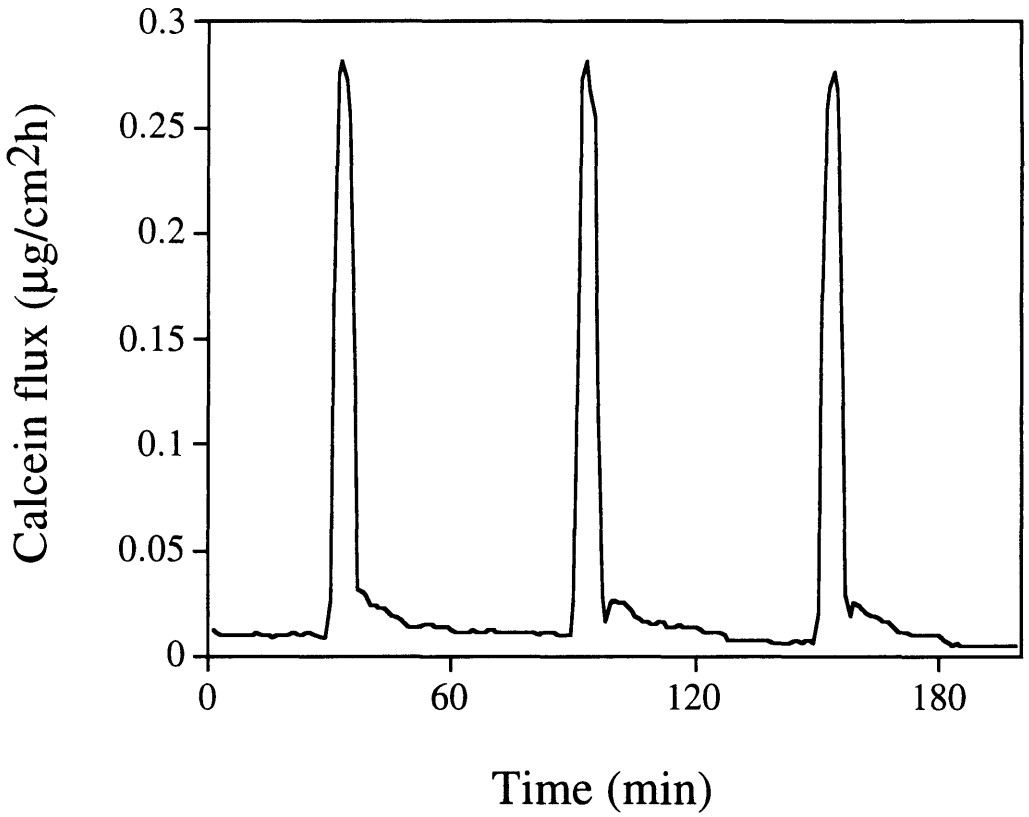


**Fig. 13-2A.** Complex delivery profiles using transdermal delivery by electroporation: continuous low-level delivery with intermittent boluses. Low-level delivery corresponded to continuous dc iontophoresis at 14 $\mu A/cm^2$. Boluses corresponded to pulsing at 115 V and 12 ppm for 5 min, each separated by 55 min of iontophoresis.

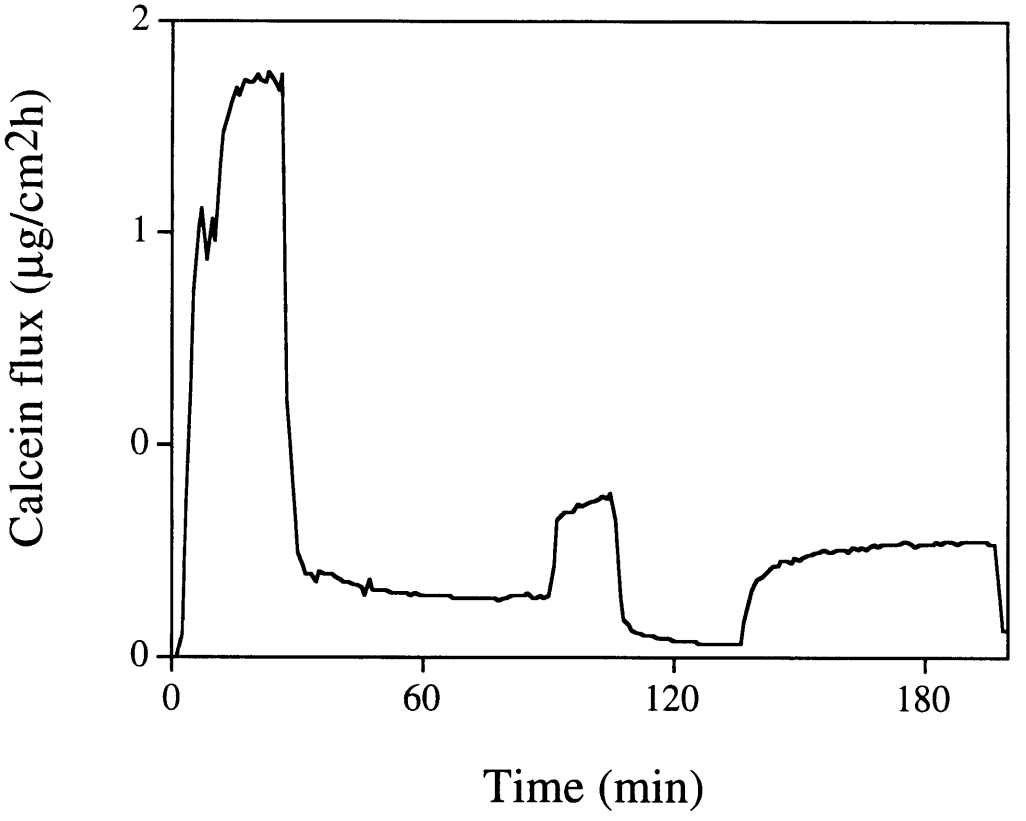


**Fig. 13-2B.** Complex delivery profiles using transdermal delivery by electroporation: a complex delivery schedule achieved by changing pulse voltage. Pulse rate was held constant at 1 ppm, while pulse voltage was changed in the following sequence: 270 V for 30 min, 115 V for 60 min, 165 V for 15 min, 0 V for 30 min, 135 V for 60 min, 0 V for 5 min.

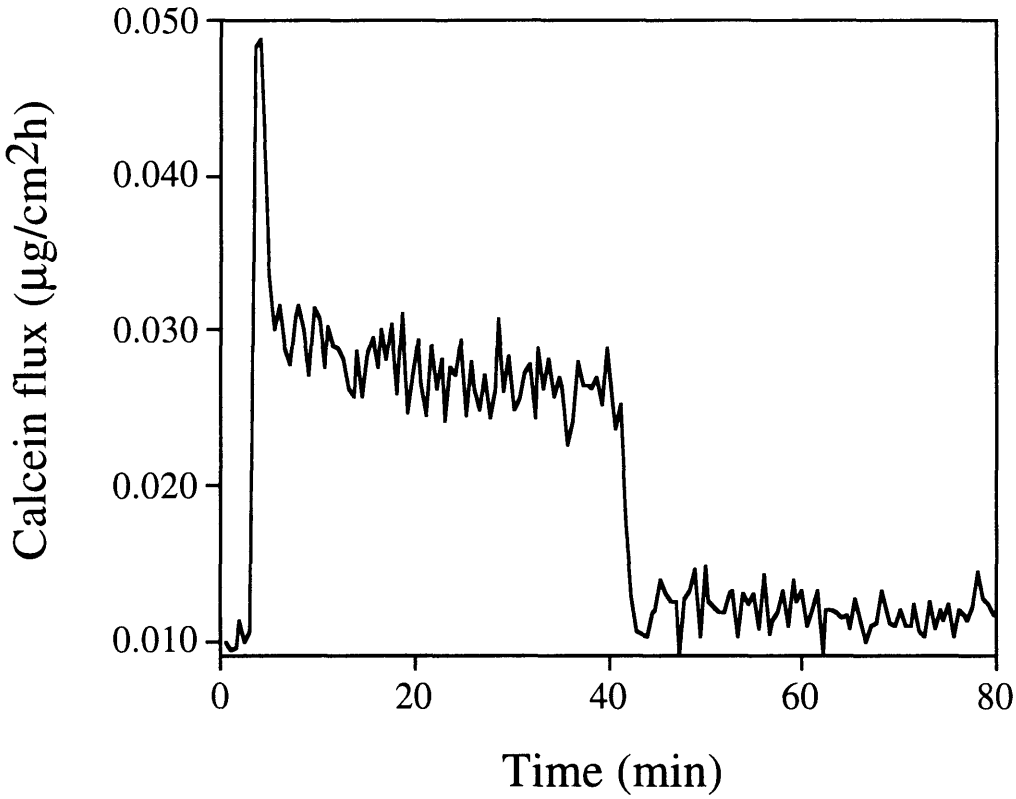


**Fig. 13-3.** More-rapid attainment of steady-state flux using a time-varying pulse protocol. Reaching steady state within approximately 1 min, transdermal flux is shown due to pulsing at 165 V initially at 12 ppm (15 s) to "prime the pump," followed by pulsing at 1 ppm (40 min) to maintain the desired steady-state flux.

achieve this type of delivery, iontophoresis was applied to supply baseline delivery, while electroporation pulses provided rapid boluses (Figure 13-2A). A more complex delivery profile is shown in Figure 13-2B. In these figures, changes in delivery rates were achieved by changing pulse voltage. However, changes in pulse rate can also achieve similar results (data not shown). Using the time-invariant pulsing protocols shown above, steady-state transport was achieved within minutes, depending on pulse rate used (e.g., Table 13-1). However, we wanted to determine whether steady state could be reached more quickly by further improving the pulsing protocol. For this reason, an initial series of three pulses were applied more rapidly (12 ppm), to "prime the pump," followed by less rapid pulsing (1 ppm) to provide the desired steady-state flux. The result is shown in Figure 13-3, where steady state was achieved within approximately 1 min.

## 13.3 Discussion

It has been previously demonstrated that electroporation of skin can cause reversible transdermal flux increases up to four orders of magnitude, which appear to involve transient structural changes within the stratum corneum [Prausnitz et al., 1993a; Prausnitz et al., in press, a]. The present study shows that during skin electroporation, steady-state lag times and onset times of minutes can be achieved, indicating rapid temporal control of transport. In contrast, steady-state lag times associated with other methods of transdermal transport are often hours to days [Bronaugh and Maibach, 1989; Hadgraft and Guy, 1989].

Flux versus time profiles were characterized by a simple set of empirical equations, which could be used to (a) predict delivery profiles under a given set

of electroporation conditions and (b) select the pulsing conditions required to achieve a desired delivery schedule. While these equations have been determined only with limited data, additional characterization could yield equations which are more broadly applicable.

Examples of how specialized delivery profiles can be created using the rapid temporal control of electroporation are shown in Figures 13-2 and 13-3. Sequential application of different sets of pulsing conditions allowed creation of complex delivery profiles, limited by temporal control not faster than minutes. Better understanding of skin electroporation and further optimization of pulsing protocols may lead to still more rapid control of transport.

## 13.4 Conclusions

Many unresolved issues must be addressed before transdermal drug delivery by electroporation finds clinical application. However, an ability to increase transdermal transport by orders of magnitude with lag times of only minutes may be significant. Rapid onset of therapeutic action and/or complex drug delivery profiles could be achieved, where delivery rates could be swiftly adjusted by medical personnel, patients, or a microprocessor either (a) controlled by preprogrammed schedules or (b) interfaced with sensors for automatic feedback.

# CONCLUSIONS

## 14 Conclusions

### 14.1 Cell Electroporation

Most applications of electroporation have the common goal of transporting useful numbers of molecules across cell membranes. However, few studies have measured the actual number of molecules transported, making efforts to advance both applications and basic modeling difficult. Here, flow cytometry has been used because of its quantitative nature at the single cell level, to conduct a systematic study of the effects of electric and other parameters on molecular transport due to electroporation, considering pulse field strength, pulse length, pulse rate, number of pulses, temperature, molecule size and charge, molecule-membrane interactions, and the time scale of transport.

While the quantitative characterization of transport performed in this thesis should serve as an important guide to both applications and modeling, this study yielded two particular results which may provide deeper insight into mechanisms of transport. First, uptake was found to plateau at high field strength. However, this was not necessarily an absolute maximum in transport. Instead, it represented the maximum effect of increasing field strength, for a particular pulse protocol. Second, maximum uptake under any conditions used here corresponded to approximately one fourth of apparent equilibrium with the external solution. These results constrain mechanisms and are probably a consequence of the complex, interactive behavior of the dynamic pore population associated with electroporation.

Although the early literature often assumed that transport due to electroporation occurred by post-pulse diffusion through long-lived electropores,

more recent studies suggested that electrically-driven transport during the pulse may be dominant (see Chapter 9). However, electroporation transport kinetics had only been measured on time scales at least an order of magnitude longer than that of the pulse, making it difficult to compare transport rates during and after the pulse. To determine the time scale of transport and the mechanism(s) by which it occurred, we measured transport with sub-millisecond time resolution during and after electroporation pulses of a few milliseconds duration. We found that under some conditions transport occurred predominantly by electrophoresis and/or electroosmosis during a pulse, while under other conditions transport occurred in part or almost completely by diffusion within seconds after a pulse. The short time resolution of these studies should make them especially useful for developing models of electroporation transport.

Because pore formation is a heterogeneous, time-dependent, and highly nonlinear phenomenon, understanding mechanisms of transport through a population of electropores is challenging. This thesis provides (a) a systematic study of the absolute number of molecules transported over a range of electroporation conditions and (b) measurements of electroporation transport with time resolution shorter than that of the pulse. These results give insight into mechanisms and form a basis for future study, where the present challenges lie in developing a theoretical framework which can fully explain the experimental findings.

## 14.2 Tissue Electroporation

Our study of tissue electroporation was motivated primarily by potential applications in transdermal drug delivery. Although electroporation of cells within tissue has received limited attention, electroporation of the multilamellar,

intercellular, nonphospholipid bilayers of the skin has not been investigated previously. We wanted to determine (a) whether electroporation occurs in skin and (b) if so, whether the associated transport occurs at levels useful for transdermal drug delivery or other applications.

Our measurements suggest that electroporation occurs in the skin by a mechanism involving transient structural changes in the intercellular lipid bilayers of the stratum corneum. Flux increases up to four orders of magnitude have been observed with human skin *in vitro* for three molecules having charges between -1 and -4 and molecular masses up to 1000 Da. Similar flux increases have been observed *in vivo* with hairless rat skin. The area fraction of skin available to transport during electroporation was determined to be up to 0.1 %. Skin electroporation was also theoretically characterized, indicating that changes in transport due to electroporation of lipid bilayers within the stratum corneum were consistent the observed results.

Electroporation-mediated transport is rapidly responsive to changes in electrical conditions, where (a) skin transport properties change over a time scale of microseconds or faster and (b) steady-state transdermal flux can be achieved on a time scale of minutes. Thus, the ability of electroporation to achieve both dramatic flux enhancement and short lag times could make possible transdermal delivery of many drugs at therapeutic rates.

Having demonstrated that electroporation appears to occur in skin and that rates of transport are at levels useful for some applications of transdermal drug delivery, challenges for future research lie primarily in two areas. First, a deeper understanding is required of skin structural alterations responsible for the observed changes in electrical and transport properties and whether they might allow transport of macromolecules. Assessment of other skin properties could be

employed, as assessed by various forms of spectroscopy, microscopy, and molecular indicator probes. Moreover, the transition region between 1 V and 100 V across the skin should be more fully studied to identify differences between conventional iontophoresis and skin electroporation. Experimental studies should be guided by further theoretical treatment.

The second area concerns medical applications. Although electrical and transport measurements suggest that changes in stratum corneum barrier properties due to electroporation are largely or fully reversible, consequences in viable tissues have not been studied. Electroporation of living cells in the epidermis, dermis and deeper tissues, and any subsequent damage, should be considered. Also, possible stimulation of nerves which can lead to unpleasant sensation and/or muscle stimulation should be addressed. Because these effects will be strongly affected by electric field properties and distribution within the skin, careful design of electrodes and pulsing protocols will be essential to the reduction of unwanted side-effects and to the eventual utility of skin electroporation in a clinical setting.

## References

Abidor, I. G., V. B. Arakelyan, L. V. Chernomordik, Y. A. Chizmadzhev, V. F. Pastushenko and M. R. Tarasevich (1979) Electric breakdown of bilayer membranes: I. The main experimental facts and their qualitative discussion. *Bioelectrochem. Bioenerget.* **6**:37-52.

Abidor, I. G. and A. E. Sowers (1992) Kinetics and mechanism of cell membrane electrofusion. *Biophys. J.* **61**:1557-1569.

Abramson, H. A. (1941) Skin reactions. X. Preseasonal treatment of hay fever by electrophoresis of ragweed pollen extracts into the skin: preliminary report. *J. Allergy* **12**:169-175.

Abramson, H. A. and M. H. Gorin (1940) Skin reactions. IX. The electrophoretic demonstration of the patent pores of the living human skin; its relation to the charge of the skin. *J. Phys. Chem.* **44**:1094-1102.

Antich, T. J. (1982) Phonophoresis: the principles of the ultrasonic driving force and efficacy in treatment of common orthopaedic diagnoses. *J. Orthop. Sports Phys. Ther.* **4**:99-102.

Arvidsson, S. B., R. H. Ekroth, A. M. C. Hansby, A. H. Lindholm and G. William-Olsson (1984) Painless venipuncture. A clinical trial of iontophoresis of lidocaine for venipuncture in blood donors. *Acta Anaesthesiol. Scand.* **28**:209-210.

Atkins, P. W. (1986) Physical Chemistry. W. H. Freeman and Co., New York.

Auer, D., G. Brandner and W. Bodemer (1976) Dielectric breakdown of the red blood cell membrane and uptake of SV 40 DNA and mammalian cell RNA. *Naturwiss.* **63**:391.

Bagniefski, T. and R. R. Burnette (1990) A comparison of pulsed and continuous current iontophoresis. *J. Controlled Release* **11**:113-122.

Banga, A. K. and Y. W. Chien (1988) Iontophoretic delivery of drugs: fundamentals, developments and biomedical applications. *J. Controlled Release* **7**:1-24.

Barnett, A. and J. C. Weaver (1991) A unified, quantitative theory of reversible electrical breakdown and rupture. *Bioelectrochem. and Bioenerg.* **25**:163-182.

Bartoletti, D. C., G. I. Harrison and J. C. Weaver (1989) The number of molecules taken up by electroporated cells: quantitative determination. *FEBS Lett.* **256**:4-10.

Bazile, D., L. M. Mir and C. Paoletti (1989) Voltage-dependent introduction of a d[α]octothymidylate into electropermeabilized cells. *Biochem Biophys Res Commun* **159**:633-639.

Belehradek, J., S. Orlowski, B. Poddevin, C. Paoletti and L. M. Mir (1991) Electrochemotherapy of spontaneous mammary tumors in mice. *Eur. J. Cancer* **27**:73-76.

Belehradek, J., S. Orlowski, L. H. Ramirez, G. Pron, B. Poddevin and L. M. Mir (1994) Electropermeabilization of cells in tissues assessed by the qualitative and quantitative electroloading of bleomycin. *Biochim. Biophys. Acta* **1190**:155-163.

Belehradek, M., C. Domenge, B. Luboinski, S. Orlowski, J. Belehradek and L. M. Mir (1993) Electrochemotherapy, a new antitumor treatment. *Cancer* **72**:3694-3700.

Bell, R. P. (1945) A problem of heat conduction with spherical symmetry. *Proceedings of the Physical Society London* **57**:45-48.

Benson, H. A. E., J. C. McElnay, R. Harland and R. Hadgraft (1991) Influence of ultrasound on the percutaneous absorption of nicotinate esters. *Pharm. Res.* **8**:204-209.

Benz, R. and U. Zimmermann (1980) Relaxation studies on cell membranes and lipid bilayers in the high electric field range. *Bioelectrochem. and Bioenerg.* **7**:723-739.

Benz, R. F., F. Beckers and U. Zimmermann (1979) Reversible electrical breakdown of lipid bilayer membranes: a charge-pulse relaxation study. *J. Membrane Bio.* **48**:181-204.

Berglund, D. L. and J. R. Starkey (1991) Introduction of antibody into viable cells using electroporation. *Cytometry* **12**:64-67.

Bliss, J. G., G. I. Harrison, J. R. Mourant, K. T. Powell and J. C. Weaver (1988) Electroporation: the population distribution of macromolecular uptake and shape changes in red blood cells following a single 50 μs square wave pulse. *Bioelectrochem. Bioenerg.* **20**:57-71.

Bockris, J. O. and A. K. N. Reddy (1970) Modern Electrochemistry. Plenum Press, New York.

Boddé, H. E., M. A. M. Kruithof, J. Brussee and H. K. Koerten (1989) Visualisation of normal and enhanced $HgCl_2$ transport through human skin in vitro. *Int. J. Pharm.* **53**:13-24.

Boddé, H. E., I. van den Brink, H. K. Koerten and F. H. N. de Haan (1991) Visualization of in vitro percutaneous penetration of mercuric chloride; transport through intercellular space versus cellular uptake through desmosomes. *J. Controlled Release* **15**:227-236.

Bommannan, D., L. Leung, J. Tamada, J. Sharifi, W. Abraham and R. Potts (1993) Transdermal delivery of luteinizing hormone releasing hormone: comparison between electroporation and iontophoresis in vitro. *Proceed. Intern. Symp. Control. Rel. Bioact. Mater.* **20**:97-98.

Bommannan, D., G. K. Menon, H. Okuyama, P. M. Elias and R. H. Guy (1991a) Sonophoresis: II. Examination of the mechanism(s) of ultrasound-enhancer transdermal drug delivery. *Pharm. Res.* **9**:1043-1047.

Bommannan, D., H. Okuyama, P. Stauffer and R. H. Guy (1991b) Sonophoresis: I. The use of ultrasound to enhance transdermal drug delivery. *Pharm. Res.* **9**:559-564.

Bommannan, D., J. Tamada, L. Leung and R. O. Potts (submitted) Effect of electroporation on transdermal iontophoretic delivery of luteinizing hormone releasing hormone (LHRH) in vitro.

Bose, V. G. (1994) Electrical Characterization of Electroporation of Human Stratum Corneum. M. S. thesis, Massachusetts Institute of Technology, Cambridge, MA.

Bouwstra, J. A., M. A. d. Vries, G. S. Gooris, W. Bras, J. Brussee and M. Ponec (1991) Thermodynamic and structural aspects of the skin barrier. *J. Controlled Release* **15**:209-220.

Brenner, H. and D. A. Edwards (1993) Macrotransport Processes. Butterworth-Heinemann, Boston.

Bronaugh, R. L. and H. I. Maibach, eds. (1989) Percutaneous Absorption, Mechanisms -- Methodology -- Drug Delivery. Marcel Dekker, New York.

Brown, R. E., D. C. Bartoletti, K. T. Powell, J. G. Bliss, G. I. Harrison and J. C. Weaver (1992) Multiple-pulse electroporation: macromolecule uptake by intact *Saccharomyces cerevisiae*. *Bioelectrochem. Bioenerget.* **28**:235-245.

Burnette, R. R. and D. Marrero (1986) Comparison between the iontophoretic and passive transport of thyrotropin releasing hormone across excised nude mouse skin. *J. Pharm. Sci.* **75**:738-743.

Burnette, R. R. and B. Ongpipattanakul (1988) Characterization of the pore transport properties and tissue alteration of excised human skin during iontophoresis. *J. Pharm. Sci.* **77**:132-137.

Campbell, S. D., K. K. Kranino, E. G. Schibli and S. T. Momii (1977) Hydration characteristics and electrical resistivity of stratum corneum using a noninvasive four-point microelectrode method. *J. Invest. Dermatol.* **89**:290-296.

Casabiance-Pignède, M. R., L. M. Mir, J. B. Le Pecq and A. Jacquemin-Sablon (1991) Protection against ricin conferred by the introduction of antiricin antibodies into chinese hamster cells by electropermeabilization. *J. Cell Pharmacol.* **2**:27-33.

Chakrabarti, R., D. E. Wylie and S. M. Schuster (1989) Transfer of monoclonal antibodies into mammalian cells by electroporation. *J. Biol. Chem.* **264**:15494-15500.

Champion, R. H., J. L. Burton and F. J. G. Ebling, eds. (1992) Textbook of Dermatology. Blackwell Scientific, London.

Chang, D. C., B. M. Chassy, J. A. Saunde and A. E. Sowers, eds. (1992) Guide to Electroporation and Electrofusion. Academic Press, New York.

Chang, D. C. and T. S. Reese (1990) Changes in membrane structure induced by electroporation as revealed by rapid-freezing electron microscopy. *Biophys. J.* **58**:1-12.

Chang, K.-P. and R. S. Bray, eds. (1985) Leishmaniasis. Elsevier, New York.

Chernomordik, L. V., S. I. Sukharev, I. G. Abidor and Y. A. Chizmadzhev (1983) Breakdown of lipid bilayer membranes in an electric field. *Biochim. Biophys. Acta* **736**:203-213.

Chernomordik, L. V., S. I. Sukharev, S. V. Popov, V. F. Pastushenko, A. V. Sokirko, I. G. Abidor and Y. A. Chizmadzhev (1987) The electrical breakdown of cell and lipid membranes: the similarity of phenomenologies. *Biochim. Biophys. Acta* 360-373.

Chien, Y. W., ed. (1991) Novel Drug Delivery Systems: Fundamentals, Developmental Concepts, Biomedical Assessments. Marcel Dekker, New York.

Chien, Y. W. and A. K. Banga (1989) Iontophoretic (transdermal) delivery of drugs: overview of historical development. *J. Pharm. Sci.* **78**:353-354.

Chien, Y. W., O. Siddiqui, Y. Sun, W. M. Shi and J. C. Liu (1987) Transdermal iontophoretic delivery of therapeutic peptides/proteins. *Ann. N. Y. Acad. Sci.* **507**:32-51.

Chizmadzhev, Y. A., V. G. Zarnytsin, J. C. Weaver and R. O. Potts (submitted) Mechanism of electroinduced ionic species transport through a multilamellar lipid system.

Corbett, J. D. and D. E. Golan (1993) Band 3 and glycophorin are progressively aggregated in density-fractionated sickle and normal red blood cells: evidence from rotational and lateral mobility studies. *J. Clin. Invest.* **91**:208-217.

Coster, H. G. L. and U. Zimmermann (1975) The mechanism of electrical breakdown in the membranes of *Valonia utricularis*. *J. Membrane Biol.* **22**:73-90.

Crank, J. (1975) The Mathematics of Diffusion. Clarendon Press, Oxford.

Cullander, C. (1992) What are the pathways of iontophoretic current flow through mammalian skin? *Adv. Drug Deliv. Rev.* **9**:119-135.

Cullander, C. and R. H. Guy (1992) Transdermal delivery of peptides and proteins. *Adv. Drug Deliv. Rev.* **8**:291-329.

Deen, W. M. (1987) Hindered transport of large molecules in liquid-filled pores. *AIChE J.* **33**:1409-1425.

Dekeyser, R. A., B. Claes, R. M. U. De Rycke, M. E. Habets, M. C. Van Montagu and A. B. Caplan (1990) Transient gene expression in intact and organized tissues. *Plant Cell* **2**:591-602.

Dev, S. B. and G. A. Hofmann (1994) Electrochemotherapy -- a novel method of cancer treatment. *Cancer Treat. Reviews* **20**:105-115.

Dimitrov, D. S. and A. E. Sowers (1990) Membrane electroporation -- fast molecular exchange by electroosmosis. *Biochim. Biophys. Acta* **1022**:381-392.

Dodge, J. T., C. Mitchell and D. J. Hanahan (1963) The preparation and chemical characteristics of hemoglobin-free ghosts of human erythrocytes. *Arch. Biochem. Biophys.* **100**:119-130.

Duvanel, T., M. Harms and J. Saurat (1988) New technique to perform local anesthesia: pulsed iontophoresis. *Dermatolog* **177**:30.

Edelberg, R. (1967) Electrical properties of the skin. *In* Methods in Psychophysiology. Brown, C. C., ed. Williams & Wilkins, Baltimore, pp. 1-53.

Edwards, D. A. and R. Langer (in press) A linear theory of transdermal transport phenomena. *J. Pharm. Sci.*

Edwards, D. A., M. R. Prausnitz, R. Langer and J. C. Weaver (submitted) Analysis of enhanced transdermal transport by skin electroporation.

Elias, P. M. (1988) Structure and function of the stratum corneum permeability barrier. *Drug Develop. Res.* **13**:97-105.

Elias, P. M. (1991) Epidermal barrier function: intercellular lamellar lipid structures, origin, composition and metabolism. *J. Controlled Release* **15**:199-208.

Escande-Geraud, M. L., M. P. Rols, M. A. Dupont, N. Gas and J. Teissié (1988) Reversible plasma membrane ultrastructural changes correlated with electropermeabilization in chinese hamster ovary cells. *Biochim. Biophys. Acta* **939**:247-259.

Fisher, H. B., E. J. List, R. C. Y. Koh, J. Imberger and N. H. Brooks (1979) Mixing in Inland and Coastal Waters. Academic Press, New York.

Foster, K. R. and H. P. Schwann (1986) Dielectric properties of tissues. *In* CRC Handbook of Biological Effects of Electromagnetic Fields. Polk, C. and E. Postow, eds. CRC Press, Boca Raton. pp. 27-96.

Freeman, S. A., M. A. Wang and J. C. Weaver (in press) Theory of electroporation of planar membranes: predictions of the aqueous area, change in capacitance and pore-pore separation. *Biophys. J.*

Frenkel, J. (1944) On the theory of seismic and seismoelectric phenomena in a moist soil. *J. Phys. U.S.S.R.* **8**:230-241.

Friend, D. R. (1992) In vitro skin permeation techniques. *J. Controlled Release* **18**:235-248.

Fung, Y. C. B. and S. S. Sabin (1977) Mechanics of pulmonary circulation. *In* Cardiovascular Flow Dynamics and Measurements. Hwang, N. H. C. and N. A. Norman, eds. University Park Press, Baltimore. pp. 665-730.

Furry, J. W. (1985) Preparation, Properties and Applications of Calcein in a Highly Pure Form. PhD. thesis, Iowa State University, Ames, IA.

Glaser, R. W., S. L. Leikin, L. V. Chernomordik, V. F. Pastushenko and A. I. Sokirko (1988) Reversible electrical breakdown of lipid bilayers: formation and evolution of pores. *Biochim. Biophys. Acta* **940**:275-287.

Glogauer, M. and C. A. G. McCulloch (1992) Introduction of large molecules into viable fibroblasts by electroporation: optimization of loading and identification of labeled cellular compartments. *Exp. Cell Res.* **200**:227-234.

Goldstein, L., eds. (1977) Introduction to Comparative Physiology. Holt, Rinehart and Winston, New York.

Grasso, R. J., R. Heller, J. C. Cooley and E. M. Haller (1989) Electrofusion of individual animal cells directly to intact corneal epithelial tissue. *Biochim. Biophys. Acta* **980**:9-14.

Graziadei, L., P. Burfeind and D. Bar-Sagi (1991) Introduction of unlabeled proteins into living cells by electroporation and isolation of viable protein-loaded cells using dextran-fluorescein isothiocyanate as a marker for protein uptake. *Anal. Biochem.* **194**:198-203.

Grimnes, S. (1984) Pathways of ionic flow through human skin in vivo. *Acta Derm. Venereol. (Stockh)* **64**:93-98.

Gummer, C. L. (1989) The in vitro evaluation of transdermal delivery. *In* Transdermal Drug Delivery: Development Issues and Research Initiatives. Hadgraft, J. and R. H. Guy, eds. Marcel Dekker, New York. pp. 177-186.

Hadgraft, J. and R. H. Guy, eds. (1989) Transdermal Drug Delivery: Developmental Issues and Research Initiatives. Marcel Dekker, New York.

Hamilton, R. T. and E. W. Kaler (1990) Akali metal ion transport through thin bilayers. *J. Phys. Chem.* **94**:2560-2566.

Hashimoto, K., N. Tatsumi and K. Okuda (1989) Introduction of phalloidin labeled with fluorescein isothiocyanate into living polymorphoneclear leukocytes by electroporation. *J. Biochem. Biophys. Met.* **19**:143-154.

Heller, R. and R. Gilbert (1992) Development of Cell-Tissue Electrofusion for Biological Applications. *In* Guide to Electroporation and Electrofusion. Chang, D. C., B. M. Chassy, J. A. Saunders and A. E. Sowers, eds. Academic Press, New York. pp. 393-410.

Heller, R. and R. J. Grasso (1990) Transfer of human membrane surface components by incorporating human cells into intact animal tissue by cell-tissue electrofusion in vivo. *Biochim. Biophys. Acta* **1024**:185-188.

Hibino, M., M. Shigemori, H. Itoh, K. Nagayama and K. Kinosita Jr. (1991) Membrane conductance of an electroporated cell analyzed by submicrosecond imaging of transmembrane potential. *Biophys. J.* **59**:209-220.

Hsieh, D. S., ed. (1994) Drug Permeation Enhancement. Marcel Dekker, New York.

Hui, L. (1994) Electroporative Molecular Uptake by Saccharomyces Cerevisiae. B.S. thesis, Massachusetts Institute of Technology, Cambridge, MA.

Hulsheger, H., H. Potel and E. G. Niemann (1981) Killing of bacteria with electric pulses of high field strength. *Radiat. Environ. Biophys.* **20**:53-65.

Inada, H., A.-H. Ghanem and W. I. Higuchi (1994) Studies on the effects of applied voltage and duration on human epidermal membrane alteration/recovery and the resultant effects upon iontophoresis. *Pharm. Res.* **11**:687-697.

Jayaram, S., G. S. P. Castle and A. Margaritis (1992) Kinetics of sterilization of lactobacillus-brevis cells by the application of high voltage pulses. *Biotechnol. Bioeng.* **40**:1412-1420.

Kanesada, H. (1990) Anticancer effect of high voltage pulses combined with concentration dependent anticancer drugs on Lewis lung carcinoma, in vivo. *J. Jpn. Soc. Cancer. Ther.* **25**:2640-2648.

Kasting, G. B. (1992) Theoretical models for iontophoretic delivery. *Adv. Drug Deliv. Rev.* **9**:177-199.

Kasting, G. B. and L. A. Bowman (1990) DC electrical properties of frozen, excised human skin. *Pharm. Res.* **7**:134-143.

Kinosita, K. and T. Y. Tsong (1977a) Formation and resealing of pores of controlled sizes in human erythrocyte membrane. *Nature* **268**:438-441.

Kinosita, K. and T. Y. Tsong (1977b) Hemolysis of human erythrocytes by a transient electric field. *Proc. Natl. Acad. Sci USA* **74**:1923-1927.

Kinosita, K., Jr. and T. Y. Tsong (1977c) Voltage-induced pore formation and hemolysis of human erythrocytes. *Biochim. Biophys. Acta* **471**:227-242.

Klenchin, V. A., S. I. Sukharev, S. M. Serov, L. V. Chernomordik and Y. A. Chizmadzhev (1991) Electrically induced DNA uptake by cells is a fast process involving DNA electrophoresis. *Biophys. J.* **60**:804-811.

Klotz, K.-H., M. Winterhalter and R. Benz (1993) Use of irreversible electrical breakdown of lipid bilayers for the study of interaction of membranes with surface active molecules. *Biochim. Biophys. Acta* **1147**:161-164.

Knight, D. E. and M. C. Scrutton (1986) Gaining access to the cytosol: the technique and some applications of electropermeabilization. *Biochem. J.* **234**:497-506.

Kost, J. and R. Langer (1993) Ultrasound-mediated transdermal drug delivery. *In* Topical Drug Bioavailability, Bioequivalence, and Penetration. Shah, V. P. and H. I. Maibach, eds. Plenum Press, New York. pp. 91-104.

Kost, J., D. Levy and R. Langer (1989) Ultrasound as a transdermal enhancer. *In* Percutaneous Absorption. Mechanisms -- Methodology -- Drug Delivery. Bronaugh, R. L. and H. I. Maibach, eds. Marcel Dekker, New York. pp. 595-601.

Kwee, S., H. V. Nielsen and J. E. Celis (1990) Electropermeabilization of human cultured cells grown in monolayers. *Bioelectrochem. Bioenerg.* **23**:65-80.

Kydonieus, A., ed. (1992) Treatise on Controlled Drug Delivery. Marcel Dekker, New York.

Lambert, H., R. Pankov, J. Gauthier and R. Hancock (1990) Electroporation-mediated uptake of proteins into mammalian cells. *Biochem. Cell Biol.* **68**:729-734.

Lampe, M. A., A. L. Burlingame, J. Whitney, M. L. Williams, B. E. Brown, E. Roitman and P. M. Elias (1983a) Human stratum corneum lipids: characterization and regional variations. *J. Lipid Res.* **24**:120-130.

Lampe, M. A., M. L. Williams and P. M. Elias (1983b) Human epidermal lipids: characterization and modulations during differentiation. *J. Lipid Res.* **24**:131-140.

Lange, Y., A. Gough and T. L. Steck (1982) Role of the bilayer in the shape of the isolated erythrocyte membrane. *J. Membr. Biol.* **69**:113-23.

Langer, R. (1990) New methods of drug delivery. *Science* **249**:1527-1533.

Lau, B. S., C. D. Milano, M. R. Prausnitz, R. S. Langer and J. C. Weaver (1993) Quantitative determination of molecular transport across erythrocyte ghost membranes by electroporation. *In* Electricity and Magnetism in Biology and Medicine. Blank, M., ed. San Francisco Press, San Francisco. pp. 141-143.

Ledger, P. W. (1992) Skin biological issues in electrically enhanced transdermal delivery. *Adv. Drug Deliv. Rev.* **9**:289-307.

Lee, R. C., E. G. Cravalho and J. F. Burke, eds. (1992a) Electrical Trauma: the Pathophysiology, Manifestations and Clinical Management. Cambridge University Press, Cambridge.

Lee, R. C., L. P. River, F. Pan, L. Ji and R. L. Wollmann (1992b) Surfactant induced sealing of electropermeabilized skeletal muscle membranes in vivo. *Proc. Natl. Acad. Sci. USA*

Levy, D., J. Kost, Y. Meshulam and R. Langer (1989) Effect of ultrasound on transdermal drug delivery to rats and guinea pigs. *J. Clin. Invest.* **83**:2074-2078.

Liang, H., W. J. Purucker, D. A. Stenger, R. T. Kubiniec and S. W. Hui (1988) Uptake of fluorescence-labeled dextrans by 10T 1/2 fibroblasts following permeation by rectangular and exponential-decay electric field pulses. *Biotechniques* **6**:550-558.

Lieber, M. R. and T. L. Steck (1982a) A description of the holes in human erythrocyte membrane ghosts. *J. Biol. Chem.* **257**:11651-11659.

Lieber, M. R. and T. L. Steck (1982b) Dynamics of the holes in human erythrocyte membrane ghosts. *J. Biol. Chem.* **257**:11660-11666.

Lyderson, A. L. (1955) Estimation of critical properties of organic compounds. Univ. Wisconsin Coll. Eng., Eng. Exp. Stn. Rep. 3, Madison, WI.

Mak, V. H. W., R. O. Potts and R. H. Guy (1991) Does hydration affect intercellular lipid organization in the stratum corneum? *Pharm. Res.* **8**:1064-1065.

Malone, D. M. and J. L. Anderson (1978) Hindered diffusion of particles through small pores. *Chem. Eng. Sci.* **33**:1429-1444.

Marszalek, P., D.-S. Liu and T. Y. Tsong (1990) Schwan equation and transmembrane potential induced by alternating electric field. *Biophys. J.* **58**:1053-1058.

Mavrovouniotis, G. M. and H. Brenner (1988) Hindered sedimentation, diffusion and dispersion coefficients for Brownian spheres in culindrical pores. *J. Colloid Interface Sci.* **124**:269-283.

Melamed, M. R., T. Lindmo and M. L. Mendelsohn (1990) Flow Cytometry and Sorting. Wiley-Liss, New York.

Meyer, B. R., W. Kreis, J. Eschbach, V. O'Mara, S. Rosen and D. Sibalis (1990) Transdermal versus subcutaneous leuprolide: a comparison of acute pharmacodynamic effect. *Clin. Pharmacol. Ther.* **48**:340-345.

Michel, M. R., M. Eligizoli, H. Koblet and C. Kempf (1988) Diffusion loading conditions determine recovery of protein synthesis in electroporated P3X63 Ag8 cells. *Experientia* **44**:199-203.

Mir, L. M., H. Banoun and C. Paoletti (1988) Introduction of definite amounts of nonpermeant molecules into living cells after electropermeabilization: direct access to the cytosol. *Exp. Cell Res.* **175**:15-25.

Mir, L. M., M. Belehradek, C. Domenge, S. Orlowski, B. Poddevin, J. Belehradek, G. Schwaab, B. Luboinski and C. Paoletti (1991a) Electrochemotherapy, a novel antitumor treatment: first clinical trial. *C. R. Acad. Sci. (Paris)* Sér III **313**:613-618.

Mir, L. M., S. Orlowski, J. Belehradek and C. Paoletti (1991b) Electrochemotherapy: potentiation of antitumor effect of bleomycin by local electric pulses. *Eur. J. Cancer* **27**:68-72.

Mir, L. M., S. Orlowski, B. Poddevin and J. Belehradek (1992a) Electrochemotherapy tumor treatment is improved by interleukin-2 stimulation of the host's defenses. *Eur. Cytokine Netw.* **3**:331-334.

Mir, L. M., C. Roth, S. Orlowski, J. Belehradek, F. Fradelizi, C. Paoletti and P. Kourilsky (1992b) Potentiation of the antitumoral effect of electrochemotherapy by an immunotherapy with allogenic cells producing interleukin 2. *C. R. Acad. Sci. Paris* **314**:539-544.

Mishra, K. P. and B. B. Singh (1986) Temperature effects on resealing of electrically hemolysed rabbit erythrocytes. *Indian J. Exp. Biol.* **24**:737-741.

Miyazaki, S., H. Mizuoka, M. Oda and M. Takada (1991) External control of drug release and penetration: enhancement of the transdermal absorption of indomethacin by ultrasound irradiation. *J. Pharm. Pharmacol.* **43**:115-116.

Monteiro-Riviere, N. A. (1991) Comparative anatomy, physiology, and biochemistry of mammalian skin. *In* Dermal and Ocular Toxicology. Hobson, D. W., ed. CRC Press, Boca Raton, FL. pp. 3-71.

Neumann, E. (1989) The relaxation hysteresis of membrane electroporation. *In* Electroporation and Electrofusion in Cell Biology. Neumann, E., A. E. Sowers and C. A. Jordan, eds. Plenum Press, New York. pp. 61-82.

Neumann, E., A. E. Sowers and C. A. Jordan (1989) Electroporation and Electrofusion in Cell Biology. Plenum Press, New York.

Neumann, E., E. Werner, A. Sprafke and K. Kruger (1992) Electroporation phenomena. Electrooptics of plasmid DNA and of lipid bilayer vesicles. *In* Colloid and Molecular Electro-Optics 1992. Jennings, B. R. and S. P. Stoylov, eds. IOP Publishing, Bristol.

Novak, F. J. (1964) Experimental transmission of lidocaine through intact skin by ultrasound. *Arch. Phys. Med. Rehabil.* **64**:231-232.

O'Neill, R. J. and L. Tung (1991) Cell-attached patch clamp study of the electropermeabilization of amphibian cardiac cells. *Biophys. J.* **59**:1028-1039

Okino, M. and K. Esato (1990) The effects of a single high voltage electrical stimulation with an anticancer drug on in vivo growing malignant tumors. *Jpn. J. Surg.* **20**:197-204.

Okino, M., M. Marumoto, H. Kanesada, K. Kuga and H. Mohri (1987) Electrical impulse chemotherapy for rat solid tumors. *Proc. Jpn. Cancer Congress* **46**:420.

Okino, M. and H. Mohri (1987) Effects of a high voltage electrical impulse and an anticancer drug on *in vivo* growing tumors. *Jpn. J. Cancer Res.* **78**:1319-1321.

Okino, M., H. Tomie, H. Kanesada, M. Marumoto, K. Esato and H. Suzuki (1992) Optimal electric conditions in electrical impulse chemotherapy. *Jpn. J. Cancer Res.* **83**:1095-1101.

Okino, M., H. Tomie, H. Kanesada, M. Marumoto, N. Morita, K. Esato and H. Suzuki (1991) Induction of tumor specific selective toxicity in electrical impulse chemotherapy -- analysis of dose-response curve. *Oncologia* **24**:71-79.

Orlowski, S. and L. M. Mir (1993) Cell electropermeabilization: a new tool for biochemical and pharmacological studies. *Biochim. Biophys. Acta* **1154**:51-63.

Parsegian, V. A. (1969) Energy of an ion crossing a low dielectric membrane: solutions to four relevant electrostatic problems. *Nature* **221**:844-846.

Phipps, J. B. and J. R. Gyory (1992) Transdermal ion migration. *Adv. Drug Deliv. Rev.* **9**:137-176.

Pliquett, U., M. R. Prausnitz, Y. A. Chizmadzhev and J. C. Weaver (submitted) Measurement of rapid release kinetics for transdermal and other types of drug delivery.

Pliquett, U. and J. C. Weaver (submitted, a) The change in the passive electrical properties of human stratum corneum due to electroporation.

Pliquett, U. and J. C. Weaver (submitted, b) Transport of a charged molecule across the human epidermis due to electroporation.

Poddevin, B., S. Orlowski, J. Belehradek and L. M. Mir (1991) Very high cytotoxicity of bleomycin introduced into the cytosol of cells in culture. *Biochem Pharmacol* **42**:S67-S75.

Potts, R. O. and R. H. Guy (1991) A pore pathway is not necessary to explain skin permeability. *Proceed. Intern. Symp. Control. Rel. Bioact. Mater.* **18**:

Potts, R. O., R. H. Guy and M. L. Francoeur (1992) Routes of ionic permeability through mammalian skin. *Solid State Ionics* **53-56**:165-169.

Powell, K. T., A. W. Morgenthaler and J. C. Weaver (1989) Tissue electroporation: observation of reversible electrical breakdown in viable frog skin. *Biophys. J.* **56**:1163-1171.

Prausnitz, M. R., V. G. Bose, R. Langer and J. C. Weaver (1992) Transdermal drug delivery by electroporation. *Proceed. Intern. Symp. Control. Rel. Bioact. Mater.* **19**:232-233.

Prausnitz, M. R., V. G. Bose, R. Langer and J. C. Weaver (1993a) Electroporation of mammalian skin: a mechanism to enhance transdermal drug delivery. *Proc. Natl. Acad. Sci. USA* **90**:10504-10508.

Prausnitz, M. R., V. G. Bose, R. Langer and J. C. Weaver (in press,a) Electroporation. *In* Percutaneous Penetration Enhancers. Maibach, H. I. and E. W. Smithe, eds. CRC Press, Boca Raton, FL.

Prausnitz, M. R., V. G. Bose, R. S. Langer and J. C. Weaver (1993b) Transtissue molecular transport due to electroporation of skin. *In* Electricity and Magnetism in Biology and Medicine. Blank, M., ed. San Francisco Press, San Francisco. pp. 122-124.

Prausnitz, M. R., V. G. Bose, C. S. Lee, J. C. Pang, R. Langer and J. C. Weaver (1993c) Effects of electroporation conditions on transdermal delivery. *Proceed. Intern. Symp. Control. Rel. Bioact. Mater.* **20**:95-96.

Prausnitz, M. R., V. G. Bose, U. Pliquett, C. H. Liu, T. P. Singh, J. A. Gimm, R. Langer and J. C. Weaver (in press, b) Changes in skin properties due to electroporation. *Proceed. Intern. Symp. Control. Rel. Bioact. Mater.*.

Prausnitz, M. R., J. D. Corbett, J. A. Gimm, D. E. Golan, R. Langer and J. C. Weaver (submitted, a) Sub-millisecond measurement of transport during and after an electroporation pulse.

Prausnitz, M. R., B. S. Lau, C. D. Milano, S. Conner, R. Langer and J. C. Weaver (1993d) A quantitative study of electroporation showing a plateau in net molecular transport. *Biophys. J.* **65**:414-422.

Prausnitz, M. R., C. S. Lee, C. H. Liu, J. C. Pang, T.-P. Singh, R. Langer and J. C. Weaver (submitted, b) Transdermal transport efficiency during skin electroporation and iontophoresis.

Prausnitz, M. R., C. D. Milano, J. A. Gimm, R. Langer and J. C. Weaver (1994) Quantitative study of molecular transport due to electroporation: uptake of bovine serum albumin by erythrocyte ghosts. *Biophys. J.* **66**:1522-1530.

Prausnitz, M. R., U. Pliquett, R. Langer and J. C. Weaver (submitted, c) Rapid temporal control of transdermal drug delivery by electroporation.

Prausnitz, M. R., D. S. Seddick, A. A. Kon, V. G. Bose, S. Frankenburg, S. N. Klaus, R. Langer and J. C. Weaver (in press, c) Methods for in vivo tissue electroporation using surface electrodes. *Drug Delivery* .

Raptis, L. and K. L. Firth (1990) Electroporation of adherent cells *in situ*. *DNA Cell Biol.* **9**:615-621.

Reid, R. C., J. M. Prausnitz and T. K. Sherwood (1977) The Properties of Gases and Liquids. McGraw-Hill, New York.

Reilly, J. P. (1992) Electrical Stimulation and Electropathology. Cambridge University Press, New York.

Robinson, J. R. and V. H. Lee, eds. (1988) Controlled Drug Delivery: Fundamentals and Applications. Marcel Dekker, New York.

Rols, M.-P. and J. Teissié (1990) Electropermeabilization of mammalian cells: quantitative analysis of the phenomenon. *Biophys. J.* **58**:1089-1098.

Rosemberg, Y. and R. Korenstein (1990) Electroporation of the photosynthetic membrane: a study by intrinsic and external optical probes. *Biophys. J.* **58**:823-832.

Rougier, A., C. Lotte, P. Corcuff and H. I. Maibach (1988) Relationship between skin permeability and corneocyte size according to anatomic site, age, and sex in man. *J. Soc. Cosmet. Chem.* **39**:15-26.

Rudoy, J., R. Kohan and J. Ben-Ari (1987) Externally applied abdominal vibration as a method for improving efficiency in peritoneal dialysis. *Nephron* **46**:364-366.

Sale, A. J. H. and W. A. Hamilton (1967) Effects of high electric fields on microorganisms. I. Killing of bacteria and yeasts. *Biochim. Biophys. Acta* **148**:781-788.

Sale, A. J. H. and W. A. Hamilton (1968) Effects of high electric fields on microorganisms. III. Lysis of erythrocytes and protoplasts. *Biochim. Biophys. Acta* **163**:37-43.

Salford, L. G., B. R. R. Persson, A. Brun, C. P. Ceberg, P. C. Kongstad and L. M. Mir (1993) A new brain tumour therapy combining bleomycin with in vivo electropermeabilization. *Biochem. Biophys. Res. Com.* **194**:938-943.

Santus, G. C. and R. W. Baker (1993) Transdermal enhancer patent literature. *J. Controlled Release* **25**:1-20.

Scheuplein, R. (1978) The skin as a barrier. *In* The Physiology and Pathophysiology of the Skin. eds. Plenum, New York.

Schwarz, V., C. H. Sutcliffe and P. P. Style (1968) Some hazards of the sweat test. *Arch. Dis. Childh.* **43**:695-701.

Schwister, K. and B. Deuticke (1985) Formation and properties of aqueous leaks induced in human erythrocytes by electrical breakdown. *Biochim. Biophys. Acta* **816**:332-348.

Scott, E. R., A. I. Laplaza, H. S. White and J. B. Phipps (1993) Transport of ionic species in skin: contribution of pores to the overall skin conductance. *Pharm. Res.* **10**:1699-1709.

Scott, E. R., H. S. White and J. B. Phipps (1992) Direct imaging of ionic pathways in stratum corneum using scanning electrochemical microscopy. *Solid State Ionics* **53-56**:176-183.

Serpersu, E. H., K. Kinosita and T. Y. Tsong (1985) Reversible and irreversible modification of erythrocyte membrane permeability by electric field. *Biochim. Biophys. Acta* **812**:770-785.

Shah, V. P. and H. I. Maibach, eds. (1993) Topical Drug Bioavailability, Bioequivalence, and Penetration. Plenum Press, New York.

Shapiro, H. M. (1988) Practical Flow Cytometry. Alan R. Liss, New York.

Singh, J. and M. S. Roberts (1989) Transdermal delivery of drugs by iontophoresis: a review. **4**:1-12.

Sixou, S. and J. Teissié (1990) Specific electropermeabilization of leucocytes in a blood sample and application to large volumes of cells. *Biochim. Biophys. Acta* **1028**:154-160.

Sixou, S. and J. Teissié (1993) Exogenous uptake and release of molecules by electroloaded cells: a digitized videomicroscopy study. *Bioelectrochem. Bioenerg.* **31**:237-257.

Sloan, J. B. and K. Soltani (1986) Iontophoresis in dermatology. *J. Am. Acad. Dermatol.* **15**:671-684.

Sloan, K. B., ed. (1992) Prodrugs. Topical and Ocular Drug Delivery. Marcel Dekker, New York.

Sontag, W. (1980) An automatic microspectrophotometric scanning method for the measurement of bone formation rates in vivo. *Calcif. Tissue Int.* **32**:63-68.

Sowers, A. E. and M. R. Lieber (1986) Electropore diameters, lifetimes, numbers, and locations in individual erythrocyte ghosts. *FEBS Lett.* **205**:179-184.

Stephens, W. G. S. (1963) The current-voltage relationship in human skin. *Med. Electron. Biol. Eng.* **1**:389-399.

Sukharev, S. I., A. V. Titomirov and V. A. Klenchin (1994) Electrically-induced DNA transfer into cells. Electrotransfection in vivo. *In* Gene Therapeutics: Methods and Applications of Direct Gene Transfer. Wolff, J. A., ed. Birkhäuser, Boston, pp. 210-232.

Suprynowicz, F. A. and D. Mazia (1985) Fluctuation of the $Ca^{2+}$ -sequestering activity of permeabilized sea urchin embryos during the cell cycle. *Proc. Natl. Acad. Sci. USA* **82**:2389-2393.

Suzuki, H. K. and A. Mathews (1966) Two-color fluorescent labeling of mineralizing tissues with tetracycline and 2,4-bis[N,N'-di-(carbomethyl)aminomethyl] fluorescein. *Stain Techn.* **41**:57-60.

Swezey, R. R. and D. Epel (1988) Enzyme stimulation upon fertilization is revealed in electrically permeabilized sea urchin eggs. *Proc. Natl. Acad. Sci. USA* **85**:812-816.

Tachibana, K. and S. Tachibana (1991) Transdermal delivery of insulin by ultrasonic vibration. *J. Pharm. Pharmocol.* **43**:270-271.

Tachibana, K. and S. Tachibana (1993) Use of ultrasound to enhance the local anesthetic effect of topically applied aqueous lidocaine. *Anesthesiology* **78**:1091-1096.

Taketo, A. (1988) DNA transfection of *Escherichia coli* by electroporation. *Biochim. Biophys. Acta* **949**:318-324.

Tekle, E., R. D. Astumian and P. B. Chock (1991) Electroporation by using bipolar oscillating electric field: an improved method for DNA transfection of NIH 3T3 cells. *Proc. Natl. Acad. Sci. USA* **88**:4230-4234.

Titomirov, A. V., S. Sukharev and E. Kistanova (1991) In vivo electroporation and stable transformation of skin cells of newborn mice by plasmid DNA. *Biochim. Biophys. Acta* **1088**:131-134.

Tojo, K. and A. R. C. Lee (1991) Penetration and bioconversion of drugs in the skin. *J. Chem. Eng. Japan* **24**:297-301.

Tsong, T. Y. (1991) Electroporation of cell membranes. *Biophys. J.* **60**:297-306.

Tyle, P., ed. (1988) Drug Delivery Devices: Fundamentals and Applications. Marcel Dekker, New York.

Tyle, P. and P. Agrawala (1989) Drug delivery by phonophoresis. *Pharm. Res.* **6**:355-361.

Wagner, J. G. (1975) Fundamentals of clinical pharmacokinetics. Drug Intelligence Publications, Hamilton, IL.

Wang, M., S. Freeman, V. Bose, S. Dyer and J. C. Weaver (1993) Theoretical modeling of electroporation: electrical behavior and molecular transport. *In* Electricity and Magnetism in Biology and Medicine. Blank, M., ed. San Francisco Press, San Francisco. pp. 138-140.

Weast, R. C., ed. (1985) CRC Handbook of Chemistry and Physics. CRC Press, Boca Raton, FL.

Weaver, J. C. (1993a) Electroporation: a dramatic nonthermal electric field phenomenon. *In* Electricity and Magnetism in Biology and Medinine. Blank, M., ed. San Francisco Press, San Francisco. pp. 95-100.

Weaver, J. C. (1993b) Electroporation: a general phenomenon for manipulating cells and tissues. *J. Cell. Biochem.* **51**:426-435.

Weaver, J. C. and A. Barnett (1992) Progress towards a theoretical model for electroporation mechanism: membrane electrical behavior and molecular transport. *In* Guide to Electroporation and Electrofusion. Chang, D. C., B. M. Chassy, J. A. Saunders and A. E. Sowers, eds. Academic Press, New York. pp. 91-118.

Weaver, J. C., G. I. Harrison, J. G. Bliss, J. R. Mourant and K. T. Powell (1988) Electroporation: high frequency of occurrence of a transient high-permeability state in erythrocytes and intact yeast. *FEBS Lett.* **229**:30-34.

Webster, J. G., ed. (1988) Encyclopedia of Medical Devices. Wiley, New York.

Wilson, A. K., J. Horwitz and P. De Lanerolle (1991) Evaluation of the electroinjection method for introducing proteins into living cells. *Am. J. Physiol.* **260**:C355-C363.

Xie, T.-D., L. Sun and T. Y. Tsong (1990) Study of mechanisms of electric field-induced DNA transfection I: DNA entry by surface binding and diffusion through membrane pores. *Biophys. J.* **58**:13-19.

Zhelev, D. V. and D. Needham (1993) Tension-stabilized pores in giant vesicles: determination of pore size and pore line tension. *Biochim. Biophys. Acta* **1147**:89-104.

Zimmermann, U., G. Pilwat and F. Riemann (1975) Preparation of erythrocyte ghosts by dielectric breakdown of the cell membrane. *Biochim. Biophys. Acta* **375**:209-219.

Zimmermann, U., F. Riekmann and G. Pilwat (1976) Enzyme loading of electrically homogeneous human red blood cell ghosts prepared by dielectric breakdown. *Biochim. Biophys. Acta* **436**:460-474.

Zlotogorski, A. (1987) Iontophoresis in dermatology. *J. Am. Acad. Derm.* **17**:690.

# Appendix 1 Red Blood Cell Ghost Preparation[22]

## A1.1 Protocol Sheet

- Obtain at least 6 ml freshly-drawn whole human blood in a test tube containing heparin ("green top").

- Put 6 ml of blood in a plastic centrifuge tube (orange cap). Centrifuge in the IEC Centra-7R centrifuge in E25-344 at 1500 rpm, T = 10 °C for 10 min.

- With a Pasteur pipette, aspirate off the clear phase on top. Remove yellow "buffy coat" as much as possible. Add 3 ml PBS (isotonic, pH 7.4). Mix gently by hand. Centrifuge as above (1500 rpm) for 10 min. Repeat two more times. After final centrifugation and aspiration, do not add PBS.

- Put 1.5 ml cleaned red blood cells (RBC) into each of two round-bottom plastic centrifuge tubes. Add 30 ml PBS (5 mM saline, pH 8.5). Mix gently by hand. Let sit on ice for 20 min.

- Centrifuge both samples in Sorvall RC-5B centrifuge with SA-600 rotor in E25-345 at 8300 rpm, T = 10 °C for 20 min.

For loaded ghosts:

  - With Pasteur pipette, aspirate off pink phase on top of each sample. Add 2 ml of fluorescent molecule solution in PBS (5 mM saline, pH 8.5) to ghost button. Mix gently by hand. Let sit 1 h on ice.

  - Add 2 ml fluorescent molecule solution in PBS (40 mM saline, pH 8.5). Mix gently by hand. Let sit for 2 h at room temperature.

  - Centrifuge in Sorvall RC-5B centrifuge with SA-600 rotor in E25-345 at 8300 rpm, T = 10 °C for 20 min.

- With Pasteur pipette, aspirate off pink phase on top of each sample. Add 2 ml PBS (20 mM saline, pH 8.5) to ghost button. Mix gently by hand. Centrifuge as above (8300 rpm) for 20 min. Repeat two more times.

- Transfer cleaned RBC ghosts to microcentrifuge tubes (1.5 ml) with adjustable pipetter. Add PBS (20 mM saline, pH 8.5) almost to rim of tubes. Mix gently by hand. Centrifuge in Biofuge A at 10700 rpm, room temperature for 20 min.

- Remove top phase and store ghosts in tubes in the refrigerator until needed.

---

22 This section supplements Section 4.1.2

Solutions needed:

PBS (isotonic, pH 7.4) -- Prepare from Dulbecco's packet. Follow directions on box. Adjust pH after filtration to 7.4 (isotonic = 150 mM).

PBS (5 mM saline, pH 8.5) -- 0.0325 ml isotonic PBS/ml to make 5 mM PBS (i.e., add 16.25 ml isotonic PBS to 484 ml DI water. Filter. Adjust pH to 8.5.)

PBS (20 mM saline, pH 8.5) -- 0.13 ml isotonic PBS/ml to make 20 mM PBS (i.e., add 65 ml isotonic PBS to 435 ml DI water. Filter. Adjust pH to 8.5.)

PBS (40 mM saline, pH 8.5) -- 0.26 ml isotonic PBS/ml to make 40 mM PBS (i.e., add 130 ml isotonic PBS to 370 ml DI water. Filter. Adjust pH to 8.5.)

1e-5 M coumarinamino-dextran (70 kDa) in PBS (5 mM saline, pH 8.5) -- 0.712 mg/ml (i.e., add 1.424 g coumarinamino-dextran to 2 ml PBS. Mix well until all dissolved. Transfer with adjustable pipetter to syringe. Push through 0.2 μm filter.)

1e-5 M coumarinamino-dextran (70 kDa) in PBS (40 mM saline, pH 8.5) -- 0.712 mg/ml (i.e., add 1.424 g coumarinamino-dextran to 2 ml PBS. Mix well until all dissolved. Transfer with adjustable pipetter to syringe. Push through 0.2 μm filter.)

# Appendix 2 Red Blood Cell Ghost Electroporation[23]

## A2.1 Protocol Sheet

Materials

- labeled and/or unlabeled cleaned red blood cell ghosts
- PBS (20 mM, pH 8.5)
- 1e-5 M labeled dextran or lactalbumin or bovine serum albumin or 1e-4 M calcein in PBS (20 mM, pH 8.5).
- 1e6/ml FITC-equivalent reference beads in PBS (20 mM, pH 8.5)
- Gene Pulser or BTX electroporator, 5 Ω safety resistor box, and 0.2 cm cuvettes.
- Orbitron shaker, vortexer, Biofuge A microcentrifuge, bucket of ice, DI water squirt bottle, Pasteur pipettes and bulbs, adjustable pipetters and tips, syringes and 0.2 μm filter tips.

Preparation of Solutions

- Weigh out needed amount of fluorescent molecule and put into centrifuge tube. Add needed amount of PBS and mix in vortexer. Put on orbitron shaker until completely dissolved.
- Pour solution into syringe with 0.2 μm filter on tip. Push solution through into a new centrifuge tube. Vortex.
- Add RBC ghosts in 1:1000 ratio (i.e., 1 μl ghosts per 1 ml solution). Mix gently by hand and put on ice until needed for experiment.

Running the Experiment

- Put 0.4 ml of sample into pulser cuvette, using adjustable pipetter. Make sure there are no bubbles on top of the solution. Load cuvette into pulser and apply pulse(s) with desired parameters [i.e., 1 kV (5 kV/cm), 0.25 μF ($\tau$ = 1 ms)]. Listen for arcing.

---

[23] This section supplements Section 4.1.3

- Quickly remove cuvette and empty contents into microcentrifuge tube, without spilling. Let sample sit on ice for 5 min after the pulse. Then add 0.4 ml of PBS (20 mM, pH 8.5), mix gently by hand, and spin sample in Biofuge A microcentrifuge at 7200 rpm (4500 g) for 3 min.

- Carefully remove sample from microcentrifuge and still more carefully remove and discard supernatant from tube with a Pasteur pipette, leaving behind the often invisible ghost pellet. It is better to leave a little of the supernatant behind that it is to suck up and throw away the sample.

- Add 0.8 ml PBS (20 mM, pH 8.5), mix by hand, and spin sample in the Biofuge A microcentrifuge at 7200 rpm (4500 g) for 3 min.

- Remove supernatant again, as above, and add 0.8 ml of FITC-equivalent reference beads in PBS (20 mM, pH 8.5) to ghost pellet. Mix by hand and store sample on ice until ready for flow cytometry analysis.

- Clean out cuvette with DI water squirt bottle, dry off outside electrode contacts, and load in another sample. Do not use cuvettes more than 5 - 10 times each.

# Appendix 3. Flow Cytometry[24]

## A3.1 Flow Cytometer Set-Up

A FACStar Plus flow cytometer was used to collect data. The Epics flow cytometer at the Cell Sorter Facility did not appear to be sensitive enough to detect ghosts by light scatter. Typically, 20,000 events were collected from each sample. Forward scatter (manual amplification set to "fully noisy," digital setting on "LO"), side scatter (manual amplification set to "fully quiet," digital setting on "LO" and ~375), and fluorescence (excitation = 488 nm, emission = 530 nm band pass; manual amplification set to "fully quiet," digital setting on "LO" and ~510) were collected. The laser was set to 50 mW. No neutral density filter was used. When red fluorescence (i.e., Texas Red) was needed, the dye laser was set to 610 nm (setting = 5.715).

A side scatter (SS) trigger was found to be best, where the threshold was set at ~310 and a gate at ~380 was used as the final collection threshold. An artifact of the system made the use of a collection window work properly, whereas simply setting a threshold did not. To set up, generally a few samples representing extreme conditions (i.e., unpulsed controls, samples pulsed at high voltage) were initially run. Using SS histograms, the SS of unpulsed ghosts was noted. Then, using samples pulsed at high voltage, or other conditions which might destroy ghosts, SS histograms usually showed many events at SS values lower than control ghosts. These low SS events were interpreted as debris from destroyed ghosts. A threshold gate was set at a SS between the control ghosts and the debris (usually ~ 380). This allowed collection only of apparently intact ghosts.

---

[24] This section supplements Section 4.1.4 and 4.1.5

## A3.2 Data Analysis Protocol Sheet

- Print contour plots (i.e., 14FEB001.FCS) using the DISP2D program. Put a window on the beads and any other relevant sub-populations. Include percent of events within each window on print out (to later calculate ghost/bead ratio).

- Create edited data files (ED14FEB001.FCS) with beads and any other undesired populations edited out. Do this by putting a window around the desired population on a FS vs. FL contour plot (DISP2D) and making edited files containing the contents of the window.

- Print log-scale fluorescence histograms (ED14FEB001.FCS) of desired cell populations selected above. Use the DISP2D program. Define the "electroporation threshold" value (maximum fluorescence of ghosts with no uptake, i.e., unpulsed controls). Identify any artifacts which should be edited out (i.e., channels 15 and 31). Include any relevant statistics (i.e., % of ghosts above electroporation threshold) on print outs.

- Create linear-scale data files (ED14FEB001.FCC) using CALC4 program (P3=1000.^%3/1000.*1023) (see section A3.4).

- Print linear-scale fluorescence histograms (ED14FEB001.FCC) using DISP4. Include relevant statistics, especially mean values of ghosts above the electroporation threshold.

- Enter data into an Excel spreadsheet on the Macintosh. Make graphs of
  - Calibration curve (fluorescence of calibration beads vs. equivalent fluorescent molecules/bead)
  - # of molecules taken up vs. voltage (or vs. any other parameters investigated, such as pulse length.)

### A3.3 Data Analysis Procedure

Data are shown in Fig. A3-1 from a representative pulsed sample. To facilitate analysis and editing, windows have been created, where window #1 contains the reference beads, window #2 contains ghosts having fluorescence corresponding to unpulsed controls (no uptake), and window #3 contains all ghosts. Note that the diagonal collection of events at large fluorescence and forward scatter is not included in window #3. These events are believed to be aggregates of debris, where fluorescence appears to vary linearly with size (or forward scatter). Therefore, they should not be included in calculations of ghost fluorescence.

Ghost concentration can be calculated by taking the ratio of the percent of events in window #3 (3.8 % in Fig. A3-1) to the percent of events in window #1 (75.8 % in Fig. A3-1). By multiplying this ratio times the bead concentration, which is known, the ghost concentration can be determined. This is useful to identify if significant numbers of ghosts were destroyed or otherwise lost during the electroporation procedure.

New files containing only the data within window #3 can be created to facilitate statistical analysis of the ghost population only. A log-scale fluorescence histogram of the contents of an edited file containing only ghosts is shown in Fig. A3-2. After linearization of the data using the CALC4 program (see section A3.4), a linear-scale fluorescence histogram can be made (Fig. A3-3), from which average fluorescence can be calculated. Using calibration beads with known fluorescence (see section 4.2.4), a calibration curve can be generated to convert ghost fluorescence values into numbers of fluorescent molecules associated with each ghost. Whether this fluorescence is associated with

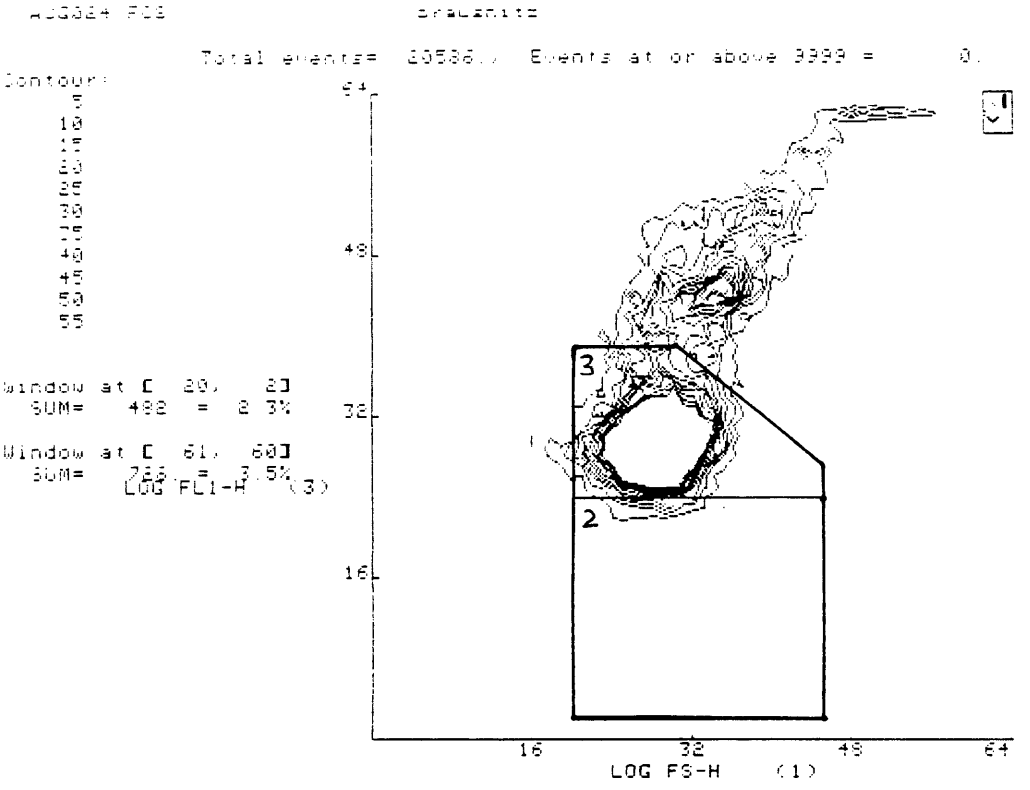


**Fig. A3-1.** Typical log contour plot of forward scatter (FS-H) versus fluorescence (FL1-H) obtained from flow cytometry. Window #1 contains reference beads, window #2 contains ghosts having background fluorescence, and window #3 contains all ghosts. Window #1 contains 728 events (3.8 %) and window #3 contains 15614 events (75.8 %). Here, ghosts suspended in $10^{-3}$ M calcein were exposed to a single exponential-decay electric field pulse (2.75 kV/cm, $\tau$ = 1.3 ms). See text for discussion.

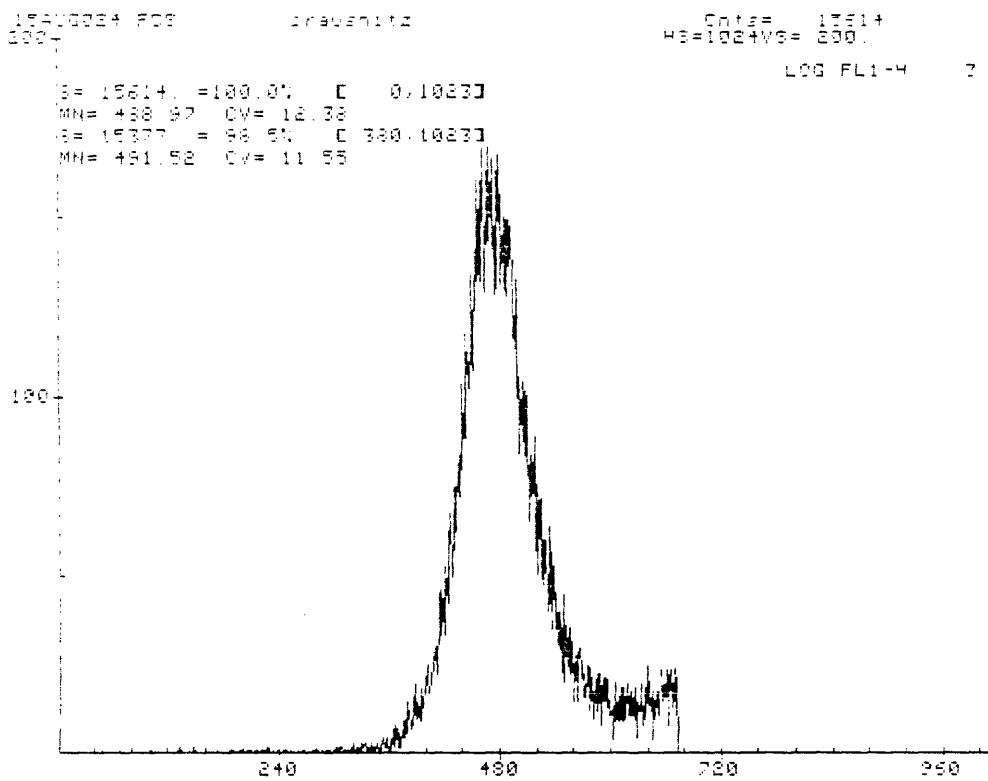


**Fig. A3-2.** Log fluorescence histogram containing the contents of window #3 in Fig. A3-1 (ghosts only; debris and beads edited out).

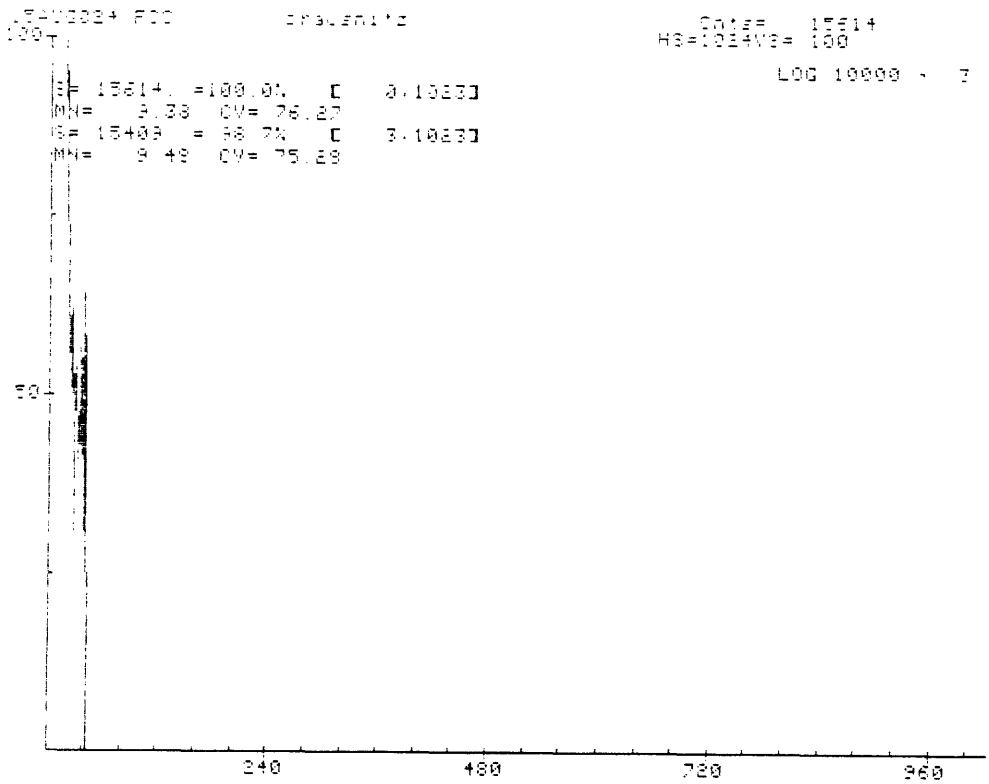


**Fig. A3-3.** Linear fluorescence histogram containing the data shown in Fig. A3-2. Linear data are needed to correctly calculate average fluorescence. Here, the average fluorescence is 9.38, with a coefficient of variation of 76.27 (standard deviation = 7.15). After calibration, average fluorescence can be converted to average number of calcein molecules associated with each ghost.

membranes or appears to exist throughout the ghost interior can be assessed by fluorescence microscopy.

### A3.4 CALC4 Progam Operation

CALC4 is a program, available on the Cell Sorter Facility's VAX, which can be used to manipulate data obtained from the flow cytometer. Because data is collected on a log scale, it is often necessary to convert that data to a linear scale. Instructions on how to use CALC4 are outlined below (technical support and instruction manuals are apparently not available). Input keystrokes are **bold-face**, computer output is plain-face.

Converting one file to linear scale

```
$ calc4                                                          A
CALC4  V02-17
CALC4> input                                                     B
INPUT FILE:  14feb001                                            C
Reading from FCS file 14feb001.FCS
CALC4> new                                                       D
CALC4__Parameter definition> p1=10000.^%1/10000.*1023            E
CALC4__Parameter definition> p2=10000.^%2/1000.*1023             F
CALC4__Parameter definition> p3=1000.^%3/1000.*1023              G
CALC4__Parameter definition>
CALC4> output 14feb001a.fcs                                      H
Output file is SYS$SYSDEVICE:[CONSORT.PRAUSNITZ]14FEB001A.FCS
[Buffers completed: . . . . . ]
CALC4> ex                                                        I
```

Meanings of bold-face keystrokes

A enters CALC4 program
B tells progam in accept input file
C gives name of input file (file with log data to be converted to linear data)
D allows definition of new parameters
E parameter 1 converted from 4-log scale to linear scale
F parameter 2 converted from 4-log scale to linear scale times 10 (fourth decade is off scale.
G parameter 3 converted from 3-log scale to linear scale
H gives name of output file (file into which converted data should be put)
I exits CALC4

Batch File Operation

```
$ calc4                                                                    A
CALC4  V02-17
CALC4> do 14feb0*                                                          B
CALC4> input/next                                                          C
Next file is SYS$SYSDEVICE:[CONSORT.PRAUSNITZ]14FEB001.FCS;1
Reading from FCS file SYS$SYSDEVICE:[CONSORT.PRAUSNITZ]14FEB001.FCS;1
CALC4> new                                                                 D
CALC4__Parameter definition> p3=1000.^%3/1000.*1023                        E
CALC4__Parameter definition>
CALC4> output                                                              F
Output file is SYS$SYSDEVICE:[CONSORT.PRAUSNITZ]14FEB001A.FCC
[Buffers completed: . . . . . ]
CALC4> enddo                                                               G
CALC4> input/next                                                          H
Next file is SYS$SYSDEVICE:[CONSORT.PRAUSNITZ]14FEB002.FCS;1
Reading from FCS file SYS$SYSDEVICE:[CONSORT.PRAUSNITZ]14FEB002.FCS;1
etc.
```

Meanings of bold-face keystrokes

A enters CALC4 program
B designates files for batch conversion
C instructs program to identify first file to be converted
D allows definition of new parameters
E parameter 3 converted from 3-log scale to linear scale
F tells program to create an output file (which automatically ends with .FCC)
G completes the set of batch instructions
H initiates batch processing (C through G will be repeated for all files identified in B).

# Appendix 4 Skin Preparation[25]

## A4.1 Protocol Sheet

Fresh tissue is kept in the refrigerator if to be used within 1 week. Otherwise, tissue should be frozen at -80 °C (flash freezing optional).

Preparing the Bench Top
All skin preparation should be on a designated biohazard benchtop. Prepare by covering the bench with bench paper (one side absorbent, one side waxy -- available from Lab Supplies), with the absorbent side up.

Materials required: "gentle" forceps (no teeth or pointed ends), forceps with teeth, large (8 - 12") forceps, scalpel handle, scalpel blades, spatula, dissecting scissors (rounded tips), hole punch (1" diameter), soft headed mallet, plastic dissecting board, floating tray (any large pan, i.e., 6" x 12") filled with DI water, extra bench paper (> twice the size of skin being prepared), waste can containing a biohazard bag.

Preparing Yourself
Wear a plastic surgical gown (from Lab Supplies), double layered latex gloves, and a surgical mask and glasses or a face shield to protect from biohazards.

Preparing Skin
If frozen, place skin in refrigerator to defrost overnight. If skin is needed immediately, it can be placed in a warm (i.e., 37 °C) incubator or a warmed (DI) water bath to expedite defrosting. Record all available information (i.e., sample #; date of death, receipt, and preparation; age; sex; etc.) in skin log book.

To remove any fat (yellow tissue) from the underside of the skin, use forceps to grasp the fat and cut carefully with dissecting scissors or a scalpel. Be careful not to puncture the epidermis with the forceps or scissors. Once only a little fat remains (the white of the dermis can be seen), scrape away the remaining fat with the blunt part of a scalpel handle (with no blade). If full-thickness skin is needed, as much fat as possible should be removed. If skin will be heat-stripped, then some remaining fat is OK.

Heating Skin
If the skin is bigger than the floating tray, cut the skin up so that all pieces are smaller than the tray. Then, cut two pieces of bench paper for each piece of skin, where each piece of paper is a little bigger than each piece of skin.

Heat > 500 ml DI water to 60 °C (59 - 62 °C is OK) in a beaker. Place skin in the water, stirring occasionally and gently with a spatula. After 2 min, remove skin and place on one of the prepared pieces of bench paper, where the dermis side

---

[25] This section supplements Section 5.2

of the skin faces the absorbent side of the paper. Spread the skin so that it makes a flat surface.

Stripping Skin

Grab the dermis of a corner of the skin with the toothed forceps. Then scrape at the epidermis immediately above the forceps with the rounded end of a spatula. Use a light, short scooping motion, where more force is applied downward (toward the dermis), than laterally (toward the epidermis). It may be difficult to get started, but the epidermis should separate from the dermis. The dermis should be white, while the epidermis will have color (depending on the donor's skin color). Slowly and patiently scrape the epidermis from the dermis, rolling the epidermis into a cylinder. Beware of skin defects (i.e., mole, laceration, belly button) -- do not let a small hole turn into a big hole. Also, be especially careful around hair follicles, where skin has a tendency to snag. Do not pull at the epidermis.

Finding Holes in the Skin

Once the epidermis has been removed, lift it from the dermis (keeping track of which side is the stratum corneum), and place it stratum corneum side up in the floating tray with DI water. The epidermis should spread out on top of the water. If it does not spread out fully, carefully use the big (dull) forceps or, preferably, a gloved finger to spread it out. If it does not spread at all, then carefully spread it out by hand. Be careful not to rip it.

Once the skin is spread, remove water puddles on the skin with Kimwipe paper towels. Rather than wiping off water, just rest the Kimwipe on the skin and let it soak the water up. Then, look for holes in the epidermis. This can be done by gently probing the skin with blunt-tipped forceps and looking for reflections from water crossing the skin through holes. Because holes can be seen much more easily when the skin is floated than when it is on paper, any identified holes should be made obvious by cutting from the hole to the nearest edge of the skin with scissors. Try to damage as little skin as possible in the process.

Take the second piece of bench paper and slide it under the skin (in the floating tray) with the waxy side up. Because the paper tend to curl under water, place forceps on the end of the paper to weigh it down and slowly slide the paper until it is fully under the skin. Then, lift the end of the paper without the forceps up to the edge of the skin and let the skin stick to the paper. The skin should stick by itself. The stratum corneum side should still be up. Slowly lift the paper out of the tray, with the skin sticking to it all the way. At the end, the skin should be out of the tray and completely on the paper.

Cutting and Storing Skin

Place the skin and paper on the dissecting board. If not already, smooth out the skin with a gloved finger so that it is flat. Identify the holes marked while the skin was floated. With the hole punch and hammer, punch out discs of skin and underlying paper. Position the punch to get as many discs as possible. Place the discs in large plastic weigh-boat trays. Label each tray on the outer-bottom

surface with the skin identification number. Place trays in a large dessicator, with saturated $K_2SO_4$ solution at the bottom to maintain 95 % humidity. Keep refrigerated until needed. Skin should be used as soon as possible. Within a few days is best, within a week is OK, or up to 2 - 3 weeks may be OK too (check electrical and passive transport properties -- see Section A5.1).

Clean Up

Throw all biohazardous materials (i.e., fat, dermis, other contaminated disposables) into a biohazard bag. Place scalpel blades into a sharps container. Place all tools into a large plastic tub and spray everything generously with 70% ethanol in water. Pour bleach into the floating tray and beaker to > 10% bleach (i.e., Clorox). If may be necessary first to remove any pieces of fat in the beaker with Kimwipes. Spray anything which may have become contaminated with 70% ethanol.

After soaking in 70% ethanol or 10% bleach for 10-15 min, rinse all items off with lots of tap water. Place metal tools in the ultrasonicator bath for 10 - 15 min. Remove and rinse again with tap water. Scrub the dissection board. Give all items a final rinse with DI water.

Biohazard bags should be double-bagged, taped shut, and labeled with "Biohazard, Human Tissue, Please Burn," as well as the researchers name and the date. Bring bags to the animal facility in the basement of E25 (a key card is needed for access). Bags can be placed in the walk-in refrigerator for incineration. Check with the facility staff for details.

# Appendix 5 Tissue Electroporation[26]

## A5.1 Protocol Sheet

Set-Up For Experiment

Prepare isotonic phosphate-buffered saline. A typical 10-chamber experiment requires 0.5 - 1 liters. Set out magnetic stirrers (2 chambers/stirrer). Cover each stirrer with a paper towel. Set out chambers with their metal holders, but do not tighten the holders yet. Put glass (or plastic) stoppers in any ports on the sides of chambers, unless the ports are to be used for some special purpose. Put an Ag/AgCl electrode into each side of each chamber through the outer (furthest from the skin) upper port. Use tape to secure each electrode. Attach tubing to the chambers and connect the ends to the water bath. Make sure all tubing connections are good and continuous before turning the water bath pump on. Set the water bath to 4 °C. Check the water bath level and add DI water to the fill line, if needed. Air bubbles within the water jackets of the chambers can be removed by tipping the chambers, starting with the one closest to the pump outlet, and moving the air through the pump inlet into the water bath.

Loading The Skin

Remove skin from the dessicator in the refrigerator. Get forceps (no teeth or pointed tips) and a small dish of DI water for floating skin. Place a spacer (3-4 microscope slides taped together) under the chamber to be loaded with skin. The spacer helps center the chamber in the metal holder. Place the left side of the chamber with the hole facing up. Using forceps, moisten a piece of skin (with waxy paper underneath) briefly in the DI water. Carefully separate the epidermis from the paper beneath. Be careful not to separate the waxy part of the paper (with epidermis attached) from the absorbent part of the paper by mistake. Make sure only the epidermis has been removed and all paper is left behind. Float the skin in the DI water.

Use forceps to pick up the paper disc from which the skin was removed, waxy side up. Position the paper under the floating skin and slowly scoop it up, stratum corneum side up. One arm of the forceps should remain between the skin and paper, while the other arm is below the paper. Place the skin and paper on the up-turned left side of the chamber, paper side down. With one gloved finger, gently press down on the skin while pulling the paper disc out from underneath the skin. This is something like the famous trick of pulling the tablecloth from the table without disrupting the dishes. Carefully remove the finger from the skin, making sure that the skin does not stick to the finger. The end result should be that the paper is removed and the skin is lying flat on the chamber surface, covering the hole. If the skin is not flat, gently smooth it out with a gloved finger. If this cannot be done easily, then refloat the skin and start the process over again.

---

26 This section supplements Section 5.3.1

Once the skin is on the chamber, position both sides of the chamber within the holder so that their large holes are opposite each other. Be careful not to let the two chambers touch, thereby disturbing the skin. Then, in one smooth motion, bring the two chambers together, sandwiching the skin. Hold the chambers tightly in place with one hand, while tightening the holder with the other hand. The holder can be made quite tight without breaking the chambers. Once the chamber is secure within the holder, fill both sides of the chamber with saline. Fill to the joint between the main chamber compartment and the upper sampling port. Using the Ag/AgCl electrodes already in the chambers, measure skin resistance with an ohm meter. If the resistance is > 70 kΩ (it can be as high as 1 MΩ), the skin will probably be good. If the skin is < 20 kΩ, it probably has a hole in it. If it is between 20 - 70 kΩ , the skin is not worthless, but will probably be a leaker (in general, do not use). Bad skin should be removed, discarded, and replaced with another piece. While sometimes all the skin from a given donor is good, often half or more of the pieces from another donor may have to be discarded. Once a good piece of skin is secured, place a small stir bar in each side of the chamber.

Repeat this process until all chambers are filled. Turn on the magnetic stirrers and leave overnight. Leaving overnight accomplishes a number of goals. First it hydrates the skin fully, although this probably takes less than an hour. However, the main purpose is that it facilitates fluorescence measurements. There appear to be fluorescent particles associated with skin, which distort fluorescence measurement used to determine transdermal flux. If the skin is soaked overnight, most of this fluorescence appears to be removed. If the skin is kept at 4 °C, little degradation occurs overnight. In contrast, degradation is much more rapid at higher temperatures. Thus, if fluorescence measurements will not be made, such as in experiments involving radioactivity assay, this overnight soak is not needed.

Starting The Experiment

Turn off the magnetic stirrers and empty and discard the saline from both sides of the chambers using plastic pipettes and refill with fresh saline. Turn the stirrers back on. Switch the temperature bath to 37 °C. Measure skin resistance with an ohm meter and record the values.

To prepare the donor solution, weigh out the needed compound and add to saline. Mix. Each donor compartment holds approximately 3.5 ml. Thus ~40 ml of donor solution should be more than sufficient for a 10 chamber experiment. Turn off the magnetic stirrers, empty and save (put in labeled fluorimeter cuvette) the contents of the receptor compartment (facing the viable epidermis -- should be on the left) and empty and discard the contents of the donor compartment (facing the stratum corneum). Refill the receptor with saline and the donor with the prepared donor solution. Turn the stirrers back on. Make sure the donor and receptor fluid levels are the same. Wait 30 - 60 min before taking the next sample.

Start up the SPEX spectrofluorimeter, by turning on the power strip, turning on the lamp and pushing the start button, and turning on the computer and monitor. Select "fluorescence measurement" and wait for the program to load. When prompted, enter the excitation (left of sample chamber of the fluorimeter) and emission (on right) wavelengths which appear on the fluorimeter. Once the program has loaded fully, press F10 and turn both high voltage sources on. Then select "define experiment" and select either an emission scan or a time-based scan. For an emission scan, the data acquisition parameters should be: excitation at 488 nm, emission at 505 - 535 nm, step 2 nm, and collection time of 1 s. For a time-based scan, data acquisition parameters should be: excitation at 488 nm, emission at 515 nm, and sample time of 1 to 5 s.

Prepare a calibration curve, by making serial dilutions (1/10) of the donor solution. Also prepare saline and DI water samples for background measurements. Obtain fluorescence of each and establish the relationship between fluorescence and concentration. There should be a 3 - 4 order of magnitude linear range.

To sample the receptor compartments, stop the stirrers, remove the receptor solution and put it in a fluorimeter cuvette, refill and empty the receptor compartment with saline to rinse, refill the receptor compartment again, and finally turn the stirrers back on. Measure the fluorescence of each receptor solution, which can be converted into a quantitative molecular flux.

Based on the first samples taken (before the donor solution was added), the cleanliness of the chamber can be assessed. Measurements made after donor solutions were added can be used to assess passive transport as a measure of the integrity of the skin barrier properties. If the fluorescence is more than 4 - 5 times higher than PBS-only background, then the skin in probably leaking (assuming a molecule which cannot cross skin is used). Data from leaky skin is of questionable value. While the resistance measurements provide a useful guide, the quality of a piece of skin is ultimately determined by passive flux measurements.

Pulsing Skin

Once good pieces of skin have been identified, electrical protocols can be applied. Using one of the electroporators (BTX or Gene Pulser), one of the square-wave pulsers (Velonex), a constant-current or constant-voltage generator, or some other power supply, electrical protocols can be applied across the Ag/AgCl electrodes to the skin. Typically, protocols are applied for 1 h, after which the receptor compartment is samples. Additional washes (2 - 4) should be performed after protocols which increase transdermal flux. Additional samples may be taken at different times after pulsing.

Clean-Up

Collect all liquids (donor compartment, receptor solution in cuvettes, etc.) in a beaker and add bleach to > 10%. Detach tubing from chambers, loosen metal holders, and separate chambers into halves. With forceps and a paper towel,

remove skin from the chambers and clean off residue. Collect stir bars, electrodes, and stoppers and place them in a plastic tub. Place the chambers in the tub too and fill with 10% bleach. Set the tubing, holders, and other metal or plastic objects (i.e., forceps) aside and spray generously with 70% ethanol. Spray the lab bench, including stirrers, with 70% ethanol. Let everything soak (in bleach or ethanol) for 10 - 15 min.

Rinse everything off well with tap water. Tubing and metal holders are shaken dry and put away. Everything else is put into the ultrasonic cleaner for 10 - 15 min, rinsed again with tap water, and given a final DI water rinse. Chambers may need extra scrubbing before ultrasonication to remove all skin residue. Be careful not to lose stir bars or stoppers; they easily go down the drain. Sand the electrodes with fine sandpaper until the surfaces become shiny. Sand as little as possible, to prolong the electrodes' lifetime.

## A5.2 Data Sheet

Skin donor #: _____ Died: ___/___/___ Stripped: ___/___/___

Load into chambers -- Date: ___/___/___ Time: ____:_____
at 4 °C in isotonic PBS (pH 7.4), stirred

---

Date ___/___/___ Your name: _____

Donor compartment: stratum corneum side, negative (-) electrode,
$10^{-3}$ M calcein in isotonic PBS (pH 7.4)
Receptor compartment: epidermis side, positive (+) electrode,
isotonic PBS (pH 7.4)
at 37°C (time switched ____:____), stirred

pH of PBS: _____ (filter and adjust pH if off)

$10^{-3}$ M calcein = 0.623 mg/ml = _____ mg/_____ ml

Spex excitation: _____ nm, slit width: _____ mm
Spex emission: _____ nm to _____ nm, step ____,
slit width: _____ mm, right angle collection

donor and receptor emptied, replaced with fresh PBS: ____:____

calcein added to donor compartment: ____:____

| Sample # | Calcein concentration | Peak + Background |
|---|---|---|
| 1 | $10^{-4}$ M | |
| 2 | $10^{-5}$ M | |
| 3 | $10^{-6}$ M | |
| 4 | $10^{-7}$ M | |
| 5 | $10^{-8}$ M | |
| 6 | $10^{-9}$ M | |
| 7 | $10^{-10}$ M | |
| 8 | DI water | |
| 9 | PBS 1 | |
| 10 | PBS 2 | |

| Sample # | Chamber# | Time/Conditions | Peak + Background |
|---|---|---|---|
| 11 | | | |
| 12 | | | |
| 13 | | | |
| 14 | | | |
| 15 | | | |
| 16 | | | |
| 17 | | | |
| 18 | | | |
| 19 | | | |
| 20 | | | |
| 21 | | | |
| 22 | | | |
| 23 | | | |
| 24 | | | |
| 25 | | | |
| 26 | | | |
| 27 | | | |
| 28 | | | |
| 29 | | | |
| 30 | | | |
| 31 | | | |
| 32 | | | |
| 33 | | | |
| 34 | | | |
| 35 | | | |
| 36 | | | |
| 37 | | | |
| 38 | | | |
| 39 | | | |
| 40 | | | |
| 41 | | | |
| 42 | | | |
| 43 | | | |
| 44 | | | |